Université catholique de Louvain
Institut de la matière condensée et des nanosciences (IMCN)
Molecules, Solids and Reactivity (MOST)

REACTIVE PROCESSING OF POLYOLEFINS : A STUDY ON POLYMERS AND MODEL COMPOUNDS

Promoteurs de thèse: Prof. J. Marchand-Brynaert & Prof. P.Godard

Dissertation présentée par

Xavier Drooghaag

En vue de l'obtention du grade de docteur en sciences

Novembre 2012

Université catholique de Louvain
Institut de la matière condensée et des nanosciences (IMCN)
Molecules, Solids and Reactivity (MOST)

REACTIVE PROCESSING OF POLYOLEFINS : A STUDY ON POLYMERS AND MODEL COMPOUNDS

Xavier Drooghaag

COMPOSITION DU JURY :

Prof. J-F. Gohy (UCL), Président du Jury
Prof. J. Marchand-Brynaert (UCL), Promoteur de thèse
Prof. P. Godard (UCL), Promoteur de thèse
Prof. J. Devaux (UCL)
Prof. B. Champagne (FUNDP)
Dr. B. Roekens (3B The Fibreglass Company)
Dr. Michaël Alexandre (ULg)

A mon grand-père

Je ne saurais débuter cette dissertation sans exprimer ma profonde gratitude à ma promotrice de thèse, le Professeur Jacqueline Marchand-Brynaert, d'une part pour la confiance qu'elle m'a accordée tout au long de ce projet mais également pour son soutien au quotidien, sa disponibilité, sa générosité, son écoute et ses nombreux conseils.

Je voudrais remercier de tout cœur le Dr. Véronique Carlier, pour son support au démarrage de ce projet de thèse, ainsi que le Professeur Pierre Godard, pour avoir assuré la co-promotion de cette thèse.

J'exprime également toute ma reconnaissance aux membres du jury pour l'intérêt porté à ce travail de recherche, leur jugement, leurs conseils et commentaires avisés.

Je remercie par ailleurs le Fonds pour la formation à la Recherche dans l'Industrie et dans l'Agriculture (FRIA), dépendant du Fonds de la Recherche Scientifique (FNRS), dont le soutien financier a permis la concrétisation de cette thèse.

Mes remerciements vont aussi à mes collaborateurs qui m'ont encadré ou qui ont participé à ce travail de thèse. Merci à Michel Sclavons, Gaëtan Henry, Dimitri Rousseaux, Cécile Le Duff, Adrien Vandormael, Leila Amajod, Geoffroy le Hardÿ, Vincent Liégeois, Florian Stadler. Merci également à Chantal pour sa bonne humeur au

quotidien et pour toute l'attention qu'elle porte à toute l'équipe de chercheurs.

Merci également à Pascal, François, Guido, Sunil, Cédric, Xavier, Anne-Christine, Julian, Pierre, Guillaume, Vincent P., Sonia, Aline, Martin, Benoît, Vincent R. Cédric, Frédéric, Catheline et Tanguy.

Merci à mes parents, ma famille et mes amis pour leur soutien et leurs encouragements tout au long de ces années.

Summary

The reduction in crystallinity of isotactic polypropylene by reactive extrusion was first described in 1970. However this process, which involves both a radical initiator and at least one molecule bearing labile bromine atoms (such as N-bromosuccinimide), has never been further investigated ever since.

Recently, our group demonstrated using high-temperature solution-state ^{13}C NMR that the bromine radicals issued from N-Bromosuccinimide were responsible for the random epimerization of polypropylene tertiary carbons by fast and reversible hydrogen abstraction, turning the isotactic into a stereoblock structure and providing the elastomer feature.

This dissertation discloses how this process could be advantageously extended to the grafting of maleic anhydride onto polypropylene, providing highly-grafted stereoblock polypropylene elastomers with preserved molecular weights. Besides, the grafts structure was identified as isolated succinic rings distributed all along the polymer chains whereas small anhydride oligomers grafted almost exclusively at chain extremities are usually observed with common grafting processes. Both the polarity and the crystallinity of the starting polypropylene could therefore be fine-tuned. Those innovative materials were investigated as a source of ionomers and led to a follow-up dissertation in the field of polypropylene/clay nanocomposites. It was also observed that N-bromossuccinimide had almost no-effect on the grafting mechanism of maleic anhydride onto high-density polyethylene because secondary hydrogen atoms cannot be reversibly abstracted by bromine radicals from polyethylene chains.

Several attempts were made to substitute bromine radicals in the grafting reaction by other mediating species borrowed from controlled radical polymerization techniques but none of the molecules tested were able to simultaneously enhance the grafting levels while preserving the molecular weights.

A five-unit oligomer of propylene was also synthesized and all the corresponding dia-stereoisomers were isolated as model compounds of polypropylene of various tacticities. In collaboration with the FUNDP, those model compounds were used to validate theoretically simulated Raman spectra of propylene oligomers. Those models were also used as a substrate to investigate the epimerization reaction in the presence of N-bromosuccinimide.

Finaly, our group contributed to an international collaboration through the elucidation of the co-monomer content and co-monomer structure of several samples of polyethylenes of various densities using high-temperature solution-state ^{13}C NMR. Melt-sate rheometry was used as a probe for short- and long-chain branched polyethylenes and the results were correlated to the molecular strcutrure.

Abbreviations

%CL	percentage of crystallinity loss
|G*|	complex modulus
A.U.	absorbance unit
Ad_2NO	1,1-diadamantyl nitroxide
aPP	atactic polypropylene
a_T	horizontal shift factor
$Br^{\bullet}$	bromine radical
Br/Ox	bromine to oxygen ratio
b_T	vertical shift factor
ccPP	controlled-crystallinity polypropylene
cND	corrected neutralizaton degree
Cp	cyclopentadienyl
CRP	controlled radical polymerization
CTA	chain transfer agent
δ	phase angle
DBTB	benzyl dithiobenzoate
DCM	dichloromethane
ΔCp	variation of heat capacity
DFT	density functional theory
DHBP	2,5-dimethyl-2,5-di-(*t*-butylperoxy)hexane
ΔH_m	melting enthalpy
DME	1,2-dimethoxyethane
DMSO	dimethyl sulfoxide
DSC	differential scanning calorimetry
E_a	activation energy
ELPP	polypropylene elastomer
elPP-g-MA	polypropylene elastomer grafted with maleic anhydride
ESR	electron spin resonance
Flu	fluorenyl
FTIR	Fourier transform infrared spectroscopy
G'	storage modulus
G''	loss modulus
GC	gas chromatography
GPC	gel permeation chromatography

η^*	complex viscosity
η_0	Newtonian viscosity
HDPE	high density polyethylene
HMHD	3,5,7,9,11,13,15-heptamethylpentadecane
HPLC	high-performance liquid chromatography
HRMS	high-resolution mass spectroscopy
HWE	Horner-Wadsworth-Emmons
Ind	Indenyl
INIFERTER	initiator-transfer-termination
iPP	isotactic polypropylene
i-PrOH	isopropanol
IUPAC	International Union of Pure and Applied Chemistry
L/D	length to diameter ratio
LCB	long-chain branching
LDPE	low density polyethylene
LLDPE	linear low density polyethylene
M	molar mass
m	mettalocene
$M^{\bullet}$	mediating radical
MA	maleic anhydride
MALLS	multiangle laser-light scattering
MAO	Methyl aluminoxane
m-CPBA	meta-chloroperbenzoic acid
MFI	melt flow index
mLLDPE	Metallocene-catalyzed linear low density polyethylene
M_{LS}	Molar Mass (light scattering method)
M_n	number-average molecular weight
MPLC	medium-pressure liquid chromatography
M_W	weight-average molecular weight
MWD	molecular weight distribution
M_z	z-average molecular weight
NBS	N-bromosuccinimide
ND	neutralization degree
NMP	nitroxide-mediated polymerization
NMR	nuclear magnetic resonance
$Ox^{\bullet}$	oxygen-based radical

P	probability of local displacement
P_a	probability for segmental motion
PDI	polydispersity index
PE	polyethylene
PET	Polyethylene terephthalate
PMU	2,4,6,8,10-pentamethylundecane
PP	polypropylene
PP-g-MA	polypropylene grafted with maleic anhydride
PP-g-TEMPO	polypropylene grafted with TEMPO
PRE	persistant radical effect
PS	polystyrene
P_v	probability for free volume
PVC	poly(vinyl chloride)
ρ	density
RAFT	reversible addition-fragmentation chain transfer
R_f	retention factor
r_g	radius of gyration
$RO^{\bullet}$	alkoxy radical
rpm	revolutions per minute
SCB	short-chain branching
SCP	scattered circularly polarized
SDTA	simultaneous differential thermal analysis
SEC	size exclusion chromatography
sPP	syndiotactic polypropylene
SSA	successive self-nucleation and annealing
SSC	single-site catalyst
T_0	reference temperature
T_a	annealing temperature
TCB	1,2,4-trichlorobenzene
TCE	1,1,2,2-tetrachloroethane
TDHF	time-dependent Hartree Fock
^{t}DSH	*tert*-dodecanethiol
TEMPO	2,2,6,6-tetramethylpiperidine-1-oxyl
T_g	glass-transition temperature
TGA	thermogravimetric anaysis
THF	Tetrahydrofurane

T_m	melting temperature
TMTDS	tetramethylthiuram disulfide
TPE	thermoplastic elastomer
UV	Ultraviolet
v/v	volume/volume
VROA	vibrational Raman optical activity
WLF	Williams–Landel–Ferry
wt.%	weight percentage
ZN	Ziegler-Natta
PMA	poly(maleic anhydride)
XRF	X-ray fluorescence
PMUBr	6-bromo-2,4,6,8,10-pentamethylundecane

Table of content

Chapter One

Introduction

1.1 Plastics – A few numbers

In 2010, the global production of synthetic polymers (referred to as «plastics») reached 265 million tons across the world, 21.5% of which were produced in Europe (57 million tons), including 3.5% (9.3 million tons) in Benelux.[1] The plastics market is constantly growing at a rate of almost 5% per year over the last 20 years, worldwide. Interestingly, only five polymers account for 75% of the market share. These are polyethylene (29%, including high density (HDPE), low density (LDPE) and linear low density (LLDPE)), polypropylene (PP - 19%), polyvinyl chloride (PVC - 12%), polystyrene (PS - 8%) and polyethylene terephthalate (PET - 6%). The main application sectors for plastics in Europe are packaging (39%), building and construction (20.6%), automotive (7.5%) and electrical and electronic equipments (5.6%).

It is remarkable that half of the European demand in polymer materials consists of polyolefins (i.e. polyethylene together with polypropylene). This can be easily understood as polyethylene is the number one polymer for the packaging industry and find its main applications as plastic bags, wrapping films, bottles and containers, etc. Polypropylene is a more polyvalent material that is also used for packaging (heavy-duty bags and bulk bags, food containers, bottle caps, etc), microwave/dishwasher compatible food containers, disposable objects, but also for several car parts (bumpers, body panels, lateral trims, dashboards, door cladding, etc.), household appliance, containers suitable for autoclaves, medical devices, etc. Fibers of polypropylene can also be drawn to make textiles (carpets, etc.) and impact-reinforced concrete.

Belgium is a key player in the field of plastics, producing almost 10 million tons of plastics per year.[2] It is also the biggest plastics producer in

the world on a *per capita* basis with over 530kg of plastics *per capita*, followed by the Netherlands (278kg *per capita*) and Germany (210kg *per capita*). For example, Belgium meets more than 15% of the European polypropylene demand thanks to the production capacity of 685000 tonnes of Borealis in Kallo and Beringen, and the production capacity of 930000 tonnes of Total Petrochemicals in Feluy. On the same basis, Belgium is also the biggest plastics converter in the world with 190kg of plastics converted *per capita*, followed by Germany (130kg *per capita*) and northern America (120kg *per capita*).

1.2 Polypropylene

TACTICITY OF POLYPROPYLENE

Because propylene is a prochiral vinyl monomer, its polymerization leads to macromolecules whose tertiary carbons are asymmetric centers. Nevertheless, it is obvious that when considering long polymer chains, each side of the chain has virtually the same priority and the assignment of stereo-descriptor for absolute chirality (R or S) to each asymmetric carbon is of no practical interest. It is therefore more common to describe the stereochemistry of macromolecules in terms of the relative configuration of its monomers. If the two monomers within a pair of successive monomers, defined as a steric dyad, have the same relative configuration, the dyad is given the *m* stereo-descriptor (meso dyad). On the contrary, if the two monomers have the opposite relative configuration, the dyad is given the *r* stereo-descriptor (racemo dyad).

To draw the polypropylene chains according to the Fischer projection, the symbols depicted on Figure 1.1 are used.[3] Symbol a represents a monomer unit -CH_2-$CH(CH_3)$-, symbol b is a meso dyad, symbol c is a

racemo dyad and symbol d is used to describe a random configuration of the monomer.

The tacticity of polymers is defined as the relative arrangement of adjacent chiral centers in a stereo-regular macromolecule. Therefore, polypropylene chains consisting of meso dyads only are called isotactic (iPP - Figure 1.2a) whereas those containing racemo dyads only are called syndiotactic (sPP - Figure 1.2b). If the relative configuration of each monomer is totally random, the macromolecule is referred to as atactic (aPP - Figure 1.2c). Other configurations exist, which can be considered as intermediate between completely stereo-regular (i.e. isotactic or syndiotactic) and stereo-irregular (i.e. atactic). Figure 1.2d depicts the hemi-isotactic sequence (monomers alternate between isotactic and random configuration) and Figure 1.2e illustrates an atactic-isotactic stereoblock sequence.

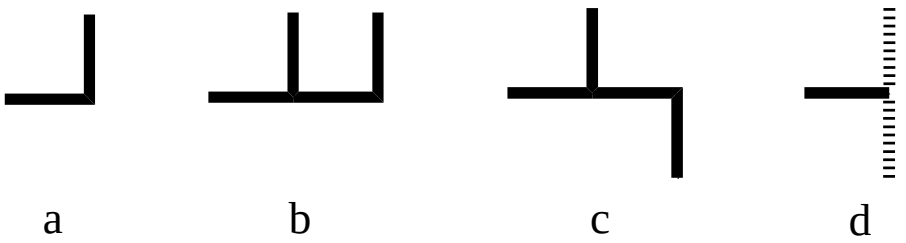

Figure 1.1 : Fischer projection for a) propylene monomer, b) meso dyad, c) racemo dyad, d) uncontrolled configuration of the monomer

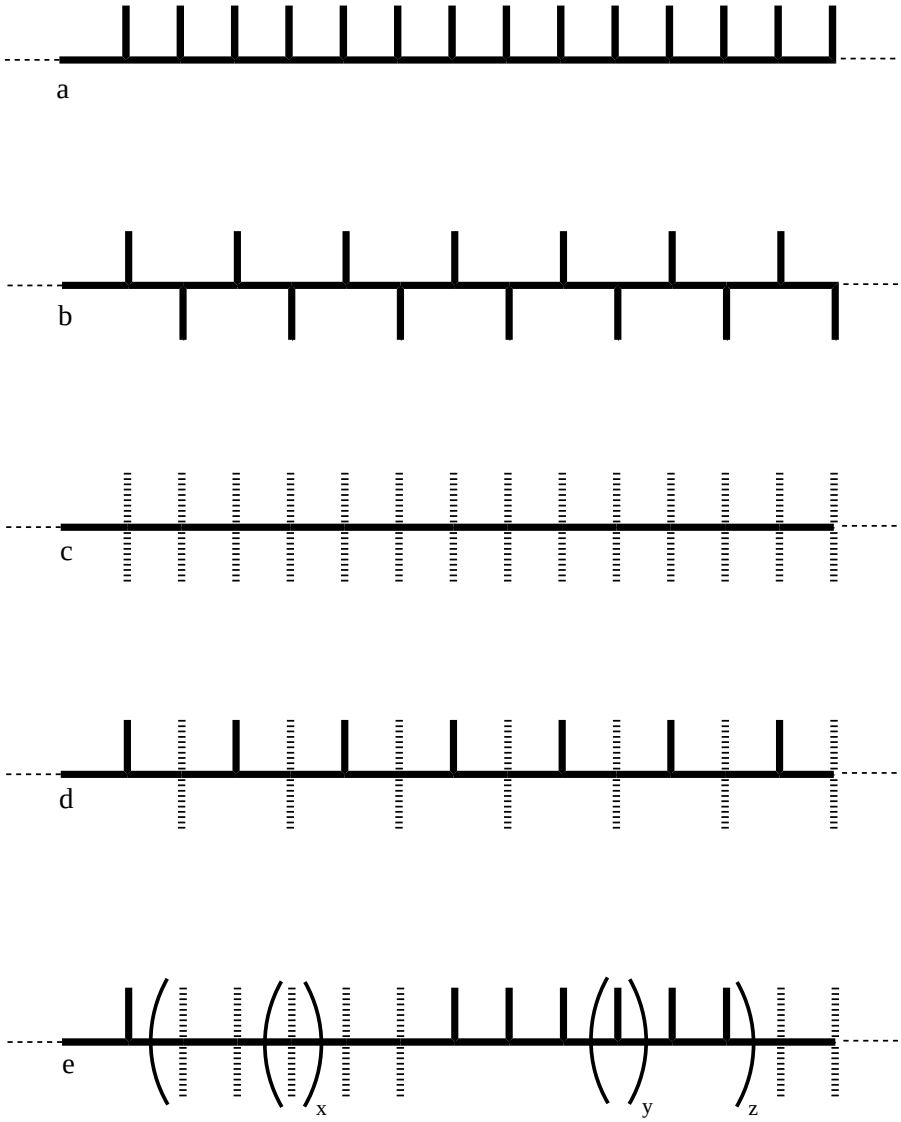

Figure 1.2 : Fischer representation for a) isotactic polypropylene, b) syndiotactic polypropylene, c) atactic polypropylene, d) hemiisotactic polypropylene, e) atactic/isotactic stereo-block polypropylene

SYNTHESIS OF POLYPROPYLENE

Polypropylene was first synthesized by Natta in 1954 using a catalytic system developed by Ziegler for the low pressure polymerization of ethylene.[4] This catalytic system consisted of $TiCl_3$ activated by $AlEt_2Cl$. The low regio- and stereo-selectivity of these early generation catalysts provided a mixture of products that could be separated in three parts : (i) an atactic polypropylene that was soluble in acetone or ether; (ii) a highly isotactic polypropylene that was not soluble in refluxing heptanes; (iii) a partially soluble isotactic-atactic polypropylene elastomer.[5,6] Even though the stereo-selectivity of this catalytic system was quite poor with respect to isotactic polypropylene, many applications quickly came out from the plastics industry for this stereo-regular polypropylene because of its interesting properties (stiffness, high melting point, chemical resistance to solvent, electrical insulation, good fatigue resistance, etc.). As a consequence, the catalytic systems were progressively modified during the next decades to improve the activity and the regio- and stereo- specificity of the polymerization process. Today, the most efficient systems are the supported catalysts [$MgCl_2/TiCl_4$/«internal» Lewis base] together with a co-catalyst consisting of $AlEt_3$ and an «external» Lewis base.[7] Such systems reach isotacticities ranging from 96% up to >99% (based on *mm* triads), making isotactic polypropylene one of the main and cheapest commodity polymer available on the market.

In 1980, Sinn and Kaminsky discovered that homogeneous metallocene catalysts could be used advantageously for the polymerization of propylene if activated with methyl aluminoxane (MAO).[8,9] Metallocene catalysts for the polymerization of olefins consist of a metal atom (mostly from group IV : Ti, Zr, Hf,) coordinated through π-electrons to two aromatic ligands in a sandwich structure (Figure 1.3). The aromatic ligands are mostly derived

from cyclopentadienyl (Cp), indenyl (Ind) or fluorenyl (Flu) structures that are sometimes connected through one or more carbon atoms (symbolized with «E» in Figure 1.3). These are called bridged or «*ansa*» metallocenes.

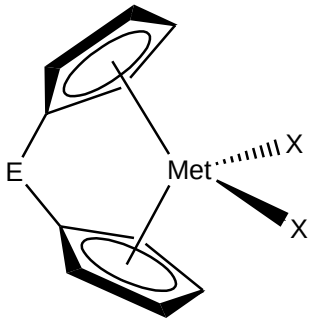

Figure 1.3 : general structure of ansa metallocene catalysts. Met = metal atom, X = halogen atom, E = bridge between the two aromatic ligands

The dichloride precursor of those metallocene catalysts must be activated by MAO that is obtained by controlled hydrolysis of trimethyl aluminium. MAO consists of linear and cyclic oligomers that are able to create cage structures containing centers of very high Lewis acidity.[10,11] The role of MAO is two-fold as it first methylates the catalyst by substitution of the chloride atoms from Cp_2ZrCl_2 , then abstracts a methyl anion to create the active catalyst as a contact ion-pair (scheme 1.1). However, this ion pair is loose enough to be separated by a substituted olefin during coordination.

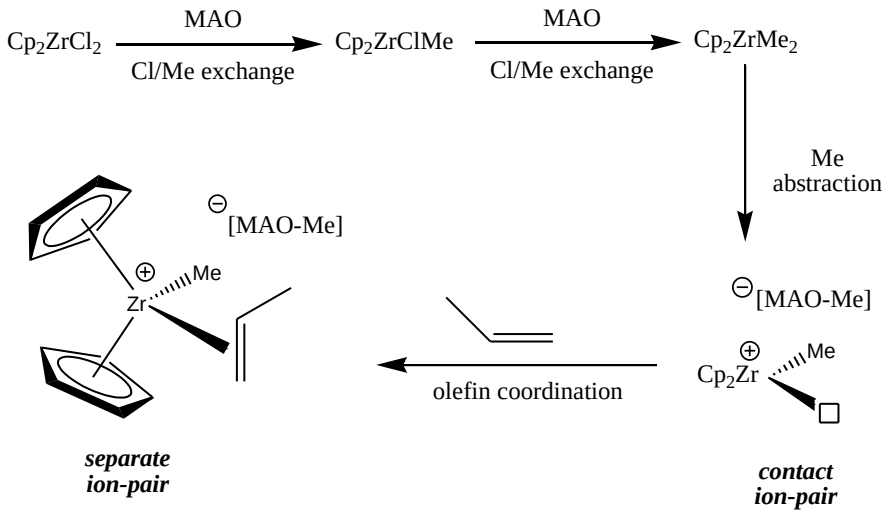

Scheme 1.1 : Mechanism of activation of metallocene

For a prochiral olefin like propylene, four coordination modes are possible, with the methyl group in position A, B, C or D (Figure 1.4). To achieve good stereo-specificity, one mode of coordination must be significantly lower in energy than the three others. The polymer chain then migrates towards the olefin while the latter creates a bond with the metal atom. The growing polymer chain thus switches back and forth from one coordination site to the other at each insertion step. Chain termination mainly occurs through β-H transfer from the growing chain to the monomer, leading to chain-end unsaturations.[12,13]

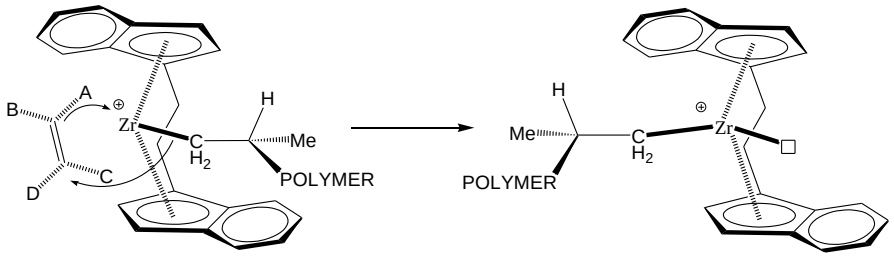

Figure 1.4 : olefin insertion in metallocene catalysts

The stereo-specificity strongly depends on the symmetry of the catalyst and the morphology of the aromatic ligands.[14] Although many exceptions exist, the following rule of thumb for ansa metallocene catalysts can be considered : complexes of C_{2v} symmetry usually produce atactic polymers. If the plane of symmetry of C_S catalyst contains the coordination sites, atactic polymer will be also produces. On the contrary, if the two coordination sites are reflected by the plane of symmetry, syndiotactic polymers will be obtained. Complexes of C_2 catalysts produce isotactic polymers. The stereo-specificity of C_1 catalysts cannot be generalized as almost any kind of tacticity can be obtained.

Two kinds of interactions were suggested to explain the stereo-specificity of metallocene catalysts (Figure 1.5) : (i) α-agostic interactions between one α-hydrogen atom and the metal atom were suggested.[15] The formation of a rigid 3-atom cycle stabilizes the transition state during the insertion step of the olefin in the metal-alkyl bond. The hydrogen atom that is involved in the α-agostic interaction in the one for which the steric hindrance between the C_α-C_β bond and the aromatic ligands is the lowest. (ii) Repulsive Van der Waals interactions between the C_α-C_β bond dominate the enantio-facial selectivity in such a way that the methyl group is located *trans* with respect to the C_α-C_β bond.[11]

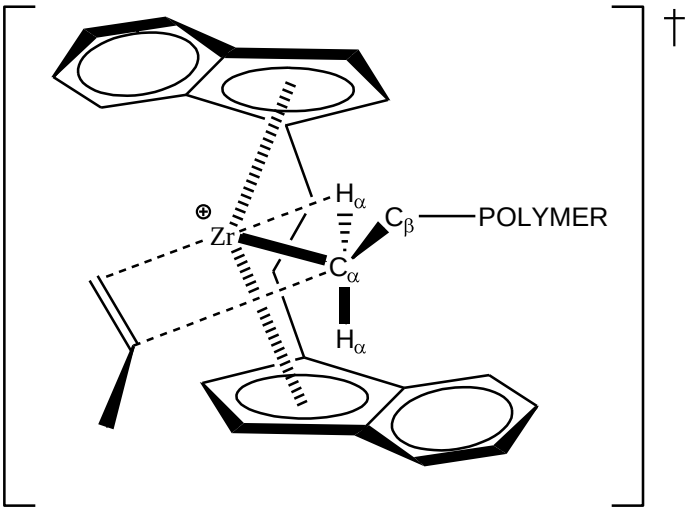

Figure 1.5 : stabilization of the transition state through α-agostic interactions and repulsive Van der Waals interactions

Metallocene catalysts offer many advantages compared to Ziegler-Natta systems.[10,11] They are soluble and have therefore much higher activities. They are single-site catalyst, i.e. there is only one family of propagating species, providing macromolecules with narrow molecular weight distribution and homogeneous co-monomer distribution in case of co-polymerization. They allow the synthesis of polypropylene of various tacticities with a very high degree of stereo-control, including polypropylene elastomers. They are also able to control the insertion of short and long chain branches in the backbone of a polyolefin (i.e. mLLDPE).

POST-SYNTHESIS MODIFICATION OF POLYPROPYLENE

Low crystallinity polypropylene

Because of their low stereo-selectivity, the early generations of Ziegler-Natta catalysts produced large amounts of low-crystallinity polypropylene

that had to be separated from the isotactic polypropylene and scraped. In the early 1970's, this by-product found a few applications in roofing membranes and hot-melt adhesives. Because of the improvement of the stereo-selectivity of the catalytic systems, this source of cheap raw material got progressively depleted, creating a real demand of low-crystallinity polypropylene. As explained here above, metallocene-based atactic or isotactic/atactic polypropylene elastomers are now available on the market but are still much too expensive for such applications.

In the late 1960's, Listner & Park issued patent applications for a reactive extrusion process that modifies the stereo-regularity of iPP by epimerization of the tertiary carbon atoms, creating a polypropylene elastomer defined as a «*sterically rearranged polymer characterized by isotactic-randiotactic blocks along the polymer chains*».[16-18] This process involves a radical initiator such as a peroxide and a molecule carrying a labile bromine atom such as N-bromosuccinimide (NBS). Another very interesting fact regarding this method is that the molecular weight of the polymer remained remarkably high in spite of the quite high concentration of peroxide involved in the extrusion process. It is indeed well-known that peroxy radicals issued from the radical initiator thermal decomposition readily abstract tertiary hydrogen atoms from polypropylene to create unstable macroradicals that quickly lead to chain scission through cleavage of the β C-C bond (Figure 1.6). This β-scission mechanism seems somehow inhibited in the presence of bromine radical.

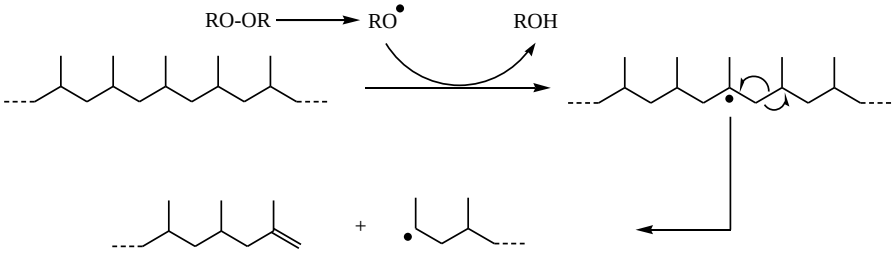

Figure 1.6 : peroxide-induced chain degradation through β-scission

Although Stehling & Knox used this process in 1975 to study the ^{1}H NMR configuration of polypropylene,[19] it has never been revisited or considered in any industrial valorization routes for iPP ever since. A few other epimerization methods involving either very high hydrogen pressure[20,21] or γ-irradiation[22] were published but are even less prone to industrialization.

Maleic anhydride grafted polypropylene

Because of its aliphatic structure, polypropylene is totally hydrophobic and offers no chemical reactivity towards other materials. This is a drawback in terms of adhesion to polar substrate (e.g. in adhesives or in composites with clay or glass) and miscibility with polar polymers (e.g in blends with polyamide). To overcome this issue, the polarity and reactivity of polypropylene is often increased by melt grafting of polar molecules such as maleic anhydride (MA) and its derivatives onto the aliphatic backbone through reactive extrusion.[23,24] Here again, peroxide-induced chain scission always compete with the grafting of maleic anhydride and a compromise must always be found between the degree of functionalization and the molecular weight. Besides, as different kinds of macroradicals are created, the position of the grafted molecules cannot be controlled. In-chain (prior to chain scission) and end-chain (after chain scission) grafting may occur. The

fate of the grafted moieties is also ambiguous as many termination reactions are possible such as radical transfer by hydrogen abstraction, homopolymerization, coupling with another macroradical, termination with degradation products of the radical initiator, etc. Several structures for the grafted moieties have been suggested and may co-exist within the material.[25,26]

1.3 Context of the thesis

As explained throughout the previous paragraphs, polypropylene is a key polymer in the world of plastics. The very high stereoregularity of iPP and its lack of reactivity are limitations for several applications for which polypropylene would be appreciated. The post-synthesis modification of polypropylene physico-chemical properties by reactive extrusion offers a way to overcome these drawbacks but still needs optimization to control the molecular weight, the tacticity/crystallinity and the polarity/reactivity through the number of grafted entities as well as their chemical structure and position onto the polypropylene backbone.

In this project, we propose to take a closer look at Listner & Park's epimerization process and adapt it to the grafting of maleic anhydride. The idea is to simultaneously reduce the crystallinity of polypropylene while enhancing its polarity/reactivity. If the molecular weights are preserved during the extrusion, as previously observed by Listner & Park, it should be possible to deliver a range of innovative polypropylene-based materials with controlled crystallinity and polarity, in a single extrusion step. The feasibility of this process was demonstrated earlier in a patent application filled by Flat & Lambla[27] (as well as a Ph.D. thesis[28]) who used bromomaleic anhydride in the grafting process. Although they observed a decrease in crystallinity (and isotacticity) and some level of retention in the molecular weight, the grafts

structure could not be controlled (succinic and bromosuccinic anhydrides were reported) and the grafting level remained quite low (<2%). The system iPP/peroxide/NBS/MA was also reported. However, Flat did not use the same range of peroxide/brominated molecule concentrations as recommended in Listner & Park's patent and there are still lots of room for improvement.

Our approach to keep optimizing this grafting process is to clearly understand the underlying chemical mechanisms responsible for the epimerization of polypropylene and for the retention of the molecular weight. In order to do so, this epimerization reaction will be studied on polymer and on a low molecular weight propylene oligomer. The model compound that was chosen is 2,4,6,8,10-pentamethylundecane (PMU), a linear five-unit oligomer that is the shorter polypropylene model whose stereoisomers are able to simulate the different tacticities of the polymer (Figure 1.7). This model compound is not available on the market and needs to be synthesized.

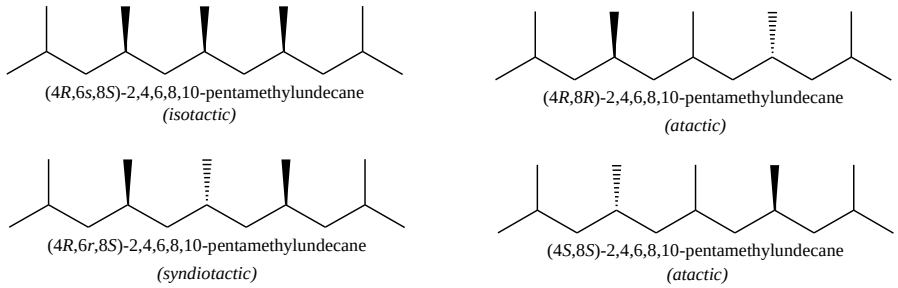

Figure 1.7 : The four stereoisomers of 2,4,6,8,10-pentamethylundecane.

Also, it would be interesting to find non-brominated mediators that would provide the same control on tacticity and molecular weight to preclude to toxicity and corrosion issue related to the use of brominated derivatives. As the reversible coupling of bromine radicals with

polypropylene macroradicals was suggested earlier,[28] a few mediators borrowed from the field of controlled radical polymerization techniques were considered for the grafting process instead of NBS.

This thesis was carried out in the continuity of a previous project called *AM-PP*,[29] funded by the Région Wallonne. The main results from this work were published as a Ph.D. Thesis.[30] The most important outcomes were a clear establishment of the tacticity of the modified polypropylene processed in the presence of a peroxide and NBS and the relationship between the reduction in crystallinity and the modification of the stereo-regularity of the starting iPP. A practical small-scale synthesis route towards PMU was also established and a first insight into the chromatographic separation of the PMU diastereoisomers was also presented but still required significant improvement.

1.4 Objectives of the thesis

The finality of this project is the synthesis of a range of polypropylene-based materials with tailored physico-chemical properties through the fine tuning of the crystallinity and polarity of the backbone while preserving the molecular weight. This implies the understanding of the underlying chemical mechanisms via the model compound. As a consequence, the following specific achievements must be fulfilled in this work :

- The synthesis and complete characterization of a highly-grafted PP-g-MA elastomer obtained in the presence of NBS. The characterization must clearly state the number, position and structure of the grafted moieties. Tacticity and crystallinity must also be clearly elucidated.
- To evaluate whether or not NBS is able to mediate the grafting of maleic anhydride on other polyolefins such as HDPE.

Ethylene-based polymers quickly react with peroxides to create branched/crosslinked chain architectures. This side reaction competes with PE functionalization and produce high molecular weight materials with severe lack of flowability/processability. Although NBS was efficient to hamper the negative effect of peroxides on PP, it might not necessarily be transposable to PE as the reactivity of the many tertiary carbons of PP largely differs from the reactivity of the secondary carbons of PE.

- The evaluation of several potential substitutes for NBS as grafting mediators. Despite the high efficiency of NBS in the grafting reaction, it has several drawbacks that preclude its intensive use in reactive extrusions, e.g. toxicity and corrosivity. As radical stabilization through reversible coupling between bromine radicals and PP tertiary macroadicals was suggested to explain the inhibition of PP degradation in the presence of NBS, other molecules known for their ability to react reversibly with macroradicals were investigated. The idea was to evaluate how common transfer agents, such as those utilized in controlled/living polymerization techniques (i.e. INIFERTERS, RAFT and NMP transfer agents), behave in the extreme conditions of reactive processing.
- The establishment of a high-yield synthesis of 2,4,6,8,10-pentamethylundecane that can be easily performed at gram-scale. A small-scale synthesis of PMU was elaborated by Gaëtan Henry during his doctoral thesis.[30] This route was amended to allow a larger production of PMU precursor, namely 6-hydroxymethyl-2,4,8,10-tetramethylundecane, whose stereoisomers would be further separated by preparative chromatography.

- The separation of the stereoisomers of at least one of the key precursor of PMU by preparative chromatography. This also implies that PMU models must be efficiently recovered without altering their stereochemistry.
- The use of the model compounds to elucidate the mechanism of tacticity/grafting enhancement reactions with NBS or other mediators.

1.5 Structure of the manuscript

The results from our investigations are thoroughly discussed throughout the following chapters. Chapter two is devoted to the reactive processing of isotactic polypropylene in the presence of N-bromosuccinimide and is divided into three sections. The first section explains how NBS altered isotactic polypropylene micro-structure and turned it into an isotactic-atactic stereoblock elastomer. The effect of NBS on the grafting of maleic anhydride on iPP is discussed in the second section of chapter two. The third section compares the grafting of maleic anhydride onto polypropylene and high-density polyethylene in order to see whether or not NBS is also able to preclude crosslinking of polyethylene when in the presence of a radical initiator.

Chapter three explores the possibility to substitute N-bromosuccinimide with bromine-free mediators in the grafting reaction of maleic anhydride onto iPP.

Chapter four is divided into three parts. The first part deals with the large scale synthesis of PMU, the second parts with and the chromatographic separation of the diastereoisomers and the third part gives the first insight of the epimerization reaction onto the model compounds.

Chapter five describes three side-projects for which the new materials or the skills developed during this thesis could be valorized through collaborations with inter-university/international projects. The first part explains how the grafted polypropylene elastomers could be neutralized to obtain ionomers. The second project describes how Raman spectroscopy could be use on the PMU models to explore the molecular structure. The third one is related to the use of rheology to probe the molecular structure of polyethylene of different chain architecture and detect low amounts of long-chain branching.

General conclusions are drawn in chapter six and further projects based on the findings described in this work are introduced.

1.6 References

[1] Numbers from "Plastics - The facts 2011". Annual report of PlasticsEurope. Available online at www.plasticseurope.org.

[2] Numbers from Belgium, a powerhouse of the plastics and rubber industry. General Assembly report of Federplast.be. Available online at www.federplast.be.

[3] Busico, V.; Cipullo, R. *Prog. Polym. Sci*. **2001**, 26, 443-533.

[4] Natta, G.; Pino, P. et al. *J. Am. Chem. Soc.* **1955**, 77, 1708-1710.

[5] Natta, G. *J. Polym. Sci.* **1959**, 34, 531-549.

[6] Natta, G.; Mazzanti, G. et al. *Chim. Ind (Milan).* **1957**, 39, 275-283.

[7] Mülhaupt, R. Ziegler-Natta catalysis and propylene polymerization. In *Polypropylene: An A-Z Reference;* Kluwer Academic Publishers: Dordrecht, The Netherlands, 1999; pp 896-920.

[8] Sinn, H.; Kaminsky, W. *Adv. Organomet. Chem.* **1980**, 18, 99-149.

[9] Sinn, H.; Kaminsky, W. et al. *Angew. Chem., Int. Ed. Engl.* **1980**, 19, 390-392.

[10] Alt, H. G.; Köppl, A. *Chem. Rev.* **2000,** 100, 1205-1221.

[11] Brintzinger, H. H.; Fisher, F.; et al. *Angew. Chem. Int. Ed. Engl.* **1995,** 34, 1143-1170.

[12] Stehling, U.; Diebold, J.; et al. *Organometallics* **1994**, 13, 964-970.

[13] Busico, V.; Cipullo, R.; et al. *Makromol. Chem. Rapid Commun.* **1993**, 14, 97-103.

[14] Coates, G. W. *Chem. Rev.* **2000,** 100, 1223-1252.

[15] Leclerc, M.; Brintzinger, H. H. *J. Am. Chem. Soc*. **1995**, 117, 1651-1652.

[16] Listner, G. J.; Park, K. FR 1 567 883, **1969**.

[17] Listner, G. J.; Park, K. US 3,511,824, **1970**.

[18] Listner, G. J.; Park, K. US 3,515,687, **1970**.

[19] Stehling, F. C.; Knox, J. R. *Macromolecules* **1975,** 8, 595-603.

[20] Suter, U. W.; Neuenschwander, P. *Macromolecules* **1981,** 14, 528-532.

[21] Suter, U. W.; Pucci, S.; Pino, P. *J. Am. Chem. Soc.* **1975,** 97, 1018-1023.

[22] Busfield, W. K.; Hanna, J. V. A. *Plym. J.***1991**, 23, 1253-1263

[23] Rzayev, Z. M.O. *I.RE.CH.E*. **2011**, 3, 153-215.

[24] Moad, G. *Prog. Polym. Sci.* **1999**, 24, 81-142.

[25] De Roover, B.; Sclavons, M.; et al. *J. Polym. Sci., Part A: Polym. Chem.* **1995**, 33, 829-842.

[26] Heinen, W.; Rosenmoeller, C. H.; et al. *Macromolecules* **1996**, 29, 1151-1157.

[27] Flat, J. J.; Lambla, , M. EP0,534,830, **1992**.

[28] Flat, J.J. Ph.D. Thesis, Université Louis Pasteur, Strasbourg, Septembre **1991**.

[29] Convention AM-PP 001/4519.

[30] Henry, G. Ph.D. Thesis, Université catholique de Louvain, Louvain-la-Neuve, Avril 2006.

Chapter Two

Reactive Extrusion of Polyolefins in the Presence of N-bromosuccinimide

Chapter two is devoted to the exhaustive investigation of the reactive extrusion of iPP in the presence of N-bromosuccinimide. This chapter consists of three consecutive parts.

Part one describes how NBS affected iPP crystallinity through different kinds of calorimetric measurements to explain the elastomeric behavior of the modified materials. High temperature NMR was used to take a closer look at chain microstructure and it was found that the stereo-regularity of the starting iPP was greatly altered. These modified polypropylenes had microstructures similar to isotactic-atactic stereoblock elastomers. Chain morphology was also investigated through size-exclusion chromatography and melt-state rheometry. It appeared that even though large amounts of peroxides were used, the molecular weights were somehow preserved and chains remained mainly linear. Attempts to turn the starting iPP into a completely atactic polypropylene through multiple extrusion steps failed but a cross-linked polypropylene elastomer was recovered instead. This first section makes the transition between the AM-PP project with Gaëtan Henry's doctoral thesis and the current project. It also states the current knowledge and skills of the team at the time. For this section, I performed the reactive extrusions, GPC, DSC/SSA and rheological measurements during a Master Degree preceding this Ph.D. thesis and under the sponsorship of Gaëtan Henry. Gaëtan recorded the NMR spectra and gathered and discussed all the results in his own Ph.D. thesis. I was also in charge of writing and submitting the paper on the basis of Gaetan Henry's Ph.D. Thesis.

Part two relates how NBS could be advantageously utilized in the melt-grafting of maleic anhydride onto iPP to provide a range of heavily-grafted PP elastomers. Complete characterization of the modified materials revealed that the presence of NBS could prevent excessive molecular weight

degradation and, more interestingly, could improve the graft content while controlling the grafts structure. It appeared that the great majority of the grafted moieties were located all along the PP chains (and not exclusively at chain ends) and consisted of saturated succinic rings (as evidenced by FTIR spectroscopy). The isotactic-atactic stereoblock elastomer microstructure was also observed on those materials. For this section, I preformed the reactive extrusions, acide-base titrations, viscosimetric titration, GPC and DSC measurements and recorded the FTIR spectra. Gaëtan Henry recorded the NMR spectra. I was also in charge of writing and submitting the paper.

Part three investigates whether or not NBS is able to mediate the grafting of maleic anhydride on high density polyethylene. Infrared spectra of PP-g-MA and PE-g-MA were put side by side to compare the structure of the grafted entities. The grafting mechanisms are discussed with respect to both polyolefins. Those results were presented as an oral communication during the 5th international meeting of the Polymer Processing Society held in Goa, India. I was fully in charge of this part of the thesis and performed all the reactive extrusions and characterizations. However, Dimitri Rousseaux performed many reactive extrusions on HDPE during a Master Degree performed under my own sponsorship. None of those results are presented here but his work helped selecting the starting materials and characterization methods (MFI measurements).

2.1 Controlled reduction of polypropylene isotacticity and crystallinity by epimerization during reactive processing

Gaëtan R. P. Henry[1,2], Xavier Drooghaag[2], Mikaël Vandeuren[1], Michel Sclavons[1], André Schanck[3], Jacques Devaux[1], Véronique Carlier[1], Jacqueline Marchand-Brynaert.[2]

Published as J.Polym.Sci, Part A : Polym. Chem. ***2009****, 47, 4505-4518*

[1]Université catholique de Louvain, Unité de Physique et de Chimie des Hauts Polymères, Place Croix du Sud, 1, B-1348 Louvain-la-Neuve, Belgium

[2]Université catholique de Louvain, Unité de Chimie Organique et Médicinale, Place L. Pasteur, 1, B-1348 Louvain-la-Neuve, Belgium

[3]Université catholique de Louvain, Unité de Chimie Structurale et des Mécanismes Réactionnels, Place L. Pasteur, 1, B-1348 Louvain-la-Neuve, Belgium

Abstract

Amorphous and low crystallinity polypropylenes were produced by reactive processing of commercial isotactic polypropylenes in the presence of a peroxide (2,5-dimethyl-2,5-di(*tert*-butylperoxy)hexane) and N-bromosuccinimide. Characterization of the modified polypropylene microstructures using ^{13}C NMR spectroscopy revealed that crystallinity loss is correlated with the epimerization of numerous methynes randomly along the polymer backbone, leading to decreasing isotacticities ([*mmmm*]) and average isotactic block lengths. Moreover, degradation usually induced by peroxide was shown to be comparatively limited in additional presence of N-

bromosuccinimide. This fast and easy process therefore allows the production of polypropylene plastomers and elastomers with controlled and homogeneous crystallinities and isotacticities, and relatively low molecular weight distributions.

2.1.1 Introduction

In the early times of heterogeneous Ziegler-Natta catalysis, polypropylene (PP) was obtained by Natta and his group as a heterogeneous mixture of prevailingly isotactic (iPP), atactic (aPP) and elastomeric (ELPP or isotactic/atactic stereoblock) polypropylenes;[1-7] Natta showed that these fractions of various tacticities and crystallinities could be segregated by sequential extractions using solvents of increasing boiling points.[4,8-10] Because of the many appreciable properties of the semi-crystalline iPP (thermoplasticity, rigidity, thermal and chemical stabilities, electrical resistance, low density, etc), the stereospecificity of the heterogeneous Ziegler-Natta catalytic systems was progressively improved, thus reducing the amounts of amorphous and elastomeric by-products. Nowadays, most commercial polypropylenes are highly isotactic (and regioregular), making of iPP one of the most widely used commodity polymers.

On the other hand, amorphous and elastomeric polypropylenes exhibit interesting properties for applications such as bitumens, (hot-melt) adhesives, water-proofing membranes, elastomeric objects, etc. More specially, stereoblock ELPP's are of great commercial interest because of their "thermoplastic elastomeric" behaviour:[11] these polymers are soluble and can be reversibly melted and solidified (unlike the chemically cross-linked materials), which is advantageous to processability and recyclability.

As a consequence, the selective synthesis of low crystallinity PP's, especially those exhibiting isotactic/atactic stereoblock microstructures, has been the object of intensive researches since their discovery by Natta. Before the late 1970's, and besides the successive extractions of conventional PP's as firstly described by Natta,[9] the production of ELPP's has been shown possible, for example, by polymerization using particular Ziegler-Natta catalytic systems[12] and by sequential polymerization processes,[13] but not in practical and efficient ways (low catalyst productivity, low content in elastomeric material, etc).

In 1978, the high-yield synthesis of significant amounts of ELPP has been achieved by Collette, Tullock *et al.* at Du Pont,[14-21] using alumina supported tetraalkyl zirconium and titanium as catalysts. However, this process yields heterogeneous products (containing fractions of various degrees of isotacticities and molecular weights), with a relatively limited control over the isotacticity extent.

In the late 1970's again, advances in homogeneous Ziegler-Natta catalysis led to the development of methyl aluminoxane (MAO) activated group IV metallocene catalysts, for the polymerization of propene (and higher olefins).[22,23] Stereoselectivity in homogeneous polypropylene synthesis was achieved a few years later independently by Ewen[24] and by Kaminsky & Brintzinger[25] using chiral bridged (*ansa*) metallocenes; nowadays, this catalysts family makes possible the synthesis of polypropylenes with very diversified and well-controlled microstructures.[26-31]

The first homogeneous polymerization of propene into thermoplastic elastomeric polypropylene was reported by Chien *et al* in 1990 using a chiral (C_1-symmetric) *ansa* titanocene;[32-37] a related class of C_1-symmetric *ansa*

metallocenes was also developed by Collins *et al*, leading to similar types of products[38-40] (in both cases, ELPP's with low isotacticities, low melting points and narrow molecular weight distributions (MWD) can be obtained but with variable M_w and catalyst activities). However, the detailed microstructural analyses made in these studies do not give unambiguous evidence of an isotactic/atactic stereoblock microstructure : it is then thought that, if blocks are present in such polymers, these should be relatively short.[28] More recently, Rieger *et al* designed several bridged, asymmetric indenyl-fluorenyl zirconocene complexes,[41-43] which enabled the authors to tailor the properties of polypropylene from semicrystalline thermoplastic to thermoplastic elastomeric, with moderate to high molecular weights; the control of both isotacticity (20 % ≤ [*mmmm*] ≤ 80 %) and crystallinity (50 °C ≤ T_m ≤ 134 °C) arises in most cases from the strong dependence of stereoerrors formation with respect to monomer concentration and polymerization temperature.[42,43] Subsequent studies from the same research group led to the development of related indenyl-fluorenyl metallocene complexes with various substitution patterns, for the synthesis of (ultra)high molecular weight polypropylene elastomers and plastomers.[44-47]

Aside from C_1-symmetric *ansa* metallocenes, some unbridged conformationnally dynamic ("oscillating") metallocenes, and more especially those derived from 2-arylindene metallocenes initially developped by Waymouth & Coates, have been reported to produce isotactic-atactic stereoblock ELPP's.[48-51] The origin of the alternating stereoselectivities has been firstly explained to arise from interconversion between stereoselective (*rac*-like) and nonstereoselective (*meso*-like) conformations of the catalysts during propagation,[49] although other research groups recently suggested the hypothesis of a reversible conformational "locking" of the *rac*-like species by counteranion association.[52,53] Although this class of metallocenes yields a broad range of polypropylene microstructures (from elastomers to high-

melting thermoplastics), it is rather difficult to predict the stereoselectivity of one particular catalytic system, because of its sensitivity to the polymerization conditions (temperature, pressure, monomer concentration) and to the nature of the ligands, transition metal and cocatalyst.[54,55] Moreover, ELPP's produced by these 2-arylindene catalysts are more heterogeneous than those made from C_1-symmetric *ansa* metallocenes, as indicated by fractionation experiments, NMR characterization and thermal analysis (distribution of isotacticities, isotactic block lengths and molecular weights).[50,55]

More recently, Eisen *et al* developed a dynamic MAO-activated titanium complex, which alternates between octahedral (stereoselective) and tetrahedral (nonstereoselective) configurations, resulting in isotactic/atactic stereoblock ELPP's.[56] However, this catalyst offers a poor control over isotacticity and block lengths, and yields polymers with a MWD increasing linearly with polymerization time.

The synthesis of discrete, multiblock, isotactic/atactic stereoblock ELPP was finally achieved very recently by Sita *et al*, using a programmable stereomodulated living Ziegler-Natta catalytic system.[57]

This non exhaustive review of synthetic methods proves the interest of making elastomeric PP with tailored microstructures and properties. Nevertheless, catalyzed polymerization is not the only way towards elastomeric and amorphous PP’s: the latter can also be obtained from stereoregular PP by epimerization of its tertiary carbon atoms. It is worth mentioning that the term "epimerization" refers here to a succession of epimerization reactions along the PP backbone, leading to a randomization of the relative configuration of the methyne groups. For instance, Prosser discovered a method to convert crystallizable stereoregular PP into

amorphous atactic PP by epimerization in the presence of a hydrogenation catalyst (e.g. Raney nickel or cobalt, powdered platinum or palladium, etc) at high temperatures (250 to 350 °C) and pressures (> 35 bars, preferably hydrogen) for several hours.[58] Although the same process was later used by Suter *et al* for epimerization studies of propylene oligomers and polymers,[59,60] it is not economically viable for the production of low crystallinity PP's, due to the severe reaction conditions and the use of solvent and high concentration of catalyst.

Another method was reported by Listner & Park in the late 1960's in a series of patents,[61-63] which is based on epimerization of non stabilized stereoregular PP in the presence of an organic peroxide and a brominated additive (e.g. tris-(2,3-dibromopropyl)phosphate) in the melt (e.g. by reactive extrusion). Peroxides are usually utilized to create PP macroradicals, leading either to degradation by β-scission (useful for the control of PP average molecular weight and polydispersity) or to grafting of additives (useful for functionalization of PP). However, the presence of a brominated additive in the aforementioned method seems to hamper the β-scission reaction, while no (or very low) grafting of bromine (or brominated additive) is observed. As a matter of fact, the combination of a peroxide with a brominated additive leads to a decrease of isotacticity, crystallinity and tensile strength, a slight decrease of the average molecular weight, and to an increase of elasticity and solubility in diethyl ether (the extent of modification depending on the reagents proportions). Although the microstructural study of PP, especially by NMR spectroscopy, was technically limited at that time, Listner & Park described the obtained polymers as "(…) *sterically rearranged isotactic-randiotactic polymers characterized by blocks of isotactic polymer and blocks of randiotactic polymer along the polymer chain* (…)". Even if this method has been later used by Stehling & Knox in order to study the stereochemical configuration

of PP by ^{1}H NMR,[64] no work has been devoted ever since to develop this epimerization process, or to understand its underlying chemical mechanisms. More recently, the transformation of an isotacic PP into an amorphous or elastomeric product was also observed by Flat & Lambla, upon extrusion in the presence of a peroxide and a brominated additive (e.g. N-bromosuccinimide, 2- or 3-bromoacrylic acid, or bromomaleic anhydride).[65,66] However, Flat & Lambla did not proceed to an extensive study of this reaction, and did not correlate their results with Listner & Park's patents.

In this context, and taking into account the potential commercial interest of producing cheap low crystallinity PP from semicrystalline PP wastes, it was decided to perform a more comprehensive study of the reactive processing of iPP in the presence of peroxide and brominated additive. Indeed, a more detailed analysis of the microstructural modifications induced in the polymer is required for a better understanding of the underlying chemical mechanisms. This study should lead to a better control of the properties of the modified polymer while making this process as reliable as catalyzed polymerization techniques but much more convenient and much less expensive. High temperature ^{13}C NMR and successive self-nucleation/annealing (SSA) were used as they are the most convenient tools to establish the correlations between the tacticity and the crystallinity of the modified polymers obtained by such a random process.

2.1.2 Experimental Section

Reagents selection

In this work, the selected brominated additive was N-bromosuccinimide (NBS), as the latter decomposes at extrusion temperatures (thermal decomposition at about 180°C), meaning that each NBS molecule would

give rise to one active bromine, and that no succinimidyl radical would graft onto the PP backbone (as confirmed by Flat[65]). According to Listner & Park, a more pronounced crystallinity loss is obtained if the production of bromine radicals occurs as the decomposition rate of the peroxide is the highest.[61-63] It was thus decided to chose a peroxide which exhibits a half-life time of less than 1 minute at 180 °C, but also a good solubility in molten PP (aliphatic peroxides rather than aromatic), a low volatility at the reaction temperatures (bis-peroxides rather than single peroxides), and which yields free radical species able to abstract efficiently hydrogen atoms from alkyl chains (e.g. *tert*-butoxy radicals). Taking all these requirements into account, 2,5-dimethyl-2,5-di-(*tert*-butylperoxy)hexane (DHBP) was selected as free radical initiator.

Materials

Isotactic polypropylene homopolymer HF500N from Basell has been used as the starting material. Two commercial formulations, one solid and one liquid, of 2,5-dimethyl-2,5-di-(*tert*-butylperoxy)hexane (DHBP) were used: Luperox® 101XL45 (45-48 wt% DHBP supported on $SiO_2/CaCO_3$) was purchased from *Arkema*, and Trigonox 101® (liquid DHBP, purity >92 %) from *Akzo Nobel*. N-bromosuccinimide (NBS), from *Acros* (99 % purity), was used as received.

Reactive extrusion (single step)

The required amounts of polypropylene, peroxide and NBS were thoroughly dry-mixed before reaction. Batch compositions are summarized in Table 2.1. The acronym ccPP stands for controlled-crystallinity polypropylene.

Table 2.1 : Composition of each controlled-crystallinity polypropylene

	wt.% DHBP [a]	*wt.% $Ox^{\bullet}$*	*wt.% NBS*	*wt.% $Br^{\bullet}$*	*$Br^{\bullet}/Ox^{\bullet}$*
iPP	-	-	-	-	-
ccPP-1	0.009	0.001	0.033	0.015	16.6 ± 0.2
ccPP-2	0.046	0.005	0.167	0.075	
ccPP-3	0.091	0.009	0.334	0.150	
ccPP-4	0.181	0.018	0.668	0.300	

[a] Luperox® 101XL45

The "Br/Ox" ratio is defined as the ratio between the maximum weight percentage of active bromine radicals and the maximum weight percentage of active oxygen-based radicals that can be produced during the reaction. The "active bromine radical" term is defined as the portion of the total bromine content of a brominated compound that can be released at the processing temperature. The "active oxygen-based radical" term is defined as the portion of the total oxygen content of the free radical initiator that shall react at the processing temperature to abstract a hydrogen radical to the molten PP.

The reactive extrusions of the mixtures were performed using a Brabender single screw extruder. The screw speed was set at 25 rpm which corresponds to a residence time of about 90 seconds. Successive extrusion steps were performed on a Shaw single screw extruder. The screw speed was set to 30 rpm which corresponds to a residence time of about 60 seconds. The barrels of both extruders comprise three independent heating zones set at 220-240-260 °C respectively. The extruded polymers were quenched in cold water, and pelletized.

Multiple reactive extrusion

The production of multi-extruded samples was carried out as follows : A 600 g sample of ccPP-4 was ground and poured into the extruder in the presence of Trigonox 101 and NBS. This material will be further referred to as ccPP-4/2x. A 300 g sample of ccPP-4/2x was re-processed in the same way to provide ccPP-4/3x. Five extrusion steps were also performed using ccPP-1 as the starting material. The compositions of the multi-extruded ccPP-4 samples and multi-extruded ccPP-1 samples are given in Tables 2.2 and 2.3 respectively. The given peroxide and NBS contents are cumulated concentrations.

Table 2.2 : Compositions of multi-extruded ccPP-4

	wt.% DHBP [a]	*wt.% Ox•*	*wt.% NBS*	*wt.% Br•*	*Br•/Ox•*
ccPP-4/2x	0.315	0.064	2.33	1.05	16.5
ccPP-4/3x	0.542	0.11	4.00	1.80	

[a] : Trigonox 101

Table 2.3 : Compositions of multi-extruded ccPP-1

	wt.% DHBP [a]	*wt.% Ox•*	*wt.% NBS*	*wt.% Br•*	*Br•/Ox•*
ccPP-1/2x	0.010	0.002	0.067	0.030	16.6
ccPP-1/3x	0.015	0.003	0.100	0.045	
ccPP-1/4x	0.020	0.004	0.134	0.060	
ccPP-1/5x	0.025	0.005	0.167	0.075	

[a] : Trigonox 101

Differential scanning calorimetry (DSC) and successive self nucleation/annealing (SSA).

DSC analyses were performed using a *Mettler Toledo* DSC821e, equipped with a liquid nitrogen cooling system. Experiments were performed in 20 µL aluminum hermetic pans. The temperature program consisted of a first heating run from -20 °C to 200 °C followed by a crystallization run from 200 °C to -20 °C and finished by a second heating run to 200 °C. Each heating/cooling rate was 3 °C/min. Melting temperatures and enthalpies of melting (ΔHm) were extracted from the second heating run.

SSA experiments were performed on a *Perkin Elmer* DSC 7 with 40 µL aluminium pans. A first heating run to 200 °C was used to erase the thermal history of each sample. The temperature was then decreased to 30 °C. A series of heating/cooling cycles was then performed. Cycles were composed of a one minute isotherm at 30 °C followed by a heating run at 10 °C/min to an annealing temperature T_a. This temperature was held constant for one hour and was then decreased to 30 °C at a rate of 10 °C/min. Another cycle then started. These successive annealing cycles were performed for T_a ranging from 170 °C to 30 °C with steps of 5 °C. The so-annealed samples were finally cooled at a rate of 10 °C/min to -10 °C and heated at the same rate to 210 °C in order to observe the melting temperatures of the formed crystalline lamellaes. Relative crystallinity losses are expressed with respect to the enthalpy of melting of the starting isotactic polypropylene according to the following relationship:

$$\text{Crystalinity Loss (\%)} = 100 \times (\Delta Hm_{iPP} - \Delta Hm_{ccPP}) / \Delta Hm_{iPP} \qquad (2.1)$$

Nuclear magnetic resonance

Prior to NMR analysis, a sample of about 1 g of ccPP has been purified by dissolution into refluxing toluene followed by precipitation into cold acetone. High temperature solution state NMR experiments were performed on a *Brüker* 500MHz AVANCE operating at 500.13 MHz for ^{1}H (125.76 MHz for ^{13}C), equipped with a 10 mm SeX-$^{13}C/^{1}H$ high temperature probe linked to a thermoregulator unit. The spectra were acquired and processed using the software XWIN-NMR. Either d_2-tetrachloroethane (d_2-TCE) was used as a solvent as well as an internal reference ($\delta[^{1}H]$ = 6.0 ppm and δ $[^{13}C]$ = 73.7 ppm), or a mixture of 1,2,4-trichlorobenzene/d_6-DMSO 75:25 v/v. Before analysis, a sample of polymer (about 100 mg) was dissolved in the appropriate solvent (2.5 mL) at 135 °C under argon atmosphere in a 10 mm *Wilmad* NMR tube. For ^{13}C NMR analysis (under total ^{1}H decoupling), a relaxation time of 15 seconds was selected and 6000 transients were recorded, in order to obtain a semi-quantitative spectrum with a good signal-to-noise ratio

Gel Permeation Chromatography (GPC)

Molecular weights were determined by high temperature size exclusion chromatography. Measurements were performed on a *Waters Alliance* GPCV 2000 equipped with two Styragel HT 6E and one Styragel HT 2 columns along with a differential refractometer and a viscometer. The mobile phase was 1,2,4-trichlorobenzene (TCB). The concentration of the sample was 2 mg/mL in TCB and dissolution was achieved by shaking at 160 °C for 1 h. Injection volume was 215 µL. Temperature was held constant at 145 °C throughout the analysis. The system was calibrated prior to the analysis with PS standards according to ISO 16014-2 specification.

Rheological investigations

Rheological experiments have been carried out on a *Ares* rheometer equipped with 25 mm plate-plate geometries. Elastic and viscous moduli (*G'* and *G''*, respectively) and complex viscosity (η^*) were recorded from 100 to 0.1 rad.s^{-1}. The temperature was set at 200 °C. The applied strain was 10 % and remained in the linear visco-elastic region. Samples were compression-molded in a 2 mm thick disc at 200 °C prior to analysis.

2.1.3 Results

GPC measurements

Table 2.4 gathers the number-, weight-, and z-average molecular weights (*Mn*, *Mw* and *Mz*, respectively) as well as polydispersities (*PDI*) of iPP and each ccPP.

Table 2.4 : Average molecular weights as obtained by GPC measurements

	Mn (kDa)	*Mw (kDa)*	*Mz (kDa)*	*PDI*
iPP	56.1	337	1704	6.0
ccPP-1	49.0	210	704	4.3
ccPP-2	50.6	222	780	4.4
ccPP-3	41.5	155	434	3.7
ccPP-4	27.5	77	155	2,8

Taking into account the considerably large amounts of peroxide introduced in the reactive mixtures, it appears that although the unavoidable PP degradation still occurs, molecular weights remain remarkably high. *PDI's* are systematically lower than that of iPP as a consequence of peroxide-induced degradation.

Thermal behavior

The thermal behavior of all the ccPP's has been evaluated by DSC and SSA measurements. The most interesting feature of the SSA mode is the slow step by step crystallization process that enables the formation of crystalline lamellae whose thicknesses and stabilities are dependent on the lengths of the isotactic sequences. Figure 2.1 shows the final heating run of the SSA experiment performed on the starting iPP.

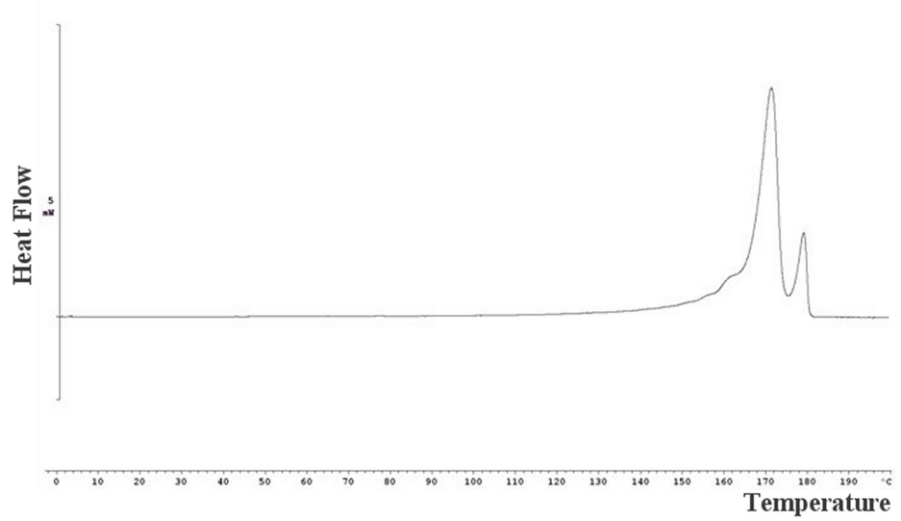

Figure 2.1 : Final heating run of SSA experiment performed on iPP

Two main melting peaks can be observed at 170 and 175 °C, revealing the presence of large crystalline lamellas as the result of the great stereo-regularity of iPP. The shoulders at lower temperatures are due to the presence of shorter chains (quite large molecular weight distribution) or chains with a few stereo-errors. Figure 2.2 shows an overlay of the final heating runs of all the SSA experiments.

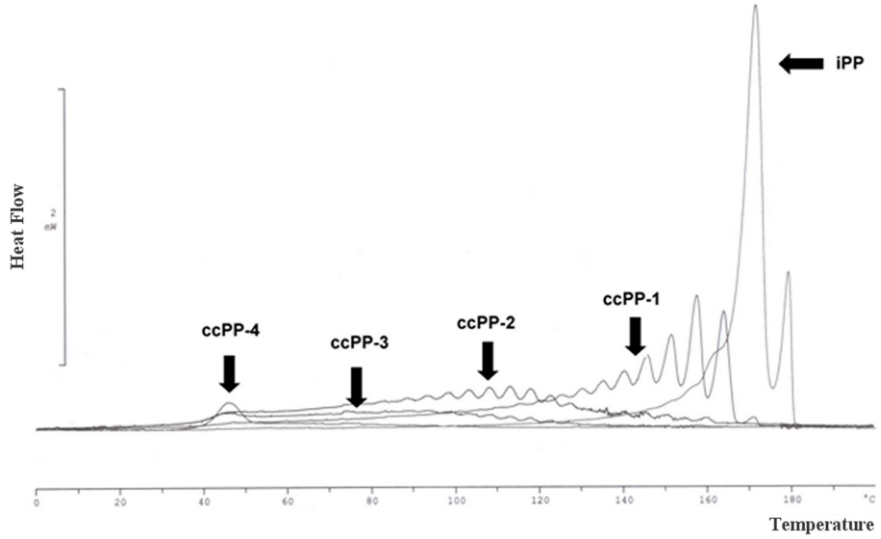

Figure 2.2 : Overlay of the SSA final heating runs of iPP and ccPP-1 to 4

Contrastingly, when NBS is present in the reactive medium, broader distributions of weaker melting peaks are observed at lower temperatures, reflecting smaller lamellar thicknesses and suggesting shorter isotactic sequence lengths.[55] Such broad distributions of melting peaks cannot be related to broad molecular weight distributions as they narrow with increasing amounts of peroxide and NBS (*vide supra – gel permeation chromatography section*). The intense melting peak of iPP at 170 °C has totally disappeared in the other samples. These have therefore been modified homogeneously and it is assumed that no chain remains unaltered (i.e. fully isotactic) after reactive processing. Besides, enthalpies of melting, obtained by integrating the area under each curve, allow the calculation of the crystallinity reduction that occurred in each ccPP. Enthalpies of melting obtained from DSC and SSA and the calculated crystallinity losses (%CL) are summarized in Table 2.5.

Table 2.5 : Melting enthalpies and crystallinity losses obtained for each ccPP according to DSC and SSA data

	ΔH_m DSC (J/g)	%CL DSC	ΔH_m SSA (J/g)	%CL SSA
iPP	111	_	142	_
ccPP-1	97	13	130	8
ccPP-2	68	39	82	42
ccPP-3	49	56	61	57
ccPP-4	11	90	14	90

SSA measurements reveal higher melting enthalpies as the long annealing periods induce a more complete crystallization. The calculated crystallinity losses remain however quite similar to those obtained from the common DSC experiments. Figure 2.3 shows a log-log plot of the crystallinity reduction measured by SSA as a function of the concentration of active oxygen in the reactive medium.

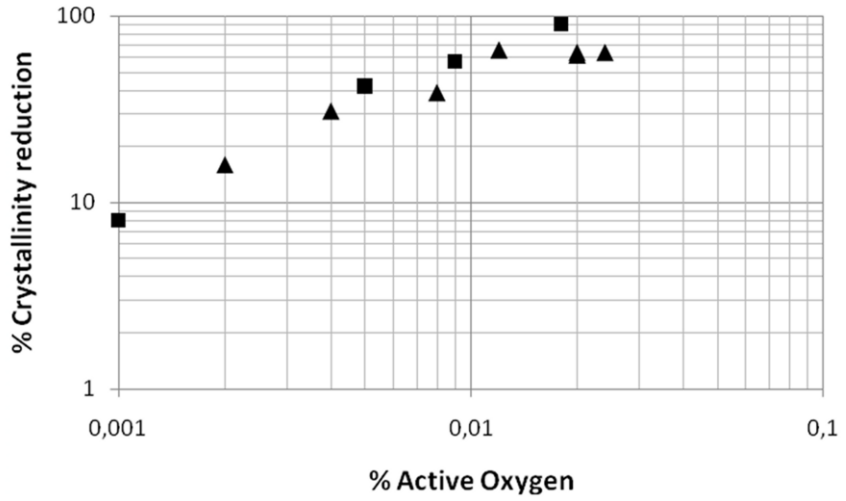

Figure 2.3 : Log-Log plot of crystallinity reduction as a function of the concentration in active oxygen. Triangles refer to Listner's data;[61-63] squares refer to this work

In such a plot, a somewhat linear relationship is observed. These results are well correlated with those previously obtained by Listner et al. for active oxygen concentrations up to 0.01%.[61-63] The crystallinity reductions deduced from Listner's data seem to level off below 70% for concentrations beyond 0.01% of active oxygen, whereas linearity up to 90% has been achieved in the present work. A more linear relationship is therefore obtained within the investigated range of peroxide concentrations.

NMR investigations - Microsctructure elucidation

^{13}C NMR spectroscopy was used for investigating the microstructure of these low crystallinity polypropylenes in order to elucidate the origin of the crystallinity reduction observed by thermal analysis. The methyl groups region of the ^{13}C NMR spectra was used to examine the tacticity of each sample as their chemical shifts are the most sensitive toward the chain configurations. Figure 2.4 illustrates the nine signals arising from the ten different methyl pentads of atactic polypropylene.[55]

It is of primary importance to be able to quantify the percentage of isotactic pentads [*mmmm*] because it is closely correlated to several macroscopic properties, including crystallinity.

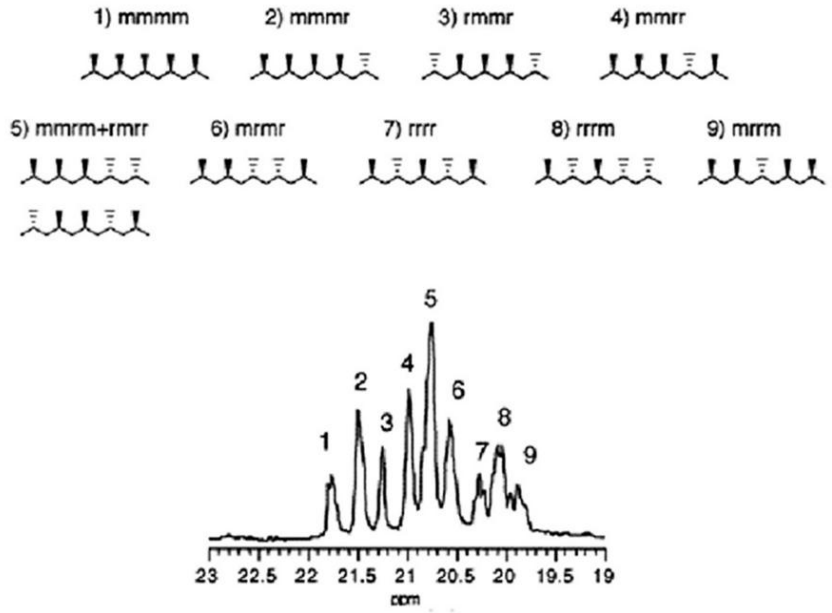

Figure 2.4 : ^{13}C NMR signals arising from the ten methyl pentads of atactic polypropylene. Adapted from Lin and Waymouth.[55]

This can be done by integrating all nine signals on the spectrum and applying the following relationship:

$$\mathbf{[}\boldsymbol{mmmm}\mathbf{]} = I^{\mathbf{mmmm}} / \Sigma\, I^{\mathbf{xxxx}} \quad (2.2)$$

Where I^{mmmm} is the intensity of the [*mmmm*] pentad signal and ΣI^{xxxx} , the sum of the intensities of the signals arising from all pentads, thus including [*mmmm*]. Enlargements of the methyl groups region of the ^{13}C NMR spectra of the starting iPP and ccPP-1 to 4 are presented on Figures 2.5 to 2.9 respectively.

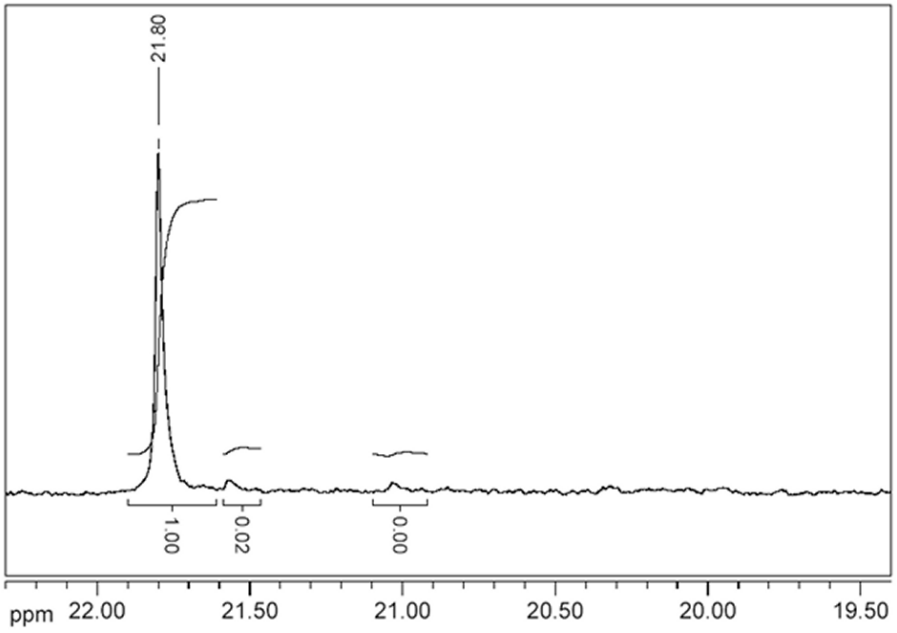

Figure 2.5 : Methyl region of the ^{13}C NMR spectrum of iPP recorded in TCB/*d6*-DMSO 75:25 [v/v] at 135°C

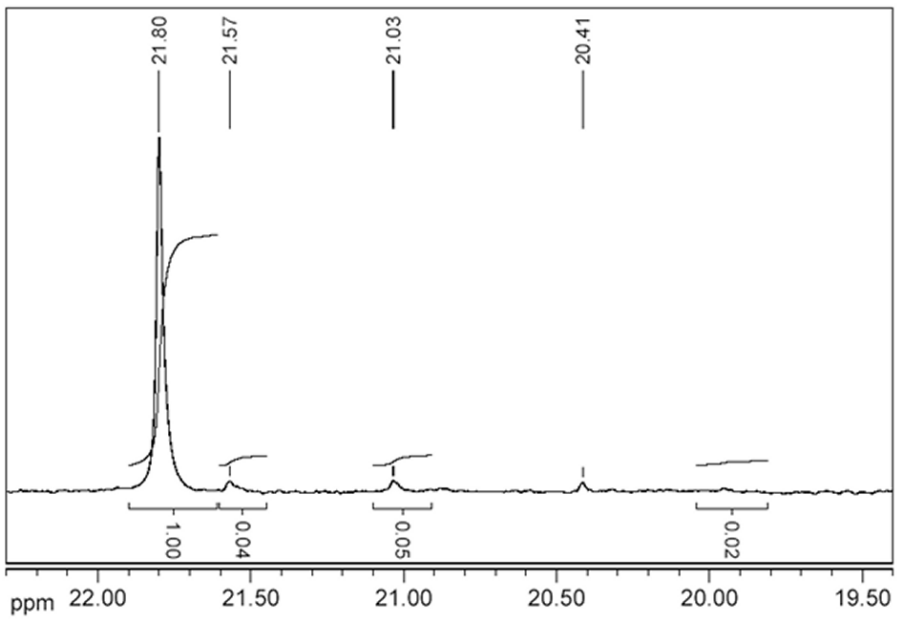

Figure 2.6 : Methyl region of the ^{13}C NMR spectrum of ccPP-1 recorded in TCB/*d6*-DMSO 75:25 [v/v] at 135°C

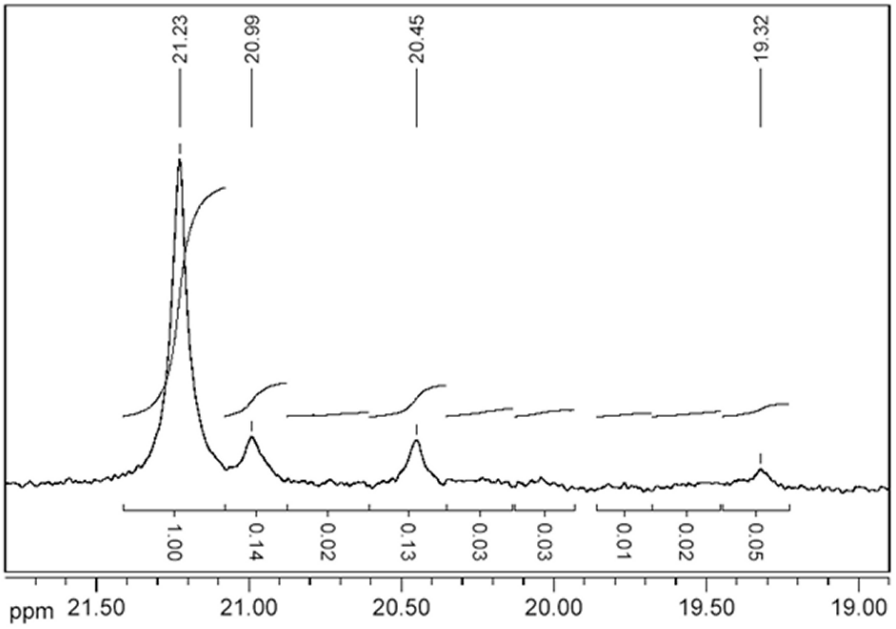

Figure 2.7: Methyl region of the ^{13}C NMR spectrum of ccPP-2 recorded in *d2*-TCE at 135°C

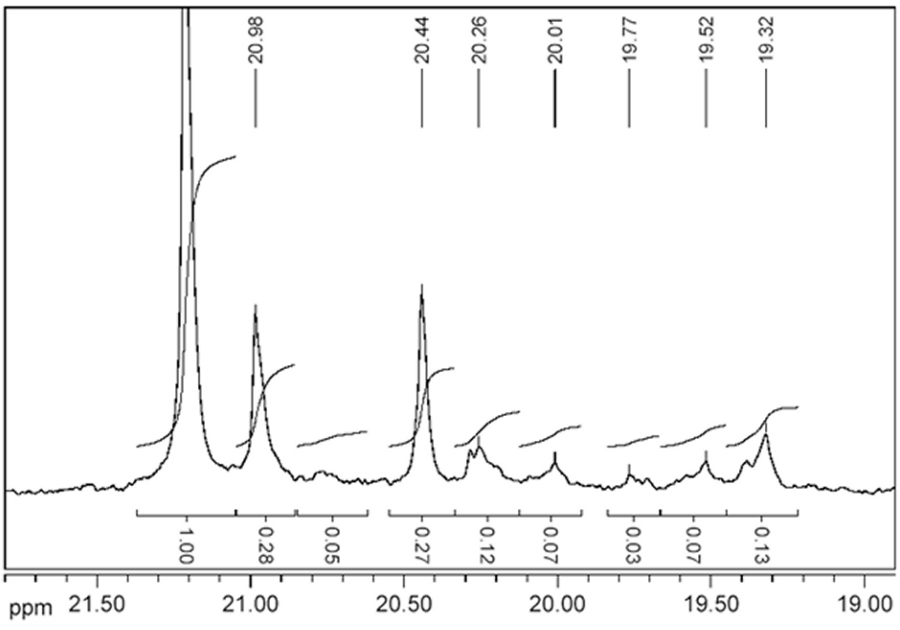

Figure 2.8 : Methyl region of the ^{13}C NMR spectrum of ccPP-3 recorded in *d2*-TCE at 135°C

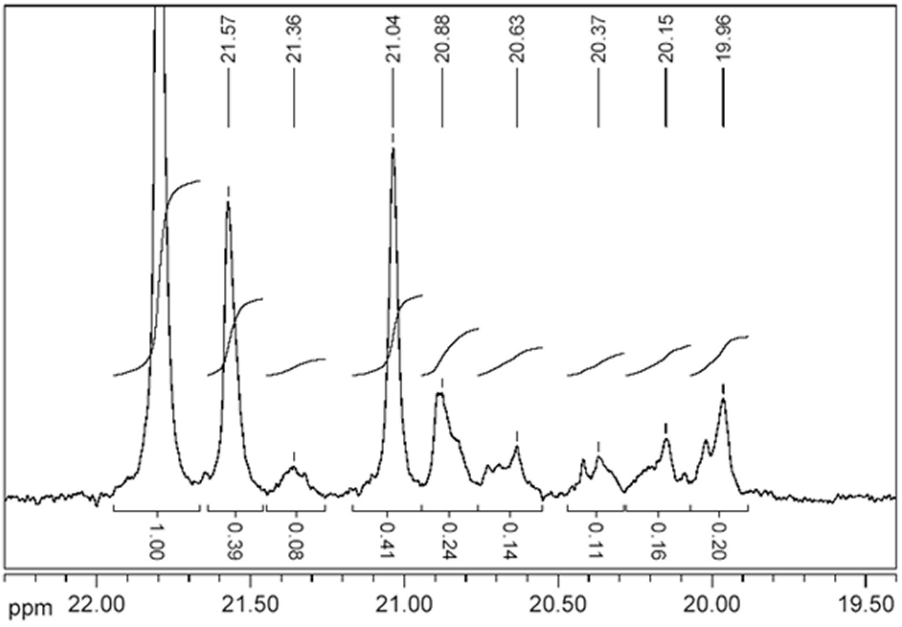

Figure 2.9 : Methyl region of the ^{13}C NMR spectrum of ccPP-4 recorded in TCB/*d6*-DMSO 75:25 [v/v] at 135°C

Table 2.6 summarizes the integrations of each pentad that can be found in each ccPP. The triads contents of each material has been calculated according to several mathematical equations derived from basic statistical considerations.[67,68] As can be seen in Figures 2.5 to 2.9, aside from the intense [*mmmm*] signal, iPP, ccPP-1 and ccPP-2 mainly exhibit signals arising from the [*mmmr*], [*mmrr*] and [*mrrm*] pentads. This means that for active oxygen concentrations below 0.005%, the inversions of configuration are mostly isolated along the PP backbone (at least 4 monomer units apart). These signals also remain highly intense in ccPP-3 and 4. All ccPPs, including ccPP-4 which is almost totally amorphous, exhibit the [*mmmm*] signal as the most intense peak of the spectrum. The structure of the amorphous ccPP-4 thus largely differs from an atactic polypropylene, whose [*mmmm*] signal represents about 6%. The spectrum of ccPP-4 appears very

similar to that of, for instance, an ELPP with alternating isotactic/atactic stereo-sequences synthesized using metallocene catalysis.[55]

On the basis of the integrations of the [*mmmm*] and [*mmmr*] signals, the average length of the isotactic sequences containing at least four monomers can be calculated using the following relationships :[15,39]

$$n\ (\geq 4) = 2[mmmr] + [mmmm] \quad (2.3)$$

$$b\ (\geq 4) = [mmmr] / 2 \quad (2.4)$$

$$N\ (\geq 4) = n\ (\geq 4) / b\ (\geq 4) = 4 + 2[mmmm] / [mmmr] \quad (2.5)$$

where n (≥4) is the fraction of the monomers belonging to the isotactic blocks whose lengths are ≥ 4 monomer units; b (≥4) is the fraction of the isotactic blocks whose lengths are ≥ 4; and N (≥4) is the average length of the isotactic blocks which contain at least 4 monomer units. N typically ranges from 23 to 104 for iPP.[15] Table 2.7 summarizes the crystallinity losses, the remaining isotacticities and N (≥4) values of each ccPP.

Table 2.6 : Pentads and triads contents of iPP and ccPPs

	Pentads									*Triads*		
	mmmm	*mmmr*	*rmmr*	*mmrr*	*mmrm + rmrr*	*mrmr*	*rrrr*	*rrrm*	*mrrm*	*mm*	*mr*	*rr*
iPP	1	0.02	-	-	-	-	-	-	-	1.02	0.02	-
ccPP-1	1	0.04	-	0.05	-	-	-	-	0.02	1.04	0.04	0.02
ccPP-2	1	0.14	0.02	0.13	0.03	0.03	0.01	0.02	0.05	1.16	0.23	0.08
ccPP-3	1	0.28	0.05	0.27	0.12	0.07	0.03	0.07	0.13	1.33	0.51	0.23
ccPP-4	1	0.39	0.08	0.41	0.24	0.14	0.11	0.16	0.20	1.47	0.81	0.47

Table 2.7 : Crystallinity losses, residual isotacticities and N(≥4) values for iPP and ccPPs

	%CL	*[mmmm] (%)*	*N (≥4)*
iPP	0	98	104
ccPP-1	10.5	90	54
ccPP-2	40.5	70	18
ccPP-3	56.5	49	11
ccPP-4	90	37	9

The average length of the atactic sequences cannot be precisely calculated but are assumed to be rather short with respect to the isotactic sequences. Furthermore, Busico *et al*. reported that the junctions between isotactic and atactic blocks in ELPPs can be evidenced by ^{13}C NMR spectroscopy.[69] Two heptads, one at the lowest field extremity of the [*mmrm*]+[*rmrr*] pentads region and one at the highest field extremity of the [*mrmr*] pentad region are peculiar to a stereoblock structure and preclude the hypothesis of a mixture of isotactic and atactic chains. According to figure 2.10 related to ccPP-4, and despite a rather poor resolution, one can verify that these heptads (indicated with small marks) are present in significant amounts in ccPP-4.

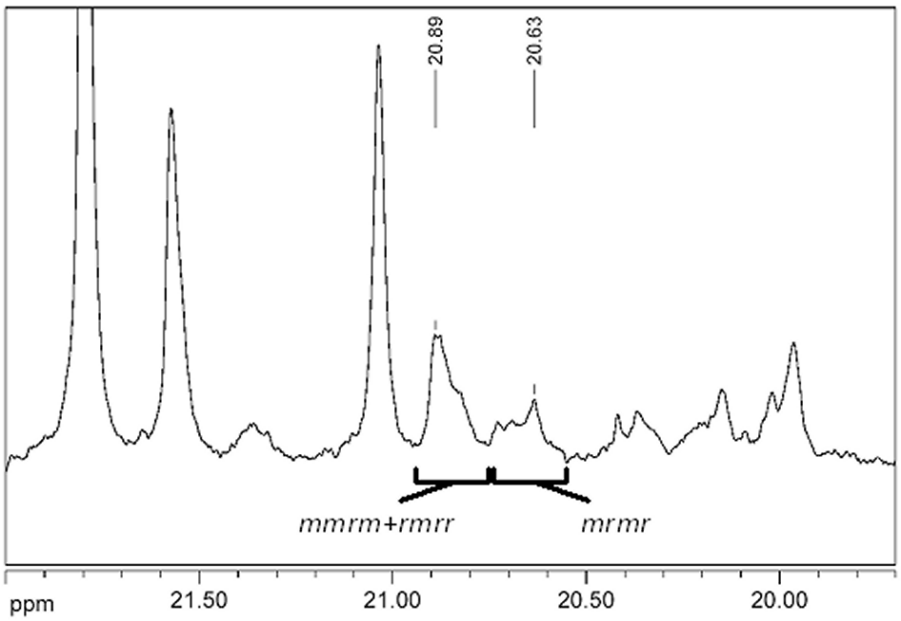

Figure 2.10 : Methyl region of ccPP-4. The peaks indicated by small marks are peculiar to isotactic/atactic junctions

Finally, as already mentioned in the thermal analysis section (*vide supra*), each ccPP is assumed to be homogeneously altered during reactive processing. This hypothesis was confirmed since no pure atactic fraction could be recovered, even after a 60 h extraction of ccPP-4 with *o*-xylene at room temperature.

All these observations support the *in-situ* formation of a homogeneous isotactic/atactic stereoblock structure for ccPP-1 to 4.

Tacticity-crystallinity correlation

Properties related to PP crystallinity such as crystallization/melting temperatures and enthalpies are directly dependent on the isotacticity level. As shown in Figure 2.11, many ELPP homopolymers obey the following empiric relationship:[29,70]

$$[mmmm] \approx 0.6 \times T_m \qquad (2.6)$$

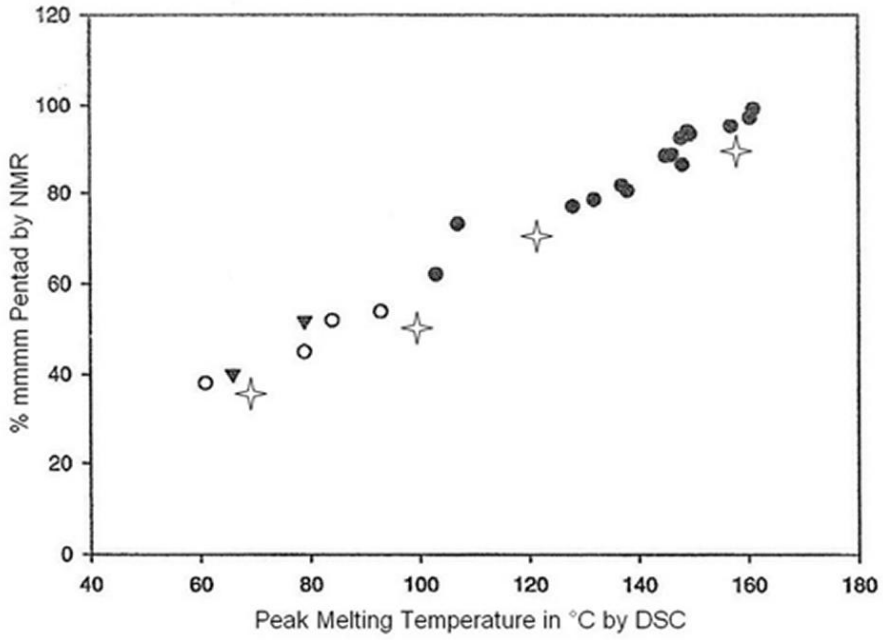

Figure 2.11 : Correlation between isotacticity and melting temperature. Empty and filled circles as well as triangles are original data from Gauthier.[70] Stars are ccPP1 to 4 from this work.

ccPPs-1 to 4 are in good agreement with equation (2.6). However, Burfield et al. have defined a calorimetric index for a more accurate determination of PP isotacticity, regardless of stereo-errors distribution, molecular weights and possible sample fractionation.[71] The best correlation

is obtained with isotactic triads [*mm*] and melting/crystallization enthalpies, as follows:

$$\log (\Delta H) = \log k + n/3 \times \log [mm] \qquad (2.7)$$

where k is a constant value; n is the critical length of the sequences that can crystallize and [*mm*] is the percentage of isotactic triads. This relationship has been validated for polypropylenes whose crystallinity ranges from 35 to 100%. Figure 2.12 shows how ccPP-1 to 4 obey equation (2.7). Both [*mmmm*] and [*mm*] were used as isotacticity factors.

Although ccPPs-1 to 3 are in good agreement with equation (2.7), a significant deviation is observed for ccPP-4. This deviation can be understood in terms of length and distribution of the isotactic sequences because they are the critical parameters that determine the amount of crystalline phase in ELPPs and hence their elastomeric feature.[19,72-74] The minimum length of the isotactic blocks must be at least 11-20 units to be able to crystallize.[15,18,69,72-75] Figure 2.13 plots the relative crystallinity (with respect to iPP) of iPP and of ccPPs-1 to 4 as a function of $N\ (\geq 4)$ as determined by equation (2.5).

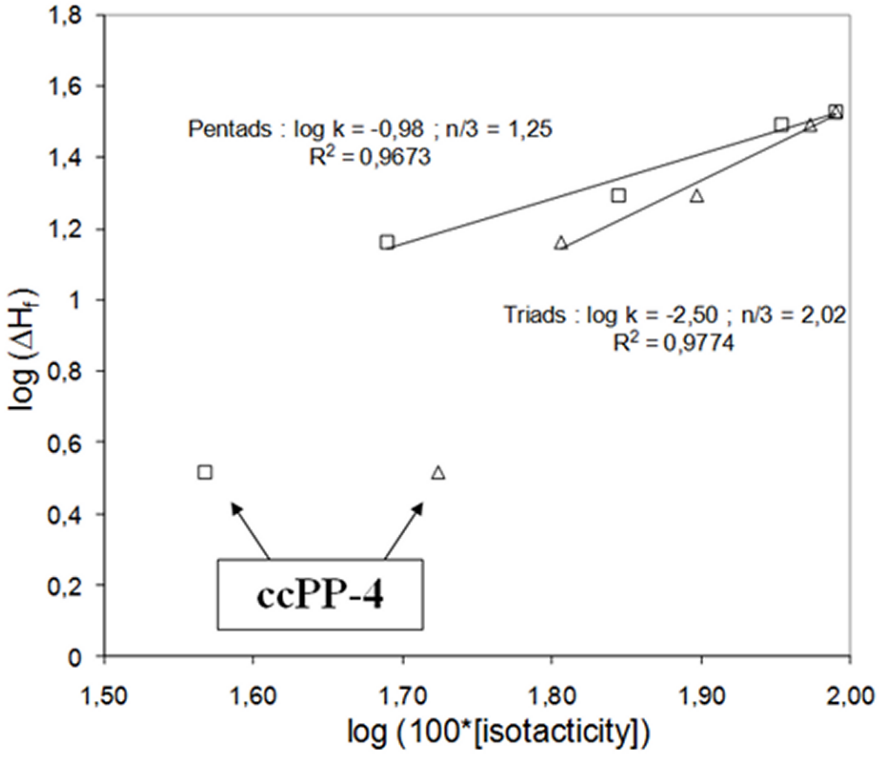

Figure 2.12 : Correlation between melting enthalpies and isotacticities for ccPP1 to 4. Triangles refer to triads and squares refer to pentads.

It can be seen that the crystallinity decreases drastically for values of N (≥ 4) lower than 20. As the length of the isotactic blocks decreases, they become too short to crystallize and hence deviate from equation (2.7).

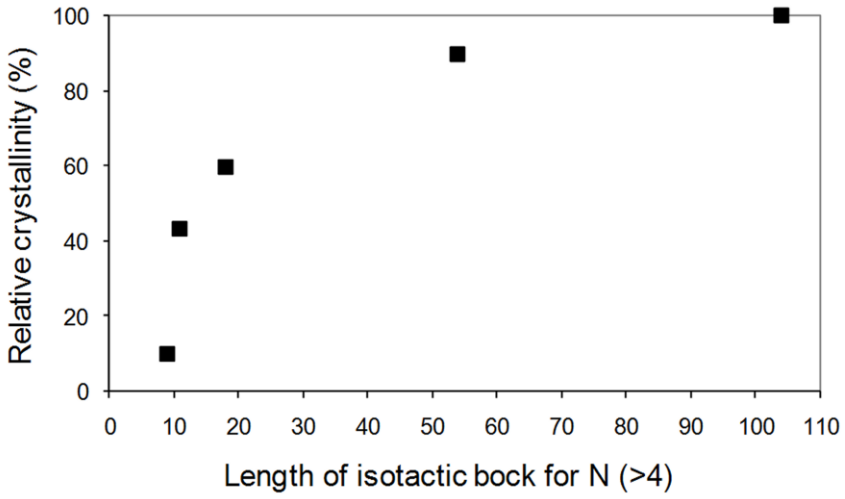

Figure 2.13 : Relative crystallinity of iPP and ccPP1 to 4 as a function of the average isotactic block lengths.

Successive extrusion steps.

As discussed above, the residual isotacticity of ccPP-4, which is yet almost totally amorphous, remains of about 37% (Table 2.7). The direct transformation of iPP into aPP was evaluated by successive extrusion steps. These materials have also been analyzed by ^{13}C NMR and the residual isotacticities as well as $N(\geq 4)$ values and crystallinity losses are reported in Table 2.8. The two additional extrusion steps could not significantly decrease the remaining isotacticties of ccPP-4/2x and 3x despite the considerable amount of peroxide and NBS introduced. This means that either the radical species are consumed by a side-reaction or the epimerization process is inhibited. Such multiple extrusion steps have also been performed with lower amounts of peroxide and NBS, starting from ccPP-1. Five successive extrusion steps have been performed. Results are also gathered in Table 2.8.

Table 2.8 : residual isotacticities, average block lengths and crystallinity losses for multi-extruded ccPPs

	[mmmm] (%)	*N (≥4)*	*% CL*
iPP	98	104	0
ccPP-4	37	8	> 90
ccPP-4/2x	31	8	> 90
ccPP-4/3x	33	8	> 90
ccPP-1	90	54	4
ccPP-1/2x	89	44	9
ccPP-1/3x	88	37	14
ccPP-1/4x	n.d	n.d	18
ccPP-1/5x	88	37	17

Once again, the isotacticity hardly decreases upon reprocessing. Although ccPP-1/5x contains as much peroxide and NBS as ccPP-2, the [*mmmm*] levels off at 88% with respect to the 70% calculated for ccPP-2. This clearly demonstrates an inhibition of the epimerization upon successive re-processing.

It is well established that halogen radicals damage extruder parts as they can abstract hydrogen atoms from the polymer to create the corresponding acid (i.e. the formation of hydrochloric acid during reactive processing of PVC). Comparatively, bromine radicals can abstract hydrogen from the PP backbone to create bromohydric acid. The corrosive action of HBr is suspected to be responsible for damaging the extruder screw with subsequent liberation of iron in the reactive medium. Elemental analysis revealed the presence of relatively large concentrations of iron in all ccPPs, up to 1700 ppm. Iron salts are known to accelerate peroxides decomposition and therefore should have a negative impact on the epimerization process

efficiency. Sealed glass tubes have been used to conduct the epimerization process in the absence of any metallic contaminants and again, no [*mmmm*] lower than 28 % could be obtained. This inhibition of the epimerization process and the limited solubility of multi-extruded ccPPs in NMR and GPC solvents let us suggest the formation of long chain branches within these materials as a side reaction. Rheological experiments have been performed to elucidate their macroscopic structure.

Rheological investigations

The rheological behavior of a polymer can be used to investigate its molecular architecture. Linear polymers are known to exhibit several peculiar properties. For instance, the loss modulus G" and the storage modulus G' decrease in the low shear rate region of a log-log plot with a slope of 1 and 2 respectively while the complex viscosity η^* tends to a plateau. In this plateau, the viscosity reaches a constant value called the Newtonian or zero-shear viscosity, η_o. For linear polymers of relatively high molecular weights, η_o is dependent on M_w according to the relationship[76]

$$\eta_o = K. M_w^{\alpha} \qquad (2.8)$$

where K is a constant value dependent on the polymer type and temperature. α lies between 3.4 and 3.6. Any deviation from those rheological properties can be due to a modification of the polymer architecture (i.e. type of branching) or molecular weight distribution and it is often very difficult to discriminate between those parameters to explain the deviation.

In his patents, Listner described that the sterically rearranged polymers obtained in the presence of bromine radicals were substantially linear.[61-63] Figures 2.14 to 2.16 show the frequency sweep tests for ccPP-4, ccPP-4/2x and ccPP-4/3x respectively.

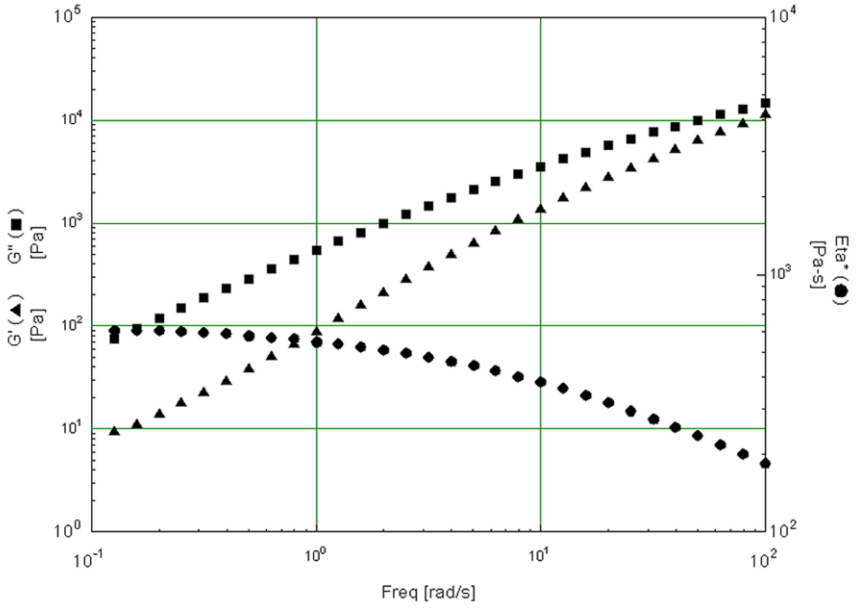

Figure 2.14 : Evolution of the storage modulus (triangles), loss modulus (squares) and complex viscosity (circles) as a function of the frequency for ccPP-4

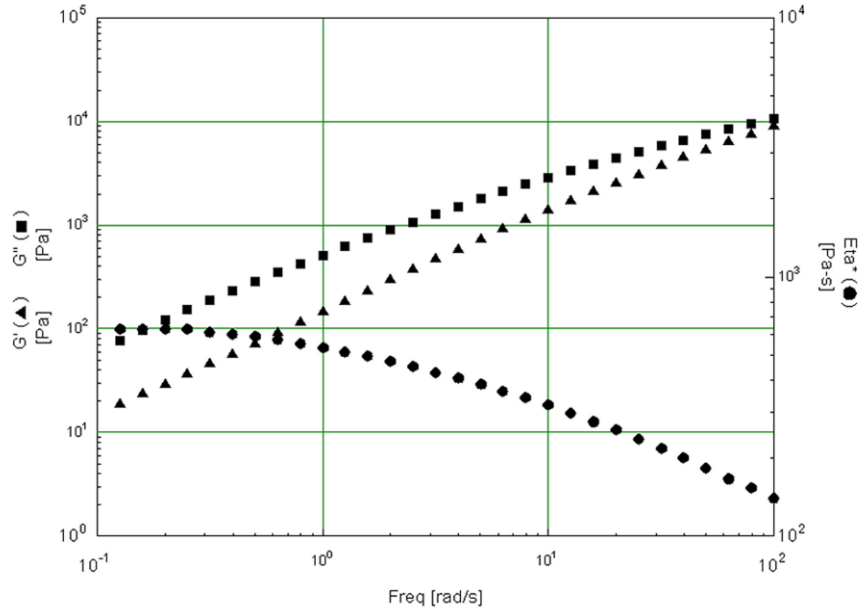

Figure 2.15 : Evolution of the storage modulus (triangles), loss modulus (squares) and complex viscosity (circles) as a function of the frequency for ccPP-4/2x

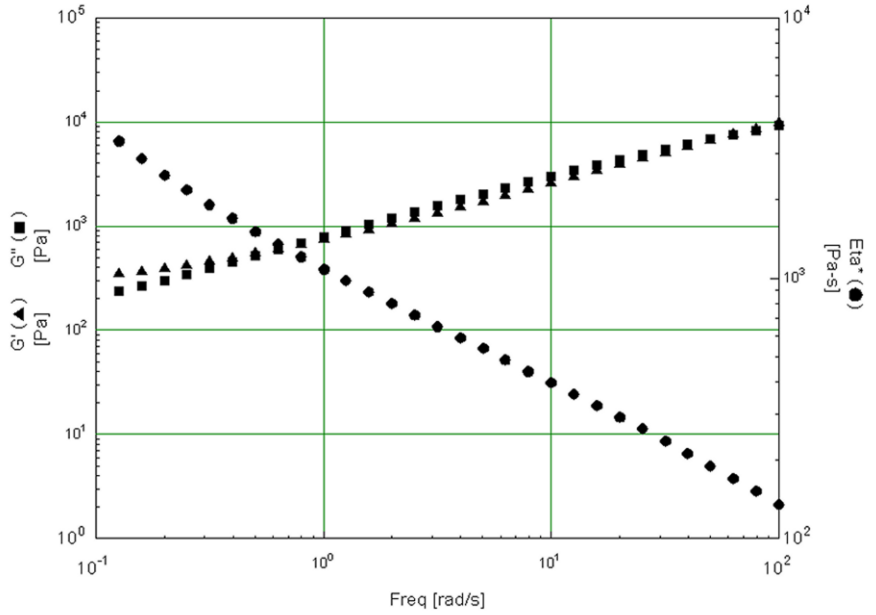

Figure 2.16 : Evolution of the storage modulus (triangles), loss modulus (squares) and complex viscosity (circles) as a function of the frequency for ccPP-4/3x

Although the beginning of the Newtonian plateau can be observed for ccPP-4 at low shear rates it is not obvious to ascertain the linearity of ccPP-4. Besides, it must be pointed out that the values of G' at low frequencies should be discarded for ccPP-4 because of too low torque. However, considering ccPP-4/2x of Figure 2.15, it becomes obvious that the slope of G' at low shear rates clearly lies below the expected value of 2 and is almost parallel to G". The situation is even more dramatic for ccPP-4/3x of Figure 2.16 where G' and G" are superimposed over a wide range of shear rates. A plateau in the storage modulus can also be observed at very low shear rates. The complex viscosity no longer tends to a Newtonian plateau but constantly increases to an infinite value. This behavior is typical for gel-like structures, indicating that a tridimensional network is being created. ccPP-4, ccPP-4/2x and ccPP-4/3x clearly do not obey equation 2.8. Therefore, it is reasonable to assume that the additional concentrations of

peroxide and NBS introduced during the second and third processing steps could not further induce epimerization reactions but contributed to the creation of long chain branches up to a pseudo-gel structure.

2.1.4 Conclusions

The reactive processing of isotactic polypropylene in the presence of a peroxide and N-bromosuccinimide enables a controlled reduction of the crystallinity of the original iPP. ^{13}C NMR analysis demonstrated that this crystallinity reduction is due to successive random epimerization of tertiary carbon atoms along the polymer backbone. Although the drastic decrease of crystallinity leads to nearly totally amorphous materials, these remain isotactic to a high extent. Isotactic/atactic stereoblock elastomers are therefore obtained whose average isotactic block lengths have been calculated from NMR data. SSA thermal analysis revealed that the polymer is homogeneously altered. The production of a pure atactic polypropylene was found impossible even upon successive extrusion steps. The progressive crosslinking of the elastomer was instead observed. The results obtained in the frame of this study were already used by our group for improving the process of polypropylene functionalization, more especially with maleic anhydride. As described in a previous publication, it was shown that N-bromosuccinimide allows higher grafting levels and prevents excessive degradation while conferring elastomeric properties to maleated polypropylenes.[77]

2.1.5 Acknowledgement

We thank La Région Wallonne (AM-PP program) and FRIA-FNRS for financial support (fellowship to X. Drooghaag). J. Marchand-Brynaert is senior research associate of FRS-FNRS.

2.1.6 References

[1] Natta, G.; Pino, P.; Corradini, P.; Danusso, F.; Mantica, E.; Mazzanti, G.; Moraglio, G. J. Am. Chem. Soc. 1955, 77, 1708-1710.

[2] Natta, G.; Corradini, P. Atti Accad. nazl. Lincei, Mem. Classe Sci. Fis., Mat. e Nat. 1955, 4 (Sez II), 73-80.

[3] Natta, G. Angew. Chem. 1956, 68, 393-403.

[4] Natta, G. J. Polym. Sci. 1959, 34, 531-549.

[5] Natta, G. Angew. Chem. 1964, 76, 553-566.

[6] Natta, G.; Pino, P.; Mazzanti, G. USA Patent US 3,112,301, 1963.

[7] Natta, G.; Pino, P.; Mazzanti, G. USA Patent US 3,582,987, 1971.

[8] Natta, G.; Mazzanti, G.; Crespi, G.; Moraglio, G. Chim. Ind. (Milan) 1957, 39, 275-283.

[9] Natta, G.; Crespi, G. Patent US 3,175,999, 1965.

[10] Natta, G.; Pino, P.; Mazzanti, G. USA Patent US 3,438,956, 1969.

[11] Rajan, G. S.; Vu, Y. T.; Mark, J. E.; Myers, C. L. Eur. Polym. J. 2004, 40, 63-71.

[12] Schrage, A.; Pless, E. J. USA Patent US 3,329,741, 1967.

[13] Gobran, R.; Kremer, L. V.; Ethier, D. O. Patent US 3,784,502, 1974.

[14] Collette, J. W.; Tullock, C. W.; MacDonald, R. N.; Buck, W. H. Macromolecules 1989, 22, 3851-3858.

[15] Collette, J. W.; Ovenall, D. W.; Buck, W. H.; Ferguson, R. C. Macromolecules 1989, 22, 3858-3866.

[16] Tullock, C. W.; Tebbe, F. N.; Mülhaupt, R.; Ovenall, D. W.; Setterquist, R. A.; Ittel, S. D. J. Polym. Sci. : Part A : Polym. Chem. 1989, 27, 3063-3081.

[17] Tullock, C. W.; Mulhaupt, R.; Ittel, S. D. Makromol. Chem., Rapid Commun. 1989, 10, 19-23.

[18] Ittel, S. D. J. Macromol. Sci., Chem. 1990, A27, 1133-1146.

[19] Ittel, S. D.; Nelson, L. T. J. Am. Chem. Soc., Polym. Prepr. 1994, 35, 665-666.

[20] Collette, J. W.; Tullock, C. W. UK Patent GB 2001080, 1979.

[21] Collette, J. W.; Tullock, C. W. Patent US 4,335,225, 1982.

[22] Sinn, H.; Kaminsky, W. Adv. Organomet. Chem. 1980, 18, 99-149.

[23] Sinn, H.; Kaminsky, W.; Vollmer, H. J.; Woldt, R. Angew. Chem., Int. Ed. Engl. 1980, 19, 390-392.

[24] Ewen, J. A. J. Am. Chem. Soc. 1984, 106, 6355-6364.

[25] Kaminsky, W.; Külper, K.; Brintzinger, H. H.; Wild, F. R. W. P. Angew. Chem., Int. Ed. Engl. 1985, 24, 507-508.

[26] Brintzinger, H. H.; Fisher, F.; Mülhaupt, R.; Rieger, B.; Waymouth, R. M. Angew. Chem. Int. Ed. Engl. 1995, 34, 1143-1170.

[27] Alt, H. G.; Köppl, A. Chem. Rev. 2000, 100, 1205-1221.

[28] Coates, G. W. Chem. Rev. 2000, 100, 1223-1252.

[29] Resconi, L.; Cavallo, L.; Fait, A.; Piemontesi, F. Chem. Rev. 2000, 100, 1253-1345.

[30] Busico, V.; Cipullo, R. Prog. Polym. Sci. 2001, 26, 443-533.

[31] Kaminsky, W.; Laban, A. Appl. Catal. A: General 2001, 222, 47-61.

[32] Mallin, D. T.; Rausch, M. D.; Lin, Y.-G.; Dong, S.; Chien, J. C. W. J. Am. Chem. Soc. 1990, 112, 2030-2031.

[33] Chien, J. C. W.; Llinas, G. H.; Rausch, M. D.; Lin, G.-Y.; Winter, H. H.; Atwood, J. L.; Bott, S. G. J. Am. Chem. Soc. 1991, 113, 8569-8570.

[34] Llinas, G. H.; Chien, J. C. W. Polym. Bull. 1992, 28, 41-45.

[35] Llinas, G. H.; Dong, S.-H.; Mallin, D. T.; Rausch, M. D.; Lin, Y.-G.; Winter, H. H.; Chien, J. C. W. Macromolecules 1992, 25, 1242-1253.

[36] Chien, J. C. W.; Rieger, B.; Sugimoto, R.; Mallin, D. T.; Rausch, M. D. Stud. Surf. Sci. Catal. 1990, 56, 535-574.

[37] Lin, Y. G.; Mallin, D. T.; Chien, J. C. W.; Winter, H. H. Macromolecules 1991, 24, 850-854.

[38] Gauthier, W. J.; Corrigan, J. F.; Taylor, N. J.; Collins, S. Macromolecules 1995, 28, 3771-3778.

[39] Gauthier, W. J.; Collins, S. Macromolecules 1995, 28, 3779-3786.

[40] Gauthier, W. J.; Collins, S. Macromol. Symp. 1995, 98, 223-231.

[41] Rieger, B.; Jany, G.; Fawzi, R.; Steimann, M. Organometallics 1994, 13, 647-653.

[42] Dietrich, U.; Hackmann, M.; Rieger, B.; Klinga, M.; Leskelä, M. J. Am. Chem. Soc. 1999, 121, 4348-4355.

[43] Müller, G.; Rieger, B. Prog. Polym. Sci. 2002, 27, 815-851.

[44] Kukral, J.; Lehmus, P.; Feifel, T.; Troll, C.; Rieger, B. Organometallics 2000, 19, 3767-3775.

[45] Deisenhofer, S.; Feifel, T.; Kukral, J.; Klinga, M.; Leskelä, M.; Rieger, B. Organometallics 2003, 22, 3495-3501.

[46] Cobzaru, C.; Deisenhofer, S.; Harley, A.; Troll, C.; Hild, S.; Rieger, B. Macromol. Chem. Phys. 2005, 206, 1231-1240.

[47] Cobzaru, C.; Hild, S.; Boger, A.; Troll, C.; Rieger, B. Coord. Chem. Rev. 2006, 250, 189-211.

[48] Hauptman, E.; Waymouth, R. M.; Ziller, J. W. J. Am. Chem. Soc. 1995, 117, 11586-11587.

[49] Coates, G. W.; Waymouth, R. M. Science 1995, 267, 217-219.

[50] Wiyatno, W.; Chen, Z.-R.; Liu, Y.; Waymouth, R. M.; Krukonis, V.; Brennan, K. Macromolecules 2004, 37, 701-708.

[51] Sacchi, M. C.; Tritto, I.; Bertini, F.; Losio, S.; Zecchi, G.; Polo, E. Kinetics Catal. 2006, 47, 268-273.

[52] Busico, V.; Castelli, V. V. A.; Aprea, P.; Cipullo, R.; Segre, A.; Talarico, G.; Vacatello, M. J. Am. Chem. Soc. 2003, 125, 5451-5460.

[53] Fujita, M.; Seki, Y.; Miyatake, T. Macromolecules 2004, 37, 9676-9680.

[54] Bruce, M. D.; Coates, G. W.; Hauptman, E.; Waymouth, R. M.; Ziller, J. W. J. Am. Chem. Soc. 1997, 119, 11174-11182.

[55] Lin, S.; Waymouth, R. M. Acc. Chem. Res. 2002, 35, 765-773.

[56] Smolensky, E.; Kapon, M.; Woollins, J. D.; Eisen, M. S. Organometallics 2005, 24, 3255-3265.

[57] Harney, M. B.; Zhang, Y.; Sita, L. R. Angew. Chem. Int. Ed. 2006, 45, 2400-2404.

[58] Prosser, T. J. US Patent 4,105,837, 1978.

[59] Suter, U. W.; Pucci, S.; Pino, P. J. Am. Chem. Soc. 1975, 97, 1018-1023.

[60] Suter, U. W.; Neuenschwander, P. Macromolecules 1981, 14, 528-532.

[61] Listner, G. J.; Park, K. Patent US 3,511,824, 1970.

[62] Listner, G. J.; Park, K. Patent US 3,515,687, 1970.

[63] Listner, G. J.; Park, K. Patent FR 1 567 883, 1969.

[64] Stehling, F. C.; Knox, J. R. Macromolecules 1975, 8, 595-603.

[65] Flat, J.-J. In Nouveaux développements dans le greffage radicalaire sur polypropylène à l'état fondu. Ph.D. Thesis, Université Louis Pasteur Strasbourg I, Strasbourg, 1991.

[66] Flat, J.-J.; Lambla, M. Patent EP 0 534 830, 1993.

[67] Ibbett, R. N. In NMR Spectroscopy of Polymers; Ibbett, R. N., Eds.; Blackie Academic & Professional: London, 1993.

[68] Tonelli, A. E.In NMR Spectroscopy and Polymer Microstucture: The Conformational Connection; VCH: New-York, USA, 1989,71-88

[69] Busico, V.; Cipullo, R.; Segre, A. L.; Talarico, G.; Vacatello, M.; Van Axel Castelli, V. Macromolecules 2001, 34, 8412-8415.

[70] Gauthier, W. J. In Polypropylene. An A-Z reference; Karger-Kocsis, J., Eds.; Kluwer Academic Publishers, 1999, pp 178-185.

[71] Burfield, D. R.; Loi, P. S. T.; Doi, Y.; Mejzik, J. J. Appl. Polym. Sci. 1990, 41, 1095-1114.

[72] Bruce, M. D.; Waymouth, R. M. Macromolecules 1998, 31, 2707-2715.

[73] Madkour, T. M.; Mark, J. E. J. Polym. Sci. : Part B : Polym. Phys. 2002, 40, 840-853.

[74] Nele, M.; Collins, S.; Dias, M. L.; Pinto, J. C.; Lin, S.; Waymouth, R. M. Macromolecules 2000, 33, 7249-7260.

[75] Madkour, T. M.; Mark, J. E. Polymer 1998, 39, 6085-6091.

[76] Barnes, H. A.; Hutton, J. F.; Walters, K. In An Introduction to Rheology; Walters, K., Eds.; Elsevier: Amsterdam, 1989,Chapter 6, pp 102.

[77] Henry, G. R. P.; Drooghaag, X.; Rousseaux, D. D. J.; Sclavons, M.; Devaux, J.; Marchand-Brynaert, J.; Carlier, V. Journal of Polymer Science, Part A: Polymer Chemistry 2008, 46, 2936-2947.

2.2 **Practical Way of Grafting Maleic Anhydride onto Polypropylene Providing High Anhydride Contents without Sacrificing Excessive Molar Mass**

Gaëtan R. P. Henry,[1] Xavier Drooghaag,[1] Dimitri D. J. Rousseaux,[1] Michel Sclavons,[2] Jacques Devaux,[2] Jacqueline Marchand-Brynaert,[1] Véronique Carlier[2]

Published as J.Polym.Sci, Part A : Polym. Chem. ***2008****, 46, 2936-2947*

[1]Unité de Chimie Organique et Médicinale, Place Louis Pasteur 1, B-1348 Louvain-la-Neuve, Belgium.
[2]Unité de Physique et de Chimie des Hauts Polymères, Place Croix du Sud 1, B-1348 Louvain-la-Neuve, Belgium.

Abstract

This study reports a reactive extrusion process leading to very high levels of anhydride grafting (2.5 to 3 *wt.*%) along polypropylene backbone without recovering grafted PP waxes at the die exit. Such high graftings are attainable without excessive degradation of the PP chain thanks to a brominated reagent. Simultaneously, this brominated reagent allows the tuning of the grafted PP crystallinity via epimerization of the PP backbone. Indeed, the synthesis of a mainly isotactic/atactic stereoblock polymer containing high levels of grafted succinic anhydride moieties is demonstrated by NMR and melting enthalpies recorded by DSC are definitely observed depressed and broadened. Grafting levels of around 3 *wt.*% have been achieved and ascertained by both chemical titration and NMR spectroscopy. In addition, FTIR spectroscopy reveals an unusual observation : for the first time, only one single pair of symmetric and

asymmetric carbonyl stretching bands are observed on those grafted PP, whilst, in other processes of anhydride grafting, those symmetric and asymmetric bands were both split in at least two bands. This suggests, for the here reported process, the absence of interacting grafted anhydride rings, i.e. absence of closely grafted anhydride moieties and absence of poly(maleic anhydride). All those observations support that this "bromine route" brings a really new grafting process for PP.

2.2.1 Introduction

Isotactic polypropylene (iPP) is a very interesting polyolefin because of its broad range of applications. However it suffers from lack of reactivity and polarity leading to low compatibility with other polymers. Besides, recent progresses in the tacticity stereo-control of the catalysts greatly reduced the amount of low molecular weight and poorly isotactic polypropylene co-produced during the synthesis of iPP.[1] However, several applications had been found for this low crystallinity polypropylene notably as hot-melt adhesives and bitumen modifiers but as this source of cheap raw material is slowly disappearing, an actual demand now exists for such a polymer. It is therefore welcome to find a way for producing from isotactic polypropylene, and at low cost, polypropylene with controlled physico-chemical properties such as reactivity, polarity, crystallinity and tacticity. Simultaneous control of these properties would help making PP a more polyvalent material and appears as an original and useful route for iPP recycling. Reactive extrusion seems the best method for polypropylene modification as it will be further detailed in the following sections, summarizing the state of the art.

Grafting of maleic anhydride onto polypropylene

Functionalization of polypropylene by maleic anhydride (MA) in the presence of organic peroxides has been intensively studied over the past decades. Extended reviews presented by Moad,[2] Hu *et al*[3] or van Duin[4] summarize the state of the art. These maleic anhydride-grafted polypropylenes (PP-g-MA's) are well known as interfacial agents because of their improved polarity and reactivity. Many applications can be found in blend compatibilization,[5-8] polymer-based nanocomposites,[9] asphalt modifiers,[10] multi-layer films, co-extrusion and many other fields.[4]

The grafting mechanisms still remain not clearly understood and different reaction pathways have been suggested. Nevertheless, it is generally accepted that grafting levels are limited by severe PP degradation, whatever the mechanism. Indeed, the unavoidable β–scission of the PP chains requires to limit the grafting to quite low contents (~0.5 *wt.*% of grafted MA) in order to maintain a PP molecular weight compatible with acceptable mechanical properties. Several approaches have been considered in order to avoid excessive degradation during melt functionalization. The use of different additives such as stearamide,[11] dimethylformamide or dimethylacetamide,[12] styrene[13-14] or furan[15] derivatives have been reported but grafting levels still remain quite low and grafting of the additive is also observed. Shi et al. recently reported an original way to limit PP degradation via the concept of nano-reactors.[16] The organic peroxide is first confined within the galleries of an organically modified montmorillonite. Primary radicals are then progressively released into the polymer melt during reactive processing providing higher grafting levels and lower extent of chain scission.

Many parameters may affect the grafting reaction and hence, the grafting levels and the grafts structures. Mixing efficiency, temperature,

pressure, residence time, venting, screw/extruder design may vary considerably even though quoted operating parameters appear rather similar.[2] This makes the elucidation of the mechanisms even more ambiguous and authors still are in disagreement.

Various methods are commonly used to ascertain grafting mechanisms. Nuclear magnetic resonance (NMR) spectroscopy is a very powerful tool for the qualitative (and sometimes quantitative) analysis of compounds grafted onto a polymer backbone. This is especially true for ^{13}C NMR, due to the superior sensitivity of the carbon nuclei to the chemical environment. Although various examples can be found in the literature,[17-20] there is a number of issues inherent to the nature of PP-g-MA that usually limits the interpretation of the NMR spectra. First, the usually low grafting yield of MA onto PP, and the limited solubility of high molecular weight PP-g-MA's often lead to signal-to-noise ratios not suitable for accurate quantitative analysis of the grafted moieties. On the other hand, various types of grafted anhydride species have been suggested in the literature (succinic,[12,17-19,21,23] maleic[23] and itaconic anhydrides,[18,19,23] as well as oligomers,[12,21] etc…); if at least two different types of grafted species are present, each one will have a particular chemical environment and therefore a specific set of chemical shifts, making both detection and interpretation more difficult.

Authors' laboratories have been greatly active toward the molecular characterization of maleic anhydride grafted polypropylenes, especially by FTIR spectroscopy.[24-27] Typical commercial PP-g-MA's exhibit strong absorption bands centered at 1792 and 1784 cm^{-1}. These bands have been assigned to symmetric stretching of the carbonyl groups in isolated succinic anhydride and interacting anhydride moieties (maleic anhydride oligomers or closely grafted succinic anhydride moieties or clusters) respectively. These two bands are accompanied with two weaker absorption bands at 1863

and 1845 cm^{-1} assigned to the corresponding asymmetric stretching of the carbonyl groups. This duality in absorption bands reflects two different types of grafted moieties. The formation of maleic anhydride oligomers during reactive processing also remains a topic of controversy. Some teams claim that radical mechanism leads to some oligomerization of MA by radical transfer,[12,24] other ones support that temperature reaction is beyond the ceiling temperature of poly(maleic anhydride)[28] and that its formation is therefore impossible. However the homopolymerization of maleic anhydride in molten polypropylene at a temperature of 190 °C was demonstrated.[21] Heinen reported the presence of such anhydride oligomerization when grafting MA onto PE but its absence when grafting onto PP.[18]

Finally, it has been suggested that the polarity of the peroxide may affect the poly(maleic anhydride) occurrence. It has already been reported in the literature that the solubility of maleic anhydride into polyolefins is very limited.[29,30] Therefore, when the anhydride concentration exceeds the solubility limit, the system is phase-separated. The peroxide partition over the apolar matrix and the polar anhydride phase is dependent upon its molecular structure and polarity. The formation of oligomeric reaction products of maleic anhydride has been observed in such phase separated systems.[30] Besides, it has been reported several times that this solubility issue is responsible for a maximum in the grafting efficiency with respect to the initial anhydride concentration. This optimum concentration is dependent upon the initiator structure and concentration.[22,23,29-31]

Polypropylene epimerization

Isotactic polypropylene tacticity can be modified in order to reduce its crystallinity. Listner patented a process for changing an isotactic polypropylene into an isotactic-randiotactic stereoblock polypropylene.[32-35] This stereochemically rearranged polypropylene is prepared by reactive

extrusion of isotactic polypropylene with a free radical initiator and a bromine compound. This stereochemical rearrangement was evidenced by NMR spectroscopy. Completely racemized polymers can be so produced and exhibit no crystallinity, low tensile strength, no discernible melting point, high elasticity and are tacky above 38 °C while less racemized polymers enabled the tuning of those properties between isotactic PP and completely racemized ones. This epimerization process has been extensively investigates in Section 2.1 of this Chapter.

Simultaneous epimerization and grafting

In 1992, Flat[14,36] introduced a European patent application describing for the first time the production of a PP-g-MA with controlled crystallinity. This process also implies the simultaneous use of a bromine compound (such as bromomaleic anhydride or *N*-bromosuccinimide (NBS)) and of maleic anhydride for promoting grafting while reducing incidence of chain scissions. However the reported operating conditions, while inducing a low level of bromination, did not allow the achievement of high levels of grafting.

In this paper, an optimized process for producing a low crystallinity isotactic/atactic stereoblock polypropylene elastomer containing high levels of grafted succinic anhydride moieties is presented together with a full structural characterization both on a macro- and micro-scale. The assumed mechanism will also be depicted.

2.2.2 Experimental Section

Materials

Isotactic polypropylene used was Moplen HF500N (powder) homopolymer supplied by Basell. Maleic anhydride, *N*-Bromosuccinimide, and *m*-xylylenediamine were 99 % purity and supplied by Acros. Free radical initiator was Luperox 101XL from Arkema (2,5-Bis(*tert*-butylperoxy)-2,5-dimethylhexane (DHBP), 45 *wt.*% blend with calcium carbonate and silica). Toluene was analytical grade. NMR solvent was 1,1,2,2-tetrachloroethane-d_2 (TCE, 99.5 % atom D) from Aldrich. All reagents were used without further purification.

Synthesis of the PP-g-MA's

Three PP-g-MA's were synthesized for a comparative study. PP-g-MA 1 is a sample processed without any brominated compound and will be used as a reference for comparison purpose. PP-g-MA 2 and 3 contain maleic anhydride, the radical initiator and the brominated compound (NBS in the present case). They differ by the amount of NBS introduced in the mixture. The amount of each reagent used is summarized in Table 2.9.

Table 2.9 : Composition of the reactive mixtures for the studied PP-g-MA's

	wt.% DHBP [a]	*wt.% NBS*	*wt.% MA*	$Br^{\bullet}/Ox^{\bullet}$
PP-g-MA 1	1.46	0	5	0
PP-g-MA 2	1.46	0.8	5	1
PP-g-MA 3	1.46	1.6	5	2

[a] support excluded

The initial MA concentration of 5 *wt.*% reported here is the optimum concentration that provided the highest grafting levels. The existence of an optimum in grafting efficiency with respect to the initial MA concentration

has already been discussed in the introduction. The $Br^{\bullet}/Ox^{\bullet}$ ratio is defined as the maximum concentration of bromine free radicals that could be produced over the maximum concentration of active oxygen-based free radicals produced by the organic peroxide. It was demonstrated that in absence of MA, the optimum $Br^{\bullet}/Ox^{\bullet}$ ratio for complete loss of crystallinity and which has the less negative effect on molecular weight ranges from 10 to 15.[34] However, as the process described here involves the additional reaction of anhydride grafting which also consumes radicals, a higher concentration of peroxide is required. The optimum $Br^{\bullet}/Ox^{\bullet}$ ratio had to be re-evaluated accordingly and was found to range from 1 to 2.

Polypropylene, maleic anhydride, NBS and peroxide were dry-mixed and then poured into the hopper of a Brabender single screw extruder equipped with a feeding screw of L/D = 20. The barrel was heated on three zones set at 220-240-260 °C. Screw speed was set to 25 rpm, which allowed a residence time of about 90 seconds. Yarns were poured into cold water and granulated.

Sample Washing

Prior to any analysis, a sample of ~1 g of PP-g-MA was dissolved into refluxing toluene and then precipitated into a large excess of acetone. The polymer was then washed with acetone and dried under vacuum at 100 °C overnight. The cleaned polymers were then rid of ungrafted maleic anhydride and short oligomers, which are soluble in acetone.

Quantification of the Grafted Species

The anhydride content of the PP-g-MA's were determined by acid-base titration according to the procedure described in a previous paper.[26] 1 g of washed polymer was dissolved in 150 ml of refluxing toluene. After complete dissolution, five drops of 1% w/v bromothymol blue in methanol

were added and the solution was titrated by a 0.05N solution of tetrabutyl ammonium hydroxide (TBAOH). The titration was stopped when the color change was stable. The AM content was calculated from the volume and concentration of TBAOH.

Size Exclusion Chromatography (SEC)

Molecular weights were determined by high temperature size exclusion chromatography. Measurements were performed on a Waters Alliance GPCV 2000 equipped with two Styragel HT 6E and one Styragel HT 2 columns along with a differential refractometer and a viscometer. The mobile phase was 1,2,4-trichlorobenzene (TCB). The concentration of the sample was 2 mg/mL in TCB and dissolution was achieved by shaking at 160 °C for 1h. The injection volume was 215 µL. Temperature was held constant at 145 °C throughout the analysis. The system was calibrated prior to the analysis with PS standards according to ISO 16014-2 specification. It must be kept in mind that hydrodynamic volume variation may occur due to the high level of grafting of maleic anhydride.

Differential Scanning Calorimetry (DSC)

Crystallinity modification of the PP-g-MA's was evaluated using Mettler Toledo DSC 821e module. A sample of about 5 mg of product was weighed and inserted into a 20 µL aluminum pan. The temperature program consisted of a first heating ramp from -20 to 220 °C followed by a cooling ramp from 220 to -20 °C and a second heating ramp from -20 to 220 °C. The heating/cooling rate of each segment was 10 °C/min. The role of the first heating run is to erase the thermal history of the sample whereas the second heating run is used for the calculation of the PP crystallinity reduction (for comparison purpose with the crystallinity of the commercial PP fed in the hopper).

FTIR Spectroscopy

FTIR spectra were recorded on a Nicolet - Nexus 670 FT-IR apparatus, over a spectral range from 4000 to 400 cm^{-1} at a resolution of 4 cm^{-1}. A thin film was compression molded at 200 °C. Spectra were normalized by setting the peak height of the 973 cm^{-1} absorption band to an absorbance of 0.5. This band, which is assigned to isotactic helices, is usually used as an internal reference for comparison of films of different thickness.[37] Although the shape of this band is slightly dependent on the length of isotactic sequences in PP,[38] its usage is still suitable in the present study as the amount of isotacticity remains rather high and does not affect the band shape. Besides, FTIR spectroscopy is use for qualitative purpose only.

NMR Spectroscopy

High temperature solution state NMR experiments were performed on a Brüker 500 MHz AVANCE operating at 500.13 MHz for ^{1}H (125.76 MHz for ^{13}C), equipped with a 10 mm SeX-$^{13}C/^{1}H$ high temperature probe linked to a thermoregulator unit. The spectra were acquired and processed using the software XWIN-NMR. TCE was used as a solvent as well as an internal reference ($\delta[^{1}H]$ = 6.0 ppm and $\delta[^{13}C]$ = 73.7 ppm). Before analysis, a sample of polymer (about 100 mg) was dissolved in TCE (2.5 mL) at 125 °C under argon atmosphere (to prevent oxidation before analysis) in a 10 mm Wilmad NMR tube (Sigma-Aldrich, Royal Imperial grade). Once the complete solubility of the sample was ascertained, the tube was inserted in the spectrometer and heated at 125 °C; the homogeneity of the magnetic field (shims) was carefully adjusted before acquisition. For ^{13}C NMR analysis (under total ^{1}H decoupling), a relaxation time of 15 seconds was selected and 6000 transients were recorded, in order to obtain a semi-quantitative spectrum with a good signal-to-noise ratio.

Viscosimetric Titration

The location of grafted species can be investigated through the ability of a grafted polypropylene to crosslink upon addition of a diamine[26]. Reactive blending of PP-g-MA with m-xylylenediamine was carried out in a Brabender plasticorder. 40 g of PP-g-MA were melted at 200 °C and, after two minutes of mixing, a stoichiometric amount of m-xylylenediamine was added. The reaction was stopped after one more minute of mixing.

2.2.3 Results and Discussion

Bulk Characterization

Characterization results of the grafted PP are summarized in Table 2.10. iPP was also analyzed for comparison.

Table 2.10 : Total anhydride contents, enthalpy of melting and molecular weights of the PP-g-MA's

	Total anhydride content [a] *(wt.%)*	ΔH_f (J/g)	*Mn (kDa)*	*Mw (kDa)*	*PDI*
iPP	/	110	49.0	230	4.68
PP-g-MA 1	1.25	88	15.5	44.3	2.85
PP-g-MA 2	2.81	35	27.4	90.8	3.31
PP-g-MA 3	2.47	24	26.0	91.9	3.53

[a] determined by acid/base titration of washed PP-g-MA. This method is non sensitive to grafts structure and position on the PP backbone.

PP-g-MA 1 has a grafting level of 1.25 *wt.*% and underwent severe degradation. It is interesting to note that in the presence of NBS (PP-g-MA's 2 and 3) both grafting contents and molecular weights are remarkably higher. This lets us suggest that bromine radicals issued from NBS decomposition act as macroradical stabilizers and promote the grafting

process instead of degradation. In addition to stabilization, bromine radicals are also responsible for polypropylene backbone epimerization.[32-34,39] The partial destruction of PP stereoregularity, as evidenced by NMR spectroscopy and reported in a following section of this paper, prevents the crystallization to occur efficiently. Figures 2.17 and 2.18 show the DSC traces of PP-g-MA 1 and 3 respectively. As the DSC trace of PP-g-MA 2 is very similar to that of PP-g-MA 3 and does not provide any further relevant information, it is not presented here.

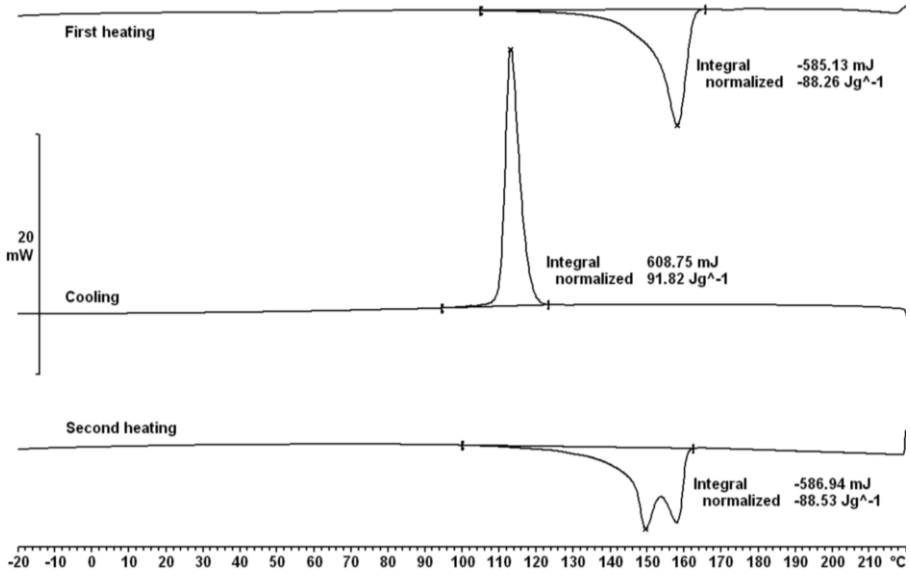

Figure 2.17 : DSC thermograms of PP-g-MA 1

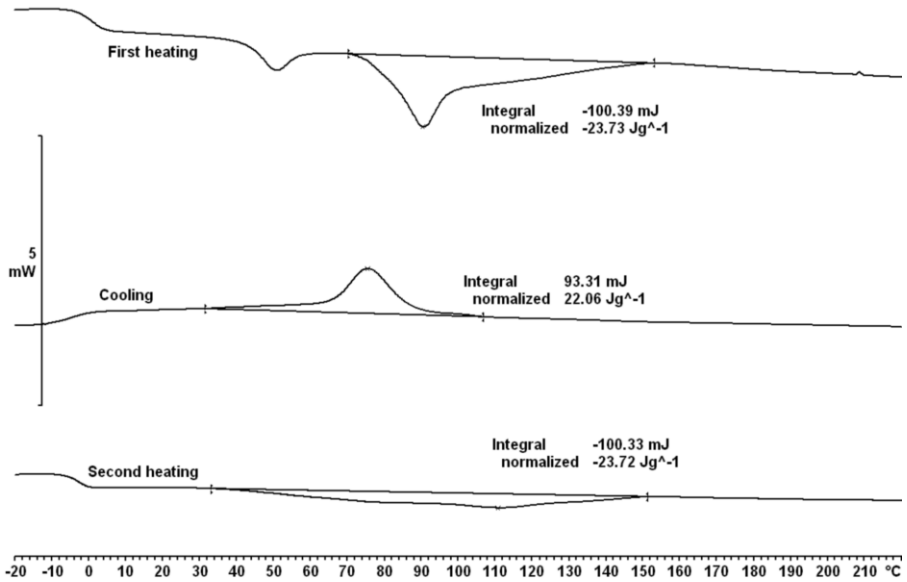

Figure 2.18 : DSC thermograms of PP-g-MA 3

PP-g-MA 1 exhibits intense thermal transitions because of its pronounced semi-crystalline nature. Integration of melting peaks reveals a decrease in crystallinity of 20 % in comparison with pure isotactic PP. This decrease in crystallinity is due to the anhydride moieties grafted along the PP backbone. They act as structural defects in the chain regularity and are rejected out of the crystallites. However, the semi-crystalline nature of this PP-g-MA 1 is preserved because its grafting process does not involve bromine radicals and therefore does not imply any change in the PP tacticity. On the other hand, PP-g-MA 3 exhibits weaker and broader thermal transitions. The crystallinity loss calculated upon integration of the second heating scan transition is of about 78 %. As the tacticity has been randomly altered, only unmodified isotactic segments of sufficient length are able to crystallize. Therefore a broad distribution of melting points appears on the DSC trace. This significant change in crystallinity confers an elastomeric behavior to PP-g-MA 3. The first heating run of this sample also exhibits a small endothermic transition at 45 °C which is related to a long-term

annealing at room temperature (several days). This transition reveals that as the tacticity of these PP-g-MA elastomers has been greatly modified, the co-crystallization of some chain segments whose isotacticity has been altered is slow. It has also been demonstrated by DSC and ^{13}C NMR that in the presence of NBS, polypropylene tacticity is homogeneously modified throughout the sample and every chain is altered similarly.

The amount of bromine radicals within the reactive medium allows the tuning of the tacticity and hence of the crystallinity as shown in table 2.10. The comparison between PP-g-MA 2 and 3 illustrates that the crystallinity of the PP-g-MA's can be tuned while maintaining grafting levels at about 2.5 *wt.*% and above, without further altering molecular weights. The chemical structures of these two samples are very similar and therefore PP-g-MA 3 will be the only sample further discussed in the microstructure investigation as it has the lowest crystallinity and therefore should be more appropriate for studying the tacticity modification.

The glass transition of the PP-g-MA 3 elastomer occurs at a temperature of -7 °C, which is close to usual values for polypropylene. This transition cannot be seen on the thermogram of PP-g-MA 1 as the contribution of isotactic PP amorphous phase to ΔCp is too low.

Microstructure Investigation – FTIR Analysis

In previous papers, the FTIR spectra of several home-made and commercial PP-g-MA's were described.[24-27] The FTIR spectrum of PP-g-MA 1 exhibits as usually a double absorption band at 1861-1844 cm^{-1} along with a broad band centered at 1784 cm^{-1} as depicted in Figure 2.19.

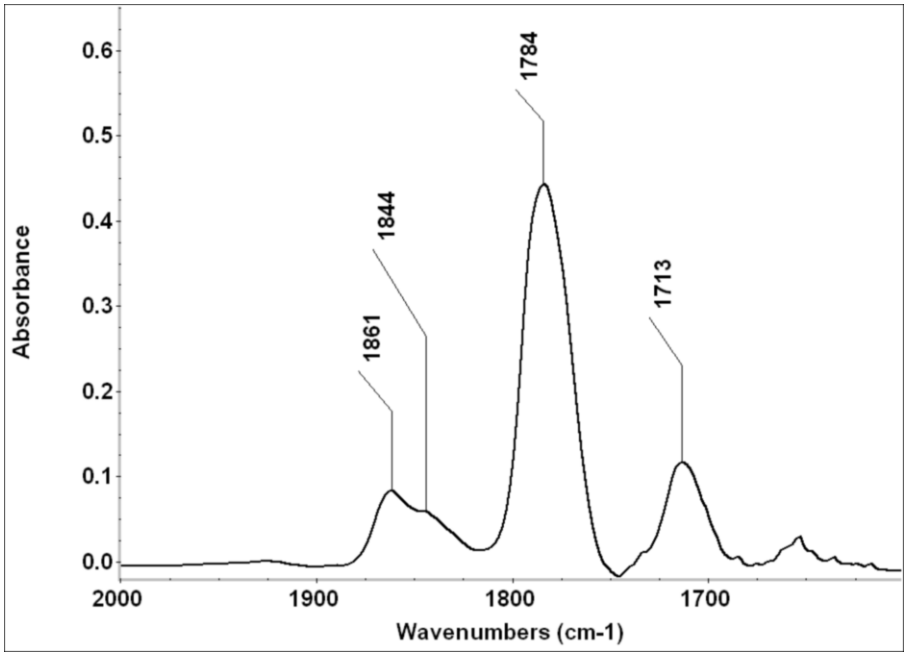

Figure 2.19 : Enlargement of the carbonyl region of the FTIR spectrum of PP-g-MA1

On the other hand, only one single absorption band for carbonyl asymmetrical stretching centered at 1863 cm^{-1} and for symmetrical stretching centered at 1790 cm^{-1} can be seen on PP-g-MA 3 as shown in Figure 2.20.

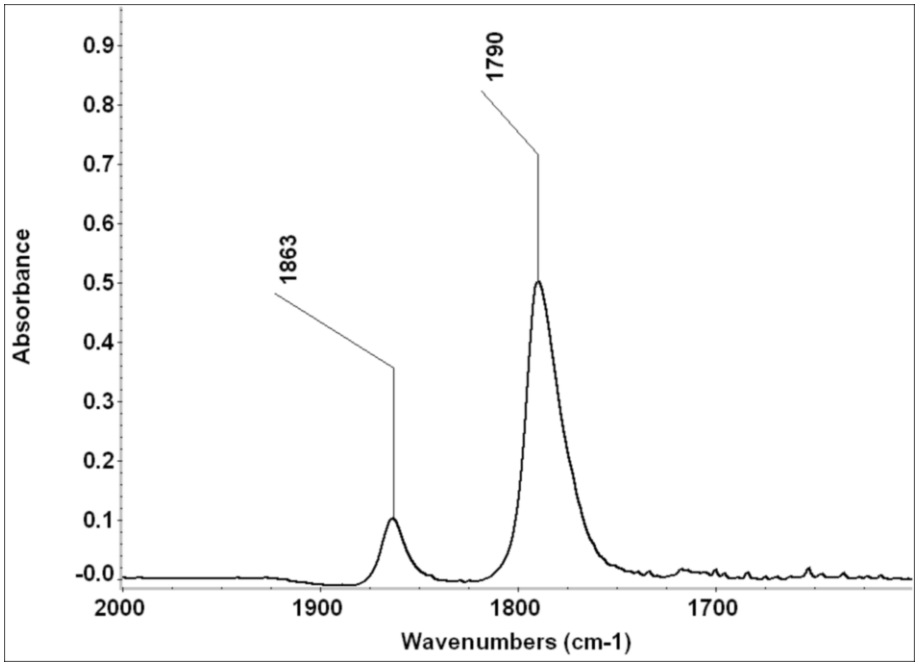

Figure 2.20 : Enlargement of the carbonyl region of the FTIR spectrum of PP-g-MA3

The absence of absorption bands at 1784 and 1844 cm^{-1} suggests the absence of poly(maleic anhydride) or any interacting carbonyl species. Grafts would therefore be isolated succinic anhydride rings only. NMR spectroscopy will further help characterize the graft structure obtained by the new process. The high grafting levels that it promotes have indeed allowed us to study this grafted polymer without need of enrichment in ^{13}C. Nevertheless, FTIR study already revealed that both processes (i.e. with or without NBS) led to different grafting schemes as different types of grafted moieties were observed.

Microstructure Investigation – NMR Analysis of the grafted species

PP-g-MA 3 was analyzed by high temperature solution-state ^{1}H NMR spectroscopy, before and after purification by precipitation from boiling toluene into acetone. From the ^{1}H spectra of Figure 2.21, it seems that

unreacted maleic anhydride (7.0 ppm) and other unidentified impurities have been removed from the crude polymer by precipitation.

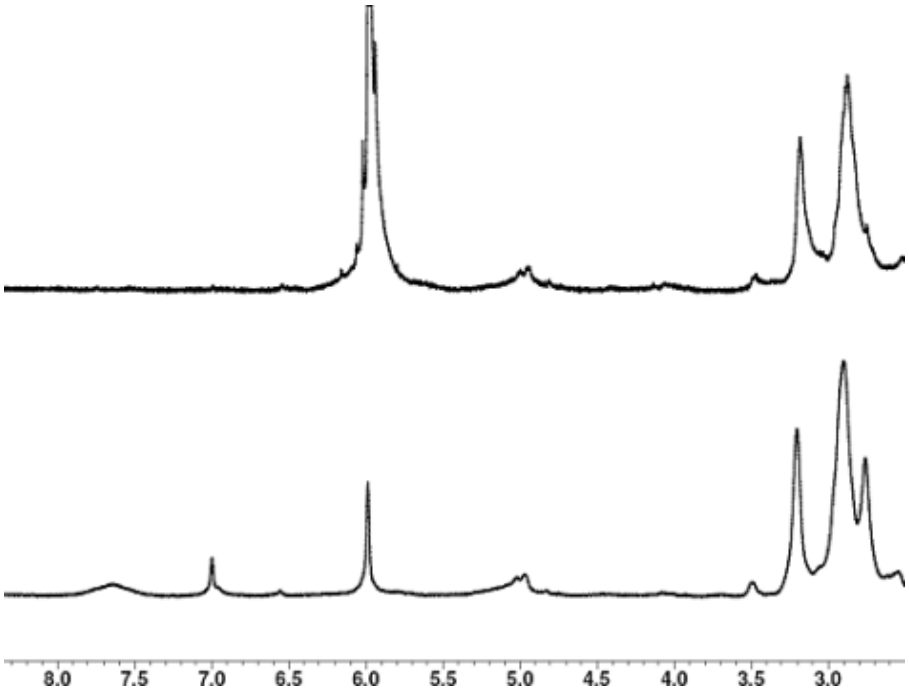

Figure 2.21 : 500 MHz ^{1}H-NMR spectra (TCE reference at 6.0 ppm) of crude PP-g-MA 3 (bottom trace) and PP-g-MA 3 precipitated into acetone (upper trace); for clarity reason, the backbone resonances at higher field are not displayed

Aside from the TCE reference at 6.0 ppm, three main peaks are observed in the spectrum of the purified polymer at 2.87, 3.18 and 5.0 ppm. The very weak peak at 5.0 ppm is probably due to backbiting and/or β-scission reactions, leading to unsaturations in the polypropylene backbone or at chain ends. The resonances at 2.87 and 3.18 ppm are assigned respectively to the methylene and methyne protons of the PP-grafted succinic anhydride species; both the chemical shifts and the relative integrations (ratio 2:1) of these peaks fit well with the structure of a grafted single (non oligomeric)

succinic anhydride. Comparable chemical shifts (2.8-2.9 and 3.1 ppm for the methylene and methyne protons, respectively)[40] were reported by Heinen et al. for a model compound of the grafted succinic anhydride moiety (2,4,6-trimethylhept-4-yl succinic anhydride).[41] Integration of these signals and those of the PP backbone provides an estimation of the anhydride grafting yield, which is found to be 1.2 succinic anhydride per 100 repeating propylene units (= 2.7 *wt.*%). In order to confirm the assignment to grafted single succinic anhydrides, the purified PP-g-MA was analyzed by ^{13}C NMR as shown in Figure 2.22.

Aside from the signals arising from the isotactic PP sequences, a number of additional peaks are observed. Most of them are of medium or high intensities and correspond to heterotactic and syndiotactic sequences that were produced from the isotactic backbone by epimerization of the stereogenic centers in the PP backbone. This phenomenon is known to occur when isotactic PP is processed at high temperatures in the presence of both a peroxide and a brominated additive.[32-34,39] This splitting of the backbone ^{13}C signals is better observed in the region of the methyl resonances (in the range 19-22 ppm), as the chemical shift of the latter is the most sensitive to the conformational changes induced by the presence of non-isotactic sequences.[42-44] Figure 2.23 depicts an enlargement of the methyl region of the ^{13}C spectrum.

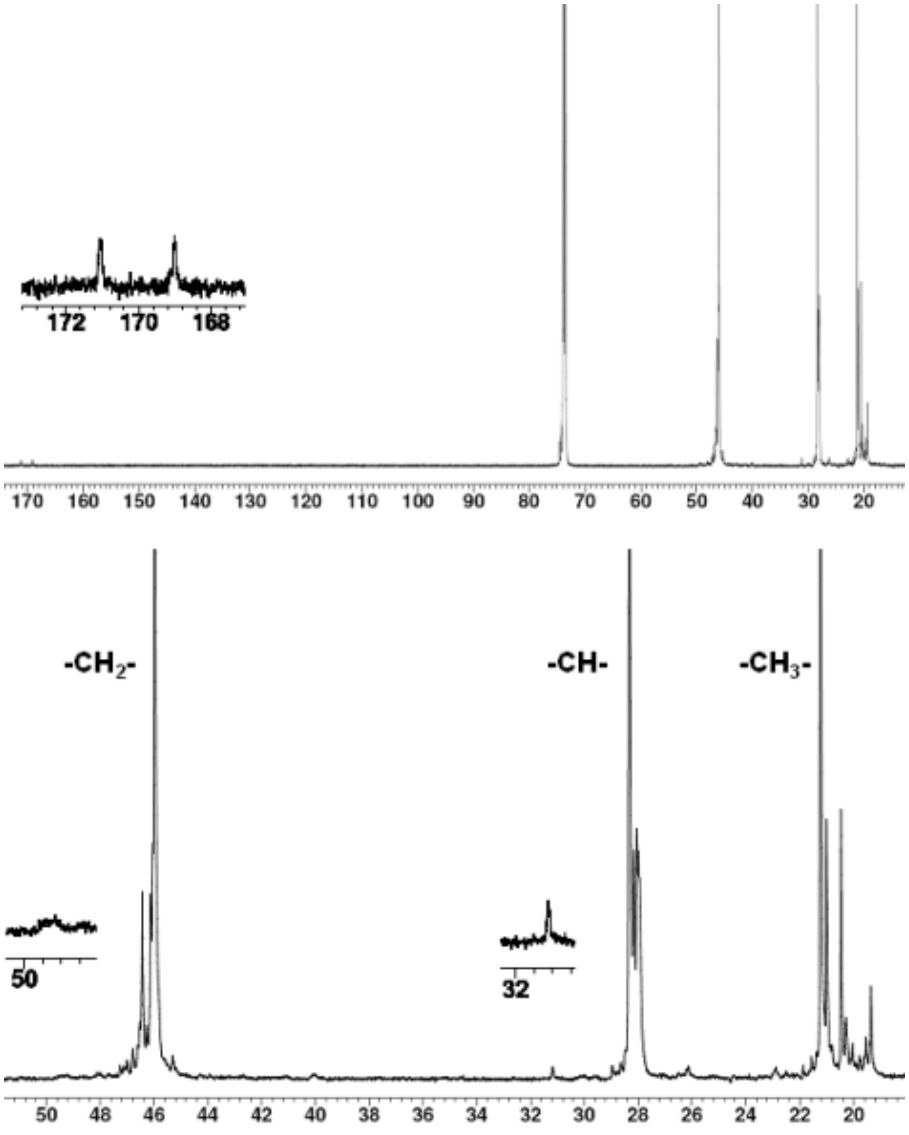

Figure 2.22 : 125 MHz ^{13}C-NMR spectrum of PP-g-MA 3 precipitated into acetone (TCE reference at 73.7 ppm); only signals assigned to succinic anhydrides were magnified

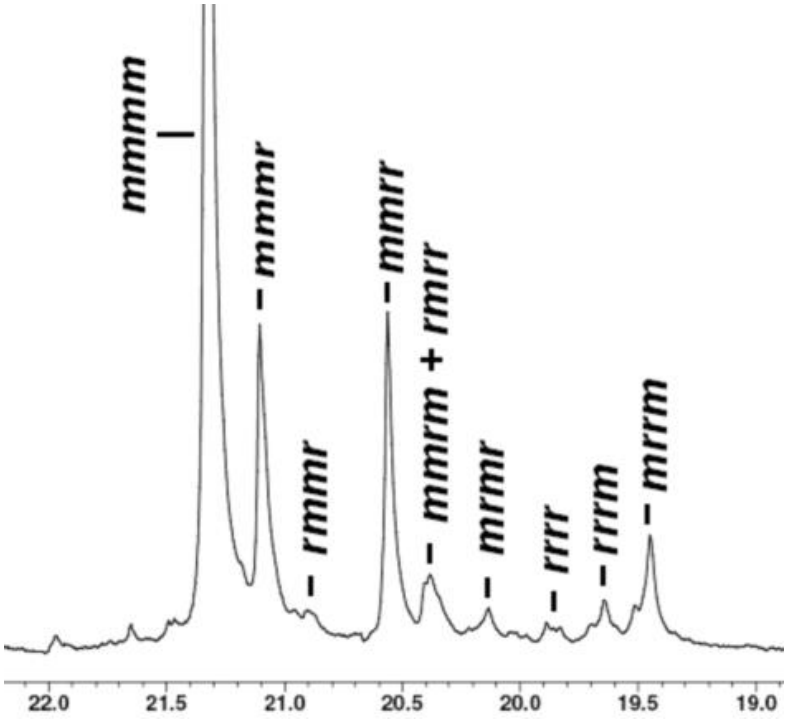

Figure 2.23 : Region of the methyl pentads of PP-g-MA 3 ^{13}C-NMR spectrum; descriptors m and r stand for meso and racemo dyads, respectively

The good resolution of the spectrum, recorded at 125 MHz, allowed us to estimate the isotacticity percentage by integration of the pentads according to:

$$[mmmm] = \frac{I^{mmmm}}{\sum I^{xxxx}} \qquad (2.9)$$

where [*mmmm*] is the percentage of isotacticity, I^{mmmm} the integration of the methyl isotactic pentad (at 21.3 ppm) and ΣI^{xxxx} the integration of all the methyl pentads together (isotactic and non isotactic, from 21.3 to 19.4 ppm).[45] It results from equation (2.9) that PP-g-MA 3 exhibits an

isotacticity of 55 %, versus 98 % for the starting iPP. It means that a lot of stereogenic centers have been epimerized during the reaction.

Amongst the smaller peaks that are visible in Figure 2.22, some of them are assigned to grafted succinic anhydride units: the methylene carbon at 31.2 ppm, and the two carbonyl carbons at 169 and 171 ppm. These values fit well with the chemical shifts reported by Heinen et al. for propylene oligomers and polymers bearing grafted succinic anhydrides (^{13}C-enriched anhydrides in the case of the polymer).[18,41] According to the same authors, one more signal should however be observed at about 49.5 ppm, corresponding to the methyne carbon of the grafted anhydride. In the spectrum presented in Figure 2.22, this signal does not appear as a well resolved peak, but rather as a broad signal. This can be explained by the fact that the chemical shift of this carbon is more sensitive to variations in its chemical environment: isotactic and non-isotactic sequences (and therefore various conformations) coexist in the polymer, leading to slightly varying chemical shifts for this carbon. The same phenomenon was observed by Heinen et al., but for MA-grafted ethylene-propylene copolymers (differences in the chemical environment were then caused by the presence of the ethylene comonomer).[18] Careful phase and baseline corrections of the spectrum enabled us to estimate the concentration of grafted anhydrides by integration of the corresponding peaks at 31.2, 169 and 171 ppm. These three peaks gave similar integration values, and therefore similar estimations for the grafting yield, which is found to be 1 succinic anhydride per 100 propylene units (= 2.3 *wt.*%). Due to the limited sensitivity of the ^{13}C NMR technique,[46] the imprecision on the measure is probably more important than for titration or ^{1}H NMR techniques. It is however satisfactory to obtain similar concentrations of anhydride from both ^{1}H and ^{13}C NMR, as it further supports the hypothesis that the great majority of the grafted species have the

same structure, i.e. succinic anhydrides. This is also corroborated by the absence of any other peak in the carbonyl region.

Microstructure investigation – Viscosimetric Titration

The addition of a stoichiometric amount of m-xylylenediamine to molten PP-g-MA is a screening method to assess in-chain or end-chain grafting. Indeed, in-chain MA grafting leads, by reaction with diamine, to crosslinking while MA end-chain grafting leads to chain lengthening or to hyperbranched structures in case of poly(maleic anhydride) end-chain grafting. Reaction of a stoichiometric amount of diamine with PP-g-MA 3 in a Brabender internal mixer led to a drastic increase in motor torque as a result of polymer crosslinking. The resulting material was totally non-soluble in refluxing toluene. When a stoichiometric amount of diamine was added to molten PP-g-MA 1, a much weaker increase in torque was observed and the resulting product remained fully soluble into refluxing toluene. These observations are consistent with the FTIR observations reported earlier. The grafting mechanism and hence grafts structure and location are expected to be different whether or not a source of bromine radicals is present in the reactive medium. End-chain grafting of succinic anhydride units or oligomers is suggested in absence of NBS and in-chain grafting of isolated succinic rings when NBS is used.

Mechanistic considerations

Scheme 2.1 depicts the MA grafting route according to De Roover et al.[24]

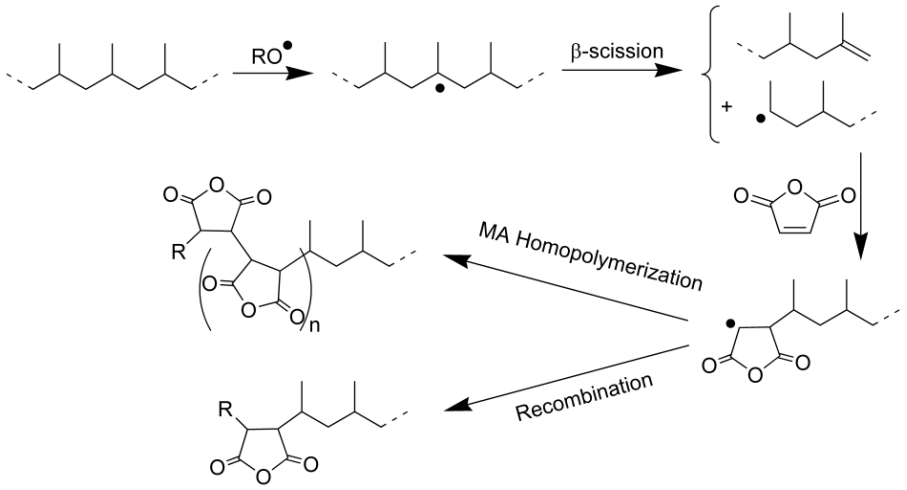

Scheme 2.1 : Grafting route according to De Roover et al.

According to these authors, PP macroradicals firstly undergo chain scission and grafting occurs afterwards on secondary macroradicals. The activated succinic units can either initiate the homopolymerization of maleic anhydride leading to oligomeric grafts, or recombine with another radical moiety. This mechanism implies that grafted moieties are exclusively located at chain ends.

Scheme 2.2 illustrates the grafting route according to Heinen et al.[18] which starts with anhydride grafting onto PP macroradicals prior to β-scission, leading to in-chain single succinic anhydride grafts.

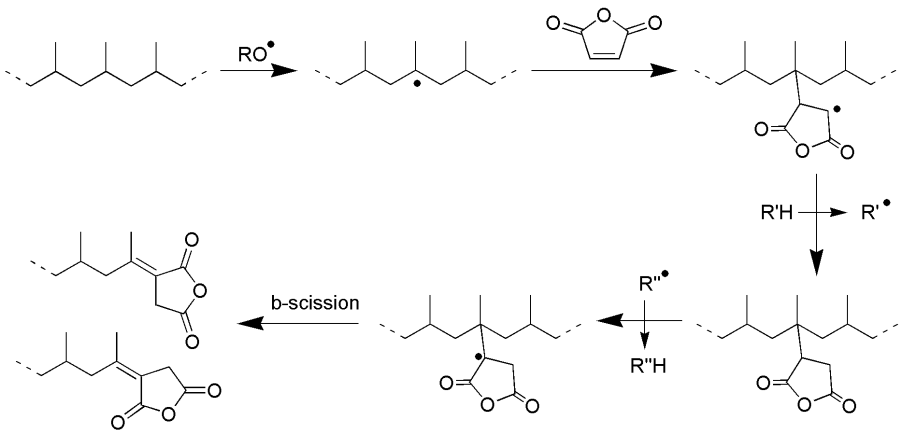

Scheme 2.2 : Grafting route according to Heinen et al.

These grafted moieties can be reactivated by hydrogen abstraction and promote chain scission. Itaconic structures would therefore be formed at chain ends as observed by NMR spectroscopy.

It has to be highlighted that these two reaction schemes cannot be readily compared because experimental conditions were not the same. Besides, each of these schemes has been mainly suggested on the basis of different characterization techniques (FTIR for Scheme 2.1, NMR for Scheme 2.2) but both techniques have never been used together to help discriminating the actual grafting mechanism.

Scheme 2.3 describes the assumed mechanism leading to epimerization and formation of a PP-g-MA elastomer from iPP, consistent with the experimental conditions used in the present work and the recorded analytical data.

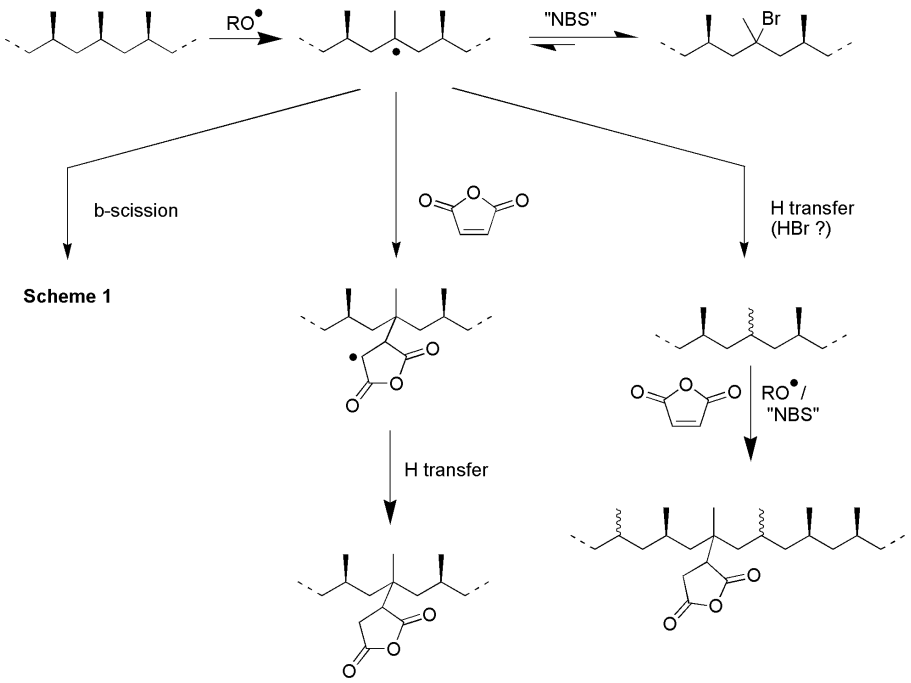

Scheme 2.3 : Suggested mechanism toward the production of a PP-g-MA elastomer

Present results seem to lead to a first step where peroxide primary radicals selectively abstract hydrogen atoms from tertiary carbons of the PP backbone. The resulting macroradicals have a great propensity to undergo degradation by β-scission. It has already been described in scheme 1 that grafting can occur at chain ends after chain breaking and hence this route cannot be discarded. However, in the presence of NBS, this tendency seems to be greatly reduced and it is postulated that bromine-containing species (Br radicals, Br_2 or HBr) issued from NBS decomposition are able to quench PP macroradicals in a reversible way. Dormant forms of PP macroradicals should therefore be created, decreasing the actual concentration of active radicals in the reactive medium and promoting grafting instead of chain scission. The formation of dormant radicals is common knowledge in controlled/living polymerization and is responsible of the lower occurrence of termination reactions which have a negative impact on polydispersity.[47]

This equilibrium between active and dormant forms of PP should temporarily and locally increase the polarity of the matrix and favor the approach of maleic anhydride and hence the efficiency of the grafting. Active forms of PP macroradicals can therefore undergo either β-scission, grafting of maleic anhydride or hydrogen transfer. The chain carrier is assumed to be bromohydric acid although this has not been demonstrated yet. The recombination of a planar macroradical with a hydrogen radical has an equiprobability to lead to retention or inversion of the tertiary carbon initial configuration. These epimerized PP chains can further be exposed to radical attack and undergo further epimerization or anhydride grafting and a PP-g-MA elastomer is thus obtained.

2.2.4 Conclusions

In this paper a process for obtaining a highly grafted PP-g-MA elastomer has been described. Grafting levels up to 2.5-3 *wt.%*, which represents an average of more than one grafted anhydride every 100 monomer units, could be achieved. This level of reaction allowed efficient characterization by ^{1}H as well as ^{13}C NMR, even without prior ^{13}C enrichment. NMR and FTIR investigations revealed that the grafts structure corresponds to isolated non-interacting succinic anhydride rings only. According to FTIR data and viscosimetric titrations, grafting is expected to be different whether or not NBS is present during the grafting process. In absence of NBS, single or interacting grafts (oligomers or closely grafted anhydride rings) are suspected to be located at or near the chain ends, hence avoiding the PP-g-MA to crosslink upon addition of a diamine. On the other hand, in the presence of NBS, in-chain grafting of single succinic anhydride moieties is suggested. Bromine radicals from NBS decomposition are assumed to be responsible for promoting grafting levels, preventing excessive degradation and simultaneously tuning the crystallinity of the

PP-g-MA via iPP backbone epimerization. The glass transition temperature is not noticeably affected by the PP modifications. A mechanistic study which uses an iPP small oligomer as model compound is currently under investigation in order to identify key intermediates and further optimize the process.

2.2.5 Acknowledgement

We thank La Région Wallone (programme "Recherche d'initiative") and FRIA for financial support. Pascal Van Velthem, Colette Douchamps, Mikhaël Vandeuren, François-Xavier Michel and Cédric Vanautgaerden are acknowledged for their contribution to the experimental work.

2.2.6 References and Notes

[1] Karger-Kocsis, J. In Polypropylene an A-Z reference; Karger-Kocsis, J., Eds.; Kluwer Publishers: Dordrecht, 1999, p 7-12.

[2] Moad, G. Prog Polym Sci 1999, 24, 81-142.

[3] Hu, G. H.; Flat, J. J.; Lambla, M. In Reactive Modifiers for Polymers; S.Al-Malaika, Eds.; Blackie Academic and Professional: London, 1997, p 1-83.

[4] Van Duin, M.; Machado, A. V.; Covas, J. Macromol Symp 2001, 170, 29-39.

[5] De Roover, B.; Devaux, J.; Legras, R. J Polym Sci, Part A: Polym Chem 1997, 35, 1313-1327.

[6] De Roover, B.; Devaux, J.; Legras, R. J Polym Sci, Part A: Polym Chem 1997, 35, 917-925.

[7] De Roover, B.; Devaux, J.; Legras, R. J Polym Sci, Part A: Polym Chem 1997, 35, 901-915.

[8] Van Duin, M.; Borggreve, R. J. M. In Reactive modifiers for Polymers; Al-Malaika, S., Eds.; Blackie Academic & Professional: London, 1997, p 133-162.

[9] Fedullo, N.; Sorlier, E.; Sclavons, M.; Bailly, C.; Lefebvre, J.-M.; Devaux, J. Prog Org Coat 2007, 58, 87-95.

[10] Yeh, P.-H.; Nien, Y.-H.; Chen, J.-H.; Chen, W.-C.; Chen, J.-S. Polym Eng Sci 2005, 45, 1152-1158.

[11] Wu, C. H.; Su, A. C. Polymer 1992, 33, 1987-1992.

[12] Gaylord, N. G.; Mishra, M. K. Journal of Polymer Science, Polymer Letters Edition 1983, 21, 23-30.

[13] Cartier, H.; Hu, G.-H. J Polym Sci, Part A: Polym Chem 1998, 36, 1053-1063.

[14] Flat, J.-J. In Nouveaux développements dans le greffage radicalaire sur polypropylène à l'état fondu. Ph.D. Thesis, Université Louis Pasteur, Strasbourg, Septembre 1991.

[15] Coiai, S.; Passaglia, E.; Aglietto, M.; Ciardelli, F. Macromolecules 2004, 37, 8414-8423.

[16] Shi, D.; Li, R. K. Y.; Zhu, Y.; Ke, Z.; Yin, J.; Jiang, W.; Hu, G.-H. Polym Eng Sci 2006, 46, 1443-1454.

[17] Bettini, S. H. P.; Agnelli, J. A. M. J Appl Polym Sci 2002, 85, 2706-2717.

[18] Heinen, W.; Rosenmoeller, C. H.; Wenzel, C. B.; de Groot, H. J. M.; Lugtenburg, J.; van Duin, M. Macromolecules 1996, 29, 1151-1157.

[19] Heinen, W.; Van Duin, M.; Rosenmoeller, C. H.; Wenzel, C. B.; De Groot, H. J. M.; Lugtenburg, J. Macromol Symp 1998, 129, 119-125.

[20] Rengarajan, R.; Parameswaran, V. R.; Lee, S.; Vicic, M.; Rinaldi, P. L. Polymer 1990, 31, 1703-1706.

[21] De Roover, B.; Devaux, J.; Legras, R. J Polym Sci, Part A: Polym Chem 1996, 34, 1195-1202.

[22] Hogt, A. Proceedings of the 46th Annual Technical Conference, Atlanta, 18-21 Apr. 1988, pp 1478-1480.

[23] Shi, D.; Yang, J.; Yao, Z.; Wang, Y.; Huang, H.; Jing, W.; Yin, J.; Costa, G. Polymer 2001, 42, 5549-5557.

[24] De Roover, B.; Sclavons, M.; Carlier, V.; Devaux, J.; Legras, R.; Momtaz, A. J Polym Sci, Part A: Polym Chem 1995, 33, 829-842.

[25] Sclavons, M.; Carlier, V.; De Roover, B.; Franquinet, P.; Devaux, J.; Legras, R. J Appl Polym Sci 1996, 62, 1205-1210.

[26] Sclavons, M.; Franquinet, P.; Carlier, V.; Verfaillie, G.; Fallais, I.; Legras, R.; Laurent, M.; Thyrion, F. C. Polymer 2000, 41, 1989-1999.

[27] Sclavons, M.; Laurent, M.; Devaux, J.; Carlier, V. Polymer 2005, 46, 8062-8067.

[28] Russel, K. E.; Kelusky, E. C. J Polym Sci, Part A: Polym Chem 1988, 26, 2273-2280.

[29] Hu, G.-H.; Flat, J.-J.; Lambla, M. In Reactive modifiers for Polymers; Al-Malaika, S., Eds.; Blackie Academic & Professional: London, 1997, p 1-83.

[30] Hogt, A. Compalloy '90, New Orleans, 1990, pp 179-193.

[31] Hu, G.-H.; Flat, J.-J.; Lambla, M. Annual Technical Conference - Society of Plastics Engineers, 1994, pp 2775-2778.

[32] Listner, G. J. (Johnson&Johnson). FR Patent 1,567,883, April 14, 1969.

[33] Listner, G. J.; Park, K. (Johnson&Johnson). U.S. Patent 3,511,824, May 12, 1970.

[34] Listner, G. J.; Park, K. (Johnson&Johnson). U.S. Patent 3,515,687, June 2, 1970.

[35] Listner, G. J.; Park, K.; Sampson, A. J. (Johnson&Johnson). U.S. Patent 3,547,870, December 15, 1970.

[36] Flat, J.-J. E.P. Patent 0,534,830 A1, 1993.

[37] Burfield, D. R.; Loi, P. S. T. J Appl Polym Sci 1988, 36, 279-293.

[38] Kissin, Y. V.; Rishina, L. A. Eur Polym J 1976, 12, 757-759.

[39] Stehling, F. C.; Knox, J. R. Macromolecules 1975, 8, 595-603.

[40] Measured in CDCl3 at room temperature

[41] Heinen, W.; Erkens, S. W.; Van Duin, M.; Lugtenburg, J. J Polym Sci, Part A: Polym Chem 1999, 37, 4368-4385.

[42] Busico, V.; Cipullo, R. Prog Polym Sci 2001, 26, 443-533.

[43] Busico, V.; Cipullo, R.; Monaco, G.; Vacatello, M.; Bella, J.; Segre, A. L. Macromolecules 1998, 31, 8713-8719.

[44] Busico, V.; Cipullo, R.; Monaco, G.; Vacatello, M.; Segre, A. L. Macromolecules 1997, 30, 6251-6263.

[45] The effect of the presence of anhydride units grafted on the backbone is not taken into account in this calculation, as their number is low enough to be neglected.

[46] The high grafting yield obtained in this work allowed us to be able to observe the anhydride signals in 13C NMR, which normally requires the use of expensive 13C-enriched maleic anhydride for the grafting reaction

[47] Greszta, D.; Mardare, D.; Matyjaszewski, K. Macromolecules 1994, 27, 638-644.

2.3 N-Bromosuccinimide Mediated Melt-Functionalization of Polyolefins

Drooghaag X.[a], Rousseaux D. D. J.[a], Sclavons M.[b], Carlier V.[b], Marchand-Brynaert, J.*[b]

[a]Unité de Chimie Organique et Médicinale, Université catholique de Louvain, Place L. Pasteur 1, B-1348 Louvain-la-Neuve, Belgium
[b]Unité de Chimie et de Physique des hauts Polymères, Université catholique de Louvain, Place Croix du Sud 1, B-1348 Louvain-la-Neuve, Belgium

Abstract

The grafting of polar monomers onto polyolefins is a very challenging process. Side reactions such as chain scission or crosslinking always compete with grafting and a compromise between the degree of functionalization and mechanical properties must be considered. This paper deals with the melt grafting of maleic anhydride (MA) onto polypropylene (PP) and high density polyethylene (HDPE) in the presence of N-bromosuccinimide as a mediator. Bromine radicals enable higher degrees of functionalization with limited side reactions.

2.3.1 Introduction

Melt grafting of polar molecules onto polyolefins is a well known process for improving the polarity and the reactivity of hydrophobic polymers. Nevertheless, those reactions are quite difficult to conduct because of the competing side reactions (i.e. chain scission and crosslinking) that greatly alter the processability of the grafted materials. Although the grafting mechanisms still remain a topic of controversy[1-3], it is generally accepted

that a compromise between grafting levels and appropriate molecular weights has to be considered. Polypropylene has a great tendency toward β-scission when peroxides are involved during reactive processing, rapidly leading to low molecular weight grafted waxes with poor mechanical properties. On the contrary, polyethylene quickly undergoes chain branching and crosslinking when processed in the presence of peroxides, leading to non-processable and non-soluble grafted materials. The use of additives such as electron donors has been suggested in the literature[4-7] to prevent crosslinking but much lower grafting levels were also observed.[8] It was demonstrated that the melt grafting of maleic anhydride in the presence of bromine radicals could hamper PP degradation to the benefit of higher grafting levels.[9] In this paper, the ability of NBS to mediate the grafting reaction onto HDPE by preventing crosslinking is presented and compared to a model grafting onto PP as a comparison reference. Mechanistic considerations are also discussed.

2.3.2 Experimental

Raw materials were Moplen HF500N propylene homopolymer, Eltex A4009 PFN 1324 HDPE (MFI 0.9 g/10' at 190 °C, 2.16 kg) and Purell GA7760 HDPE (MFI 18 g/10' at 190 °C, 2.16 kg). Two processing methods were used. Preliminary investigations were performed in a Brabender single screw extruder (D = 19mm, L/D = 20, compression ratio = 1) heated at 200 °C with a screw speed of 50 RPM, which correspond to a residence time of about 60 seconds. All reagents were manually pre-mixed and poured in the hopper of the extruder. Samples for the comparison between PP and PE graftings were processed in a Brabender kneader heated at 200 °C and 50 rpm. Purell GA7760 HDPE was ground to a coarse powder prior to reactive processing. HDPE was first introduced in the kneader until complete melting (2 minutes). The mixture of peroxide, NBS and maleic anhydride

was manually pre-mixed and then added in the kneader. The kneader was covered and flushed with a light nitrogen flow during 8 additional minutes. The peroxide was Luperox101 XLS50 provided by Arkema. N-bromosuccinimide (99 % purity) were provided by Sigma-Aldrich and maleic anhydride (98 % purity) was provided by Acros. Samples compositions are summarized in Table 2.11. After processing, PP samples were dissolved in refluxing toluene and precipitated in cold acetone. The anhydride contents were evaluated by acid-base titration according to a known procedure:[10] 1 g of washed polymer was dissolved in 150 ml of refluxing toluene. After complete dissolution, five drops of 1% w/v bromothymol blue in methanol were added and the solution was titrated by a 0.05N solution of tetrabutyl ammonium hydroxide (TBAOH). The titration was stopped when the color change was stable. The AM content was calculated from the volume and concentration of TBAOH. The grafts structures were determined by FTIR spectroscopy on compression-molded thin films. Spectra were recorded on a Nicolet-Nexus 670 apparatus, over a spectral range from 4000 to 400 cm^{-1}. Degradation of PP was assessed by high temperature size exclusion chromatography using two Styragel HT 6E and one Styragel HT 2 columns along with a differential refractometer and a viscosimeter. The mobile phase was 1,2,4-trichlorobenzene. The concentration of the sample was 2 mg/mL in TCB and dissolution was achieved by shaking at 160 °C for 1 h. Injection volume was 215 µL. Temperature was held constant at 145 °C throughout the analysis. The system was calibrated prior to the analysis with PS standards according to ISO 16014-2 specification. Crosslinking of HDPE was evaluated by Soxhlet extraction for 24 h in refluxing toluene. The crystallinity of the PP-g-MA's was evaluated on a Mettler Toledo DSC 821e module. A sample of about 5 mg of product was weighed and inserted into a 20 µL aluminum pan. The temperature program consisted of a first heating ramp from -20 °C to 220 °C followed by a cooling ramp from 220 °C to -20 °C and a second heating

ramp from -20 °C to 220 °C. The heating/cooling rate of each segment was 10 °C/min. The enthalpy of melting is calculated by the integration of the melting peak observed during the second heating ramp.

Table 2.11: Sample compositions

Sample	*Raw Material*	*method*	*wt.% Luperox*	*wt.% NBS*	*wt.% MA*	*Br/Ox*
PE-g-MA 1	Eltex	Extruder	0.5	0	5	0
PE-g-MA 2	Eltex	Extruder	0.5	2.2	5	10
PE-g-MA 3	Eltex	Extruder	0.5	4.4	5	20
PE-g-MA 5	Purell	kneader	2	0	5	0
PE-g-MA 6	Purell	kneader	2	1	5	1
PP-g-MA 1	Moplen	kneader	2	0	5	0
PP-g-MA 2	Moplen	kneader	2	1	5	1

2.3.3 Results

Preliminary investigations in single-screw extruder

In a first time, the effect of NBS on PE-g-MA flowability was evaluated on Eltex HDPE (PE-g-MA 1 to 3). As shown in Table 2.12, PE-g-MA 1 had a high anhydride content but no flowability at all. Extrusion was difficult to conduct as heavy crosslinking occurred during processing. Although the reactive extrusions of HDPE in the presence of NBS were easier to conduct, the obtained PE-g-MA's still had limited flowability and much lower anhydride contents. PE-g-MA's 2 and 3 had a dark brown color at the die exit whereas PE-g-MA 1 was only slightly yellowish. All these observations indicate a possible competition between anhydride and bromine grafting onto PE chains.

Table 2.12 : MFI and anhydride contents of the starting HDPE and PE-g-MA1 to 3

Sample	*MFI (g/10' at T/Load)*	*wt.% g-MA*
HDPE Eltex	36 (190 °C/21.6 kg)	0
PE-g-MA 1	Non flowable	2.3
PE-g-MA 2	0.5 (190 °C/21.6 kg)	1.2
PE-g-MA 3	7.0 (190 °C/21.6 kg)	1.1

Grafting onto polyethylene in reactive kneader

On the basis of these first results, it was decided to adapt the reactive conditions. MA grafting was performed on a HDPE with a higher starting MFI (Purell), in kneader and with optimized concentrations in peroxide and NBS. The concentration of peroxide had to be increased to 2 wt.% as Purell HDPE is stabilized whereas Eltex HDPE is not. As a competition between MA grafting and bromine grafting was suspected during the preliminary investigations, the concentration of NBS was decreased to 1 wt.% with respect to peroxide (Br/Ox = 1) in order to limit the extend of crosslinking without hampering the grafting reaction. In these conditions and in the absence of NBS, a fraction of 60 % of non-soluble material was recovered (Table 2.13, PE-g-MA 4). Lower grafting levels were observed compared to those obtained previously on Eltex HDPE, probably because Purell HDPE is a stabilized homopolymer. In the presence of NBS the fraction of non-soluble material that was recovered was only 25 % (Table 2.13, PE-g-MA 5) and enhanced grafting levels were observed as well.

Table 2.13 : anhydride contents and gel fractions of the PE-g-MA's

Sample	*wt.% MA*	*Gel fraction (%)*
HDPE (Purell)	/	0
PE-g-MA 4	1.22	60
PE-g-MA 5	1.47	25

FTIR spectra of those two PE-g-MA's were similar in shape and confirmed the higher grafting level in the presence of NBS. (Figure 2.24, spectrum C and D). In agreement with the literature,[11-14] two carbonyl absorption bands could be observed on the spectra : 1791 cm^{-1} (paired with the band at 1864 cm^{-1}) and 1784 cm^{-1}. The corresponding grafted structures were assigned on the basis of previous knowledge established on polypropylene to grafted succinic anhydride and grafted poly(maleic anhydride) (PMA), as small oligomers or closely grafted interacting rings, respectively (*vide infra*).

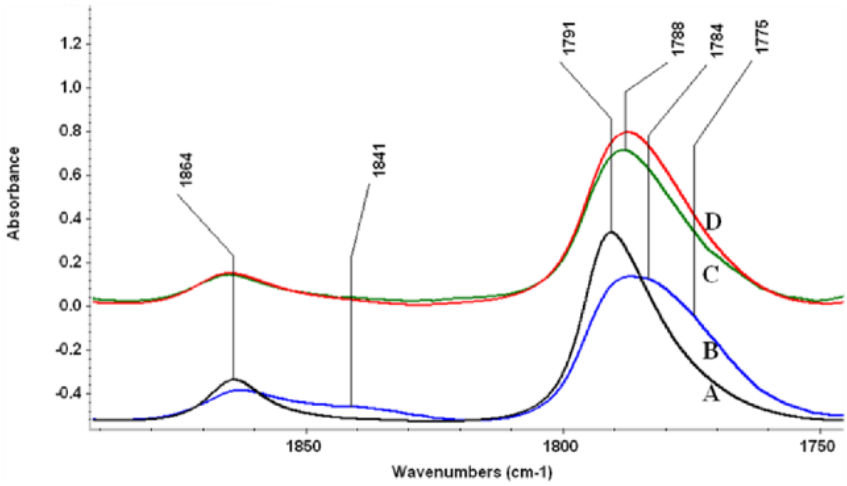

Figure 2.24 : Enlargement of the carbonyl region of the PP- and PE-g-MA's. A : PP-g-MA with NBS, B : PP-g-MA without NBS, C : PE-g-MA without NBS, D: PE-g-MA with NBS.

Grafting onto polypropylene in internal mixer

As shown in Table 2.14, the melt grafting of MA onto iPP induced heavy degradation (PP-g-MA 1). Lower grafting levels were achieved with respect to PE, as stated in the literature.[15-17] On the contrary, NBS efficiently mediated the grafting of maleic anhydride (PP-g-MA 2): the anhydride

content was higher and degradation was limited compared to the PP-g-MA 1. The crystallinity of the grafted polypropylene was also greatly reduced. The FTIR spectra of the two PP-g-MA's revealed that NBS also affected the chemical structure of the grafted moieties. Several structures coexisted in PP-g-MA 1 as multiple absorption bands could be observed (Figure 2.24, spectrum B): 1791/1864 cm^{-1} : grafted succinic anhydride rings,[9,18,19] 1784 cm^{-1} : grafted poly(maleic anhydride) (PMA) as small oligomers or closely grafted interacting rings,[14,19,20] 1775/1841 cm^{-1} : grafted unsaturated anhydride rings (maleic rings as will be explained in chapter 3.1 but itaconic rings have been suggested as well in the literature by other authors[1-4]). Conversely the proportion of saturated rings drastically increased in the presence of NBS (Figure 2.24, spectrum A). It must be pointed out that the bands at 1775/1841 cm^{-1} only appeared when MA was grafted onto PP but not onto HDPE. This is also in agreement with the literature.[11-13,22]

Table 2.14 : Anhydride contents and molecular weights of the PP-g-MA's

Sample	*wt.% g-MA*	*Mn (Da)*	*Mw(Da)*	*PDI*	*ΔH_m (J/g)*
iPP	/	49000	230000	4.68	111
PP-g-MA 1	0.9	22500	50500	2.25	108
PP-g-MA 2	1.23	31300	80900	2.82	39

2.3.4 Mechanistic considerations

The ability of bromine radicals issued from the thermal decomposition of NBS to mediate the grafting of maleic anhydride onto PP has already been described in a previous paper.[9,23] As depicted in Figure 2.25, the mediation mechanism is three-fold: (i) the reversible trapping of the PP macroradicals allowing higher grafting levels and higher molecular weight by decreasing the concentration of instantaneous concentration of PP macroradicals; (ii) the racemization of the PP backbone by fast hydrogen exchange with HBr;[23] (iii)

the control of the grafts structure by fast termination of the grafted anhydride rings by hydrogen donation from HBr preventing maleic anhydride oligomerization.

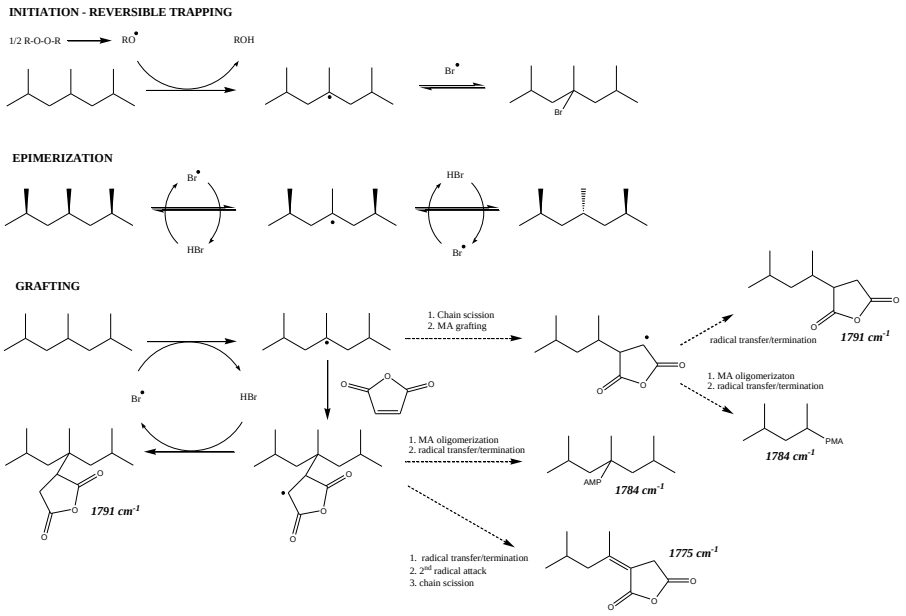

Figure 2.25 : Suggested mechanisms for the radical grafting of maleic anhydride onto PP mediated by NBS

This work demonstrates that the situation is different for HDPE. NBS did not affect the grafting reaction itself as the shape of the FTIR spectra remained identical. Relatively broad bands were observed as both single succinic anhydrides and oligomers were grafted on HDPE. It seems therefore that bromine radicals operate in a different way when exposed to tertiary (PP) or secondary (HDPE) macroradicals. Reversible trapping and hydrogen transfer are less likely to happen on HDPE as secondary hydrogen atoms are much less reactive than tertiary ones. Therefore, bromine radicals act as non-reversible radical traps for HDPE macroradicals, hampering crosslinking to the benefit of grafting. As no HBr was created during reactive processing, no

hydrogen donation was possible to promote the saturated anhydride structure as observed on PP (Figure 2.26).

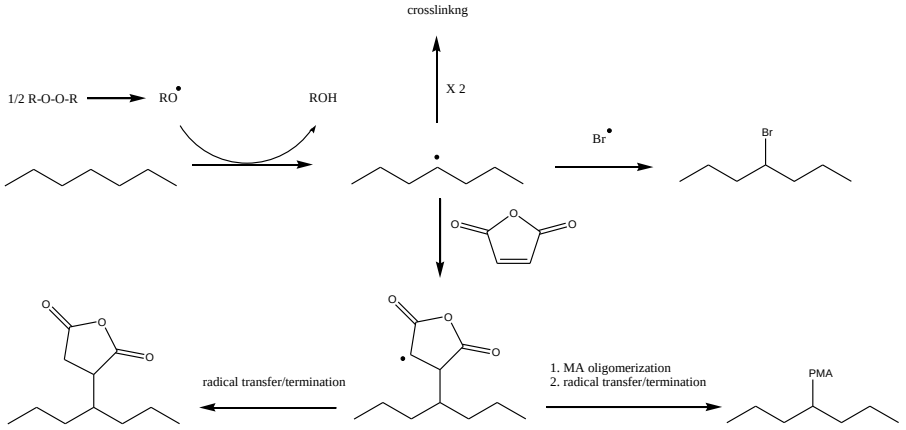

Figure 2.26 : mechanisms for the radical grafting of maleic anhydride onto HDPE in the presence of NBS

2.3.5 Conclusions

NBS-mediated grafting of maleic anhydride onto polypropylene and high density polyethylene leads to materials with enhanced properties: a higher degree of functionalization as well as limited side reactions. However, NBS does not operate in the same way on both polyolefins. Reversible hydrogen abstraction on PP leads to a highly-grafted low-crystallinity polypropylene with controlled graft structure (mainly saturated anhydride rings) whereas non-reversible macroradical trapping is suspected on HDPE, preventing chain crosslinking to the benefit of grafting. The shape of the FTIR spectra provided crucial information regarding the control of the grafts structure. Hydrogen transfer from polypropylene to the grafted anhydride rings leads to a high proportion of grafted saturated rings. The similarity between the grafts structures in the presence or in the absence of NBS confirms that hydrogen abstraction/transfer from polyethylene chains is not possible.

2.3.6 Acknowledgement

The authors thank FRIA (Fonds pour la Recherche dans l'Industrie et l'Agriculture, FRS-FNRS, Belgium) for financial support. J.Marchand-Brynaert is Senior Research Associate of the FRS-FNRS (Fond National de la Recherche Scientifique, Belgium).

2.3.7 References

[1] G. Moad. The synthesis of polyolefin graft copolymers by reactive extrusion, Progress in Polymer Science,24 (1999) 81-142.

[2] K. E. Russel. Free radical graftpolymerization and copolymerization at higher temperatures, Prog Polym Sci,27 (2002) 1007-1038.

[3] G.-H. Hu; J.-J. Flat; M. Lambla. In Reactive modifiers for Polymers; Al-Malaika, S., Eds.; Blackie Academic & Professional: London, 1997,1, pp 1-83.

[4] Gaylord N.G.; Mehta M. Role of homopolymerization in the peroxide-catalysed reaction of maleic anhydride and polyethylene in the absence of solvent, Journal of Polymer Science : Polymer Letters Edition,20 (1982) 481-486.

[5] Gaylord N.G.; Mehta R. Peroxide-catalysed grafting of maleic anhydride onto molten polyethylene in the presence of polar organic compounds, Journal of Polymer Science : Part A : Polymer Chemistry,26 (1988) 1189-1198.

[6] Gaylord N.G.; Mehta R.; Kumar V.; Tazi M. High density polyethylene-g-maleic anhydride preparation in presence of electron donoors, Journal of Applied Polymer Science,38 (1989) 359-371.

[7] Gaylord N.G.; Mehta R.; Mohan D.R.; Kumar V. Maleation of linear low-density polyethylene by reactive processing, Journal of Applied Polymer Science,44 (1992) 1941-1949.

[8] H. R. Z. Sheshkali; H. Assempour; H. Nazockdast. Parameters Affecting the Grafting Reaction and Side Reactions involved in the Free-Radical Melt Grafting of Maleic Anhydride onto High-Density Polyethylene, J Appl Polym Sci,105 (2007) 1869-1881.

[9] G. Henry; X. Drooghaag; D. D. J. Rousseaux; M. Sclavons; J. Devaux; J. Marchand-Brynaert; V. Carlier. A Practical Way of Grafting Maleic Anhydride onto Polypropylene Providing High Anhydride Contents Without Sacrificing Excessive Molar Mass, J Polym Sci, Part A: Polym Chem,46 (2008) 2936-2947.

[10] M. Sclavons; P. Franquinet; V. Carlier; G. Verfaillie; I. Fallais; R. Legras; M. Laurent; F. C. Thyrion. Quantification of the maleic anhydride grafted onto polypropylene by chemical and viscosimetric titrations, and FTIR spectroscopy, Polymer,41 (2000) 1989-1999.

[11] W. Heinen; S. W. Erkens; M. Van Duin; J. Lugtenburg. Model compounds and 13C NMR increments for the characterization of maleic anhydride-grafted polyolefins, J Polym Sci, Part A: Polym Chem,37 (1999) 4368-4385.

[12] W. Heinen; C. H. Rosenmoeller; C. B. Wenzel; H. J. M. de Groot; J. Lugtenburg; M. van Duin. 13C NMR Study of the Grafting of Maleic Anhydride onto Polyethene, Polypropene, and Ethene-Propene Copolymers, Macromolecules,29 (1996) 1151-1157.

[13] W. Heinen; M. Van Duin; C. H. Rosenmoeller; C. B. Wenzel; H. J. M. De Groot; J. Lugtenburg. 13C NMR study of the grafting of 13C labeled maleic anhydride onto PE, PP, and EPM, Macromol Symp,129 (1998) 119-125.

[14] M. Van Duin. Production, structure and application of maleic-anhydride-grafted polyolefins, Recent Research Developments in Macromolecules,7 (2003) 1-28.

[15] Machado A.V.; Covas J.A.; Van Duin M. A Study of Grafting Reactions During Processing of Polyolefins, Advances in Polymer Technology,23 (2004) 196-210.

[16] M. Van Duin; A. V. Machado; J. Covas. A look inside the extruder: evolution of chemistry, morphology and rheology along the extruder axis during reactive processing and blending, Macromol Symp,170 (2001) 29-39.

[17] Machado A.V.; Covas J.A.; Van Duin M. Effect of polyolefin structure on maleic anhydride grafting, Polymer,42 (2001) 3649-3655.

[18] B. De Roover; M. Sclavons; V. Carlier; J. Devaux; R. Legras; A. Momtaz. Molecular characterization of maleic anhydride-functionalized polypropylene, J Polym Sci, Part A: Polym Chem,33 (1995) 829-842.

[19] M. Sclavons; V. Carlier; B. De Roover; P. Franquinet; J. Devaux; R. Legras. The anhydride content of some commercial PP-g-MA: FTIR and titration, J Appl Polym Sci,62 (1996) 1205-1210.

[20] B. De Roover; J. Devaux; R. Legras. Maleic anhydride homopolymerization during melt functionalization of isotactic polypropylene, J Polym Sci, Part A: Polym Chem,34 (1996) 1195-1202.

[21] X. Drooghaag; D. D. J. Rousseaux; G. Henry; M. Sclavons; V. Carlier; J. Marchand-Brynaert. Mediated Melt Functionalization of Polypropylene, Polym Degrad Stab,95 (2010) 342-345.

[22] Van Duin M. Grafting of Polyolefins with Maleic Anhydride: Alchemy or Technology?, Macromolecular Symposia,202 (2003) 1-10.

[23] G. R. P. Henry; X. Drooghaag; M. Vandeuren; M. Sclavons; A. Schanck; J. devaux; V. Carlier; J. Marchand-Brynaert. Controlled Reduction of Polypropylene Isotacticity and Crystallinity by Epimerization During Reactive Processing, J Polym Sci, Part A: Polym Chem,47 (2009) 4505-4518.

Chapter Three

Potential Substitutes for

N-bromosuccinimide

This chapter is devoted to the research of other mediating molecules as substitutes for bromine radicals. The results are presented as a full paper published in the Journal "Polymer Degradation and Stability" edited as a special issue after the 5th MoDeSt International Conference held in Liege, Belgium. The paper compares the ability of several molecules to mediate the grafting of maleic anhydride on iPP in the same reaction conditions with respect to NBS. A few additional results that further explore nitroxides as mediators are also presented after the paper, in section 5.1.5. As many of those mediators were borrowed from controlled radical polymerization (CRP) techniques, a brief summary of the mechanisms involved in CRP is presented in a foreword to this chapter. I was fully in charge of this chapter. However, the reactive extrusions (single step extrisions only, with each substitute) and most of the characterization of the obtained materials was performed by Geoffroy Le Hardÿ during his high school graduation work and under my supervision.I was in charge of writing and submitting the paper.

Foreword

Controlled/living radical polymerization

The concept of "living" polymerization was first introduced by Zwarc in 1956.[1] A living polymerization is defined as a chain growing process where transfer and termination reactions are excluded. This allows the synthesis of block copolymers and the control of the nature of the chain extremities but does not imply controlled molecular weight and narrow weight distribution. To achieve such a control, two additional criteria must be fulfilled: the initiator must be consumed as fast as possible and exchange reactions between reactive species must be much faster than propagation. Therefore "controlled" polymerization does not preclude the occurrence of transfer and termination reactions but they should take place to such a low extent that they do not interfere with the control of the polymer molecular structure. An ideal controlled/living polymerization implies that (i) all the chains propagate simultaneously and remain active after all the monomer has been consumed and reactivate the polymerization upon addition of a second monomer (block copolymers), (ii) The number of active chains and hence the concentration of active species remains constant throughout the polymerization. Mechanical and kinetic aspects of the different controlled radical polymerization techniques are reviewed in the literature.[2-4] The techniques of interest that meet the scope of this Thesis will be briefly introduced for the novice reader.

The concept of INIFERTER

INIFERTERS represent the first class of molecules involved in controlled radical polymerization.[5] They are commonly thiuram disulfide-based molecules or dithiocarbamates and simultaneously act as initiators (INI), transfer agents (FER) and terminators (TER). The general mechanism on polymerization is described in figure 3.8.

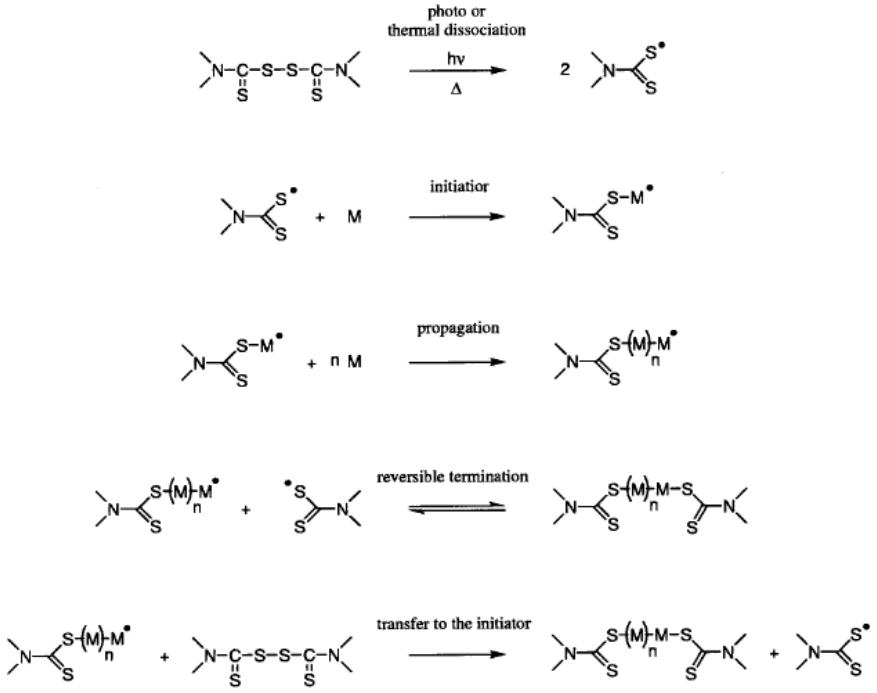

Figure 3.8 : General mechanism of INIFERTER-mediated polymerization

The process starts with photo-induced or thermal cleavage of the S-S bond creating two dithiocarbamyl radicals. These radicals initiate the polymerization and mediate the polymerization by reversible termination with the growing chains, keeping the concentration of propagating radicals as low as possible. Transfer to the initiator can also occur and maintains the polymerization process. Because of this transfer to the initiator, this type of polymerization is clearly not actually living as all the chains do not grow simultaneously. However some degree of control of the molecular weight can be achieved. Non-symmetrical INIFERTERS such as benzyl diethyldithiocarbamate are preferred for a better control of the polymerization. Upon heating, a benzyl radical will be created together with a dithiocarbamyl radical. The former will initiate the polymerization and the

latter will reversibly terminate the growing chains. Tetramethylthiuram disulfide (TMTDS) is often added as an additional transfer agent.

The reaction of main interest here is the reversible coupling of dithiocarbamyl radicals with propagating carbon-centered radicals and this property will be investigated in the conditions of reactive extrusion. Such thiuram disulfide compounds are also widely used as vulcanization accelerators in combination with zinc oxide.[6,7]

Nitroxide mediated polymerization (NMP)

NMP was invented at CSIRO (Commonwealth Scientific and Industrial Research Organization) in the mid 1980's.[8-9] The technique relies on the persistent radical effect (PRE)[10,11] between a transient propagating radical and a persistent radical, namely a nitroxide. The general mechanism of NMP is depicted in Figure 3.9.[12,13]

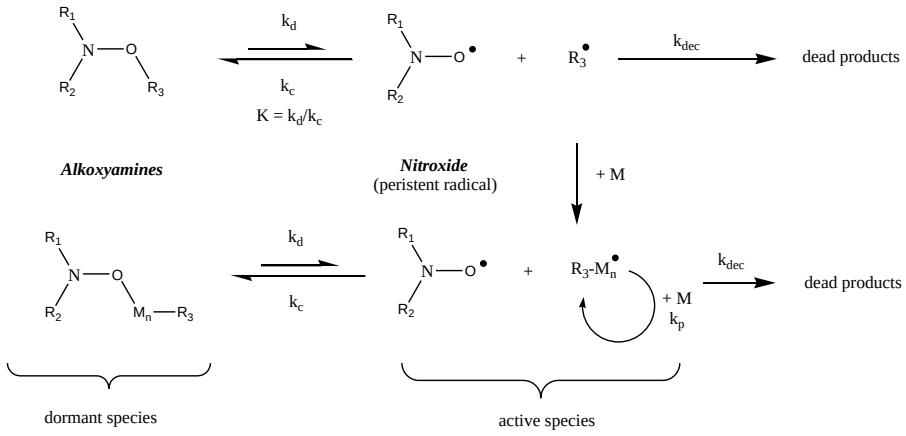

Figure 3.9 : General mechanism of NMP

The initiation starts with the reversible thermal C-ON bond dissociation of an alkoxyamine (k_d) which creates a transient carbon-centered radical $R_3^{\bullet}$ and a persistent nitroxide radical at the same rate. $R_3^{\bullet}$ can evolve in different directions: it can either recombine with the nitroxide back to the original

alkoxyamine (k_c); self-terminate with another transient radical (dimerization or disproportionation, k_{dec}), leading to dead products; or propagate by monomer addition (k_p). As the persistent radical is unable to self-terminate, the only possible route is the cross-reaction with the carbon-centered radicals. Because of the lack of termination of the nitroxide, an excess in persistent radicals rapidly builds up as time goes on. This accelerates the cross-coupling reaction between transient and persistent radicals, and shifts the equilibrium in favor of the dormant state. This cross-coupling reaction is therefore very selective, keeping the concentration of active species so low that termination of the transient radicals becomes unlikely. As the structure of the alkyl moiety $R_3^{\bullet}$ of the starting alkoxyamine is usually chosen as similar as possible to the propagating radical $R_M^{\bullet}$, their reactivities toward the nitroxide are quite similar (same K_d and K_c). As a consequence, $R_3^{\bullet}$ can add monomer and propagate during the short period of the active state. In this way, the growth of the polymer chain is expected to occur without termination, except for a very short period after the initiation (when there is no excess in persistent radical yet). The first example of styrene polymerization using NMP were conducted in the presence of a conventional radical initiator such as a peroxide and a free nitroxide, commonly 2,2,6,6-tetramethylpiperidine-1-oxyl (TEMPO).[8] Similarly, polymerization of styrene can also be initiated thermally, i.e. in the absence of initiator, and controlled by the addition of TEMPO. However, unimolecular initiators (alkoxyamines) are largely preferred and almost used exclusively nowadays.[14-17] The polymerization is defined as "living" in the sense that it will stop when the monomer is depleted and can be further re-initiated after additional monomer feed. The synthesis of block/graft copolymers is therefore possible. For successful control and livingness in NMP, the reactivity of the persistent radical must be tuned so that the equilibrium K between the propagating and the dormant chains is much faster than monomer conversion so that every chain grows simultaneously. The

equilibrium is thus largely in favor of the dormant state. This makes the polymerization rate very slow. Besides, one must keep in mind that the termination of propagating chains cannot be totally precluded and therefore the concentration of nitroxide keeps rising up during the polymerization and will ultimately inhibit it.

As stated above, the key parameter for successful NMP is the equilibrium constant K between the dormant alkoxyamine and the propagating radical. The strength of the C-ON bond of the alkoxyamine is therefore a very critical factor that strongly depends on the chemical structure of both the nitroxide and the leaving radical.

Reversible Addition-Fragmentation Chain Transfer Polymerizaton (RAFT)

The RAFT polymerization in based on radical chain transfer through successive addition/fragmentation steps involving a chain transfer agent (CTA) that bears a stabilizing group Z and a leaving group R.[18-21] The RAFT process is illustrated in Figure 3.10. After initiation, the addition of a growing chain on a dithioester-based CTA creates an intermediate adduct radical that is stabilized through the Z moiety. This intermediate further evolves through the fragmentation of the S-R bond, releasing the activated leaving group R (pre-equilibirum step). Re-initiation of the polymerization occurs until the new growing chain adds back to a thiocarbonylthio group that will release a dormant chain that will reactivate the polymerization and so on. The control of the polymerization is therefore achieved through the transfer of the thiocarbonylthio group from one chain to another.

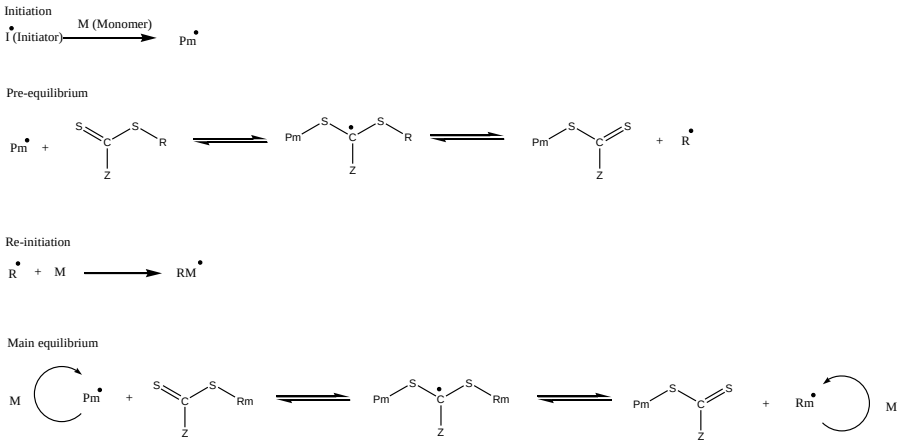

Figure 3.10 : The RAFT process

For an efficient RAFT polymerization, the release of the leaving group R in the pre-equilibrium step should be largely favored over re-fragmentation of the growing chain. Also, the R moiety should be able to rapidly and selectively initiate a new polymer chain. Concerning the main equilibrium, the structure of the CTA (Z and R groups) is of course critical and are dependent on the monomer and reaction conditions.[20-21] The Z group plays a major role in activating/deactivating the C=S double bound and therefore has a crucial impact on the addition rate. Z substituents with lone pairs directly conjugated with the C=S double bound have low transfer coefficient but additional electron withdrawing groups (such as dithiocarbamates) can enhance the reactivity of the RAFT CTA. The fragmentation ability of the R group depends on its own structure (stability of the leaving radical) but also on the (un)stability of the intermediate adduct radical and therefore also on the structure of the Z group. Steric factors, radical stability and polar effect all appear important in the fragmentation ability of R.

References

[1] Szwarc, M. *Nature* **1956,** 178, 1168-9.

[2] Braunecker, W. A.; Matyjaszewski, K. *Progress in Polymer Science* **2007,** 32, 93-146.

[3] Goto, A.; Fukuda, T. *Progress in Polymer Science* **2004,** 29, 329-385.

[4] Moad, G.; Rizzardo, E.; Thang, S. H. *Accounts of Chemical Research* **2008,** 41, 1133-1142.

[5] Otsu, T. *Journal of Polymer Science, Part A: Polymer Chemistry* **2000,** 38, 2121-2136.

[6] Nieuwenhuizen, P. J. *Applied Catalysis, A: General* **2001,** 207, 55-68.

[7] Nieuwenhuizen, P. J.; Ehlers, A. W.; Haasnoot, J. G.; Janse, S. R.; Reedijk, J.; Baerends, E. J. *Journal of the American Chemical Society* **1999,** 121, 163-168.

[8] Georges, M. K.; Veregin, R. P. N.; Kazmaier, P. M.; Hamer, G. K. *Macromolecules* **1993,** 26, 2987-8.

[9] Solomon, D. H. *Journal of Polymer Science, Part A: Polymer Chemistry* **2005,** 43, 5748-5764.

[10] Fischer, H. *Macromolecules* **1997,** 30, 5666-5672.

[11] Fischer, H. *Chemical Reviews* **2001,** 101, 3581-3610.

[12] Hawker, C. J.; Bosman, A. W.; Harth, E. *Chemical Reviews (Washington, D. C.)* **2001,** 101, 3661-3688.

[13] Studer, A.; Schulte, T. *Chemical Record* **2005,** 5, 27-35.

[14] Hawker, C. J. *Journal of the American Chemical Society* **1994,** 116, 11185-6.

[15] Hawker, C. J.; Barclay, G. G.; Orellana, A.; Dao, J.; Devonport, W. *Macromolecules* **1996,** 29, 5245-5254.

[16] Miura, Y.; Hirota, K.; Moto, H.; Yamada, B. *Macromolecules* **1998,** 31, 4659-4661.

[17] Miura, Y.; Hirota, K.; Moto, H.; Yamada, B. *Macromolecules* **1999,** 32, 8356-8362.

[18] Chiefari, J.; Chong, Y. K.; Ercole, F.; Krstina, J.; Jeffery, J.; Le, T. P. T.; Mayadunne, R. T. A.; Meijs, G. F.; Moad, C. L.; Moad, G.; Rizzardo, E.; Thang, S. H. Macromolecules 1998, 31, 5559-5562.

[19] Chiefari, J.; Mayadunne, R. T. A.; Moad, C. L.; Moad, G.; Rizzardo, E.; Postma, A.; Skidmore, M. A.; Thang, S. H. Macromolecules 2003, 36, 2273-2283.

[20] Chong, Y. K.; Krstina, J.; Le, T. P. T.; Moad, G.; Postma, A.; Rizzardo, E.; Thang, S. H. Macromolecules 2003, 36, 2256-2272.

[21] Favier, A.; Charreyre, M.-T. Macromolecular Rapid Communications 2006, 27, 653-692.

3.1 Mediated Melt Functionalization of Polypropylene

Drooghaag X.[a], Rousseaux D.J.[a], Henry G.R.P.[a], Sclavons M.[b], Carlier V.[b], Marchand-Brynaert, J.[a]*

[a]Université catholique de Louvain, Unité de Chimie Organique et Médicinale, Place Louis Pasteur 1, B-1348 Louvain-la-Neuve, Belgium

[b]Université catholique de Louvain, Unité de Physique et de Chimie des Hauts Polymères, Place Croix du Sud 1, B-1348 Louvain-la-Neuve, Belgium

Published as Polym. Degrad. Stab. ***2010****, 95, 342-345.*

Abstract

This paper investigates the ability of several kinds of molecules to mediate the melt-functionalization of polypropylene. N-Bromosuccinimide, nitroxides, iniferters, thiols and RAFT chain transfer agents were tested as potential mediators. The grafting of maleic anhydride onto polypropylene was carried out with and without mediator and the grafted polymers were discussed in terms of graft content, graft structure and molecular weights.

3.1.1 Introduction

The radical functionalization of polypropylene by reactive extrusion is a very challenging industrial process. The occurrence of side reactions such as chain scission makes the grafting process quite critical for the production of grafted polymers with high graft contents while preserving the mechanical properties or processability.[1-3] Besides, it is also very challenging to control the chemical structure of the grafts during processing and the co-existence of several types of grafts is usually observed in commercial products.[4] Many coagents have been suggested to enhance the grafting levels without altering

the molecular weights. Although many of these methods have been extensively investigated,[5,6] some of them have been mainly described in the patent literature and accurate characterization of the grafted products is often lacking. For instance, the ability of nitroxides such as 2,2,6,6-tetramethylpiperidine-1-oxyl (TEMPO) to reversibly trap carbon-centered radicals, according to the persistent radical effect,[7] has already been applied to the production of controlled-rheology polypropylene[8] and functionalized polypropylene.[9] However, those patents were barely convincing and no spectroscopic characterization of the grafted polymer was shown. Thiuram disulfide derivatives (called iniferters)[10] have also been investigated as potential mediators for the grafting of multifunctional monomers onto PP[11] but, as will be discussed in more details later on, the suggested mechanism might be controversial (*vide infra*).

In this paper, the effect of several coagents whose behaviors are still unclear with respect to PP functionalization is described. TEMPO (Figure 3.1, structure **1**), *tert*-dodecanethiol (^{t}DSH - Figure 3.1, structure **2**), tetramethylthiuram disulfide (TMTDS - Figure 3.1, structure **3**), benzyl dithiobenzoate (BDTB - Figure 3.1, structure **4**) and N-bromosuccinimide (NBS - Figure 3.1, structure **5**) were investigated as potential coagents and the modified polymers were compared in terms of graft content, graft structure and molecular weights. The molecular structures of these mediators are illustrated in Figure 3.1.

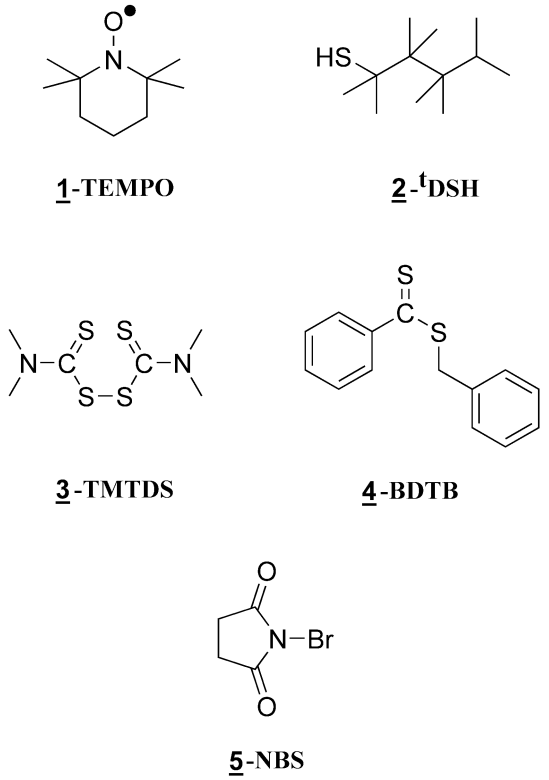

Figure 3.1 : Structures of the mediators - 1: TEMPO, 2: *tert*-dodecanethiol, 3: tetramethylthiuram disulfide, 4: benzyl dithiobenzoate, 5: N-bromosuccinimide

3.1.2 Experimental

Materials

Raw isotactic polypropylene was Moplen HF500N propylene homopolymer from Basell. Maleic anhydride (99 % purity), N-bromosuccinimide (99 % purity) and TEMPO (98 % purity) were supplied by Acros. Phosphorous pentasulfide, benzylmercaptan and benzoic acid were 99 % purity and supplied by Aldrich. *Tert*-dodecanethiol was 98.5 % purity and supplied by Aldrich as a mixture of isomers. TMTDS was 97 %

purity and also supplied by Aldrich. Free radical initiator was Luperox 101XLS50 from Arkema (2,5-bis(*tert*-butylperoxy)-2,5-dimethylhexane (DHBP), 50 wt.% blend with silica). Toluene was analytical grade. Benzyl dithiobenzoate was synthesized according to a known procedure.[12] All reagents were used without further purification.

Reactive extrusion

Reactive extrusions were performed on a Brabender single screw extruder heated at 200 °C all along the screw axis. The screw speed was set to 30 rpm which implies a residence time of 90 seconds. A mixture of polypropylene, peroxide, maleic anhydride and mediator was thoroughly dry-mixed until complete homogenization and inserted in the hopper of the extruder. The grafted polymers were poured into cold water and pelletized when possible.

Sample characterization

Prior to any analysis, a sample of about 3 g of crude product was dissolved into refluxing toluene and precipitated into a large excess of cold acetone, filtered and dried under vacuum at 90 °C overnight. Anhydride contents were determined according to a known procedure:[13] 1 g of washed polymer was dissolved in 150 ml of refluxing toluene. After complete dissolution, five drops of 1% w/v bromothymol blue in methanol were added and the solution was titrated by a 0.05N solution of tetrabutyl ammonium hydroxide (TBAOH). The titration was stopped when the color change was stable. The AM content was calculated from the volume and concentration of TBAOH. FTIR spectra were recorded from compression-molded films on a Nicolet - Nexus 670 FT-IR apparatus, from 4000 cm^{-1} to 400 cm^{-1} with a resolution of 2 cm^{-1}. Baselines were corrected manually and the height of the peak at 973 cm^{-1} (used as a reference) was set to 1 A.u for comparison purposes. Molecular weights were determined by high temperature gel

permeation chromatography on a Waters Alliance GPCV 2000 equipped with two Styragel HT 6E and one Styragel HT 2 columns along with a differential refractometer. The mobile phase was 1,2,4-trichlorobenzene (TCB). The concentration of the sample was 2 mg/mL in TCB and dissolution was achieved by shaking at 160 °C for 1 h. Injection volume was 215 µL. Temperature was held constant at 145 °C throughout the analysis. The system was calibrated prior to the analysis with PS standards according to ISO 16014-2 specification.

3.1.3 Results and discussion

Table 3.1 gathers the composition of all the samples together with their anhydride contents and GPC measurements. A blank PP-g-MA was extruded without any mediator, as a reference for all the experiments that are discussed in this paper. In this table, the concentrations of peroxide and maleic anhydride are expressed in weight percentage (2 wt.% and 5 wt.%, respectively) as it is widely used in the literature and in the industrial world. However, it would not be reasonable to simply use the weight percentage of the mediators as the screening parameter for their relative efficiency as their molecular weight and functionality differ from one to another. Therefore, to assess the efficiency of the mediating species, the amount of mediator introduced in the reactive mixture was determined on the basis of the ratio between the molar concentration of the mediating radicals ($M^{\bullet}$) issued from the mediator and the molar concentration of alkoxy radicals ($RO^{\bullet}$) issued from the peroxide.

Table 3.1 : Sample compositions, grafting levels and molecular weights

Sample	*wt.% DHBP*	*wt% MED.*	*wt% MA*	*$M^{\bullet}/RO^{\bullet}$*	*wt% g-MA*	*Mn (Da)*	*Mw (Da)*	*PDI*
iPP	0	0	0	-	0	75300	239400	3.18
Blank PP-g-MA	2	0	5	-	1.14	21900	46300	2.11
PP-g-MA NBS 1	2	0.24	5	0.20	2.18	39700	93500	2.36
PP-g-MA NBS 2	2	0.49	5	0.50	2.62	44100	110400	2.50
PP-g-MA NBS 3	2	0.73	5	1.00	1.27	46400	136600	2.94
PP-g-MA NBS 4	2	1.22	5	2.00	0.61	48800	151000	3.10
PP-g-MA TEMPO 1	2	0.43	5	0.20	0.76	41700	102400	2.46
PP-g-MA TEMPO 2	2	1.07	5	0.50	0.70	46100	126700	2.75
PP-g-MA TEMPO 3	2	2.15	5	1.00	0.56	53900	170800	3.17
PP-g-MA TMTDS 1	2	0.13	5	0.08	1.26	20500	44000	2.14
PP-g-MA TMTDS 2	2	0.33	5	0.20	1.17	20000	47000	2.36
PP-g-MA TMTDS 3	2	0.66	5	0.40	1.11	47200	127300	2.69
PP-g-MA TMTDS 4	2	1.32	5	0.80	0.93	54900	154600	2.81
PP-g-MA TMTDS 5	2	1.99	5	1.20	0.62	82100	196700	2.40
PP-g-MA TMTDS 6	2	3.31	5	2.00	0.61	141000	367400	2.00

Table 3.1 (continued) : Sample compositions, grafting levels and molecular weights

Sample	*wt% DHBP*	*wt% MED.*	*wt% MA*	*M•/RO•*	*wt% g-MA*	*Mn (Da)*	*Mw (Da)*	*PDI*
PP-g-MA ^{t}DSH 1	2	0.56	5	0.20	1.21	20600	44900	2.18
PP-g-MA ^{t}DSH 2	2	1.39	5	0.50	1.36	19800	43700	2.21
PP-g-MA ^{t}DSH 3	2	2.79	5	1.00	0.69	29700	69800	2.35
PP-g-MA ^{t}DSH 4	2	5.57	5	2.00	0.59	39300	92900	2.36
PP-g-MA BDTB 1	2	0.67	5	0.20	0.69	28300	63500	2.24
PP-g-MA BDTB 2	2	1.68	5	0.50	0.39	44100	114300	2.59
PP-g-MA BDTB 3	2	3.36	5	1.00	0.15	53900	191700	3.56
PP-g-MA BDTB 4	2	6.73	5	2.00	0.12	60900	205200	3.37

Grafting in the absence of mediator

As expected, because of the quite high concentration of peroxide involved in the process, a relatively high graft content of 1.14 wt.% could have been obtained (Table 3.1, Blank PP-g-MA) but severe degradation with respect to the starting polymer (Table 3.1, iPP) also occurred as a result of peroxide-induced chain scissions. The carbonyl region of the FTIR spectrum of Blank PP-g-MA (Figure 3.2, spectrum F) exhibits several weak overlapping absorption bands. The grafts structure is not controlled and several species co-exist. The assignment of these bands will be discussed throughout the following sections.

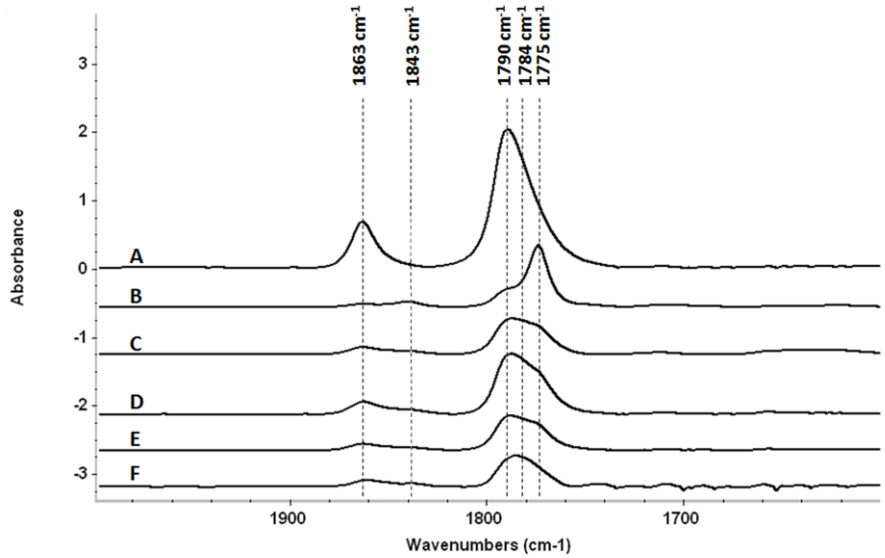

Figure 3.2 : Effect of the mediator on the grafts structure. Enlargement of the carbonyl region of the FTIR spectra of A : PP-g-MA NBS 2; B : PP-g-MA TEMPO 1; C: PP-g-MA TMTDS 1; D: PP-g-MA ^{t}DSH 3; E: PP-g-MA RAFT 1, F: Blank PP-g-MA.

N-bromosuccinimide as mediator

The NBS-mediated functionalization of PP (Table 3.1, PP-g-MA NBS 1 to 3) leads to remarkably enhanced grafting levels and molecular weights. As previously reported in Chapter 2, the propensity of bromine radicals to rapidly transfer hydrogen atoms from one tertiary carbon to another, creates numerous short-life transient macroradicals as potential grafting sites.[14] Large amounts of NBS eventually lead to non-reversible grafting of bromine atoms,[15] permanently decreasing the number of potential grafting sites and therefore preventing both degradation and maleic anhydride grafting (Table 3.1, PP-g-MA NBS 4). The FTIR spectrum of NBS-mediated grafted polypropylene (Figure 3.2, spectrum A) exhibits strong absorption bands at 1790 cm^{-1} and 1863 cm^{-1}. These bands have been assigned previously to saturated succinic anhydrides grafted along the backbone.[14,16] The large predominance of saturated rings is another consequence of the fast hydrogen transfer that readily occurs from both the PP backbone and the *in situ* generated hydrogen bromide. A small shoulder at 1775 cm^{-1} can also be discerned as a broadening in the low wavenumber region of the large peak at 1790 cm^{-1}. A small proportion of unsaturated rings would therefore be created as well, probably by disproportionation (*vide infra*). It must be pointed out that NBS-mediated grafted polypropylenes were low crystallinity (less than 10 %) isotactic/atacitc stereoblock elastomers due to successive, random hydrogen transfers leading to progressive racemization of PP tertiary carbons.[14,15,17]

TEMPO as mediator

A set of extrusions were carried out in the presence of increasing amounts of TEMPO (Table 3.1, PP-gMA TEMPO 1 to 3), up to $M^{\bullet}/RO^{\bullet} = 1$, conditions required for the persistent radical effect to establish.[7] Increasing the concentration of nitroxide considerably maintained the molecular weights to higher values. When considering both the grafting levels and the

molecular weights, it appears that they evolved in opposite directions: the higher the molecular weight, the lower the anhydride content. In the carbonyl region of the FTIR spectrum related to TEMPO-mediated grafting (Figure 3.2, spectrum B), two pairs of absorption bands are clearly discernible: 1790 cm^{-1}/1863 cm^{-1} and 1775 cm^{-1}/1843 cm^{-1}. The former pair has already been assigned to succinic rings (*vide supra*) but the origin of the latter is still unclear. It has already been reported that chain-end functionalization of nitroxide-terminated polystyrene can easily be done it the presence of maleic anhydride at temperatures above 125 °C.[18] This reaction consists in the insertion of a single anhydride unit (no oligomers were observed) which readily undergoes disproportionation, leading to grafted unsaturated anhydride moieties. Maleic anhydride insertion also occurred when TEMPO-heptene was heated at 111 °C for 25 minutes.[19] TEMPO-heptene dissociation led to the formation of an allylic radical onto which maleic anhydride can graft. The grafts structure was also identified as single unsaturated anhydride. It seems thus reasonable to ascribe the bands at 1843 cm^{-1} and 1775 cm^{-1} to grafted unsaturated rings as the presence of a conjugated double bond would decrease the absorption frequencies of the carbonyl groups. Besides, as no absorption band is observed at 1784 cm^{-1}, all the grafted anhydrides are believed to be monomeric as well.[16] It can therefore be stated that the majority of the grafted anhydrides interact with the nitroxide and terminate by disproportionation instead of hydrogen transfer from the PP backbone.

The reactive grafting of maleic anhydride in the presence of nitroxides will be further discussed in section 3.1.5.

TMTDS as mediator

TMTDS was chosen as it decomposes thermally into two dithiocarbamyl radicals that are able to interact selectively and reversibly

with carbon-centered radicals but not with oxygen.[20] Increasing the concentration of TMTDS progressively suppressed the degradation of the polymer but also prevented the grafting (Table 3.1, PP-g-MA TMTDS 1 to 6). Three kinds of grafted anhydrides can be observed on the FTIR spectrum (Figure 3.2, spectrum C): Succinic anhydrides (1790 cm^{-1}/1863 cm^{-1}), maleic anhydride oligomers (1784 cm^{-1}) and unsaturated maleic anhydrides (1775 cm^{-1}/1843 cm^{-1}). TMTDS was therefore unable to control the grafts structure. More surprisingly, when very high concentrations of TMTDS were introduced (PP-g-MA TMTDS 6), the measured molecular weights exceeded those of the starting iPP, probably as a result of crosslinking. Therefore, it seems that TMTDS did not actually mediate the grafting process but was involved in side reactions. The concept of iniferter-mediated grafting of unsaturated monomers onto polypropylene was already described in the literature.[11] Graebling used several iniferters to mediate de grafting of trimethylol propane triacrylate, a crosslinking agent, onto PP in the presence of DHBP. He observed that even in the absence of DHBP, some degree of branching occured. However, a peroxide was still required to allow sufficient grafting and the presence of the iniferter was only useful to limit the extent of peroxide-induced degradation. The author claimed that dithiocarbamyl radicals interacted with PP macroradicals, and that this reaction was reversible. This would lower the instantaneous concentration of active radicals and hence favor the grafting over degradation. However, neither spectroscopic evidences of the grafted intermediates nor evidences of reversibility were provided. Since the grafting reaction was only monitored by rheometry and not by any spectroscopic methods, it was impossible to directly correlate the degree of branching with the amount of grafted monomer and therefore exclude the occurrence of any other side reactions which the iniferter might be held responsible for. Some data concerning the thermal dissociation of thiuram disulfides in solution are available in the literature. It was found that tetraisopropylthiuram disulfide dissociated

reversibly in decalin above 50 °C and could be recovered unchanged even after 30 minutes at 178 °C.[20] Tetraethyl- and tetramethylthiuram disulfides required higher temperature for ESR evidence of dissociation. Evidence of thermal decomposition of the disulfide was also observed for tetraetyhlthiuram disulfide at temperatures above 120 °C. A comprehensive investigation of rubber-curing accelerator systems, including TMTDS, was published by Coleman, et al.[21,22] A free radical decomposition mechanism of TMTDS was suggested on the basis of Raman and ESR observations of the intermediate species. The thermal decomposition of TMTDS led to the formation of di-, tri-, and polysulfides as well as elemental sulfur. More recently the thermal dissociation and stability of TMTDS have been investigated through computational studies.[23] It was calculated that the homolytic cleavage of the S-S bond in TMTDS was much more favorable than the dissociation of the C-S bond. Interestingly, it was also calculated that the further decomposition of the dithiocarbamyl radicals (with loss of CS_2) was less endothermic than the homolytic cleavage of the S-S bond. Consequently, at temperatures high enough to initiate the dissociation of TMTDS, the further decomposition, leading to CS_2 and dimethylaminyl radicals also takes place. As a consequence, it would be reasonable to believe that TMTDS acted as a source of sulfur in the grafting process. PP crosslinking was already observed when processed in the presence of a peroxide, sulfur and an accelerator such as TMTDS.[24] That paper also related that TMTDS together with a peroxide led to a limited degradation of PP but no mechanism was discussed and no allusion to a reversible interaction between dithiocarbamyl radicals and PP was made. The very high concentration of peroxide and TMTDS used in the present work might be the reason why the grafting reaction could not be controlled (i.e. uncontrolled grafts structures and inhibition of the reaction with increasing TMTDS concentrations), and why such a dramatic increase in molecular weights was observed.

^{t}DSH as mediator

Thiols are known as efficient hydrogen donors and have already been used to control the viscosity of polyethylene waxes during melt functionalization.[25] In that patent, no spectroscopic characterization was provided and no mechanism was discussed. It was therefore decided to further investigate the influence of thiols on polypropylene functionalization. As can be seen in Table 3.1 (PP-g-MA ^{t}DSH 1 to 4), increasing the concentration of ^{t}DSH limited the degradation of PP but also inhibited the grafting reaction. The FTIR spectrum (Figure 3.2, spectrum D) revealed that the grafts also consisted of succinic, maleic and oligomeric moieties, with a small predominance of saturated rings, probably as a consequence of hydrogen transfer from the backbone or hydrogen donation from ^{t}DSH.

BDTB as mediator

Benzyl dithiobenzoate is a common chain transfer agent (CTA) used in reversible addition-fragmentation chain transfer polymerization (RAFT). In the present work, an attempt to use this CTA to transfer a radical from one PP chain to another is described. Radical transfer is assumed to play a crucial role in the grafting process as it should diminish the instantaneous concentration of transient macroradicals without loss of potential grafting sites, in order to favor grafting over degradation. As can be seen in Table 3.1 (PP-g-MA BDTB 1 to 4), although very high molecular weights could be preserved, very low grafting levels were reached and total inhibition of the radical reaction was observed at high CTA concentration. This can be explained either by non-reversible addition of dithiobenzoate moieties (weak aromatic signals detected by ^{1}H NMR) or thermal degradation of the CTA, leading to sulfur-containing by-products that could be involved in side reactions such as chain branching/crosslinking. The FTIR spectrum (Figure 3.2, spectrum E) shows weak absorption bands at 1790/1863 cm^{-1}, 1784 cm^{-1}

and 1775/1843 cm^{-1} indicating that no control on the grafts structure could be achieved.

3.1.4 Conclusions

NBS-mediated grafting of maleic anhydride was the most effective process as both the graft content and molecular weights were enhanced. The graft structure was identified as saturated rings together with a small proportion of unsaturated rings. All the other mediators failed to significantly enhance the grafting levels while preserving the molecular weights. The presence of TEMPO in the reactive medium limited both degradation and grafting. Indirect evidence of interaction between the nitroxide and the grafted anhydrides was observed through the formation of unsaturated rings as a result of disproportionation between TEMPO and the intermediate cyclic radicals. Radical propagation was therefore precluded, leading to lower grafting levels and lower degradation. Bringing together the FTIR data presented in this paper and previously published observations of the interaction between nitroxides and maleic anhydride enabled the correct assignment of the 1775/1843 cm^{-1} absorption bands to grafted unsaturated rings. TMTDS was not an appropriate mediator for free radical grafting of maleic anhydride as the grafting levels decreased with increasing concentrations of mediator. Besides, the complexity of the FTIR spectra revealed an uncontrolled reaction (saturated/unsaturated anhydrides, oligomers, etc) and further decomposition of the mediator was suspected as crosslinking of the material occured when very high concentrations of TMTDS were used. Tert-dodecanethiol and benzyl dithiobenzoate also failed to mediate the grafting process. It must be pointed out that NBS is the only mediator able to epimerize the backbone with loss of crystallinity.

Additional unpublished data

3.1.5 Influence of sterically hindered nitroxides

As disclosed in the previous paragraphs, in TEMPO-mediated grafting, the graft content decreases with increasing concentrations of TEMPO. This can be explained by a competition between TEMPO radicals and maleic anhydride towards carbon-centered macroradicals. Besides, acknowledging that TEMPO is able to graft on PP, this reaction is expected to be reversible.[8,9] However, the rate of dissociation of this macro-alkoxyamine might be too low to further reactivate polypropylene chains and allow maleic anhydride grafting before they exit the extruder. Studies on model compounds revealed that dissociation rates of TEMPO-based alkoxyamines are highly dependent on the nature of the leaving group.[26] Aliphatic alkyl groups have extremely poor leaving ability, leading to very low dissociation constant rates. For example, experimental dissociation constant rates at 393K for methyl-, cyclohexyl- and tertbutyl-TEMPO alkoxyamines of respectively $6.6x10^{-12}$, $2.8x10^{-8}$ and $1.0x10^{-5}$ s^{-1} were found,[26-29] which are very low compared to activated leaving groups such as cumyl radicals for which a dissociation constant rate of $8.5x10^{-2}$ s^{-1} was found.[26,29] Therefore, TEMPO is suspected to act as a permanent radical trap in the experimental condtions of reactive processing. To improve the dissociation rate of the macro-alkoxyamine, the strength of the C-ON bond must be lowered. In order to do so, the structure of the nitroxide must be modified. Many studies reavealed that the strength of the C-ON bond is influenced by stereoelectronic,[25,28-30] H-bonding[28-30] and steric effecfs,[26,28-30,32-38] the latter being the strongest**.** It was decided to compare the reactivity of TEMPO with 1,1-diadamantyl nitroxide (Ad_2NO), a bulky aliphatic nitroxide whose dissociation rate should be larger than the one of TEMPO. Ad_2NO was chosen for several reasons:[34] (i) the bulkiness of the substituents borne by the nitrogen atom

increases the steric hindrance around the nitroxide free radical. This steric hindrance is held responsible for lower activation energies and faster exchange rates; (ii) it is remarkably stable at high temperatures because it has no α-hydrogen**.** α-H-bearing nitroxides are well-known for their instability and readily undergo disproportionation to the corresponding nitrone and hydroxylamine.[38-40] (iii) because of the aliphatic nature of the substituents, it should be more easily miscible to molten polyolefins.

Two processing methods were also compared in order to compare the reactivity of the two nitroxides. On the one hand, the method consisted of a direct single-step extrusion where all the reactants were dry-mixed together and poured into the hopper on an extruder. On the other hand, to further investigate the mechanism, the grafting process was divided into three individual steps: (i) melt blending of polypropylene and the nitroxide in a melt-kneader, (ii) synthesis of the macro-alkoxyamine by slow addition of the peroxide (iii) maleic anhydride insertion in the C-ON bond of the alkoxyamine.

This strategy implies that the grafting of the nitroxides to create the macro-alkoxyamine is reversible at elevated temperature to allow maleic anhydride insertion. This reversibility has already been suggested in the literature for several processes such as controlled polyolefins synthesis,[41,42] controlled degradation[8] and grafting,[9] but also for the production of crosslinked ethylene-based polymers that are able to flow at higher temperatures[43] and for the synthesis of long-chain branched polyolefins from nitroxide-based macro-initiators (grafting from approach).[44,45] However those papers are questionable because as those exemples are mainly issued in the patent literature, complete experimental characterization is often lacking or barely convincing.

EXPERIMENTAL

Synthesis of 1,1-diadamantyl nitroxide

The synthesis of 1,1-diadamantyl nitroxide was described by Debuigne et al,[34] and consists in the oxidation of 1,1-diadamantanamine with m-chloroperbenzoic acid (m-CPBA). They synthesized 1,1-diadamantanamine according to the procedure published earlier by Sarker et al,[46]. A mixture of 11.37 g of 1-bromoadamantane (52.86 mmol, 1 eq) and 15.93 g of 1-aminoadamantane (105.32 mmol, 2 eq) was distributed in 5 sealable glass tubes. The tubes were sealed under vacuum and inserted inside a home-made electric oven pre-heated at 220 °C. After 40 h, the glass tubes were removed and allowed to cool down to room temperature. They were then carefully opened and the products (a thick white solid) were dissolved together under vigorous stirring in a mixture of 200 mL NaOH 20 % and 200 mL diethyl ether. After complete dissolution (about 3 h), the phases were separated and 200 mL of aqueous HCl 20 % were added to precipitate the 1,1-diadamantanamine as the hydrochloride. The precipitate was then filtrated, washed with 50 mL of water and dissolved in a mixture of 200 mL NaOH 20 % and 200 mL diethylether to re-generate the 1,1-diadamantanamine. The organic layer was separated, dried over $MgSO_4$ and evaporated under reduced pressure. 6.454 g of crude product were recovered (22.62 mmol, 0.43 eq). The crude product was oxidized in the corresponding nitroxide without further purification.

Synthesis of 1,1-diadamantyl nitroxide

6.454 g of 1,1-diadamantanamine (22.62 mmol, 1 eq) were dissolved under argon in 100 mL of chloroform and cooled down to -78 °C. A solution of 7.809 g of m-CPBA (45.25 mmol, 2 eq) in 100 mL of chloroform was then added dropwise over 15 minutes. The temperature was allowed to warm up to room temperature in 3 hours. The solution progressively turned orange

because of the apparition of the nitroxide. The mixture was allowed to react at 0 °C for one hour. 100 mL of NaOH 20 % were then added and the organic layer was separated, washed twice with 100 mL NaOH 20 %, dried over $MgSO_4$ and evaporated under reduced pressure. The crude product was purified through column chromatography over silicagel using DCM for elution. 5.017 g of orange crystals were recovered (16.71 mmol, 0.74 eq)

Reactive extrusion

Reactive extrusions were performed on a Brabender single screw extruder heated at 200°C all along the screw axis. The screw speed was set to 30 rpm which implies a residence time of 90 seconds. A mixture of polypropylene, peroxide, maleic anhydride and mediator was thoroughly dry-mixed until complete homogenization and inserted in the hopper of the extruder. The grafted polymers were poured into cold water and pelletized when possible. Table 3.2 sumarizes the composition of the samples for reactive extrusion experiments.

Reactive kneading

A mixture of PP and mediator was thoroughly dry-mixed until complete homogenization and was introduced in the pre-heated chamber of the Brabender plasticorder (mixing volume of 7 ml), covered with a blanket of argon and kneaded for two minutes. The temperature was set at 200 °C and the rotor speed was set to 90 rpm. The cover was then removed and the peroxide was carefully added into the kneader over a period of five minutes. The reaction was still allowed to proceed for two more minutes under argon. Maleic anhydride was then added in one minute into the kneader. The plasticorder was then covered with a blanked of argon and allowed to react for one hour. Three intermediate samples were taken out after 15, 30, 45

minutes. Table 3.3 gathers the composition of the samples for the three-step grafting experiments.

Table 3.2 : Composition of the samples for nitroxide-mediated grafting

Sample	*wt% Perox sup*	*wt% nitroxide*	*wt% MA*	*$NO^{\bullet}/RO^{\bullet}$*
Blank PP-g-MA	2	0	5	0
PP-g-MA TEMPO 0	0	0.43	5	-
PP-g-MA TEMPO 1	2	0.43	5	0.20
PP-g-MA TEMPO 2	2	1.07	5	0.50
PP-g-MA TEMPO 3	2	2.15	5	1.00
PP-g-MA Ad2NO 1	2	0.83	5	0.20
PP-g-MA Ad2NO 2	2	2.07	5	0.50
PP-g-MA Ad2NO 3	2	4.13	5	1.00

Table 3.3 : Composition of the samples for the three-step grafting.

Sample	*wt% Perox*	*wt% nitroxide*	*wt% MA*	*$NO^{\bullet}/RO^{\bullet}$*
PP-g-TEMPO	9.28	10	0	1
PP-g-MA/ TEMPO	9.28	10	6.27	1
PP-g-MA/ Ad_2NO	9.28	19.28	6.27	1

Sample characterization

Characterization methods were already described in section 3.1.2.

RESULTS

TEMPO versus 1,1-diadamantyl nitroxide as mediators in reactive extrusion

The PP-g-MA TEMPO 0 sample has been extruded in the absence of peroxide in order to assess the H-abstracting ability of TEMPO. As can be seen in Table 3.4, the molecular weights remain approximately the same and H-abstraction can be neglected. Here again, the graft contents and the molecular weights evolve in opposite directions, as already observed previously. This is also in agreement with the examples disclosed in the patent literature.[9] Both TEMPO and Ad_2NO behave approximately the same way.

From the carbonyl region of the FTIR spectra of Figures 3.3 and 3.4 related to TEMPO-mediated grafting and Ad_2NO mediated grafting respectively, two pairs of absorption bands are clearly discernible : 1790 cm^{-1}/1864 cm^{-1} and 1774 cm^{-1}/1840 cm^{-1}.

Table 3.4 : Anhydride contents and molecular weights of nitroxide-mediated grafted samples

Sample	*wt% g-MA*	*Mn (Da)*	*Mw (Da)*	*PDI*
iPP	0	75300	239400	3.18
Blank PP-g-MA	1.14	21900	46300	2.11
PP-g-MA TEMPO 0	0	53100	227100	4.28
PP-g-MA TEMPO 1	0.76	41700	102400	2.46
PP-g-MA TEMPO 2	0.70	46100	126700	2.75
PP-g-MA TEMPO 3	0.56	53900	170800	3.17
PP-g-MA Ad2NO 1	0.83	29200	70500	2.41
PP-g-MA Ad2NO 2	0.52	47500	126000	2.65
PP-g-MA Ad2NO 3	0.24	55200	173500	3.14

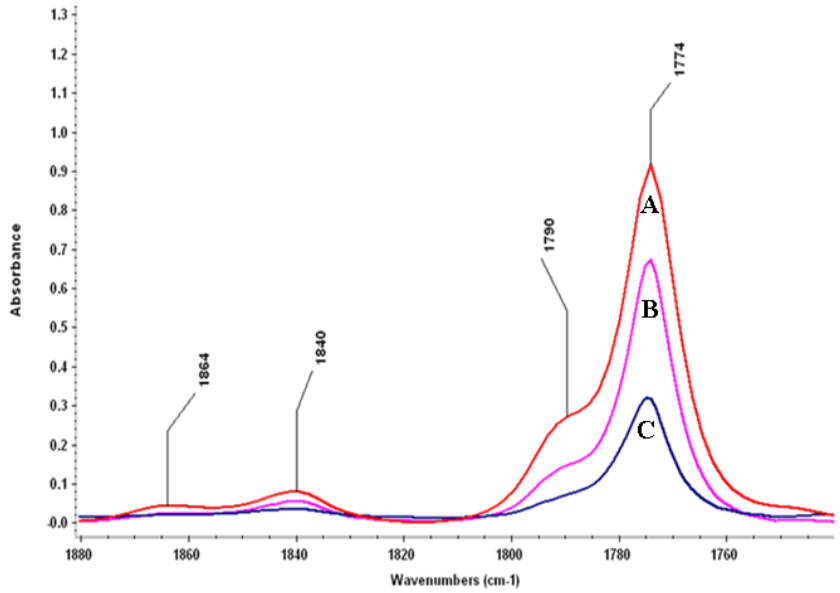

Figure 3.3: Carbonyl region of the spectra of TEMPO-mediated grafted samples. A: PP-g-MA TEMPO 1, B: PP-g-MA TEMPO 2, C: PP-g-MA TEMPO 3.

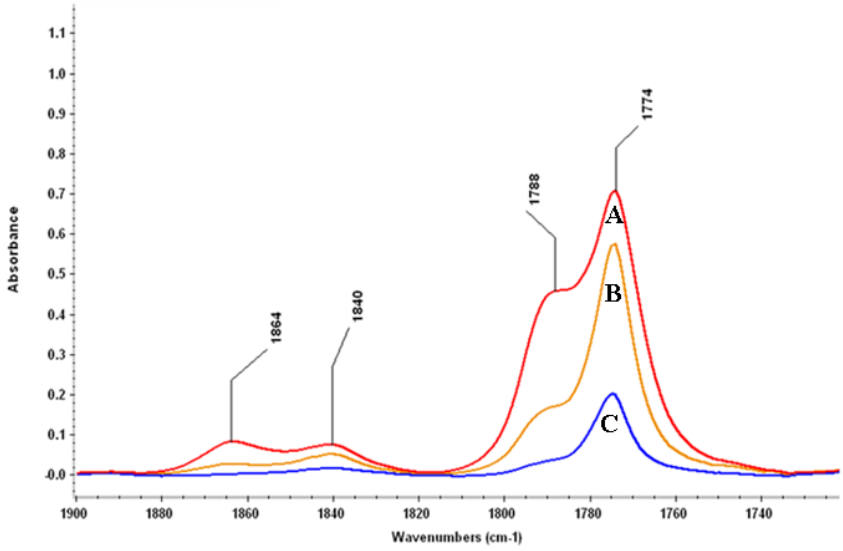

Figure 3.4 : Carbonyl region of the spectra of Ad_2NO-mediated grafted samples. A: PP-g-MA Ad_2NO 1, B: PP-g-MA Ad_2NO 2, C: PP-g-MA Ad_2NO 3.

As already discussed, the 1790 cm^{-1}/1864 cm^{-1} bands were assigned to grafted succinic rings and the 1775 cm^{-1}/1840 cm^{-1} bands were assigned to grafted unsaturated rings (a summary of chemical structure of the grafted anhydrides and their respective FTIR data is presented in Appendix at the end of this chapter). This assignment also explains why a small peak remains at 720 cm^{-1} (C-H out of plane deformation of maleic anhydride). This peak is commonly used to ascertain the complete disappearance of free maleic anhydride after the cleaning process. The absorption that remains even after cleaning the sample and drying overnight under vacuum at 90 °C would confirm the presence of maleic anhydride moieties within the material. However, some authors suggest that unsaturated rings are effectively grafted onto PP chains but would rather be itaconic rings.[47-49] It can therefore be stated that the majority of the grafted anhydrides interact with the nitroxide and terminate by disproportionation instead of by hydrogen transfer from the PP backbone. TEMPO interacts more easily with anhydride-based radicals as the proportion of grafted saturated rings is lower with respect to the unsaturated anhydrides, implying a higher extent of disproportionation.

TEMPO versus 1,1-diadamantyl nitroxide as mediators in multi-step grafting

Comparing iPP and sample PP-g-TEMPO 15' from Table 3.5, it appears that controlled-degradation of iPP occurred in the presence of peroxide and TEMPO. Considering the very large amount of peroxide introduced (>9 wt.% of supported DHBP), the molecular weights remained acceptable. The time-dependency of the molecular weights (samples PP-g-TEMPO 15' to 60' from Table 3.5) can be due to either deactivation of the macro-alkoxyamine or to oxygen-induced degradation as the protective blanket of argon must be removed while each sample is taken out of the kneader.

Table 3.5 : Molecular weights of the samples grafted in three steps.

Sample	*Mn (Da)*	*Mw (Da)*	*PDI*
iPP	75300	239400	3.18
PP-g-TEMPO 15’	29400	88200	2.99
PP-g-TEMPO 30’	26500	74500	2.81
PP-g-TEMPO 45’	25400	70300	2.77
PP-g-TEMPO 60’	24800	66900	2.70
PP-g-MA/TEMPO 15’	26500	74800	2.82
PP-g-MA/TEMPO 30’	26000	66500	2.55
PP-g-MA/TEMPO 45’	24700	64300	2.60
PP-g-MA/TEMPO 60’	22800	61000	2.67
PP-g-MA/Ad_2NO 15’	18100	47900	2.64
PP-g-MA/Ad_2NO 30’	18000	48300	2.69
PP-g-MA/Ad_2NO 45’	17800	48200	2.70
PP-g-MA/Ad_2NO 60’	17600	47800	2.67

Figure 3.5 depicts the carbonyl region of the FTIR spectra of the four PP-g-TEMPO samples. The spectrum of iPP is shown for comparison purpose. No significant differences can be observed as a function of time. When compared to the spectrum of the starting iPP, evidence of degradation can be seen as two small peaks appear at 1642 cm^{-1} and 888 cm^{-1} (vinylidene C=C stretching and vinylidene C-H deformation, respectively)[50] as well as a second peak centered at 1722 cm^{-1}. This latter is usually ascribed to the diacid form of the grafted anhydrides in PP-g-MA’s but as no anhydride was involved at this stage, this peak can reasonably be ascribed to methyl ketones or in-chain ketones that appear as a result of degradation.[50-53] The small and broad peak centered at 1692 cm^{-1} is due to in-chain double bonds.[50] It must be noted that no additional peaks have appeared which could have been

ascribed to a PP-based alkoxyamine. High-Temperature NMR was also performed on PP-g-TEMPO 15' but no additional signals were observed.

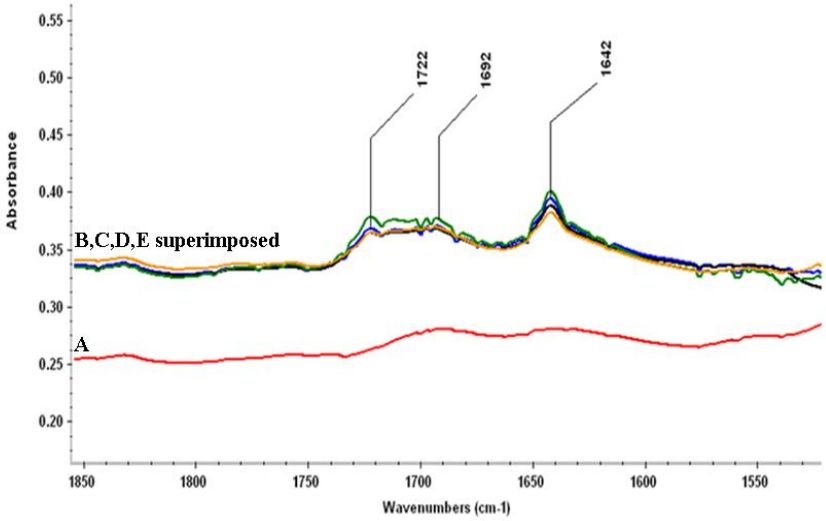

Figure 3.5 : Carbonyl region of the spectra of the samples kneaded in the absence of maleic anhydride. A: iPP, B: PP-g-TEMPO 15', C: PP-g-TEMPO 30', D: PP-g-TEMPO 45', E: PP-g-TEMPO 60'

The introduction of maleic anhydride in the kneader induced a further slight decrease of molecular weights. It also appeared that Ad_2NO is less efficient in stabilizing the systems as all the samples have similar but much lower molecular weights.

Let's now consider the carbonyl region of the spectra related to the PP-g-MA's issued from the PP-g-TEMPO (Figure 3.6). The two pairs of peaks at 1864 cm^{-1}/1790 cm^{-1} and 1840 cm^{-1}/1775 cm^{-1}, which were observed previously after reactive extrusion, are also present here but are very small. Those materials thus have very low anhydride contents. The band at 1722 cm^{-1} has increased but it was impossible to make it disappear

upon drying. This band should therefore rather be a result of further degradation than a hydrolyzed form of grafted anhydride.

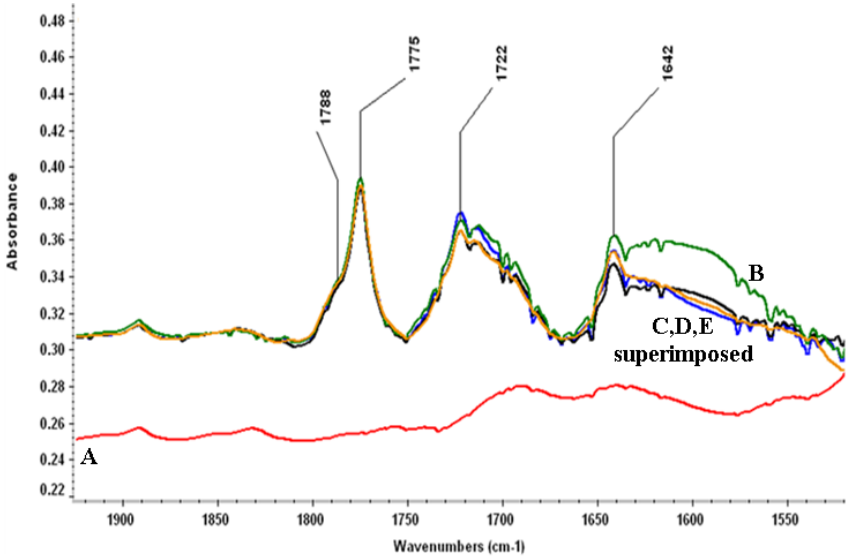

Figure 3.6 : Carbonyl region of the spectra of the PP-g-MA synthesized in three steps in the presence of TEMPO. A: iPP, B: PP-g-MA TEMPO 15', C: PP-g-MA TEMPO 30', D: PP-g-MA TEMPO 45', E: PP-g-MA TEMPO 60'

The spectra of PP-g-MA's issued from the PP-g-Ad_2NO look quite similar to those collected from PP-g-MA's issued from PP-g-TEMPO (Figure 3.7). The same bands can be found with the anhydride bands being smaller and the band at 1722 cm^{-1} being even more intense. If those bands are actually due to degradation, this correlates with the heavier reduction in molecular weight observed in GPC.

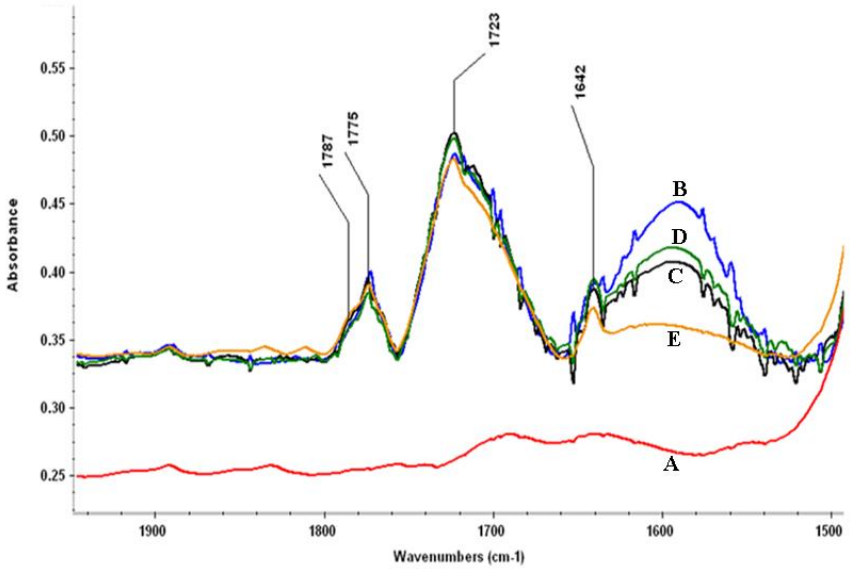

Figure 3.7 : Carbonyl region of the spectra of the PP-g-MA synthesized in three steps in the presence of Ad_2NO. A: iPP, B: PP-g-MA Ad_2NO 15', C: PP-g-MA Ad_2NO 30', D: PP-g-MA Ad_2NO 45', E: PP-g-MA Ad_2NO 60'

It is also surprising that the FTIR spectra do not evolve with time. Ideally, if a dynamic equilibrium between dormant PP-based alkoxyamines and active PP macroradicals was established, one would think that anhydride units would have been progressively grafted along the polymer backbone, presumably with a subsequent buildup in hydroxylamine due to the possible deactivation of both the propagating and persistent radicals by disproportionation. This should however not affect the PRE as those "dead" products should not shift the equilibrium in any direction.

CONCLUSIONS

From the experiments presented in the section, one can conclude that nitroxides interact with the carbon-centered radicals from both PP chains and the grafted anhydrides. Nitroxides actually compete with maleic anhydride towards PP macroradicals as they preserve the molecular weights to the expense of grafing levels. Most of the grafted anhydrides terminate by disproportionation with nitroxide radicals leading to a majority of unsaturated rings of maleic structure. Ad_2NO turned out to be less efficient than TEMPO as lower molecular weights and lower grafing levels were observed. The steric hindrance of the substituents required to increase the dissociation rate of the macro-alkoxylamine most probably lowered the trapping ability of the Ad_2NO.

3.1.6 Acknowledgement

The authors thank F.R.I.A, F.R.S-FNRS and the Walloon Government (Belgium) for financial support. Jacques Devaux is acknowledged for support and helpful suggestions.

3.1.7 References

[1] Moad, G. Progress in Polymer Science 1999, 24, 81-142.

[2] van Duin, M. Recent Research Developments in Macromolecules 2003, 7, 1-28.

[3] Russell, K. E. Progress in Polymer Science 2002, 27, 1007-1038.

[4] Sclavons, M.; Carlier, V.; De Roover, B.; Franquinet, P.; Devaux, J.; Legras, R. Journal of Applied Polymer Science 1996, 62, 1205-1210.

[5] Bettini, S. H. P.; Ruvolo Filho, A. C. Journal of Applied Polymer Science 2008, 107, 1430-1438.

[6] Coiai, S.; Passaglia, E.; Aglietto, M.; Ciardelli, F. Macromolecules 2004, 37, 8414-8423.

[7] Fischer, H. Macromolecules 1997, 30, 5666-5672.

[8] Bertin, D.; Robert, P. Patent WO 00/63260, 2000.

[9] Robert, P. M. Patent EP 0,837,080, 1998.

[10] Otsu, T. Journal of Polymer Science, Part A: Polymer Chemistry 2000, 38, 2121-2136.

[11] Graebling, D. Macromolecules 2002, 35, 4602-4610.

[12] Sudalai, A.; Kanagasabapathy, S.; Benicewicz, B. C. Organic Letters 2000, 2, 3213-3216.

[13] Sclavons, M.; Franquinet, P.; Carlier, V.; Verfaillie, G.; Fallais, I.; Legras, R.; Laurent, M.; Thyrion, F. C. Polymer 1999, 41, 1989-1999.

[14] Henry, G. R. P.; Drooghaag, X.; Rousseaux, D. D. J.; Sclavons, M.; Devaux, J.; Marchand- Brynaert, J.; Carlier, V. Journal of Polymer Science, Part A: Polymer Chemistry 2008, 46, 2936-2947.

[15] Listner, G. J.; Park, K. Patent US 3,515,687, 1970.

[16] De Roover, B.; Sclavons, M.; Carlier, V.; Devaux, J.; Legras, R.; Momtaz, A. Journal of Polymer Science, Part A: Polymer Chemistry 1995, 33, 829-842.

[17] Henry, G. R. P.; Drooghaag, X.; Vandeuren, M.; Sclavons, M.; Schanck, A.; Devaux, J.; Carlier, V.; Marchand-Brynaert, J. Journal of Polymer Sciences, Part A : Polymer Chemistry.

[18] Harth, E.; Hawker, C. J.; Fan, W.; Waymouth, R. M. Macromolecules 2001, 34, 3856-3862.

[19] Scott, M. E.; Parent, J. S.; Dupont, J.; Whitney, R. A. Industrial & Engineering Chemistry Research 2003, 42, 3662-3670.

[20] Nichols, P. J.; Grant, M. W. Australian Journal of Chemistry 1983, 36, 1379-1386.

[21] Coleman, M. M.; Shelton, J. R.; Koenig, J. L. Rubber Chemistry and Technology 1973, 46, 938-956.

[22] Coleman, M. M.; Shelton, J. R.; Koenig, J. L. Rubber Chemistry and Technology 1973, 46, 957-980.

[23] Steudel, R.; Steudel, Y.; Mak, A. M.; Wong, M. W. Journal of Organic Chemistry 2006, 71, 9302-9311.

[24] Bouhelal, S.; Cagiao, M. E.; Benachour, D.; Calleja, F. J. B. Journal of Applied Polymer Science 2007, 103, 2968-2976.

[25] Ames, W. A. Patent US 4,358,564, 1982.

[26] Bertin, D.; Gigmes, D.; Marque, S. R. A.; Tordo, P. Macromolecules **2005,** 38, (7), 2638-2650.

[27] Ciriano, M. V.; Korth, H.-G.; van Scheppingen, W. B.; Mulder, P. Journal of the American Chemical Society **1999,** 121, (27), 6375-6381.

[28] Marque, S.; Fischer, H.; Baier, E.; Studer, A. Journal of Organic Chemistry **2001,** 66, (4), 1146-1156.

[29] Marque, S.; Le Mercier, C.; Tordo, P.; Fischer, H. Macromolecules **2000,** 33, (12), 4403-4410.

[30] Fischer, H.; Kramer, A.; Marque, S. R. A.; Nesvadba, P. Macromolecules **2005,** 38, (24), 9974-9984.

[31] Beaudoin, E.; Bertin, D.; Gigmes, D.; Marque, S. R. A.; Siri, D.; Tordo, P. European Journal of Organic Chemistry **2006**, 1755-1768.

[32] Siegenthaler, K. O.; Studer, A. Macromolecules **2006,** 39, (4), 1347-1352.

[33] Marque, S. Journal of Organic Chemistry **2003,** 68, (20), 7582-7590.

[34] Debuigne, A.; Chan-Seng, D.; Li, L.; Hamer, G. K.; Georges, M. K. Macromolecules **2007,** 40, (17), 6224-6232.

[35] Lagrille, O.; Cameron, N. R.; Lovell, P. A.; Blanchard, R.; Goeta, A. E.; Koch, R. Journal of Polymer Science, Part A: Polymer Chemistry **2006,** 44, 1926-1940.

[36] Mannan, M. A.; Ichikawa, A.; Miura, Y. Polymer **2007,** 48, 743-749.

[37] Miura, Y.; Nakamura, N.; Taniguchi, I. Macromolecules **2001,** 34, 447-455.

[38] Studer, A.; Harms, K.; Knoop, C.; Mueller, C.; Schulte, T. Macromolecules **2004,** 37, (1), 27-34.

[39] Hawker, C. J.; Bosman, A. W.; Harth, E. Chemical Reviews (Washington, D. C.) **2001,** 101, (12), 3661-3688.

[40] Studer, A.; Schulte, T. Chemical Record **2005,** 5, (1), 27-35.

[41] Moffat, K. A.; Saban, M.; Veregin, R. P. N.; Georges, M. K.; Hamer, G. K.; Kazmaier, P. M. Stable free radical polymerization process and thermoplastic materials produced therefrom. US5449724, 1995.

[42] Buback, M.; Minaux, E.; Senninger, T.; Le Blevec, J.-M. Method for controlled free radical polymerisation or copolymerisation of ethylene under high pressure in the presence of an initiator-controller. WO 00/20469, 2000.

[43] Bertin, D.; Guerret, O.; Dumont, L.; Lascombe, J.-P.; Baumert, M. Heat-reversible polymers with nitroxide functions. WO 01/62804, 2001.

[44] Roth, M.; Pfaendner, R.; Nesvadba, P. Grafting of ethylenically unsaturated monomers onto polymers. WO/ 0014135, 2000.

[45] Park, E.-S.; Jin, H.-J.; Lee, I.-M.; Kim, M.-N.; Lee, H. S.; Yoon, J.-S. Journal of Applied Polymer Science **2002,** 83, 1103-1111.

[46] Sarker, H.; Greer, M. L.; Blackstock, S. C. Journal of Organic Chemistry **1996,** 61, 3177-82.

[47] Heinen, W.; Erkens, S. W.; Van Duin, M.; Lugtenburg, J. Journal of Polymer Science, Part A: Polymer Chemistry **1999,** 37, 4368-4385.

[48] Heinen, W.; Rosenmoeller, C. H.; Wenzel, C. B.; de Groot, H. J. M.; Lugtenburg, J.; van Duin, M. Macromolecules **1996,** 29, 1151-7.

[49] Heinen, W.; Van Duin, M.; Rosenmoeller, C. H.; Wenzel, C. B.; De Groot, H. J. M.; Lugtenburg, J. Macromolecular Symposia **1998,** 129, 119-125.

[50] Oktern, Z.; Cetin, S.; Akin-Oktem, G. Polymer Bulletin (Berlin) **1999,** 43, 239-246.

[51] He, P.; Xiao, Y.; Zhang, P.; Xing, C.; Zhu, N.; Zhu, X.; Yan, D. Polymer Degradation and Stability **2005,** 88, 473-479.

[52] He, P.; Xiao, Y.; Zhang, P.; Zhu, N.; Zhu, X.; Yan, D. Applied Spectroscopy **2005,** 59, 33-38.

[53] Vaillant, D.; Lacoste, J.; Dauphin, G. Polymer Degradation and Stability **1994,** 45, 355-60.

APPENDIX

Table 3.6: chemical structure and FTIR data of the grafted anhydrides.

Structure	*Name*	*Symmetrical stretching*	*Asymmetrical stretching*
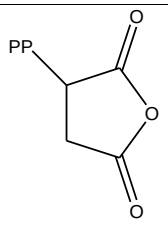	Succinic anhydride	1790 cm^{-1}	1864 cm^{-1}
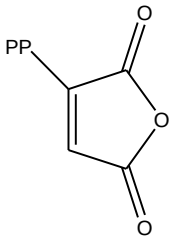	Maleic anhydride	1774 cm^{-1}	1840 cm^{-1}
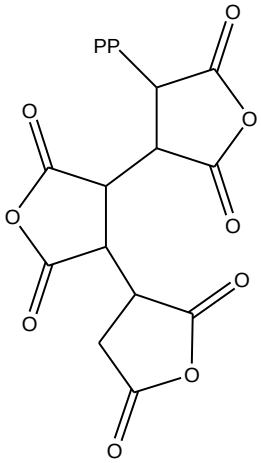	Poly(maleic anhydride)	1784 cm^{-1}	1844 cm^{-1}

Chapter Four

2,4,6,8,10-pentamethylundecane

-

Synthesis, Separation and Use of the Diastereoisomers as Model Compounds

The first section of chapter four discloses an original, simple and very efficient synthesis route toward 2,4,6,8,10-pentamethylundecane, as a statistical mixture of stereoisomers. This section also explains how this route was adapted to create two potential key precursors to PMU that could be utilized for the chromatographic separation of their diastereoisomers to provide pure models of isotactic, atactic and syndiotactic polypropylene. A few milligrams of each model compound could be isolated and an original strategy based on a comparison between the spectroscopic data available on polymeric material and those obtained on the model compounds is presented. A large-scale version of this synthetic pathway that implied only minor adjustments could also be established. Gaëtan Henry established this synthesis route toward PMU during his Ph.D. thesis. I adapted it to a larger, multi-gram scale with the help of Dimitri Rousseau who was working on this topic under my sponsorship during his Master Degree. I was also in charge of writing and submitting the paper.

The second part of chapter four describes the many efforts devoted to the preparative chromatographic separation of 6-hydroxymethyl-2-4-8-10-tetramethylundecane diastereoisomers, key precursor to PMU. Despite the many roadblocks that were encountered it was possible to isolate a few hundred milligrams of the syndiotactic and atactic models. Unfortunately the resolution remained quite poor to efficiently separate the isotactic model from the original mixture. I was fully in charge of this section and performed all the chromatographic separations reported hereafter.

Finally, the third part of this chapter discloses the very first results obtained on PMU models. Preliminary experiments for a feasibility study were performed on the PMU models available. As the isotactic model was very delicate to isolate from the mixture of stereoisomers, it was decided to conduct the preliminary experiments on a mixture of isomers and on pure

syndiotactic model, available in much more reasonable quantities. I was fully in charge of this section and performed all the experiments disclosed hereafter except for the DSC measurements that were performed by Leila Amajod, 3rd year Bachelor student from Institut Meurice, who performed a traineeship under my supervision.

4.1 A Flexible Route Toward Polypropylene Model Compounds of Various Tacticities

Xavier Drooghaag,[1] Gaëtan Henry,[1] Jacqueline Marchand-Brynaert.[1*]

*Published as Synthesis, **2010**, 21, 3755-3760*

[1]Institute of condensed matter and nanosciences (IMCN), Unité de Chimie organique et médicinale, Université catholique de Louvain, Bâtiment Lavoisier, Place Louis Pasteur 1, B-1348 Louvain-la-Neuve, Belgium.

Abstract

This paper reports the flexible synthesis of 2,4,6,8,10-pentamethylundecane as well as a chromatographic method for the separation of the diastereoisomers. This strategy offers the unique opportunity to accede to three model compounds of polypropylene of different tacticities (i.e. isotactic, syndiotactic and atactic).

4.1.1 Introduction

Isotactic polypropylene modifications (i.e. grafting of polar monomers, racemization, etc.) are very challenging industrial processes and the underlying chemical reactions are barely established.[2] The very high molecular weights of the polymers and the low graft contents make the identification of reaction products and intermediates very delicate. As a consequence, small oligomers are commonly used as model compounds to shed light on the functionalization mechanisms through the analytical tools of the organic chemist. This paper describes a flexible synthesis of

2,4,6,8,10-pentamethylundecane (PMU) and a chromatographic method for the separation of the diastereoisomers as a route to polypropylene model compounds with controlled tacticities.

The PMU synthesis was initially described about 40 years ago and never revisited since that time.[3] Reaction of 3,5-dimethylhexanal with the Grignard reagent issued from 1-bromo-2,4-dimethylpentane, followed by the oxidation of the alcohol intermediate, led to 2,4,8,10-tetramethylundecan-6-one (scheme 4.1). The central missing methyl group was then introduced by addition of methylmagnesium bromide, giving 2,4,6,8,10-pentamethylundecan-6-ol. The alcohol dehydratation by distillation over iodine afforded a mixture of isomeric olefins which hydrogenation in the presence of Raney nickel yielded PMU as a mixture of stereoisomers, separable by fractional distillation with ~90 % purity.

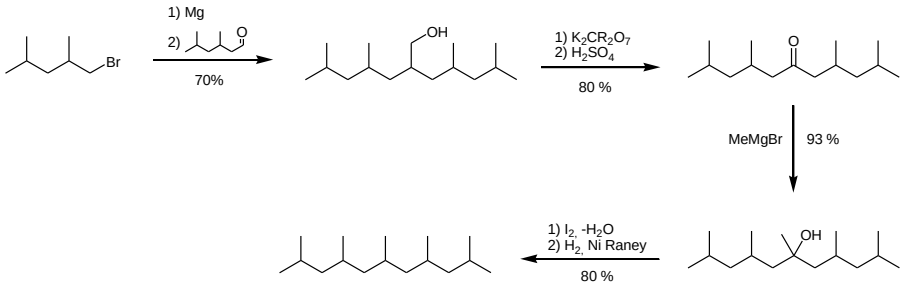

Scheme 4.1 : Synthesis of PMU according to Pino et al.[53]

In our hands, this PMU synthesis revealed to be hardly reproducible at the multi-gram scale, mainly because a competition occurred, during the first organometallic coupling, with the alkyl bromide auto-condensation. We tried to replace the aldehyde partner by the corresponding Weinreb amide in view of directly forming the ketone key-intermediate, but without success. Therefore, we investigated another route toward PMU based on Wittig-type

coupling reactions and using a flexible intermediate, namely 2,4,8,10-tetramethyl-6-methylene-undecane, to furnish either the mixture of PMU stereoisomers, or the individual stereoisomers through chromatographic separation of more polar precursors.

4.1.2 Results and discussion

Scheme 4.2 depicts the overall synthetic route to 2,4,6,8,10-pentamethylundecane as a mixture of stereoisomers. The first two steps were performed according to known procedures.[4] Unsaturated ester **1** was synthesized from 4-methyl-2-pentanone and triethyl phosphonoacetate, through a Horner-Wadsworth-Emmons (HWE) reaction, as a mixture of regio- and stereoisomers, all of them leading to ethyl 3,5-dimethylhexanoate **2** upon catalytic hydrogenation. The addition of methyl dimethylphosphonate in the presence of *n*-butyl lithium led to the β-ketophosphonate **3**. The enone **4** was synthesized through a second HWE reaction between **3** and isovaleraldehyde. The subsequent addition of methyl magnesium bromide in the presence of copper iodide allowed the insertion of the missing methyl group in the polypropylene-like structure. A simple Wittig reaction from ketone **5** led to olefin **6** as a key intermediate in the synthesis of the model compounds. Catalytic hydrogenation of **6** gave PMU **7** (mixture of isomers) with an overall yield of 41% for 7 steps, including one purification by distillation (for **1**) and 4 purifications by flash chromatography (for **3**, **4**, **5** and **6**). Synthesis of **6** at the 250 mmol-scale was performed, without purification of the intermediates, in 65% yield for 6 steps (see supporting information).

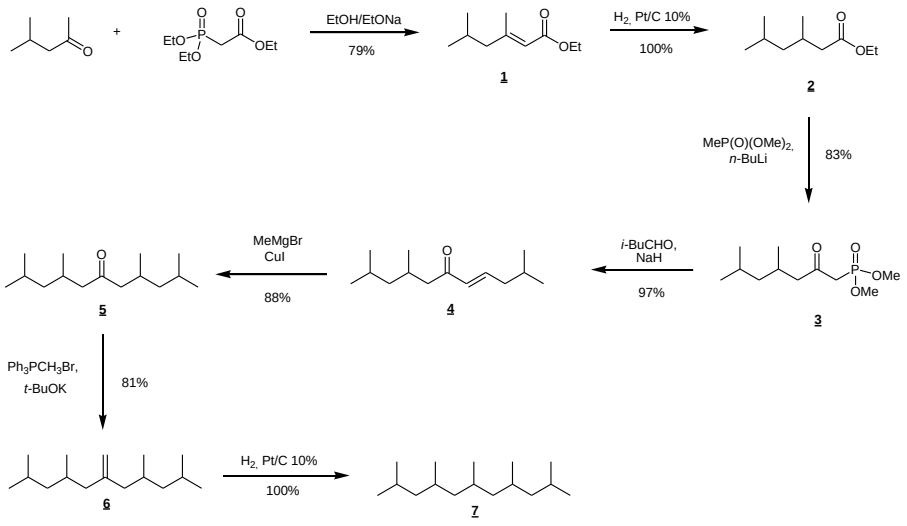

Scheme 4.2 : High-yield synthesis of PMU as a mixture of stereoisomers

Figure 4.1 shows the GC chromatogram of the mixture of stereoisomers of PMU. It consists of three peaks in a 1:2:1 ratio. Since PMU has two asymmetric carbons (C4 and C8) and one pseudo asymmetric carbon (C6), it was synthesized as a mixture of 4 stereoisomers in equivalent amounts, two of them being enantiomers to each other. The central peak of the chromatogram can unambiguously be assigned to the mixture of enantiomers but without further information it is impossible to ascribe the other peaks to any of the two remaining diastereoisomers. Those have to be isolated for accurate characterization. As no fraction of pure isomer could be retrieved by distillation, we turned to simple flash chromatography.

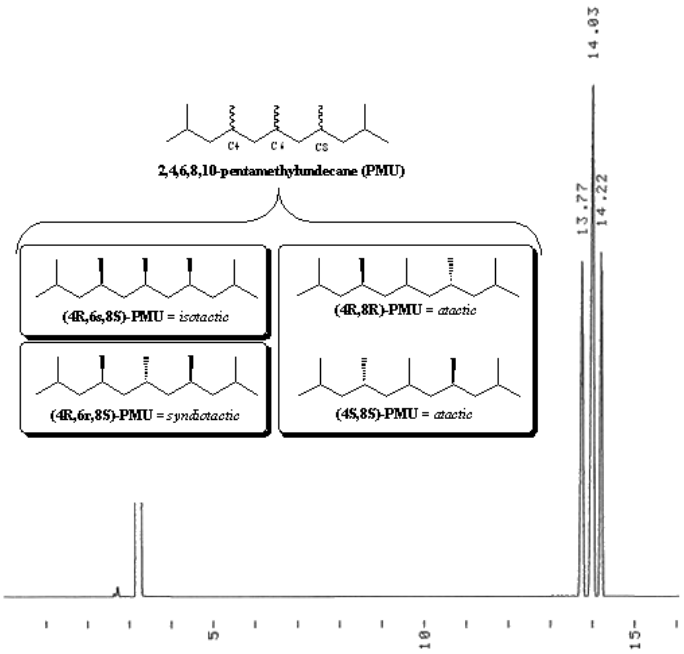

Figure 4.1 : GC chromatogram of PMU synthesized as a mixture of stereoisomers according to scheme 2. (4R,6s,8S)-PMU : 13.77 min, (4R,8R)- and (4S,8S)-PMU : 14.0 min, (4R,6r,8S)-PMU : 14.22 min. Supelco Fused Silica capillary column, SLB 5ms, 30 m x 0.25 mm

The chromatographic separation of hydrocarbons (and more specially stereoisomers) is very delicate as there are no functional groups to interact with the stationary phase. Scheme 4.3 shows how olefin **6** was derivatized to insert functional groups, i.e. a hydroxyl **8** or a tosylate **9** group, onto the main chain. PMU was then recovered through the substitution of the tosylate moiety by hydride.

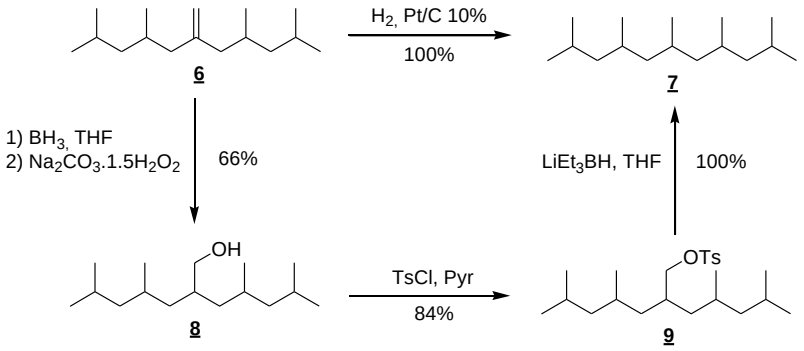

Scheme 4.3 : Derivatization of olefin **6** to introduce functional groups onto the PMU backbone for HPLC separation

The potential separation of the diastereoisomers of tosylate **9** was investigated using reverse-phase HPLC. Figure 4.2 shows that a satisfactory separation could be obtained but the very long retention times (50-60 minutes) make it difficult to scale-up the separation to preparative HPLC.

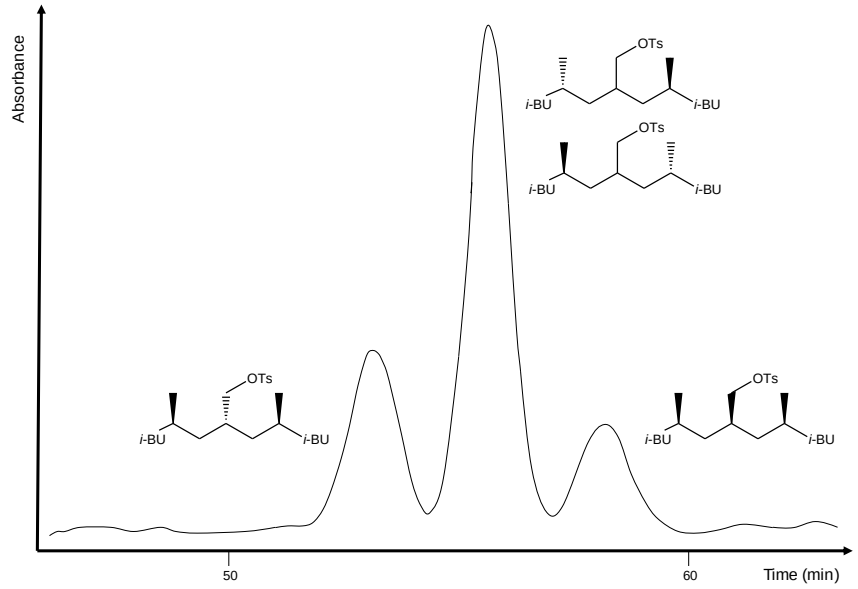

Figure 4.2 : Chromatographic separation of tosylate 13. (4R,6r,8S)-13 : 53.82 min, (4R,8R)- and (4S,8S)-13 : 56.15 min, (4R,6s,8S)-13 : 58.40 min. Xterra RP-18, 5 µm, MeOH/H_2O 85:15 v/v, 1 mL/min, 227 nm)

GC analysis of the fractions collected during the flash chromatography purification of alcohol **8** revealed that many of them contained only one diastereoisomer (single peak observed by GC whereas three peaks were observed for the crude product). Fractions containing only one of the three diastereoisomers were therefore collected separately and converted to PMU separately as well according to scheme 4.3. The correct stereochemistry of the diastereoisomers of intermediates **8** and **9** was assigned *a posteriori* based on NMR data of each PMU stereoisomer independently prepared from their pure precursors.

As can be seen in Figure 4.3a and b, isotactic and syndiotactic polypropylene (iPP and sPP, respectively) can be differentiated in ^{1}H NMR on the basis of the chemical shifts of their CH_2 hydrogen atoms as their magnetic environment differs with respect to tacticity.[5,6] These hydrogen atoms are magnetically equivalent in sPP and have the same chemical shift at $\delta \sim 1.1$ ppm. (Figure 4.3b). Conversely, the two hydrogen atoms are magnetically non-equivalent in iPP and are exposed to different shielding. Therefore those two hydrogen atoms have two distinct chemical shifts at $\delta \sim 1.3$ and 0.9 ppm (Figure 4.3a). The same principle also applies for small oligomers of propylene and can therefore be used for the stereochemical assignment of the models. ^{1}H NMR spectra of Figure 4.3c to e refer to the three stereoisomers of PMU. Figure 4.3c clearly exhibits one set of resonances at $\delta = 0.9$-1.14 ppm, very similar to that observed in sPP whereas Figure 4.3e exhibits two sets of chemical shifts at $\delta \sim 1.06$-1.22 ppm and $\delta \sim 0.95$ ppm, such as those observed in iPP. Figure 4.3d exhibits all the resonances simultaneously and is therefore consistant with the random configuration of atactic PP.

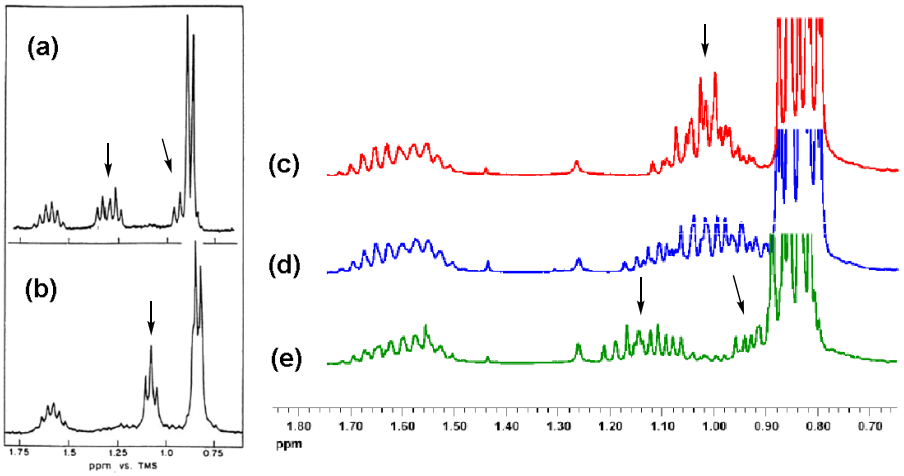

Figure 4.3 : ^{1}H NMR spectra of (a) iPP (b) sPP (c) (4R,6r,8S)-PMU (d) (4R,8R)- and (4S,8S)-PMU (e) (4R,6s,8S)-PMU. (a) and (b) recorded in ortho-dichlorobenzene at 150°C, see reference 6a; (c), (d), (e) recorded in CDCl3 at r.t.

^{13}C NMR was also used to ascertain the assignments made from ^{1}H NMR data as the chemical shifts of the methyl groups in polypropylenes are strongly dependent on the tacticity. It was reported that 3,5,7,[9-*^{13}C*],11,13,15-heptamethylpentadecane (HMHD) was used to assign the triads centered on the ^{13}C-enriched methyl group.[7] The chemical shifts of the HMHD methyl triads were very close to those observed on polypropylene. 2,4,8,10-tetramethyl-[*6-^{13}C*]-methylundecane (6-$^{13}CH_3$-PMU) was therefore synthesized from 6-($^{13}CH_2$)-**6** in order to identify the ^{13}C resonance of the central methyl group for each stereoisomer of PMU (see supporting information). Figure 4.4a to d shows the ^{13}C spectra of (4R,6s,8R)-PMU, (4R,8R)- and (4S,8S)-PMU, (4R,6r,8S)-PMU and 6-[$^{13}CH_3$]-PMU respectively.

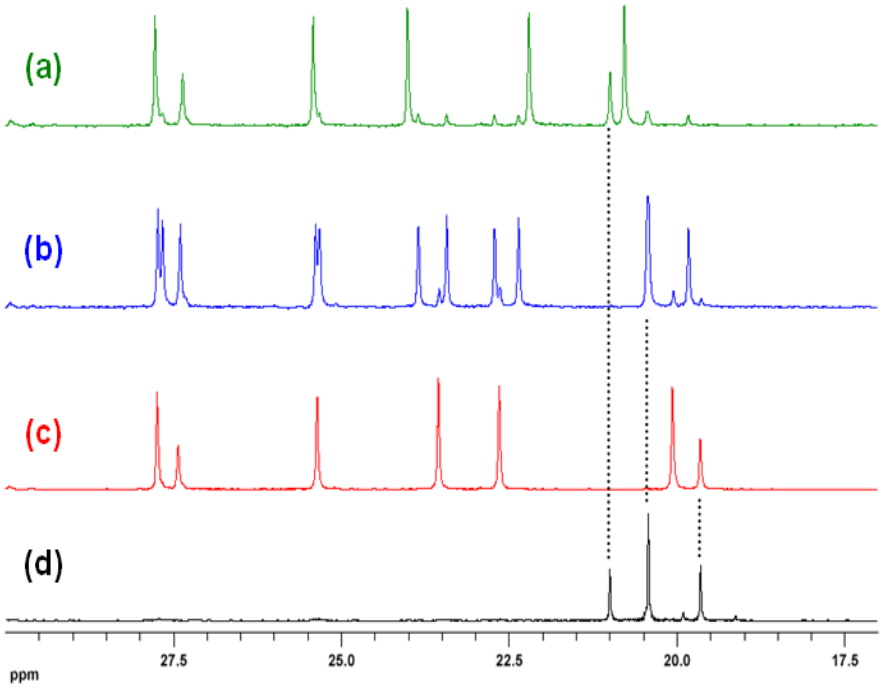

Figure 4.4 :^{13}C NMR spectrum of (a) (4R,6s,8S)-PMU, (b) (4R,8R)- and (4S,8S)-PMU, (c) (4R,6r,8S)-PMU, (d) 13C6-PMU. All spectra recorded at r.t. in CDCl3

Table 4.1 compares the chemical shifts of the methyl triads of PMU to those of HMHD[7] and polypropylene.[5] The rule of thumb "δ isotactic > δ atactic > δ syndiotactic" commonly observed for propylene oligomers and polymers also applies in the case of PMU.

Each stereoisomer being clearly identified, it was therefore possible to assign the stereochemistry of each stereoisomers of intermediates **8** and **9** and to characterize them correctly (see experimental section). The two remaining peaks of PMU **7** of the GC chromatogram in Figure 4.1 could also be assigned accurately as reported in Table 4.2.

Table 4.1 : ^{13}C chemical shifts of isotactic, atactic and syndiotactic triads in PMU, HMHD and PP

Structure	*Isotactic triad*	*Atactic triad*	*Syndiotactic triad*
(4R,6s,8S)-PMU	20.99	-	-
(4R,8R)- and (4S,8S)-PMU	-	20.43	-
(4R,6r,8S)-PMU	-	-	19.65
HMHD[7]	21.55	20.85	20.17
PP[5]	21.9-21.3	21.1-20.6	20.4-19.7

Table 4.2 : GC/HPLC retention times of isotactic, syndiotactic and atactic stereoisomers of intermediates **8**, **9** and PMU

Isomer	*GC (**8**)* [a]	*GC (**PMU**)* [a]	*HPLC (**9**)* [b]
Isotactic	21.6	13.8	58.4
Syndiotactic	22.0	14.2	53.8
Atactic (racemic mixture)	21.9	14.0	56.1

[a]Supelco Fused Silica capillary column, SLB 5ms, 30 m x 0.25 mm x 0.25 µm.

[b]Xterra RP-18, 5 µm, MeOH/H_2O 85:15 v/v, 1 mL/min, 227 nm

In conclusion, we have disclosed a practical and scalable synthesis of PMU, the model compound of PP. The isotactic stereoisomer could be isolated by flash chromatography separation of the primary alcohol intermediate **8** (obtained in 43% overall yield for 7 steps; recovery of (4R,6s,8S)-**8** = 30% of the initial content for the first run) followed by tosylation and reduction with $LiEt_3BH$ (yield of 84% for 2 steps). Knowing that the initial content in (4R,6s,8S) stereoisomers is only 25% and that the compound of interest has the highest retention time, the final recovery of 6% of pure isotactic-PMU from the initial mixture is acceptable. Moreover, the

other diastereoisomers are also accessible in pure forms. In the particular case of PMU, a molecule devoid of functional group, our stereochemically non-controlled synthesis was preferred over asymmetric synthesis using the catalytic methods recently developed in the field of biologically relevant compounds featuring polydeoxypropionate chains.[8]

4.1.3 Experimental

(E)- and (Z)-Ethyl 3,5-Dimethyl-2-hexenoate (1)

To a three-neck round-bottom flask under argon atmosphere was added sodium ethanolate (53 mL, 21 wt.% in ethanol, 142 mmol), anhydrous ethanol (100 mL) and triethyl phosphonoacetate (32.826 g, 142 mmol) at room temperature. 5 minutes later, 4-methlyl-2-pentanone (14.29 g, 0.142 mmol) was added in one portion and an exothermic reaction occurred. After 50 minutes, the mixture was heated under reflux for 1.5 hours. The mixture was then distilled under atmospheric pressure to eliminate ethanol until the temperature of the vapor reached 90 °C. The mixture was finally cooled down to room temperature and diethyl ether (100 mL) and cold water (60 mL) were added. The aqueous layer was extracted with diethyl ether (2 x 30 mL) and the combined organic layers were washed with water (3 x 50 mL), dried over $MgSO_4$. The crude product was distilled under vacuum.

Yield : 19.135g (112.4 mmol, 79 %), colorless oil.

^{1}H NMR (300 MHz, $CDCl_3$): The spectrum is very complicated because four isomers were synthesized simultaneously. Only olefinic protons are presented. Full ^{1}H NMR assignment was done after catalytic hydrogenation (*vide infra*, Ethyl 3,5-Dimethylhexanoate). δ = 5.63 (s, 1 H, *E*-α,β), 5.71 (s, 1 H, *Z*-α,β), 5.10 (d, J = 9 Hz, 1 H, *E*-β,γ), 5.15 (d, J = 9 Hz, 1 H, *Z*-β,γ).

Ethyl 3,5-Dimethylhexanoate (2)

To a three-neck round-bottom flask was added the mixture of isomers of unsaturated ester **1** (3.226 g, 18.9 mmol) and 10% Pt/C (1.221 g, 60 µmol). The atmosphere in the flask was purged three times with argon and three times with hydrogen. The reaction mixture was stirred vigorously at 30 °C under hydrogen atmosphere (~ 1 atm) for 30 hours. The catalyst was then filtered and washed with petroleum ether (3 x 50 mL). The pure product was recovered after distillation of the solvent.

Yield : 3.198 g (18.6 mmol, 98 %), colorless oil.

^{1}H NMR (300 MHz, $CDCl_3$): δ = 4.13 (q, J = 7 Hz, 2 H), 2.19-2.33 (m, 1 H), 1.93-2.12 (m, 2 H), 1.63 (m, 1 H), 1.26 (t, J = 7 Hz, 3 H), 1.01-1.18 (m, 2 H), 0.91 (d, J = 6 Hz, 3 H), 0.87 (2d, J = 6 Hz, 6 H)

Dimethyl 4,6-Dimethyl-2-oxoheptylphosphonate (3)

A two-neck flask under argon atmosphere containing BuLi (9.3 mL, 2.5 M in hexanes, 23.2 mmol) and anhydrous THF (13 mL) was cooled down to -78 °C (dry-ice / isopropanol). Dimethyl methylphosphonate (2.881 g, 23.2 mmol) was then added dropwise in 5 minutes. The colorless solution turned into a white gel. The mixture was stirred at -78 °C for 30 minutes. A solution of ethyl 3,5-dimethylhexanoate **2** (1.000 g, 5.8 mmol) in anhydrous THF (3 mL) was added dropwise. The mixture turned into a colorless liquid again. The temperature was then allowed to rise up to -20 °C in 2 h. HCl (5 mL, 18 % in water) was then added to the mixture. The aqueous layer was separated and $NaHCO_3$ is added to rise the pH to 8. The aqueous layer was extracted with CH_2Cl_2 (15 mL). The organic layers were washed with water (10 mL) and a solution of saturated NaCl (10 mL), dried over $MgSO_4$, filtered and concentrated. The crude product was purified by flash chromatography (flash silica, CH_2Cl_2/*i*-PrOH 95:5 v/v).

Yield : 1.200g (4.8 mmol, 83 %), colorless liquid.

^{1}H NMR (300 MHz, $CDCl_3$): δ = 3.79 (d, J = 11 Hz, 6 H), 2.98-3.18 (m, 2 H), 2.52-2.62 (dd, J = 5 Hz, J = 17 Hz, 1 H), 2.36-2.47 (dd, J = 8 Hz, J = 17 Hz, 1 H), 2.09 (m, 1 H), 1.62 (m, 1 H), 1.00-1.16 (m, 2 H), 0.84-0.90 (m, 9 H)

^{13}C NMR (75 MHz, $CDCl_3$) : δ = 201.62, 52.93, 51.85, 46.34, 41.76, 26.72, 25.29, 23.23, 22.17, 19.84.

^{13}P NMR (200 MHz, $CDCl_3$, external reference : H_3PO_4 at δ = 0) : δ = 23.49

2,8,10-trimethyl-4-undecene-6-one (4)

NaH (0.80 g, 20 mmol, 60 % in mineral oil) was washed in a two-neck flask under argon atmosphere with petroleum ether (3 x 20 mL) and dried under vacuum. Anhydrous DME (20 mL) was then poured onto NaH and cooled down to 0°C. Dimethyl 4,6-Dimethyl-2-oxoheptylphosphonate **3** (5.005 g, 20.0 mmol) was then added dropwise in 15minutes.When all NaH was consumed (NaH is not soluble into DME) isovaleraldehyde (2.2 mL, 20 mmol) was slowly added into the mixture. The reaction mixture was stirred at 0°C for 15 minutes. Water (40 mL) and Et_2O (40 mL) were then added. The aqueous layer was extracted with Et_2O (3 x 20 mL). The organic layers were washed with a saturated solution of NaCl (3 x 20 mL), dried over $MgSO_4$, filtered and concentrated. The crude product was purified by flash chromatography (flash silica, AcOEt 100 %). A fraction of the product still contained an impurity that was removed on a short flash chromatography (flash silica, CH_2Cl_2 100 %).

Yield : 4.069 g (19.3 mmol, 97 %), colorless liquid.

^{1}H NMR (300 MHz, $CDCl_3$): δ = 6.79 (dt, J = 7.5 Hz, J = 15 Hz, 1H), 6.09 (dd, J = 2 Hz, J = 15 Hz, 1 H), 2.44-2.52 (dd, J = 6 Hz, J = 15 Hz, 1 H) 2.27-

2.36 (dd, J = 7.5 Hz, J = 15 Hz, 1 H) 2.00-2.18 (m, 3 H), 1.78 (m, 1 H), 1.62 (m, 1 H), 1.01-1.8 (m, 2 H), 0.93 (d, J = 7 Hz, 6 H), 0.85-0.90 (m, 9 H).

^{13}C NMR (75 MHz, $CDCl_3$) : δ = 200.67, 146.13, 131.92, 48.18, 46.86, 41.92, 28.15, 27.83, 25.46, 23.49, 22.61, 22.37, 20.24.

IR : 2930-2956, 2872-2902, 1696, 1671, 1629, 1457-1468, 1367-1386, 982.

HRMS (CI, +c) : 211.2069 ($[M+H]^+$), calculated : 211.2062.

2,4,8,10-tetramethylundecan-6-one (5)

CuI (0.146 g, 0.8 mmol) and anhydrous Et_2O (10 mL) were inserted in a three-neck flask under argon atmosphere. The flask was then cooled to 0 °C and methylmagnesium bromide (5.0 mL, 3.0 M in Et_2O, 15.0 mmol) was added dropwise in 10 minutes. After 30 minutes of stirring at 0°C, a solution of (E)-2,8,10-trimethyl-4-undecene-6-one 4 (1.530 g, 7.3 mmol) in anhydrous Et_2O (30 mL) was added dropwise in 30 minutes. After 1h of stirring at 0°C, aqueous HCl (10 mL, 1N) and water (60 mL) were added and a white solid appeared. The aqueous layer was extracted with Et_2O (3 x 50 mL). The organic layers were washed with water (2 x 50 mL) and a saturated solution of NaCl (3 x 50 mL). The white solid then disappeared. The crude product was recovered after drying over $MgSO_4$, filtration and evaporation of the solvent. The crude product was purified by flash chromatography (flash silica, CH_2Cl_2 100 %).

Yield : 1.46g (6.4 mmol, 88 %), colorless liquid.

^{1}H NMR (300 MHz, $CDCl_3$): δ = 2.28-2.37 (dd, J = 5 Hz, J = 15 Hz, 2 H), 1.99-2.21 (m, 4 H), 1.61 (m, 2 H), 0.98-1.14 (m, 4 H), 0.83-0.90 (m, 18 H).

^{13}C NMR (75 MHz, $CDCl_3$) : δ = 211.28, 51.43, 51.37, 46.67, 46.63, 27.03, 25.38, 23.44, 22.26, 20.11.

IR : 2931-2958, 2875-2900, 1711, 1454-1466, 1362-1385.

HRMS (CI, +c) : 227.237145 ($[M+H]^+$), calculated : 227.237491.

2,4,8,10-tetramethyl-6-methylene-undecane (6)

Methyltriphenylphosphonium bromide (7.148 g, 20.0 mmol) and *t*-BuOK (20 ml, 1.0 M in THF, 20.0 mmol) were inserted into a three neck round bottom flask under argon atmosphere. The mixture was stirred at room temperature for 7 minutes. 2,4,8,10-tetramethylundecan-6-one (2.264 g, 10.0 mmol) was then added dropwise. The reaction was stopped after 2 hours of stirring at room temperature by addition of 30 mL of water. The aqueous layer was then extracted with AcOEt (2 x 60 mL). The combined organic layers were washed with water (2 x 30 mL), then with saturated NaCl (2 x 30 mL), dried over $MgSO_4$, filtered and concentrated. The crystallization of triphenylphosphine oxide occured during evaporation of the solvent. The solid was then triturated in pentane (40 mL) and filtered. This procedure was repeated several times. The combined filtrates were concentrated and 2.125 g of crude product were recovered. The remaining solid was ground in powder, poured into pentane (150 mL) and stirred overnight. 0.25 g of additional crude product were recovered after filtration and distillation of the solvent. The crude product was purified by flash chromatography (flash silica, petroleum ether 100 %).

Yield : 1.822 g (8.1 mmol, 81 %), colorless liquid.

^{1}H NMR (300 MHz, $CDCl_3$): δ = 4.71 (s, 2 H), 1.90-2.08 (m, 2 H), 1.58-1.80 (m, 6 H), 0.79-1.18 (m, 22 H).

^{13}C NMR (75 MHz, $CDCl_3$) : δ = 147.57, 111.94, 111.83, 47.17, 46.76, 44.48, 44.18, 28.40, 28.29, 25.43, 23.74, 23.60, 22.47, 22.30, 20.08, 19.83.

IR : 3071, 2913-2956, 2839-2869, 1641, 1437-1466, 1361-1383, 892.

HRMS (EI, +c) : 224.249788 ($[M+H]^+$), calculated : 224.250401.

6-hydroxymethyl-2-4-8-10-tetramethylundecane (8)

A two-neck round-bottom flask under argon atmopshere containing 2-4-8-10-tatramethyl-6-methylene-undecane **6** (0.561 g, 2.5 mmol) was cooled to 0 °C. Borane-THF (7.5 mL, 7.5 mmol, 1M in THF) was then inserted dropwise and stirred for 2 hours at room temperature. The mixture was then cooled again to 0 °C and water (7.5 mL) was slowly added to neutralize the excess of hydride. Sodium percarbonate (2.777 g , ~13% H_2O_2 w/w, ~22.3 mmol H_2O_2) was slowly added stirred for 1 hour at 50 °C and 48 hours at room temperature. The aqueous layer was then separated and extracted with diethyl ether (3 x 10 mL); the combined organic layers were washed with a saturated solution of NaCl (10 mL), dried over $MgSO_4$, filtered and concentrated. The crude product was purified by flash chromatography (flash silica, petroleum ether/ethyl acetate 95:5 v/v).

Yield : 0.402 g (1.7 mmol, 66 %, all isomers considered), colorless liquid.

^{1}H NMR (300 MHz, $CDCl_3$), (4R,6r,8S)-**8** : δ = 3.51 (d, J^3 = 5 Hz, 2 H), 1.46-1.72 (m, 5 H), 1.22-1.36 (m, 4 H), 0.89-1.16 (m, 4H), 0.78-0.89 (m, 18 H).

^{1}H NMR (300 MHz, $CDCl_3$), (4R,6s,8S)-**8**: δ = 3.51 (d, 2 H), 1.48-1.75 (m, 5 H), 0.91-1.30 (m, 8 H), 0.74-0.91 (m, 18 H).

^{1}H NMR (300 MHz, $CDCl_3$), (4R,8R)- and (4S,8S)-**8** δ = 3.50-3.60 (dd, J^3 = 4.8 Hz, J^2 = 10.5 Hz, 1 H), 3.39-3.49 (dd, J^3 = 5.7 Hz, J^2 = 10.5 Hz, 1 H), 1.45-1.74 (m, 5 H), 0.74-1.34 (m, 26 H).

^{13}C NMR (75 MHz, $CDCl_3$), (4R,6r,8S)-**8** : δ = 65.91, 47.31, 40.20, 35.29, 27.89, 25.38, 23.74, 22.38, 20.47.

^{13}C NMR (75 MHz, $CDCl_3$), (4R,6s,8S)-**8**: δ = 66.97, 47.21, 40.10, 35.47, 27.96, 25.39, 23.77, 22.33, 20.51.

^{13}C NMR (75 MHz, $CDCl_3$), (4R,8R)- and (4S,8S)-**8**: δ = 66.47, 47.67, 47.56, 40.41, 39.30, 35.41, 27.93, 27.70, 25.35, 23.63, 23.59, 22.47, 20.22, 20.18.

6-p-toluenesulfonyloxymethyl-2,4,8,10-tetramehtylundecane (9)

General procedure: A two-neck round-bottom flask under argon atmopshere containing 6-hydroxymethyl-2-4-8-10-tetramethylundecane **8** (0.292 g, 1.2 mmol) and anhydrous pyridine (3.6 mL) was cooled to 0 °C. Tosyl chloride (1.144 g, 6.0 mmol) was added stirred for 48 hours at room temperature. Water (8 mL) was then added and the aqueous layer was separated and extracted with diethyl ether (3 x 8 mL). The combined organic layers were washed with aqueous HCl (3 x 5 mL, 10% in water) and water (8 mL), dried oved $MgSO_4$, filtered and concentrated. The crude product was purified by flash chromatography (flash silica, chloroforme/cyclohexane 60:40 v/v).

Yield : 0.401 g (1.0 mmol, 84 %), colorless liquid.

^1H NMR (300 MHz, $CDCl_3$), (4R,6r,8S)-**9** : δ = 7.78 (d, J^3 = 8 Hz, 2 H), 7.33 (d, J^3 = 8 Hz, 2 H), 3.91 (d, J^3 = 4.5 Hz, 2H), 2.44 (s, 3 H), 1.75 (m, 1 H), 1.57 (m, 2 H), 1.42 (m, 2 H), 1.18-1.30 (m, 2 H), 0.85-1.05 (m, 6 H), 0.74-0.85 (m, 18 H).

^1H NMR (300 MHz, $CDCl_3$), (4R,6s,8S)-**9**: δ = 7.78 (d, J^3 = 8 Hz, 2 H), 7.33 (d, J^3 = 8 Hz, 2 H), 3.87 (d, J^3 = 5 Hz, 2H), 2.44 (s, 3 H), 1.75 (m, 1 H), 1.58 (m, 2 H), 1.39 (m, 2 H), 0.86-1.20 (m, 8 H), 0.83 (d, J^3 = 6 Hz, 6 H), 0.76 (d, J^3 = 6 Hz, 12 H).

^1H NMR (300 MHz, $CDCl_3$), (4R,8R)- and (4S,8S)-**9**: δ = 7.78 (d, J^3 = 9 Hz, 2 H), 7.33 (d, J^3 = 9 Hz, 2 H), 3.83-3.95 (m, 2H), 2.44 (s, 3 H), 1.75 (m, 1 H), 1.57 (m, 2 H), 1.39 (m, 2 H), 0.85-1.25 (m, 8 H), 0.72-0.85 (m, 18 H).

^{13}C NMR (75 MHz, $CDCl_3$), (4R,6r,8S)-**9** : δ = 144.75, 133.32, 129.96, 128.07, 73.13, 47.09, 39.77, 32.62, 27.57, 25.25, 23.63, 22.32, 21.81, 20.09.

^{13}C NMR (75 MHz, $CDCl_3$), (4R,6s,8S)-**9**: δ = 144.75, 133.21, 129.90, 128.07, 74.01, 46.64, 39.49, 32.54, 27.55, 25.20, 23.68, 22.07, 21.71, 20.18.

^{13}C NMR (75 MHz, $CDCl_3$), (4R,8R)- and (4S,8S)-**9**: δ = 144.75, 133.28, 129.84, 127.97, 73.57, 47.29, 46.90, 39.87, 38.73, 32.52, 27.50, 27.28, 25.11, 23.51, 23.42, 22.30, 22.16, 21.67, 19.82, 19.74.

2-4-6-8-10-pentamethylundecane (7)

From **6** : To a three-neck round-bottom flask was added 2,4,8,10-tetramethyl-6-methylene-undecane **6** (0.617 g, 2.7 mmol) and 10% Pt/C (~0.5 g, ~24.5 µmol). The atmosphere in the flask was purged three times with argon and three times with hydrogen. The reaction mixture was stirred vigorously at 25 °C under hydrogen atmosphere (~ 1 atm) for 48h. The catalyst was then filtered and washed with petroleum ether (3 x 50 mL). The pure product was recovered after distillation of the solvent.

Yield : 0.577 g, (2.5 mmol, 93 %), colorless liquid.

^{1}H NMR (300 MHz, $CDCl_3$), mixture of isomers δ = 1.45-1.75 (m, 5 H), 0.75-1.22 (m, 29 H)

^{13}C NMR (75MHz, $CDCl_3$), mixture of isomers δ = 48.08, 47.80, 47.13, 46.75, 46.20, 46.10, 45.01, 27.68-27.80, 27.40-27.43, 25.34-25.43, 24.00, 23.85, 23.54, 23.43, 22.72, 22.64, 22.37, 22.21, 21.01, 20.79, 20.43-20.46, 20.07, 19.85, 19.65.

From **9**: general procedure. in a two-neck round-bottom flask under argon atmosphere containing 6-p-toluenesulfonyloxymethyl-2,4,8,10-tetramethylundecane **9** (0.086 g , 0.22 mmol) was added lithium

triethylborohydride (0.7 mL, 0.7 mmol, 1.0 M in THF) at room temperature. The mixture was then stirred at 67 °C for 6 hours. NaOH (1.4 mL, 3N in water) was then added dropwise at room temperature. The aqueous layer was then separated and extracted with petroleum ether (2 x 5 mL). The combined organic layers were washed with water (1 mL) and a saturated solution of NaCl (1 mL), dried over $MgSO_4$, filtered and concentrated. GC and NMR measurements revealed that the product was pure and did not need to be further purified.

Yield : 0.051g (0.22 mmol, 100%), colorless liquid.

^{1}H NMR (300 MHz, $CDCl_3$), (4R,6r,8S)-**7** : δ = 1.48-1.74 (m, 5 H), 0.90-1.13 (m, 8 H), 0.78-0.90 (m, 21 H).

^{1}H NMR (300 MHz, $CDCl_3$), (4R,6s,8S)-**7**: δ = 1.47-1.74 (m, 5 H), 0.79-1.22 (m, 29 H).

^{1}H NMR (300 MHz, $CDCl_3$), (4R,8R)- and (4S,8S)-**7**: δ = 1.47-1.74 (m, 5 H), 0.76-1.20 (m, 29 H).

^{13}C NMR (75 MHz, $CDCl_3$), (4R,6r,8S)-**7** : δ = 47.80, 46.19, 27.74, 27.42, 25.35, 23.55, 22.65, 20.70, 19.65.

^{13}C NMR (75 MHz, $CDCl_3$), (4R,6s,8S)-**7**: δ = 46.69, 46.06, 27.76, 27.35, 25.41, 24.01, 22.19, 20.98, 20.78.

^{13}C NMR (75 MHz, $CDCl_3$), (4R,8R)- and (4S,8S)-**7**: δ = 48.06, 47.10, 46.73, 44.97, 27.72, 27.65, 27.39, 25.38, 25.32, 23.85, 23.42, 22.72, 22.36, 20.44, 19.83.

4.1.4 Acknowledgement

The authors thank La Région Wallonne (programme "Recherche d'initiative") and FRIA for financial support.

4.1.5 References

(1) (a) Both authors have contributed equally to this work. (b) present address of G.Henry : Total Petrochemicals Research, Zone industrielle C,B-7181 Feluy, Belgium (c) present address of X.Drooghaag : 3B-Fibreglass, Route de Maestricht, B-4651 Battice, Belgium.

(2) (a) Henry, G. R. P.; Drooghaag, X.; Rousseaux, D. D. J.; Sclavons, M.; Devaux, J.; Marchand-Brynaert, J.; Carlier, V. *J. Polym. Sci., Part A: Polym. Chem.* **2008,** 2936-2947. (b) Henry, G. R. P.; Drooghaag, X.; Vandeuren, M.; Sclavons, M.; Schanck, A.; Devaux, J.; Carlier, V.; Marchand-Brynaert, J. *J. Polym. Sci., Part A: Polym. Chem.* **2009,** 4505-4518.

(3) Pino, P.; Pucci, S.; Benedetti, E.; Bucci, P. *Sintesi Organiche*, **1968**, 91-95.

(4) Rice, K. C. *J. Org. Chem.* **1982,** 3617-3622.

(5) Busico, V.; Cipullo, R. *Prog. Polym. Sci.* **2001,** 443-533.

(6) (a) Ferguson, R. C. *Trans. N.Y. Acad. Sci.* **1967,** 495-501. (b) Resconi, L.; Cavallo, L.; Fait, A.; Piemontesi, F. *Chem. Rev.* **2000,** 1253-1345.

(7) Zambelli, A.; Locatelli, P.; Bajo, G.; Bovey, F. A. *Macromolecules* **1975,** 687-689.

(8) (a) Des Mazery, R.; Pullez, M.; Lopez, F.; Harutyunyan, S. R.; Minnaard, A. J.; Feringa, B. L. *J. Am. Chem. Soc.* **2005,** 9966-9967. (b) Liang, B.; Novak, T.; Tan, Z.; Negishi, E.-i. *J. Am. Chem. Soc.*

2006, 2770-2771. (c) ter Horst, B.; Feringa, B. L.; Minnaard, A. J. *Org. Lett.* **2007,** 3013-3015.

4.1.6 Supporting Information

4.1.6.1 Large scale synthesis of 2,4,8,10-tetramethyl-6-methylene-undecane (6)

(E)- and (Z)-Ethyl 3,5-Dimethylh-2-hexenoate (1)

To a three-neck round-bottom flask under argon atmosphere was added sodium ethanolate (933 mL, 21 wt% in ethanol, 2.50 mol) and triethyl phosphonoacetate (500 mL, 2.50 mol) at room temperature. 5 minutes later, 4-methyl-2-pentanone (313 mL, 2.50 mol) was added in one portion and an exothermic reaction occured. After 30 minutes, the mixture was heated under reflux for 1.5 hours. The mixture was then distilled under atmospheric pressure to eliminate ethanol until the temperature of the vapor reached 90 °C. The mixture was finally cooled down to room temperature and dichloromethane (400 mL) as well as cold water (800 mL) were added. The aqueous layer was extracted with dichloromethane (2 x 400 mL) and the combined organic layers were washed with water (2 x 1000 mL) and dried over $MgSO_4$. The crude product was distilled under vacuum.

Yield : 391.6 g (2.30 mol, 92 %), colorless oil.

^{1}H NMR (300 MHz, $CDCl_3$): The spectrum is very complicated because 4 isomers were synthesized simultaneously. Only olefinic protons are presented. Full ^{1}H NMR assignment was done after catalytic hydrogenation (*vide infra*, Ethyl 3,5-Dimethylhexanoate (2)). δ = 5.63 (s, 1 H, *E*-α,β), 5.71 (s, 1 H, *Z*-α,β), 5.10 (d, J = 9 Hz, 1 H, *E*-β,γ), 5.15 (d, J = 9 Hz, 1 H, *Z*-β,γ).

Ethyl 3,5-Dimethylhexanoate (2)

To a three-neck round-bottom flask was added the mixture of isomers of unsaturated ester (1) (91.88 g, 540 mmol) and 10% Pt/C (~ 3 g, ~ 150 µmol). The atmosphere in the flask was purged three times with argon and three times with hydrogen. The reaction mixture was stirred vigorously at 30 °C under hydrogen atmosphere (~ 1 atm) for 9 days. The catalyst was then filtered and washed with petroleum ether (3 x 300 mL). The pure product was recovered after distillation of the solvent.

Yield : 92.38 g (536 mmol, 99 %), colorless oil.

^{1}H NMR (300 MHz, $CDCl_3$): δ = 4.13 (q, J^3 = 7 Hz, 2 H), 2.19-2.33 (m, 1 H), 1.93-2.12 (m, 2 H), 1.63 (m, 1 H), 1.26 (t, J^3 = 7 Hz, 3 H), 1.01-1.18 (m, 2 H), 0.91 (d, J^3 = 6 Hz, 3 H), 0.87 (2d, J^3 = 6 Hz, 6 H)

Dimethyl 4,6-Dimethyl-2-oxoheptylphosphonate (3)

A two-neck flask under argon atmosphere containing BuLi (100 mL, 2.5 M in hexanes, 250 mmol) and anhydrous THF (250 mL) was cooled down to -78 °C (dry-ice / isopropanol). Dimethyl methylphosphonate (31.1 g, 250 mmol) was then added dropwise in 5 minutes. The colorless solution turned into a white gel. The mixture was stirred at -78 °C for 30 minutes. A solution of ethyl 3,5-dimethylhexanoate (2) (15 g, 87.25 mmol) in anhydrous THF (10 mL) was added dropwise. The mixture turned into a colorless liquid again. The temperature was then allowed to rise up to -20 °C in 2 h. A saturated solution of NH_4Cl (100 mL) was then added to the mixture. The aqueous layer was extracted with dichloromethane (2 x 100 mL). The organic layers were washed with water (2 x 200 mL) and with a solution of saturated NaCl (2 x 200 mL), dried over $MgSO_4$, filtered and concentrated. The crude product (21.05 g, ~ 84 mmol, ^{1}H NMR conversion 99 %) was not purified and used as such in the following step of the synthesis.

^{1}H NMR (300 MHz, $CDCl_3$): δ = 3.79 (d, J^3 = 11 Hz, 6 H), 2.98-3.18 (m, 2 H), 2.52-2.62 (dd, J^3 = 5 Hz, J^3 = 17 Hz, 1 H), 2.36-2.47 (dd, J^3 = 8 Hz, J^3 = 17 Hz, 1 H), 2.09 (m, 1 H), 1.62 (m, 1 H), 1.00-1.16 (m, 2 H), 0.84-0.90 (m, 9 H)

^{13}C NMR (75 MHz, $CDCl_3$) : δ = 201.62, 52.93, 51.85, 46.34, 41.76, 26.72, 25.29, 23.23, 22.17, 19.84.

(E)-2,8,10-trimethyl-4-undecene-6-one (4)

NaH (3.36 g, 84.1 mmol, 60 % in mineral oil) was washed in a two-neck flask under argon atmosphere with petroleum ether (3 x 30 mL) and dried under vacuum. Anhydrous THF (100 mL) was then poured onto NaH and cooled down to 0°C. Dimethyl 4,6-Dimethyl-2-oxoheptylphosphonate (3) (21.05 g, ~ 84 mmol) was then added dropwise in 15 minutes. After 15 additional minutes isovaleraldehyde (9 mL, 84 mmol) was slowly added to the mixture. The mixture was stirred at 0°C for 15 minutes. Water (150 mL) and Et_2O (150 mL) were then added. The aqueous layer was extracted with Et_2O (2 x 150 mL). The organic layers were washed with a saturated solution of NaCl (2 x 250 mL), dried over $MgSO_4$, filtered and concentrated. The crude product (17.67 g, ~ 84 mmol, ^{1}H NMR conversion 96 %) was not further purified and used as such in the following step of the synthesis.

^{1}H NMR (300 MHz, $CDCl_3$): δ = 6.79 (dt, J^3 = 7.5 Hz, J^3 = 15 Hz, 1H), 6.09 (dd, J^4 = 2 Hz, J^3 = 15 Hz, 1 H), 2.44-2.52 (dd, J^3 = 6 Hz, J^2 = 15 Hz, 1 H) 2.27-2.36 (dd, J^3 = 7.5 Hz, J^2 = 15 Hz, 1 H) 2.00-2.18 (m, 3 H), 1.78 (m, 1 H), 1.62 (m, 1 H), 1.01-1.8 (m, 2 H), 0.93 (d, J^3 = 7 Hz, 6 H), 0.85-0.90 (m, 9 H).

^{13}C NMR (75 MHz, $CDCl_3$) : δ = 200.67, 146.13, 131.92, 48.18, 46.86, 41.92, 28.15, 27.83, 25.46, 23.49, 22.61, 22.37, 20.24.

2,4,8,10-tetramethylundecan-6-one (5).

CuI (1.60 g, 8.4 mmol) and anhydrous Et_2O (250 mL) were inserted in a three-neck flask under argon atmosphere. The flask was then cooled to 0 °C and methylmagnesium bromide (56 mL, 3.0 M in Et_2O, 168 mmol) was added dropwise in 10 minutes. After 30 minutes of stirring at 0°C, a solution of 2,8,10-trimethyl-4-undecene-6-one (4) (17.67 g, ~ 84 mmol) in anhydrous Et_2O (250 mL) was added dropwise in 30 minutes. After 1h of stirring at 0°C, aqueous HCl (100 mL, 1N) and water (500 mL) were added and a white solid appeared. The aqueous layer was extracted with Et_2O (3 x 200 mL). The organic layers were washed with water (2 x 300 mL) and with a saturated solution of NaCl (2 x 300 mL). The white solid then disappeared. The crude product (17.22 g, 76 mmol) was recovered after drying over $MgSO_4$, filtration and evaporation of the solvent. The crude product was not further purified and used as such in the following step of the synthesis. ^{1}H NMR revealed that the (1,4)/(1,2)-addition ratio ws about 9:1. As a consequence, the content of 2,4,8,10-tetramethylundecan-6-one in the mixture was about 15.5 g (~ 68.5 mmol)

^{1}H NMR (300 MHz, $CDCl_3$): δ = 2.28-2.37 (dd, J^3 = 5 Hz, J^2 = 15 Hz, 2 H), 1.99-2.21 (m, 4 H), 1.61 (m, 2 H), 0.98-1.14 (m, 4 H), 0.83-0.90 (m, 18 H).

^{13}C NMR (75 MHz, $CDCl_3$) : δ = 211.28, 51.43, 51.37, 46.67, 46.63, 27.03, 25.38, 23.44, 22.26, 20.11.

2,4,8,10-tetramethyl-6-methylene-undecane (6)

Methyltriphenylphosphonium bromide (54.29 g, 152 mmol) and *t*-BuOK (152 ml, 1.0 M in THF, 152 mmol) were inserted into a three-neck round-bottom flask under argon atmosphere. The mixture was stirred at room temperature for 10 minutes. The mixture containing 2,4,8,10-tetramethylundecan-6-one (*vide supra*, 17.2 g, 68.5 mmol of (5)) was then

added dropwise. The reaction was stopped after 2 hours of stirring at room temperature by addition of water (100 mL) and AcOEt (100 mL). The aqueous layer was then extracted with AcOEt (3 x 100 mL). The combined organic layers were washed with water (2 x 200 mL), then with saturated NaCl (2 x 200 mL), dried over $MgSO_4$, filtered and concentrated. The crystallization of triphenylphosphine oxide occured during evaporation of the solvent. This solid was then triturated in pentane (100 mL) and filtered. This procedure was repeated several times. The combined filtrates were concentrated and the crude product was purified by flash chromatography (flash silica, petroleum ether 100 %).

Yield : 13.86 g (61.8 mmol, 71 % over 4 steps), colorless liquid.

^{1}H NMR (300 MHz, $CDCl_3$): δ = 4.71 (s, 2 H), 1.90-2.08 (m, 2 H), 1.58-1.80 (m, 6 H), 0.79-1.18 (m, 22 H).

^{13}C NMR (75 MHz, $CDCl_3$) : δ = 147.57, 111.94, 111.83, 47.17, 46.76, 44.48, 44.18, 28.40, 28.29, 25.43, 23.74, 23.60, 22.47, 22.30, 20.08, 19.83.

4.1.6.2. Synthesis of 2,4,8,10-tetramethyl-6-[^{13}*C*]-methylundecane

2,4,8,10-tetramethyl-6-[^{13}*C*]-methylene-undecane

^{13}C-methyltriphenylphosphonium iodide (0.245 g, 0.6 mmol) and *t*-BuOK (0.6 ml, 1.0 M in THF, 0.6 mmol) were inserted into a three neck round bottom flask under argon atmosphere. The mixture was stirred at room temperature for 7 minutes. 2,4,8,10-tetramethylundecan-6-one (0.138 g, 0.6 mmol) was then added dropwise. The reaction was stopped after 3.5 hours of stirring at room temperature by addition of 1 mL of water and 10 mL of AcOEt. The aqueous layer was then extracted with AcOEt (3 x 5 mL). The combined organic layers were washed with water (1 mL), then with saturated NaCl (3 x 1 mL), dried over $MgSO_4$, filtered and

concentrated. The crystallization of triphenylphosphine oxide occured during evaporation of the solvent. The solid was then triturated in pentane and filtered. This procedure was repeated several times. The combined filtrates were concentrated purified by flash chromatography (flash silica, petroleum ether 100 %).

Yield : 0.009 g (0.04 mmol, 7 %), colorless liquid.

^{1}H NMR (300 MHz, $CDCl_3$): δ = 4.70 (d, 2 H, $J_{1H\text{-}13C}$ = 155 Hz), 1.89-2.08 (m, 2 H), 1.58-1.81 (m, 6 H), 0.79-1.18 (m, 22 H).

^{13}C NMR (75 MHz, $CDCl_3$) : δ = 111.85, 111.74. Other signals in baseline noise.

2,4,8,10-tetramethyl-6-[*^{13}C*]-methylundecane

To a three-neck round-bottom flask was added 2,4,8,10-tetramethyl-6-*[^{13}C]*-methylene-undecane (0.009 g, 0.04 mmol) and 10% Pt/C (tip of a spatula). The atmosphere in the flask was purged three times with argon and three times with hydrogen. The reaction mixture was stirred vigorously at 25 °C under hydrogen atmosphere (~ 1 atm) for 43h.The catalyst was then filtered and the crude product was recovered after distillation of the solvent and was not further purified.

Yield : 0.010 g, (0.04 mmol, 98 % conversion), colorless liquid.

^{1}H NMR (300 MHz, $CDCl_3$), mixture of isomers δ = 1.46-1.74 (m, 5 H), 0.75-1.22 (m, 29 H)

^{13}C NMR (75MHz, $CDCl_3$), mixture of isomers δ = : 48.08, 47.80, 47.13, 46.75, 46.20, 46.10, 45.01, 27.68-27.80, 27.40-27.43, 25.34-25.43, 24.00, 23.85, 23.54, 23.43, 22.72, 22.64, 22.37, 22.21, 21.01, 20.79, 20.43-20.46, 20.07, 19.85, 19.65.

4.2 Chromatographic separation of the diastereoisomers of PMU precursors

A part of this work has been published in the supplementary data of J. Phys. Chem. B ***2010****, 114, 11753-11760. The full paper is disclosed in Chapter 4.*

4.2.1 Introduction

As stated earlier, a first attempt to separate the diastereoisomers of 6-p-toluenesulfonyloxymethyl-2,4,8,10-tetramehtylundecane (compound **9** in scheme 4.3) in analytical scale was illustrated in the previous section of this chapter (see Figure 4.2 in paragraph 4.1.2). Nevertheless, the experimental conditions were not appropriate for preparative-scale chromatography as retention times were quite long. Besides, most of the preparative phases have a coarser granulometry of at least 10µm that is less efficient than a 5µm analytical phase. No better experimental conditions could be found and no separation at all was observed in normal phase. It was therefore decided to investigate the potential separation of 6-hydroxymethyl-2,4,8,10-tetramethylundecane (compound **8** in scheme 4.3) diastereoisomers.

Considering the aliphatic structure of 6-hydroxymethyl-2-4-8-10-tetramethylundecane, it should be possible to separate its diastereoisomers in either normal or reverse phases. However, one might expect detection issues as the hydroxyl group is a really poor chromophore in the wavelength range of typical UV detectors. The acquisition of a corona discharge detector (Corona CAD® from ESA) was therefore necessary. This detector is claimed universal as it is able to detect all chemical compounds, even those devoid of chromophores, as long as their molecular weight is high enough to prevent

evaporation together with the mobile phase. This detector is very sensitive and operates in a wide range of concentrations which enables it to detect injected quantities from the nanogram up to the milligram-scales. Besides its response factor is independent of the nature of the sample. It is therefore a concentration detector. Nevertheless, it also has a few drawbacks: (i) it is destructive, (ii) it consumes up to 5 L/min of nitrogen to dry, atomize and ionize the solute, (iii) it can only handle flow rates below 1.5 mL/min. The latter is an additional complication for (semi-)preparative scale as a flow splitter is required between the preparative column upstream and the corona detector and the fraction collector downstream. This also implies additional back-pressure, peak broadening, and a possible delay between detection and fraction collection.

Equipment at our disposal

Before investigating the analytical scale separation of 6-hydroxymethyl-2,4,8,10-tetramethylundecane, it is necessary to establish the list of equipment at our disposal for the large scale separation in order to properly prepare the study at analytical scale. Here is the list of preparative equipment available for our project:

- A Waters modular semi-preparative HPLC that can deliver a mobile phase flow rate up to 20 mL/min, equipped with the Corona detector, a flow splitter and a fraction collector. The available columns are a Xterra C18 30x100 mm, 5 µm reverse phase column (the corresponding 4.6x100 mm, 5 µm analytical column is also available), a Waters Novapack 30x300mm, 6µm reverse phase column (the corresponding 3.9x300 mm analytical column is also available but with a stationary phase of 4 µm). This HPLC was setup to operate in reverse-phase mode.
- A preparative-scale HPLC specifically designed by the Union Chimique Belge (UCB) to meet the needs of UCL that consists of two Gilson

pumps which are able to operate with binary gradients of solvents, a thermostatic bath to control the temperature of the mobile phase, four 50x250 mm preparative columns (Lichrosphere Si60, 12 µm, normal phase; Kromasil C18, 10 µm, reverse phase; OD, 20 µm, chiral phase and AD, 20 µm, chiral phase), a UV detector and a 12-way serial fraction collector triggered by the UV signal of the detector. The corresponding analytical columns are available except for the Lichrosphere stationary phase.

- A Prochrom LC80 medium pressure preparative column that uses dynamic axial compression to pack bulk silica. This system consists of two pumps (out of phase with each other) that can only work in isocratic mode, a stainless steel column of 80 mm on internal diameter that must be filled with bulk stationary phase in suspension in ~2 L of solvent. The height of the bed is determined by the amount of stationary phase and can reach a maximum of 40 cm. Once poured in the column, the suspension is packed axially and a holding pressure is applied throughout the elution. The stationary phase can undergo several elution cycles before unloading. The elution is monitored with a UV detector and fractions are collected semi-automatically (on a time basis and not according to the detector signal). Although any kinds of stationary phase can be packed in the Prochrom, 40-63 µm or 15-40 µm bulk silica are usually used (reverse and chiral phases being much more expensive). No analytical scale columns were available with the same granulometry of stationary phase. Small scale trials were therefore performed on a Waters Novapack Si60, 3.9x300 mm, 4 µm, normal phase column.

4.2.2 Results

Reverse phase analytical separation of 6-hydroxymethyl-2,4,8,10-tetramethylundecane

The first attempt was performed on the Supelco Kromasil C18, 10 µm, 4.6x250 mm analytical scale column. As depicted on Figure 4.5, an acceptable separation with baseline resolution could be obtained using a mixture of acetonitrile and water (85:15 v/v) at a flow rate of 1 mL/min. Both Corona and UV signals are superimposed on the Figure. This clearly illustrates the poor UV absorption of the hydroxyl group compared to the strong detection of the Corona CAD®. Peak assignment was done by comparing the relative concentration of each stereoisomer as measured by HPLC and GC (see table 4.2 for the assignments of the GC peaks). The relative concentration of each stereoisomer was 32 % of (4R,6s,8S)-**9**, 50 % of (4R,8R)- and (4S,8S)-**9**, 18 % of (4R,6r,8S)-**9**. The isotactic stereoisomer was thus the first one to be eluted in reverse phase HPLC. Although the separation was quite good already, it still required improvement before scaling up the separation. Increasing the water content of the mobile phase helped separate the peaks (better separation factor) but as peaks broadened, the resolution could not be improved. Other columns were thus tested to improve the resolution.

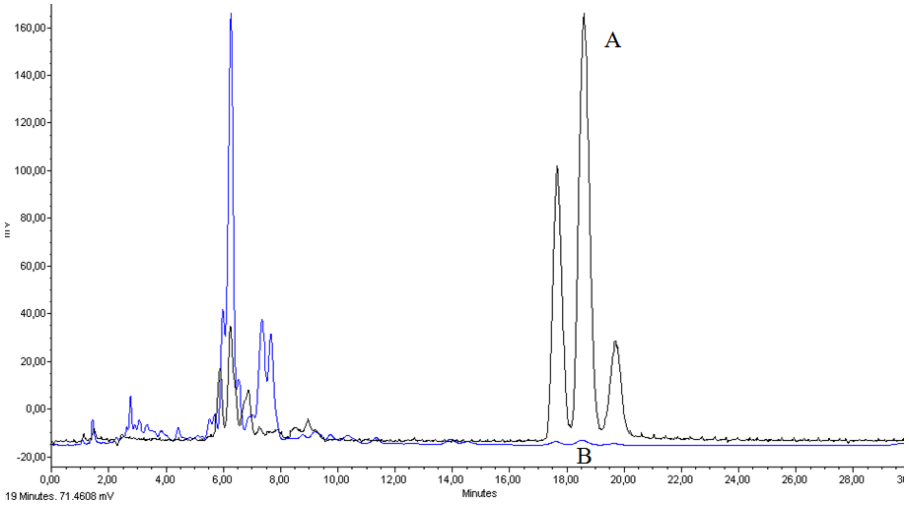

Figure 4.5 : reverse phase separation of 6-hydroxymethyl-2,4,8,10-tetramethylundecane, Supelco Kromasil C18, 10 µm, 4.6x250 mm, acetonitrile/water (85:15 v/v), 1 mL/min. A : Corona detection, B : UV detection at 227 nm.

The second attempt was performed on a Waters Xterra C18 4.6x100 mm, 5 µm. No satisfactory separation could be obtained either in isocratic or gradient mode. However, increasing the length of the column to 300 mm helped improve the separation. Figure 4.6 shows the separation of the same sample with different water content in the mobile phase. Increasing the water content increased the retention times but improved the separation factor and the resolution. However as the length of the preparative Xterra C18 column is only 100 mm, these results were left aside.

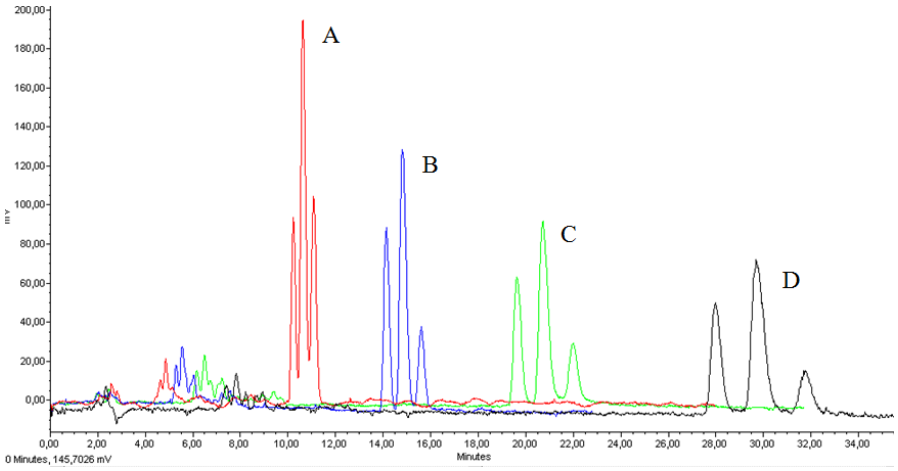

Figure 4.6 : reverse phase separation of 6-hydroxymethyl-2,4,8,10-tetramethylundecane, Xterra C18 4.6x100 mm, 5 µm, 1 mL/min. A : acetonitrile/water 85:15 v/v, B : acetonitrile/water 80:20 v/v, C : acetonitrile/water 75:25 v/v, D : acetonitrile/water 70:30 v/v

The third attempt was performed on a Waters Novapack 3.9x300 mm, 4 µm. A baseline resolution could be obtained within 12 minutes (acetonitrile/water 85:15 v/v, 1 mL/min). However, as shown in Figure 4.7, an improved resolution that could be transposed to preparative scaled was obtained when increasing the water content of the mobile phase up to 30%. Those conditions were tested on the preparative column Waters Novapack 30x300 mm, 6 µm.

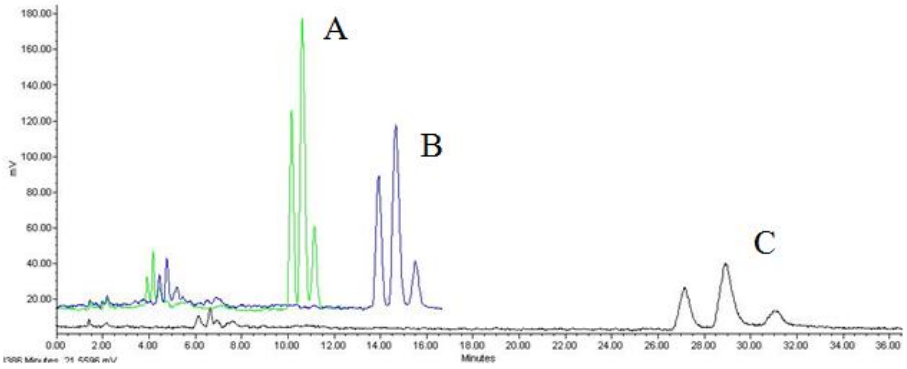

Figure 4.7 : reverse phase separation of 6-hydroxymethyl-2,4,8,10-tetramethylundecane, Waters Novapack 3.9x300 mm, 4 µm, 1 mL/min. A : acetonitrile/water 85:15 v/v, B : acetonitrile/water 80:20 v/v, C : acetonitrile/water 70:30 v/v

Reverse phase semi-preparative separation of 6-hydroxymethyl-2,4,8,10-tetramethylundecane

The preparative flow rate that must be applied can be calculated from Equation 4.1 :

$$preparative\ \ flow\ rate = analytical\ \ flow\ rate \times \frac{D_{prep}{}^2}{D_{ana}{}^2} \qquad (4.1)$$

This equation is only valid if the diameter of the column is the only parameter to vary (same stationary phase, same granulometry, etc). In this particular case, the granulometry is 4 µm in analytical scale but 6 µm in preparative scale. The efficiency is therefore expected to be lower on the preparative column. According to equation 4.1, a flow rate of approximately 60 mL/min would be required to adapt the separation of 6-hydroxymethyl-2,4,8,10-tetramethylundecane on the Waters Novapack 30x300 mm, 6 µm on the semi-preparative HPLC but the pumping device can only provide

20 mL/min. Therefore the experimental conditions have to be adapted directly on the semi-preparative column with a stronger mobile phase to compensate the low flow rate available. For these trials, a mixture containing no isotactic isomer was used in order not to waste any. The semi-preparative HPLC chain was equipped with an adjustable flow splitter set to a split ratio of 19:1. The larger portion of the flow rate was sent to the fraction collector whereas the smaller portion of the flow rate (approximately 1 mL/min) was sent to the detector. Figure 4.8 shows an overlay of 3 runs from the same sample. Elution A was performed with the 3.9x300 mm analytical column with a mobile phase consisting of acetonitrile/water 85:15 v/v at a flow rate of 1 mL/min. The chromatogram confirms that there is almost no isotactic isomer in the mixture. Elution B was performed on the 30x300 mm semi-preparative column with a mobile phase consisting of acetonitrile/water 95:5 v/v at a flow rate of 20 mL/min. The chromatogram reveals that the two peaks of interest are not correctly separated despite the quite long retention time of 17 minutes. It is also surprising to see a very broad peak preceding the two peaks of interest because the sample appeared clean on the analytical column. Elution C was performed with a weaker mobile phase consisting of acetonitrile/water 90:10 v/v. The two stereoisomers were still not correctly separated and were still contaminated with impurities. Besides, an additional difficulty that was faced was the low solubility of 6-hydroxymethyl-2,4,8,10-tetramethylundecane in acetonitrile. The sample was thus dissolved into methanol prior injection.

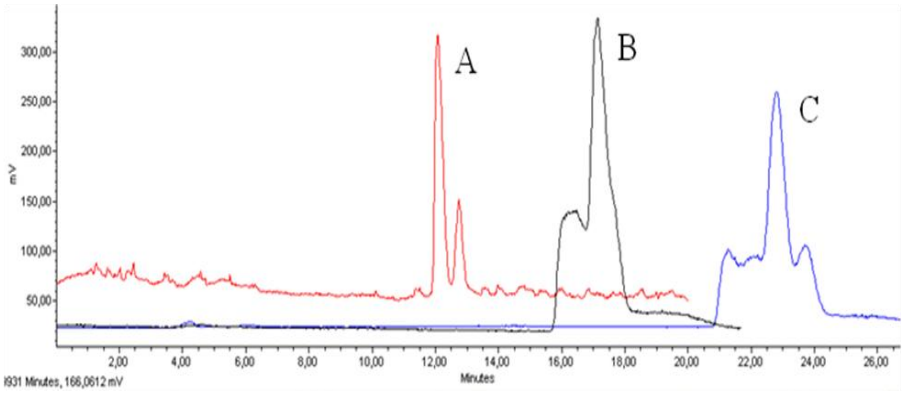

Figure 4.8 : reverse phase separation of 6-hydroxymethyl-2,4,8,10-tetramethylundecane. A : Waters Novapack 3.9x300 mm, 4 µm, acetonitrile/water 85:15 v/v, 1 mL/min, 1 µL injected, B : Waters Novapack 30x300 mm, 6 µm, acetonitrile/water 95:5 v/v, 1 mL/min, 25 µL injected, C : Waters Novapack 30x300 mm, 6 µm, acetonitrile/water 90:10 v/v, 1 mL/min, 30 µL injected.

The long retention times, the poor resolution, the low solubility of the sample and the low capacity of reverse phases made us consider the normal phase separation of 6-hydroxymethyl-2-4-8-10-tetramethylundecane.

Normal phase preparative separation of 6-hydroxymethyl-2,4,8,10-tetramethylundecane

As no identical columns were available in either analytical and (semi-)preparative scales, it was decided to search for optimal separation conditions directly with preparative columns. The first trial was done with a Lichrosphere Si60 50x250 mm, 12 µm connected to the preparative HPLC unit from UCB. Figure 4.9 shows the chromatogram of a sample containing the three diastereoisomers of 6-hydroxymethyl-2,4,8,10-tetramethyl-undecane. The mobile phase consisted of a mixture of hexane and ethyl acetate 85:15 v/v. An adjustable flow splitter was used to send 65 mL/min of mobile phase in the collecting device and 1 mL/min in the Corona detector.

Fraction collection was performed manually according to the signal observed on the Corona detector.

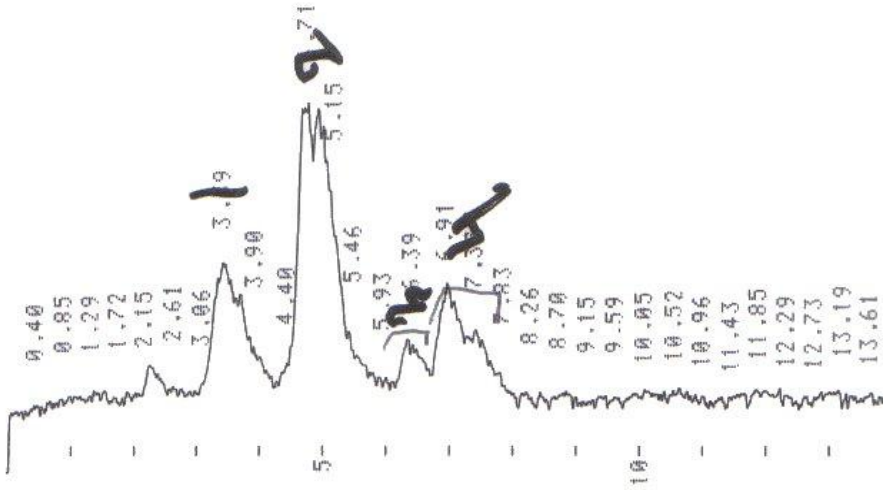

Figure 4.9 : normal phase preparative separation of 6-hydroxymethyl-2,4,8,10-tetramethylundecane. Lichrosphere Si60 50x250 mm, 12 µm, hexane/ethyl acetate 85:15 v/v, detector flow rate : 1 mL/min, collector flow rate : 65 mL/min. 30 mg injected.

The peaks identified as 1, 2, 3 and 4 were collected. The three diastereoisomers of 6-hydroxymethyl-2,4,8,10-tetramethylundecane were recovered in fractions 3 and 4 only. Peak assignment was performed by injecting each collected fraction as well as the starting mixture in the Alliance separation module equipped with the Waters Novapack Si60, 4 µm, 3.9x300 mm and a mixture of hexane and ethyl acetate 92:8 v/v as the mobile phase at a flow rate of 1 mL/min. In such conditions, the three peaks were correctly separated within 6 minutes for fast and easy identification of the streoisomers. Retention times were 4.48 min, 5.03 min and 5.30 min for (4R,6r,8S)-**9**, (4R,8R)- together with (4S,8S)-**9**, and (4R,6s,8S)-**9** respectively. The order of elution is thus the contrary of the elution order that was observed in reverse phase. A second injection was performed in the same conditions but many additional peaks that superimpose to the peaks of

interest were observed. We were able to identify the three stereoisomers as a single unresolved peak among the many others. The injections appeared therefore non reproducible. Besides, the load cannot exceed 30 to 50 mg of the initial mixture. This implies that very large amounts of solvent must be evaporated to recover only a few milligrams of product. Finally, the third run could not be correctly monitored because of repetitive software crashes. The temperature of the thermostatic bath was not correctly regulated and started to overheat until it eventually burnt.

It was then decided to give up using this HPLC equipment and started to develop a new method on the Prochrom. In a first time, it was necessary to connect the Corona detector and the adjustable flow splitter to the Prochrom. Unfortunately, the additional back pressure created by those two items was too high for the pumping system that could not deliver flow rates above 40 mL/min. Hence, the Corona detector could not be used in-line and we had to turn to an off line detection method, preventing us to run in a continuous way through successive injections. As a consequence, blind elution of the mixture of isomer was performed and the collected fractions were sampled and injected in the Alliance analytical HPLC equipped with corona detection for product identification. Fractions containing only one diastereoisomer were combined and converted into PMU separately. In these conditions, it was difficult to perform more than 3 consecutive injections because of the long analysis time of the collected fractions and collecting tubes availability. The main benefit of this technique is the capacity of the column as it can handle a sample load of at least one gram.

To determine the optimal eluting power of the mobile phase, several mixtures of solvents were tested using thin layer chromatography. Hexane / ethyl acetate 97:3 v/v provided a retention factor of 0.2-0.35 as one large

spot that obviously contains the three diastereoisomers. A first run was performed with a sample load of 1.2 g of crude 6-hydroxymethyl-2,4,8,10-tetramethylundecane (24% of (4R,6r,8S)-**9**, 54 % of (4R,8R)- and (4S,8S)-**9**, 22 % of (4R,6s,8S)-**9**) in solution in 5 mL of the mobile phase. The flow rate was set to 90 mL/min. In these conditions, it was possible to recover 81% of the syndiotactic model (the first stereoisomer to elute), 48% of the atactic models (second stereoisomer to elute) and 30% of the isotactic model (the last stereoisomer to elute). The remaining percentages were recovered as binary mixtures of isomers. A few additional attempts to improve the separation were made using finer silica (15-40µm) and different hexane / isopropanol mixtures of solvents to compensate the higher retention of the finer silica but the resolution could not be ameliorated. We kept working with the initially established conditions for a few additional runs to build up a stock of each precursor. In this manner, it was possible to accumulate up to 952 mg of pure syndiotactic precursor, 678 mg of pure atactic precursors but only 297 mg of pure isotactic precursor. Aside from these fractions of pure isomers, several other fractions were collected and gathered together according to their relative concentration in each isomer. The pure fractions were converted into pure PMU models according to scheme 3.3 and a fraction of 1.833 g containing both isotactic and atactic precursors in a 50:50 ratio was converted as well. Because each run is very time and solvent consuming it was decided not to pursue the separation any further. The total amount of each model recovered after conversion to PMU was 711 mg (3.14 mmol) of syndiotactic PMU, 506 mg (2.24 mmol) of atactic PMU, 222 mg (0.98 mmol) of isotactic PMU and 1.442 mg (6.37 mmol) of the isotactic/atactic 50:50 mixture of PMU.

4.2.3 Experimental

6-hydroxymethyl-2-4-8-10-tetramethylundecane (8)

A two-neck round-bottom flask under argon atmopshere containing 2,4,8,10-tetramethyl-6-methylene-undecane **6** (13.86 g, 61.8 mmol) was cooled to 0 °C. Borane-THF (75 mL, 1 M in THF, 75 mmol) was then inserted dropwise and stirred for 3 hours at room temperature. The mixture was then cooled again to 0 °C and water (70 mL) was carefully added to neutralize the excess of hydride. NaOH (70 mL, 3N) and then H_2O_2 (70 mL, 30 wt%) were slowly added and the mixture was stirred for 12 hours at room temperature. A saturated solution of K_2CO_3 (130 mL) and dichloromethane (50 mL) were then added. The aqueous layer was separated and extracted with dichloromethane (2 x 75 mL); the combined organic layers were washed with water (2 x 150 mL) and with a saturated solution of NaCl (2 x 150 mL), dried over $MgSO_4$, filtered and concentrated. The crude product (14.79 g, 61 mmol, ^{1}H NMR conversion: 99%) was not further purified and used as such in MPLC for the separation of the stereoisomers.

^{1}H NMR (300 MHz, $CDCl_3$), (4R,6r,8S)-**8** : δ = 3.51 (d, J^3 = 5 Hz, 2 H), 1.46-1.72 (m, 5 H), 1.22-1.36 (m, 4 H), 0.89-1.16 (m, 4H), 0.78-0.89 (m, 18 H).

^{1}H NMR (300 MHz, $CDCl_3$), (4R,6s,8S)-**8** : δ = 3.51 (d, 2 H), 1.48-1.75 (m, 5 H), 0.91-1.30 (m, 8 H), 0.74-0.91 (m, 18 H).

^{1}H NMR (300 MHz, $CDCl_3$), (4R,8R)- and (4S,8S)-**8** : δ = 3.50-3.60 (dd, J^3 = 4.8 Hz, J^2 = 10.5 Hz, 1 H), 3.39-3.49 (dd, J^3 = 5.7 Hz, J^2 = 10.5 Hz, 1 H), 1.45-1.74 (m, 5 H), 0.74-1.34 (m, 26 H).

^{13}C NMR (75 MHz, $CDCl_3$), (4R,6r,8S)-**8** : δ = 65.91, 47.31, 40.20, 35.29, 27.89, 25.38, 23.74, 22.38, 20.47.

^{13}C NMR (75 MHz, $CDCl_3$), (4R,6s,8S)-**8**: δ = 66.97, 47.21, 40.10, 35.47, 27.96, 25.39, 23.77, 22.33, 20.51.

^{13}C NMR (75 MHz, $CDCl_3$), (4R,8R)- and (4S,8S)-**8** : δ = 66.47, 47.67, 47.56, 40.41, 39.30, 35.41, 27.93, 27.70, 25.35, 23.63, 23.59, 22.47, 20.22, 20.18.

Analytical HPLC

All analytical separations were performed on a Waters Alliance 2690 separation module equipped with the Corona CAD® detector from ESA along with a Waters 2996 photodiode array detector. Trials were performed from a stock solution of 6-hydroxymethyl-2,4,8,10-tetramethylundecane at a concentration of 2 mg/mL (in acetonitrile for reverse phase separations or in hexane/ethyl acetate for normal phase separations). Mixtures of solvents were prepared automatically from HPLC-grade solvents that were degassed and filtered. The injection volume was 1µL and the flow rate was 1 mL/min.

Semi-preparative HPLC

The modular semi-preparative HPLC consisted of a Waters 600 pump that can deliver a maximum flow rate of 20 mL/min, the Corona detector together with an SSI three way stream-splitting valve to limit the inlet flow inside the Corona below 1.5 mL/min and a Waters 717plus Fraction Collector III. Trials were performed from a stock solution of 6-hydroxymethyl-2,4,8,10-tetramethylundecane at a concentration of 10 mg/mL in methanol. Mixtures of solvents were prepared automatically from HPLC-grade solvents that were degassed and filtered. The injection volume was 25 or 30µL and the flow rate was 20 mL/min.

Preparative HPLC

The preparative HPLC equipment was provided by UCB and consisted of two Gilson 305 HPLC pumps that can deliver a flow rate up to 200 mL/min. The mobile phase consisted in a manually prepared mixture of technical grade hexane and ethyl acetate 85:15 v/v that were distilled, filtered and degassed prior usage. An ASI quicksplit adjustable flow splitter was used to split the flow rate in order to provide a constant flow rate of 1 mL/min inside the Corona detector. A paper recorder was connected to the Corona and fraction collection was done manually. 3 mL of 6-hydroxymethyl-2,4,8,10-tetramethylundecane in solution in the same mixture of solvents than the mobile phase was injected. The collected fractions were injected in the Alliance separation module equipped with the Waters Novapack Si60 4 µm, 3.9x300 mm column, and using a mixture of hexane and ethyl acetate 92:8 v/v as the mobile phase at a flow rate of 1 mL/min. Retention times were 4.48 min, 5.03 min and 5.30 min for (4R,6r,8S)-**9**, (4R,8R)- and (4S,8S)-**9**, and (4R,6s,8S)-**9** respectively.

Preparative MPLC

MPLC apparatus consisted of a Prochrom LC80 (80 mm internal diameter) stainless steel column with dynamic axial compression. Bulk silica (500 g, 40-63 µm) was used as stationary phase. The flow rate of the mobile phase was 90 mL / min (hexane / ethyl acetate 97:3 v/v, R_f = 0.2-0.35 as a unique large spot). Hexane and ethyl acetate (technical grade) were distilled under vacuum and mixed together in a 10 L tank. The solvent mixture was degassed by bubbling nitrogen through the tank for 5 minutes. The sample load was 1.2 g of crude 6-hydroxymethyl-2,4,8,10-tetramethylundecane in solution in 5 mL of mobile phase (24% of (4R,6r,8S)-**9**, 54 % of (4R,8R)- and (4S,8S)-**9**, 22 % of (4R,6s,8S)-**9**). Blind elution was performed and fractions of 30 mL were collected with a Gilson 202 fraction collector. A sample of each fraction was injected in the Waters Alliance HPLC using a Waters

Novapack column (SiO_2, 4µm, 3.9 x 300 mm). The mobile phase consisted of a mixture of hexane and ethyl acetate 92:8 v/v at a flow rate of 1 mL/min. Fractions containing the same isomer(s) were gathered together.

Finally, the following fractions were recovered:

- (4R,6r,8S)-**9** : 0.2195 g (0.905 mmol, 81% of the initial stereoisomer content of the mixture)
- (4S,8S)- and (4R,8R)-**9** : 0.2927 g (1.207 mmol, 48% of the initial stereoisomer content of the mixture)
- (4R,6s,8S)-**9** : 0.0745 g (0.307 mmol, 30% of the initial stereoisomer content of the mixture)

The remaining fractions (for a total of 0.5426 g, 2.238 mol) consisted of a mixture of 2 diastereoisomers and were re-injected in a following MPLC run. The collected fractions were converted into PMU according to the procedures described in paragraph 4.1.3.

4.3 2,4,6,8,10-pentamethylundecane as a model compound for polypropylene epimerization in the presence of NBS.

4.3.1 Introduction

Low molecular weight model compounds are often used to investigate chemical reactions usually performed on polymers as they are easier to handle and their products of reaction are more easily identified through the common spectroscopic methods of the organic chemist. Many examples of mechanistic studies on polyolefin-based model compounds can be found in the literature to elucidate polyolefins reactivity,[1,2] degradation pathways,[3,4] conformational studies,[5-7] epimerization[5,8-10] and functionalization.[11-22] As demonstrated in the first section of this chapter, our team has already successfully used the close correlation between the spectroscopic data of the models and those of the different polypropylenes for the post-synthesis identification of the pure stereoisomers of PMU.

As explained throughout this chapter, tremendous efforts were devoted to set up a synthesis route of 2,4,6,8,10-pentamethylundecane as well as a separation method of its stereoisomers in order to obtain model compounds reflecting the different tacticities of polypropylene, including iPP. Despite those many efforts only a few milligrams of each stereoisomer could be recovered. Nevertheless, the last period of this thesis was devoted to the use of those models to investigate the effect of NBS on PP tacticity. Considering the difficulties encountered during the separation of the diastereoisomers of PMU and hence the very low amount of pure isotactic PMU recovered, the first investigations were conducted on a 50:50 atactic/isotactic mixture to assess the feasibility of the experiments. Finally, experiments were

performed on the pure syndiotactic model, available in a much more reasonable quantity than the isotactic model. Although syndiotactic polypropylene has never been processed in reactive extrusion in the presence of peroxide and NBS, random epimerization should occur as well.

In chapter two, the formation of "dormant species" through reversible addition of bromine radicals onto PP macroradicals was suggested to explain the higher grafting levels obtained in the presence of NBS. This reversible coupling would temporarily trap PP macroradical before chain scission occurs. PP macroradical would be progressively re-activated again to allow maleic anhydride grafting. However, no elemental analyses could demonstrate the presence of grafted bromine on polypropylene after reactive extrusion in the presence of NBS. XRF measurements revealed that only 5 to 7 wt.% of the total amount of bromine introduced in the reactive mixture was recovered in the final product after polymer washing.[23] In order to identify the presence of such a dormant species in the reaction mixture of the models, the synthesis of a brominated model compound of PMU (namely 6-bromo-2,4,6,8,10-pentamethylundecane, PMUBr) was attempted from 2,4,8,10-tetramethylundecan-6-one (compound **5** in schemes 4.2 and 4.3 in section 4.1). As depicted in Scheme 4.4, ketone **5** was engaged in a Grignard reaction to insert the central methyl group, creating the tertiary alcohol **10**. This alcohol was then reacted with BBr_3 to substitute the hydroxyl group by a bromine atom according to a known procedure.[24]

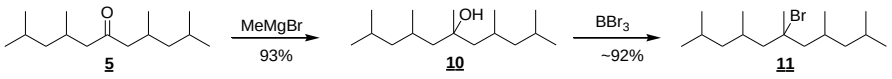

Scheme 4.4 : synthesis route towards 6-bromo-2,4,6,8,10-pentamethylundecane from intermediate ketone **5**.

4.3.2 Experimental

2,4,6,8,10-pentamethylundecan-6-ol (10)

A two-neck flask under argon atmosphere containing MeMgBr (3 M in diethyl ether, 3.5 mL, 10.6 mmol, 1.2 eq.) was cooled down to 0°C. A solution of 2,4,8,10-tetramethylundecan-6-one (2.0 g, 8.83 mmol, 1.0 eq.) in 3 mL of anhydrous diethyl ether was then added dropwise in 15 minutes. The mixture was first stirred at 0 °C for 15 minutes, then at room temperature for another 60 minutes. HCl (1 N, 4 mL) was then added dropwise at 0 °C to stop the reaction. A white precipitate appeared. 20 mL of DCM and 20 mL of water were added to the mixture. The aqueous phase was extracted with 3 x 15 mL of DCM. The combined organic layers were then washed with 3 x 30 mL of saturated NaCl and dried over $MgSO_4$. The crude product was purified over silica using DCM as eluant. 2,4,6,8,10-pentamethylundecan-6-ol (1.99 g, 8.21 mmol, 0.93 eq.) was recovered as a clear oil.

^{1}H NMR (300 MHz, $CDCl_3$): δ = 0.84-0.90 (m, 12 H), 0.91-0.97 (m, 6 H), 1.19 (s, 3 H), 0.98-1.33 (m, 8 H), 1.40-1.49 (m, 2 H), 1.54-1.76 (m, 2H).

6-bromo-2,4,6,8,10-pentamethylundecane (PMUBr, 11)

A two-neck flask under argon atmosphere containing 2,4,6,8,10-pentamethylundecan-6-ol (1.99 g, 8.21 mmol, 1.0 eq) and 20 mL of DCM was cooled down to 0°C. A solution of boron tribromide (1 M in DCM, 10 mL, 10 mmol, 1.22 eq.) was then added dropwise in 5 minutes. The mixture was stirred at 0°C for one hour. A precipitate appeared. The reaction was stopped by addition of 50 mL of water. The aqueous layer was extracted by 2 x 25 mL of DCM. The combined organic layers were washed by 2 x 75 mL of saturated NaCl and dried over $MgSO_4$. The crude product could not be further purified (PMUBr, 2.30 g, 7.55 mmol, 0.92 eq.).

^{1}H NMR (300 MHz, $CDCl_3$): δ = 0.76-0.90 (m, 12 H), 0.90-1.3 (m, 10 H), 1.78 (s, 3 H), 1.51-1.94 (m, 8 H).

Epimerization/grafting reactions

The necessary amounts of reactants and a small magnetic bar were inserted in a 3 ml HPLC glass vial. The vial was sealed with a cap/rubber-septum assembly and degassed under vacuum. The vial was then inserted into a pre-heated home-made electrical barrel-oven at 200 °C that was put down on a magnetic stirrer. The vial was kept in the oven for a certain period of time ranging from 10 min to 24 h, then pulled out of the oven and allowed to cool down to room temperature. A sample of the crude product (a dark brown liquid in each case) was taken out with a syringe, diluted in acetone and filtered through 0.2 µm prior to gas chromatography analysis. The samples were not further purified. Table 4.3 shows the real composition of isotactic/atactic 50:50 PMU models and that of pure syndiotactic model according to gas chromatography. Table 4.4 gathers the composition of all the reactive mixtures prepared for the epimerization/grafting reactions.

Table 4.3 : composition of the mixtures of model compounds engaged in epimerization reactions

Model identification	*% isotactic*	*% atactic*	*% syndiotactic*
PMU iso/ata/syn 50/50/0	52.4	46.9	0.7
PMU iso/ata/syn 0/0/100	<0.1	<0.1	~100

Table 4.4 : composition of the reactive mixtures engaged in epimerization reactions

Run	*PMU Model (iso/ata/syn)*	*PMU (mg)*	*DHBP (µL)*	*wt.% DHBP*	*NBS (mg)*	*wt.% NBS*	*Br_2 (µL)*	*wt.% Br_2*	*Br/Ox*	*MA (mg)*	*wt.% MA*
Epim. 1	PMU 50/50/0	400	10	2	3	0.75	0	0	1	0	0
Epim. 2 (solution)	PMU 50/50/0	400	10	2	3	0.75	0	0	1	0	0
Epim. 3	PMU 50/50/0	300	7.5	2	0	0	2.1	2.1	1	0	0
Epim. 4	PMU 0/0/100	100	2.5	2	0.75	0.75	0	0	1	0	0
Epim. 5	PMU 0/0/100	100	0	0	0.75	0.75	0	0	/	0	0
Grafting 1	PMU 0/0/100	400	10	2	3	0.75	0	0	1	20	5

Gas Chromatography

Fused Silica capillary column, SLB 5ms, 30 m x 0.25 mm x 0.25 µm, supplied by Supelco. Temperature ramp : 50 °C for 5 min., then 50 °C to 280 °C, 10 °C/min. Retention time of isotactic PMU : 13.03 min, atactic PMU : 13.25 min, syndiotactic PMU : 13.41 min.

DSC Measurments

Mettler Toledo 827e was used at atmospheric pressure with 20 µL aluminum pan tightly sealed with the corresponding aluminum lid. The amount of product inside the pan ranged from 3 to 6 mg. The initial temperature was set to 25 °C for 2 minutes. The temperature was then increased to 300 °C at a rate of 10 °C/min.

4.3.3 Results

Synthesis of PMUBr

No particular issues were encountered during the preparation of the tertiary alcohol **10** and a 93% yield was obtained. The efficiency of the bromination reaction was easily ascertained by ^{1}H NMR spectroscopy as the chemical shift of the three hydrogen atoms from the central methyl group of the aliphatic backbone of the model (large singlet) shifted from 1.19 ppm to 1.78 ppm. The singlet at 1.19 ppm totally disappeared, indicating complete conversion of the tertiary alcohol **10**. Unfortunately, it was not possible to further purify compound **11** as it appeared very sensitive to environmental conditions (quickly turned reddish when exposed to heat or light but also during elution on both normal and reverse phase chromatography). Despite a clean ^{1}H NMR spectrum, GC analysis of the crude product revealed many peaks (~20 peaks) distributed in an elution time range from 4 to 14 minutes. Based on their intensities, none of them can be assigned to a "main product". Those peaks are most likely due to product degradation/rearrangement upon

heating. The ^{1}H NMR spectrum of a sample of PMUBr heated at 100 °C for 15 min is very complicated but poorly resolved signals downfield (4.60 – 5.30 ppm region) indicate PMUBr rearrangement most probably due to dehydrobromination – bromination of the aliphatic backbone, leading to olefins and α-brominated olefins.

Epimerization of PMU model compounds

Table 4.5 summarizes the GC characterization of the mixtures of PMU stereoisomers after epimerization according to Table 4.4, with respect to the starting mixture of stereoisomers

Table 4.5 : Composition of the PMU mixtures after reaction according to gas chromatography.

Run	*Starting PMU model*	*Reaction time*	*% Isotactic*	*% atactic*	*% syndiotactic*
Epim. 1	PMU (50/50/0)	0’	52.4	46.9	0.7
		10’	49.1	47.6	3.3
		+60’	49.3	47.4	3.3
		24h	46.3	47.9	5.8
Epim. 2	PMU (50/50/0)	0’	52.4	46.9	0.7
		90’	48.8	46.6	4.6
Epim. 3	PMU (50/50/0)	0’	52.4	46.9	0.7
		90’	44.3	47.6	8.1
Epim. 4	PMU (0/0/100)	0’	0	0	100
		90’	3.2	5.6	91.2
Epim. 5	PMU (0/0/100)	0’	0	0	100
		90’	1.8	3	95.2
Grafting 1	PMU (0/0/100)	0’	0	0	100
		90’	3.1	5.5	91.4

The reaction mixture of the first run "Epimerization 1" led to the formation 3.3 % of the syndiotactic isomer of PMU after 10 minutes at 200 °C. A small droplet of a mixture of the 3 isomers of PMU was added into the GC vial and then re-injected in the chromatograph to ascertain the observed retention times. To conduct the reaction further, the reaction vessel was put back into the oven for one additional hour. Another sample was taken out and injected in GC. The ratio between each isomer remained unchanged. A fresh sample identical to Epimerization 1 was prepared and reacted for 24 h. The relative concentration of the syndiotactic model reached 5.8 %. The GC trace is shown on Figure 4.10.

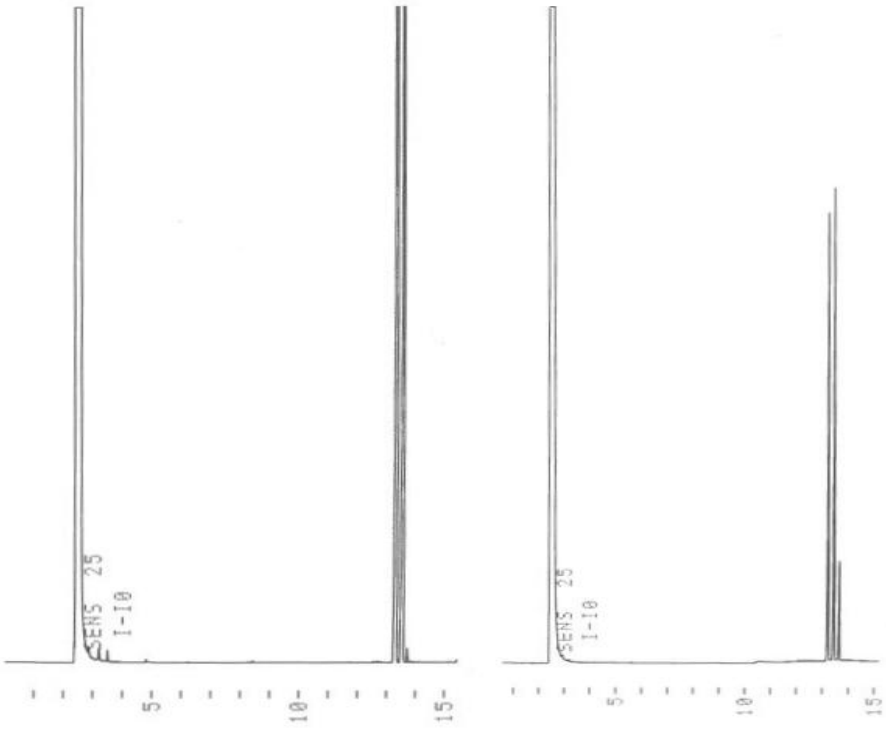

Figure 4.10 : GC trace of the starting mixture of model compounds (left, PMU iso/ata/syn 50:50:0) and GC trace of the mixture of stereoisomers obtained after epimerization for 24 h at 200 °C (right).

This first run demonstrated that epimerization could be observed on our model compounds but yields as high as those obtained on polypropylene could not be reached yet. Epimerization 2 was performed in solution (1 ml dichlorobenzene) whereas Epimerization 1 was conducted in neat PMU. The amount of syndiotactic isomer that was created was in the same range than in neat PMU. For Epimerization 3, NBS was substituted by molecular bromine. It appeared that Br_2 was slightly more efficient than NBS as 8.1 % of syndiotactic isomer could be created. No corresponding data on polypropylene are available as this reaction was never performed by reactive extrusion during this thesis. The higher conversion level reached by Br_2 can be explained by a lower dissociation energy for Br-Br bond compared to the N-Br bond (Br-Br = 194 kJ/mol; N-Br = 276 kJ/mol). All the septa of the vials caps were still airtight after reaction but were distorted because of gas buildup inside the vial. The inner part of the cap, which is made of aluminum, was partially corroded and slightly colored in red/brown under the action of bromohydric acid created during the reaction. Indirect evidence of bromohydric acid formation was also observed during reactive processing as white fumes exiting the extruder die (pH paper test).

Those three first runs were promising and it was decided to confirm those results on a pure isomer. Epimerization 4 was performed in the same way than Epimerization 1, only on a smaller amount of model compound. Both isotactic and atactic products were created in a 1:1.75 ratio, which is close to statistical control. Figure 4.11 shows the GC trace of the stereoisomers mixture after epimerization of the pure syndiotactic model.

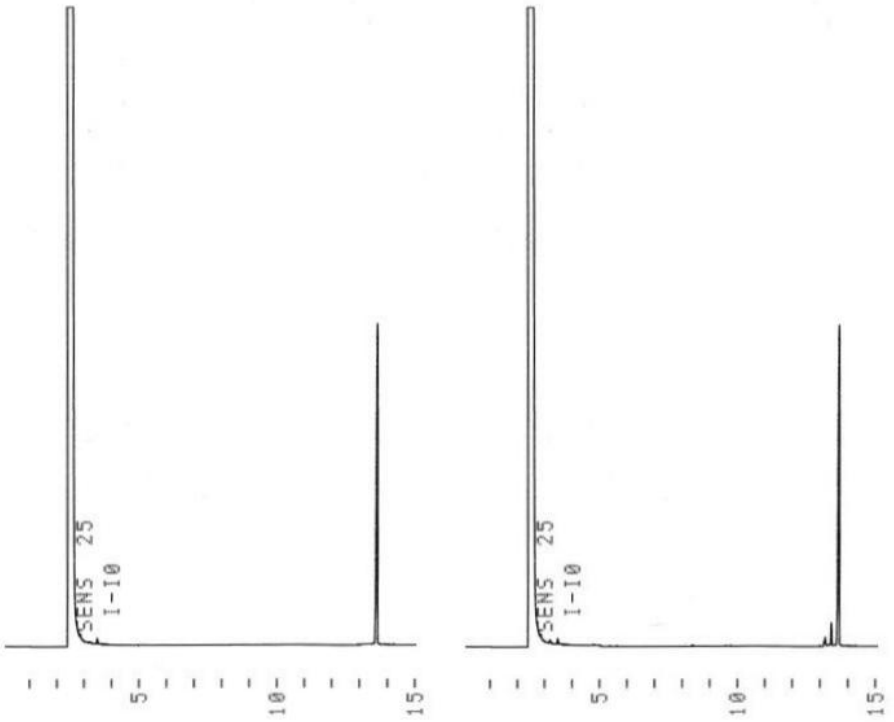

Figure 4.11 : GC trace of the starting syndiotactic PMU model (left, PMU iso/ata/syn 0:0:100) and GC trace of the mixture of stereoisomers obtained after epimerization for 90 minutes at 200 °C (right).

The corresponding reactive extrusion on isotactic polypropylene led to a decrease in crystallinity of ~ 90 % and the remaining content in [mmmm] pentads was ~ 40%. Epimerization 5 was carried out without peroxide to see whether or not a radical initiator was really necessary to epimerize PMU. The H-abstracting ability of bromine radicals is well established[25,26] and is much more selective towards tertiary carbon-centered radicals than *tert*-butoxy radicals.[27] It appeared that epimerization actually could occur in the absence of peroxide, but in a lower extent. This confirms that bromine radicals are effectively able to reversibly abstract hydrogen atoms from PMU. The reversibility of H-abstraction by bromine radicals has also been

reported in the literature.[25,28,29] However, it was observed in the past that the epimerization of polypropylene was very limited in the absence of peroxide.[30] Reactive extrusion of iPP in the presence of 0.67 wt.% NBS led to a decrease of ~ 10 % in crystallinity with respect to the starting iPP and a relative content of [mmmm] pentads of ~ 83 % was measured.

Of course, the two methods cannot be readily compared because many parameters are different between reactive extrusion of polypropylene and reaction of a model compound in a small glass vessel. The homogeneity of the reactive mixture, the solubility of the reactants in the substrate, the viscosity of the reactive medium, diffusion rates, pressure, the starting tacticity, the possible loss of reactive species out of the reactive mixture, etc. are amongst the many variables that cannot be accurately controlled and hence may differ from one processing method to the other, affecting the accuracy of the measurements.

Aside from these process-related considerations, the question that remains is: why is a peroxide required to boost the epimerization reaction ? DSC experiments were conducted to collect clues about this concern. Figure 4.12a shows the DSC scan of pure NBS. The endothermic melting peak is clearly discernable at 175-181 °C and is followed by the exothermic dissociation of the N-Br bond and subsequent degradation of the succinimidyl moiety. Figure 4.12b is the DSC scan of pure DHBP (Luperox 101). A broad exothermic peak is observed from 150 °C to 200 °C that is due to O-O bond cleavage and subsequent degradation of the initiator. Figure 4.12c shows the DSC scan of a mixture of NBS and DHBP (Br/Ox = 1). It is interesting to see that the exothermic peak observed on pure DHBP shifted to lower temperatures, ranging from 135 °C to 160 °C and the endothermic melting of NBS is no longer observable. The DSC trace of Figure 4.12d is related to the same mixture of NBS and DHBP but in the

presence of n-eicosane as hydrocarbon substrate.[31] It is remarkable that the exothermic peak has shifted to even lower temperatures, ranging from 120 °C to 140 °C. The same observation was also reported by other authors when studying the thermal decomposition of N-chlorosuccinimide in isotactic polypropylene.[32] It is therefore assumed that bromine atoms are released at temperature much lower than the decomposition temperature of NBS and before complete melting of polypropylene.

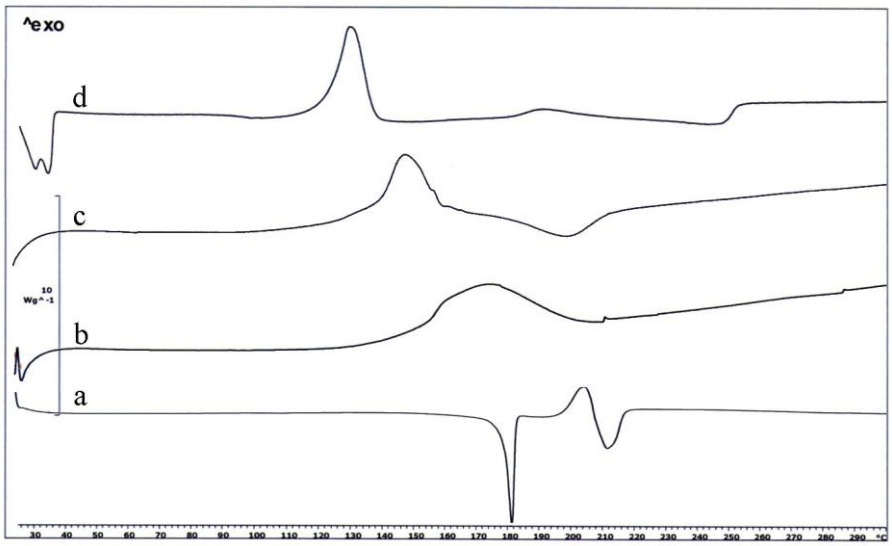

Figure 4.12 : DSC scans of a : NBS, B : Luperox 101, c : mixture of NBS and Luperox 101, d : mixture of NBS and Luperox 101 and n-eicosane.

To further understand the epimerization process, the fate of the bromine radicals must be elucidated. Surprisingly, the GC traces of the crude modified models are extremely clean despite the dark brown color of the mixture after reaction with NBS (It was the case for each experiment). Especially, no lower molecular weight degradation products corresponding to β-scission reactions were observed on the GC traces. The expected very low molecular weight by-products (e.g. from peroxide decomposition) that are highly volatile either escaped the reactive mixture or were co-eluted with

the solvent (acetone) but larger hydrocarbons and vinylidene compounds could have been created as a result of β-scission. All the NMR spectra also confirmed the absence of by-products as no other signals than those belonging to PMU stereoisomers were observed (i.e. no vinylidene or olefinic groups, no additional singlet that could have been assigned to PMUBr, etc.). The use of the model compounds with such reaction/analyses methods does not provide any further clue concerning the epimerization process.

Finally, for the last experiment, finely ground maleic anhydride was added to the reaction mixture for a grafting trial (Grafting 1 in tables 4.4 and 4.5). As expected, maleic anhydride was not soluble in PMU. (the solubility of maleic anhydride into model hydrocarbon such as squalane is estimated to 0.05 M but increases to 0.08 M at 160 °C).[13] The concentration in maleic anhydride is thus 5 to 8 times too high for homogeneous reaction. Nevertheless, the objective of the trial is to mimic the experimental conditions of reactive extrusion and a limited solubility of maleic anhydride in molten polyolefins leading to phase separation was also reported.[27,33] After the vial was pulled out of the oven and allowed to cool down to room temperature, white crystals appeared on the inner walls of the vial, above the level of model compound. A sample of those crystals was collected separately as well as a sample of model compound that was filtered as usual. NMR analyses revealed that the white crystals consisted of pure maleic anhydride. Unfortunately, analyses of the reacted model compound showed no evidence of grafted maleic anhydride. A large amount of the inserted maleic anhydride obviously left the reactive mixture, preventing grafting (the boiling point of maleic anhydride is 202 °C at 760 mmHg). The GC trace also revealed that epimerization occurred roughly to the same extent that Epimerization 5, which contained the same concentration in peroxide and NBS. It seems that the reaction occurred as if maleic anhydride was

omitted from the initial reactive mixture. Also, no by-products were observed.

4.3.4 Conclusions

The synthesis of a bromine-grafted polypropylene model (PMUBr) was achieved from an intermediate compound already available from the synthesis of PMU. However, PMUBr was not easily purified but the ^{1}H NMR signal of interest could be correctly assigned. The first trials using PMU as a model compound of polypropylene are very promising as the epimerization reaction could be correctly achieved and the modification of the stereochemistry of the starting model could easily be observed and quantified by gas chromatography, whatever the starting stereochemistry. NBS was successfully replaced by bromine, definitely confirming that the succinimidyl moiety does not play any role in the epimerization reaction. Also, epimerization of the models occurred even in the absence of radical initiator, confirming the hydrogen-abstraction and hydrogen-transfer (that is to say reversible abstraction) ability of bromine radicals. The DSC measurements demonstrated that peroxide and NBS decomposition occurred at much lower temperature when they are mixed together and is even lower when mixed with a hydrocarbon substrate. Surprisingly, no by-products could be observed on the GC traces nor on NMR spectra, i.e. no degradation products or bromine-grafted hydrocarbons. This complicates the identification of reaction intermediates required to further elucidate the epimerization process. Unfortunately, the grafting of maleic anhydride on PMU failed because of maleic anhydride left the reactive mixture. Further work is therefore required to elucidate the epimerization process and in particular the fate of bromine radicals as they do not graft on polypropylene and do not lead to conjugated dienes as a result of dehydrobromation. Further work is also required to investigate the grafting reaction using

adapted reaction conditions (lower temperature, lower anhydride concentration, etc).

4.3.5 References

[1] Camara S.; Gilbert B.C.; Meier R.J.; Van Duin M.; Whitwood A.C. *Organic Biomolecular Chemistry* **2003,** 1, 1181-1190.

[2] Drillieres, S.; Mestanza, R.; Graebling, D. *International Polymer Processing* **1998,** 13, 149-153.

[3] Van Drumpt, J. D.; Oosterwijk, H. H. J. *Journal of Polymer Science, Polymer Chemistry Edition* **1976,** 14, 1495-511.

[4] Tabata, M.; Sohma, J.; Yokota, K.; Yamaoka, H.; Matsuyama, T. *Radiation Physics and Chemistry* **1990,** 36, 551-8.

[5] Benedetti, E.; Pucci, S.; Pino, P.; Schettino, V. *Spectrochim. Acta* **1973,** 29A, 1313-1320.

[6] Zambelli, A.; Locatelli, P.; Bajo, G.; Bovey, F. A. *Macromolecules* **1975,** 8, 687-689.

[7] Ferro, D. R.; Zambelli, A.; Provasoli, A.; Locatelli, P.; Rigamonti, E. *Macromolecules* **1980,** 13, 179-186.

[8] Gorodetsky, M.; Kogan, D.; Mazur, Y. *Journal of the American Chemical Society* **1970,** 92, 1094-1096.

[9] Gorodetsky, M.; Mazur, Y. *J. Am. Chem. Soc.* **1968,** 90, 6540-6541.

[10] Suter, U. W.; Pucci, S.; Pino, P. *J. Am. Chem. Soc.* **1975,** 97, 1018-1023.

[11] Russel, K. E. *Progress in Polymer Science* **2002,** 27, 1007-1038.

[12] Russell, K. E.; Kelusky, E. C. *Journal of Polymer Science, Part A: Polymer Chemistry* **1988,** 26, 2273-80.

[13] Sipos, A.; McCarthy, J.; Russell, K. E. *Journal of Polymer Science, Part A: Polymer Chemistry* **1989,** 27, 3353-62.

[14] Russell, K. E. *Journal of Polymer Science, Part A: Polymer Chemistry* **1995,** 33, 555-61.

[15] Ranganathan, S.; Baker, W. E.; Russell, K. E.; Whitney, R. A. *Journal of Polymer Science, Part A: Polymer Chemistry* **1999,** 37, 1609-1618.

[16] Ranganathan, S.; Baker, W. E.; Russell, K. E.; Whitney, R. A. *Journal of Polymer Science, Part A: Polymer Chemistry* **1999,** 37, 3817-3825.

[17] Clark, D. C.; Baker, W. E.; Russell, K. E.; Whitney, R. A. *Journal of Polymer Science, Part A: Polymer Chemistry* **2000,** 38, 2456-2468.

[18] Heinen, W.; Erkens, S. W.; Van Duin, M.; Lugtenburg, J. *Journal of Polymer Science, Part A: Polymer Chemistry* **1999,** 37, 4368-4385.

[19] Sulek, P.; Knaus, S.; Liska, R. *Macromolecular Symposia* **2001,** 176, 155-165.

[20] Knaus, S.; Spoljaric-Lukacic, L.; Liska, R.; Saf, R. *European Polymer Journal* **2005,** 41, 2240-2254.

[21] Jois, Y. H.; Bronk, J. M. *Polymer* **1996,** 37, 4345-4356.

[22] Pan, B.; Viswanathan, K.; Hoyle, C. E.; Redfearn, R.; Moore, R. B. *Polymer Preprints* **2001,** 42, 278-279.

[23] Heny, G.; Ph.D. Thesis, **2006**, Faculté des Sciences, Université Catholique de Louvain.

[24] Pelletier, J. D.; Poirier, D. *Tetrahedron Letters* **1994,** 35, 1051-1054.

[25] Thaler, W. A., In Methods in Free-Radical Chemistry, Dekker: New-York, 1969; pp 121-242.

[26] Bottoni, A.; Poggi, G. Journal of Molecular Structure (Theochem) 1995, 337, 161-172.

[27] Hu, G.-H.; Flat, J.-J.; Lambla, M., In *Reactive modifiers for Polymers*, Al-Malaika, S., Ed. Blackie Academic & Professional: London, 1997; pp 1-83.

[28] Tanner, D. D.; Rowe, J. E.; Pace, T.; Kosugi, Y. Journal of the American Chemical Society 1972, 95, 4705-4711.

[29] Tanner, D. D.; Pace, T.; Ochiai, T. Canadian Journal of Chemistry 1975, 53, 2202-2209.

[30] Convention AMPP 001/4519, semestrial report August 2004

[31] DSC measurments were performed by L.Amajod for her graduation work as Bachelor in Chemistry in April 2007. As PMU was not yet available at the time, n-eicosane was chosen as a model compound for polyethylene.

[32] Janigova, I.; Rychly, J. Chemical Papers 1991, 45, 845-854.

[33] Hogt, A. In Modification of polyolefins with maleic anhydride, Compalloy '90, New Orleans, 1990; pp 179-193.

Chapter Five

Valorization of the acquired experience through collaborations

Chapter five reports how the knowledge, expertise and skills as well as new materials could contribute to the accomplishment of several interesting projects through collaborations within our group as well as on an international level.

The "Unité de Chimie Physique Théorique et Structurale" from the "Facultés Universitaires Notre-Dame de la Paix" in Namur is very active in the theoretical modeling of the relationships between Raman-based spectroscopies and the conformational aspects of alkanes of low and high molecular weights. Therefore, the model compounds of polypropylene that were synthesized in chapter 3 were a real opportunity to validate the theoretical calculations of Raman and VROA spectra of PMU and confront them to their respective experimental spectra. The results of this very interesting work combining both theoretical and experimental characterization of PMU stereoisomers are disclosed in section 1. My contribution to this work was simply to provide the separated diastereoisomers of PMU as model compounds. I have also tried many separation protocols for the enantiomers (not presented here) but none of them succeeded. The Servier Laboratories also explored many separation protocols and the best separation that could be obtained is presented. I also wrote the part of the paper dedicated to the synthesis of the model compounds.

A new project, in the form of a PhD thesis in the continuity of this work, was started also in collaboration between POLY and CHOM. The goal of this new project is to investigate the behavior of the highly-grafted polypropylene elastomers upon hydrolysis and neutralization of the grafted anhydrides as an alternative source of ionomers that play a major role in PP/clay nanocomposites. Section 2 describes the first results concerning the hydrolysis and the neutralization of PP-g-MA elastomers. My contribution to this work is minor in the sense that the very first trials of neutralization were performed by our team on the materials acquired by the process described in chapter two. However, Dimitri Rousseaux reproduced and improved the neutralization/characterization process with fresh materials and all the results presented hereafter are his.

Finally, the third section deals with the molecular characterization of short- and long-chain branched polyethylenes and explores how rheometry can be used as a probe for the molecular structure of branched polyethylenes. This work was carried out in collaboration between the "Institute of Polymer Materials" of the "Friedrich-Alexander-University" in Erlangen (Germany), the "School of Semiconductor and Chemical Engineering" from "Chonbuk National University" in Jeonju (Korea) and CHOM. Although it may sound off-topic with respect to the original project involving polypropylene grafting, this work is really interesting as it requires the skills and the expertise of CHOM laboratory for the correct

characterization of the molecular structure of the different polyethylenes through high temperature ^{13}C NMR as was used to characterize the modified polypropylenes. My contribution to this work was to identify and quantify the co-monomer content of most of the polyethylene samples considered in this paper. Those spectra were recorded following the same protocol as used for the NMR investigation of polypropylene tacticity in chapter two but with an improved acquisition sequence developed by Cécile Le Duff.

5.1 Combined Experimental and Theoretical Study on the Raman and Raman Optical Activity Signatures of Pentamethylundecane

Xavier Drooghaag,[1] Jacqueline Marchand-Brynaert,[1] Benoît Champagne,[2] Vincent Liégeois[2]

Published as J. Phys. Chem. B ***2010,*** *114, 11753–11760*

[1] Institute of Condensed Matter and Nanosciences, Université Catholique de Louvain, Place Louis Pasteur 1,B-1348 Louvain-la-Neuve, Belgium.
[2] Laboratoire de Chimie Théorique, Unité de Chimie Physique Théorique et Structurale, Facultés Universitaires Notre-Dame de la Paix, rue de Bruxelles, 61, B-5000 Namur, Belgium.

Abstract

The synthesis and the separation of the four stereoisomers of 2,4,6,8,10-pentamethylundecane (PMU) are described together with their characterization by Raman spectroscopy. In parallel, theoretical calculations of the Raman and vibrational Raman optical activity (VROA) spectra are reported and analyzed in relation with the recorded spectra. A very good agreement is found between the experimental and theoretical spectra. The Raman spectra are also shown to be less affected by the change of configuration than the VROA spectra. Nevertheless, by studying the overlap between the theoretical Raman spectra, we show clear relationships between the spectral fingerprints and the structures displaying a mixture of the TGTGTGTG conformation of the (4R,6s,8S)-PMU (isotactic compound) and of the TTTTTTTT conformation of the (4R,6r,8S)-PMU (syndiotactic compound). Then, the fingerprints of the VROA spectra of the five

conformers of the (4R,8R)-PMU have been be related to the fingerprints of the regular $(TG)_N$ isotactic compound as a function of the torsion angles. Since the $(TT)_N$ syndiotactic compound has no VROA signatures, the VROA spectroscopy is very sensitive to the helical structures as demonstrated here.

5.1.1 Introduction

Raman spectroscopy is a widely used technique to study the structure of molecules as well as of macromolecules and polymers. For instance, Raman spectroscopy is well-known to be sensitive to the chain conformation and thereof to the temperature changes[1] and the related disorder in the chain.[2,3] recent studies have revealed relationships between the Raman spectral signatures and the conformation of alkanes[4,5] and alkasilanes.[6] The Raman technique is also sensitive to the environment of the molecules and can therefore be used to study chain packing and conformational disorder.[7] Moreover, the structures and properties of conducting polymers (like polypyrrole, polythiophene, polyaniline) can be studied by Raman spectroscopy to probe the existence of self-localized excitations, i.e. polarons, bipolarons, and/or solitons.[8] In many cases, these experimental characterizations can benefit from complementary ab initio simulations, which provide further insight into the possible structures and their associated Raman pattern. For instance, density functional theory (DFT) simulations combined with experimental measurements provide information to interpret the vibrational bands and to deduce the molecular structure.[9-11] The optically active evolution of Raman spectroscopy, namely, the vibrational Raman optical activity (VROA), has also inherited a huge sensitivity to conformation and configuration, owing to the use of incident circularly polarized light.[12-17] The VROA technique has been applied to the analysis of biomacromolecules[18-22] and synthetic polymers.[23,24]

Following a recent theoretical modeling of the relationship between conformational structure, Raman and VROA spectra of model polypropylene (PP) chains,[5] we carried out a joined experimental-theoretical investigation for substantiating these initial theoretical conclusions. We report here the results obtained on a series of small PP-oligomers, namely, pentameric diastereoisomers. Indeed, low molecular weight model compounds are often used to mimic the behavior of polymers, while the lower viscosity and higher solubility in common organic solvents of small oligomers of ethylene and propylene make them excellent alternatives to polyolefins for analytical characterization. Many readily accessible or easily prepared model compounds of polyolefins have been used to elucidate the mechanisms of postsynthesis modifications such as degradation,[25] cross-linking,[26-28] and grafting[29-33] or to retrieve structural information through spectroscopic investigations.[34-37] Among those, 2,4,6,8,10-pentamethylundecane (PMU) is of particular interest when it comes to investigate the tacticity-related properties of PP.[34,36] As already explained in chapter 4 and illustrated in Figure 4.1, PMU consists of four stereoisomers that mimic the three main tacticities of PP: (4*R*,6*s*,8*S*)-PMU and (4*R*,6*r*,8*S*)-PMU correspond to isotactic and syndiotactic PP, respectively, whereas both (4*R*,8*R*)-PMU and (4*S*,8*S*)-PMU correspond to atactic PP and are enantiomers to each other.

The following paragraphs disclose the synthesis of PMU stereoisomers according to the synthetic route described in details in chapter 4 as well as their experimental Raman characterization. Those experimental Raman spectra were interpreted by comparing them with the simulated ones. In particular, similarities between the spectra are highlighted and associated with chain conformations, while the key vibrational modes are described. Theoretical VROA spectra are also presented and analyzed as a function of the chain configurations and conformations.

5.1.2 Materials and Methods

Synthesis of Pentamethylundecane Stereoisomers.

The stereochemical control of methyl substituents in the 1,3-relative positions along a linear alkane chain is a very challenging problem, addressed in few specific cases by catalytic asymmetric synthesis. For instance, the total synthesis of phthioceramide acid has been achieved by an iterative catalytic asymmetric 1,4-addition protocol,[38] and the *all*-(*R*)-2,4,6,8-tetramethyldecanoic acid synthesis makes use of Zr-catalyzed asymmetric carboalumination reactions.[39]

Since we are interested in all the stereoisomers of PMU, we decided to perform a nonasymmetric, high-yielding synthesis of PMU and to achieve the stereoisomers via separation. The synthesis of PMU was initially described by Pino et al. in 1968.[40] A fractional distillation was used to separate the diastereoisomers, but this method was revealed to be poorly efficient. Therefore, as disclosed previously in Chapter 3, we established another large-scale, practical route toward PMU where synthetic intermediates could be used for chromatographic separations. The key intermediate is 2,4,8,10-tetramethyl-6-methyleneundecane **1**, which furnished the mixture of PMU stereoisomers (Figure 5.1) upon hydrogenation. On the other hand, hydroboration of **1** led to the mixture of primary alcohol **2** stereoisomers, usable in the liquid chromatography technique for resolution. Next, tosylation of the alcohols **2**, giving tosylates **3**, followed by borohydride substitution led to the PMU stereoisomers.

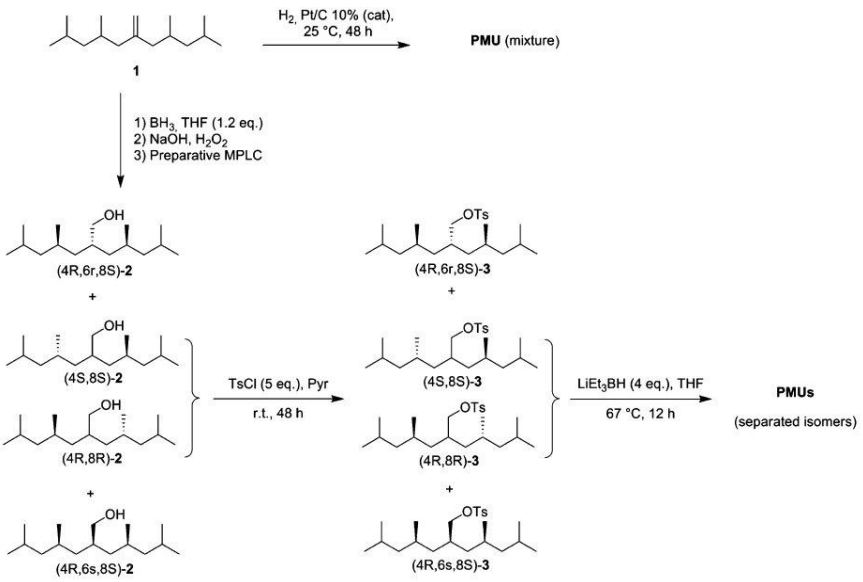

Figure 5.1 : Synthetic route toward PMU and HPLC separation of the diastereoisomers

Preparative (1 g scale) normal-phase medium-pressure liquid chromatography (MPLC) was therefore performed to separate the diastereoisomers of alcohol **2**. Because of the absence of chromophore group, common UV detection was impossible. The use of a Corona CAD universal detector was therefore mandatory.[41] Although excellent separation of the diastereoisomers could be obtained in analytical HPLC, the use of such a detector turned out to be much more critical on preparative scale. As the maximum flow rate allowed in the Corona detector is 1.5 mL/min, a flow splitter had to be installed, but the extra backpressure from both the flow splitter and the detector were too high for the solvent-pumping device. As a consequence, blind elution with automated collection was performed instead. Sampling of the collected fractions and automated injections in an analytical HPLC equipped with Corona detection was used as an off-line detection method. Fractions containing only one diastereoisomer were combined and

converted into PMU separately. Despite a quite poor resolution (only 52 % of the total sample load was recovered as pure stereoisomers), it was possible to recover the syndio- and atactic models of PMU at the 100 mg scale. The isotactic model was much more delicate to isolate as pure material, but could be recovered at the 10 mg scale.

Many efforts were also devoted to the separation of the enantiomers (4*R*,8*R*)/(4*S*,8*S*) to provide models for VROA spectroscopy. Despite the very large number of conditions tested on both alcohol **2** and tosylate **3**, only partial separation could be obtained on analytical-scale chiral HPLC (Figure 5.2) Because of the poor resolution and the very low capacity of the chiral HPLC columns, it was not possible to scale up the separation.

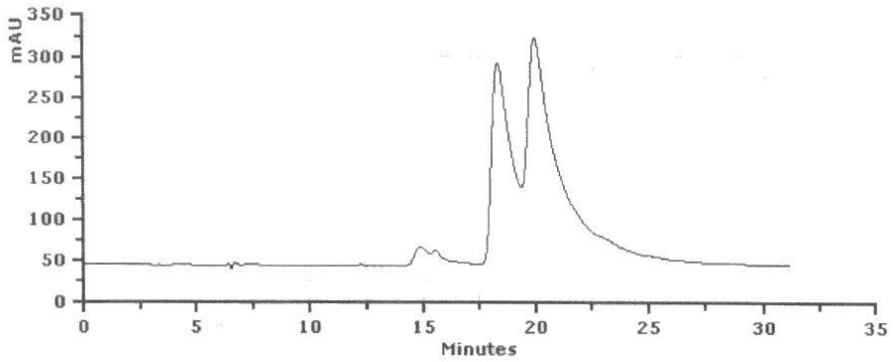

Figure 5.2 : Chiral separation of (4R,8R)- and (4S,8S)-3. Cyclobond I 2000, 4.6 x 250 mm, 5 µm, MeOH/H_2O 55:45 v/v, 0.5 mL/min, UV 230 nm, load 1.5 µg

Raman Experimental Setup.

The Raman spectra have been recorded on a Fribourg instrument in a capillary with a 10.0 µL sample size. The exposure time is typically 10 min while the laser wavelength is 532 nm and the laser power at the sample amounts to 300 mW.

Theoretical and Computational Aspects on Raman and VROA Spectroscopies.

Within the harmonic approximation, the differential Raman and VROA scattering cross section for a naturally polarized incident light (n) in the scattered circularly polarized (SCP) scheme for backward-scattering detection (scattering angle $\theta = \pi$) read for the p vibrational normal mode[13,42,43] is

$$^{n}\mathrm{d}\sigma(\pi)_{\mathrm{SCP}} = \frac{1}{90}\left(\frac{\mu_0}{4\pi}\right)^2 \omega_{\mathrm{p}}{}^3\omega_0 \frac{\hbar}{2\Delta\omega_{\mathrm{p}}}[90a_{\mathrm{p}}{}^2 + 14\beta_{\mathrm{p}}{}^2]\,\mathrm{d}\Omega \qquad (5.1)$$

$$-\Delta^{n}\mathrm{d}\sigma(\pi)_{\mathrm{SCP}} = \frac{1}{90}\left(\frac{\mu_0}{4\pi}\right)^2 \omega_{\mathrm{p}}{}^3\omega_0 \frac{\hbar}{2\Delta\omega_{\mathrm{p}}}\frac{2}{\mathrm{c}}[24\beta_{G\mathrm{p}}{}^2 + 8\beta_{A\mathrm{p}}{}^2]\,\mathrm{d}\Omega \qquad (5.2)$$

where $\omega_0 = 2\pi\nu_0$ is the pulsation of the laser beam, ω_{p} is the pulsation of the scattered light, $\Delta\omega_{\mathrm{p}}$ corresponds to the vibrational transition associated with the normal mode coordinate Q_{p}, μ_0 is the permeability constant, and c is the speed of light in a vacuum. The cross section σ, expressed in m^2 in SI units, describes the linear dependence of the scattered light intensity with respect to the incident irradiance and it contains all the information about the molecular system under study. One can notice that the Raman backward-scattering intensity is the same as the more classical Raman polarized experiment for which, starting from an incident naturally polarized light, the scattered light at 90° that goes through a polarizer perpendicular to the scattering plane is measured. The two Raman invariant quantities ($\alpha_{\mathrm{p}}{}^2$ and $\beta_{\mathrm{p}}{}^2$) in eq 5.1 require the evaluation of the first-order derivatives with respect to the atomic Cartesian coordinates of the electric dipole-electric dipole polarizability, α, while the two VROA invariant quantities ($\beta_{G\mathrm{p}}{}^2$ and $\beta_{A\mathrm{p}}{}^2$) in eq 5.2 require in addition the evaluation of the first-order derivatives of the

electric dipole-electric quadrupole polarizability, *A*, and of the electric dipole-magnetic dipole polarizability, *G′*. A review by Buckingham[44] defines all these polarizabilities. They are evaluated within the TDHF scheme using a recently developed and implemented fully analytical procedure.[45] The vibrational frequencies and the normal modes were determined at the B3LYP/6-31G* level of approximation. Then, due to the relatively big size of the systems but also owing to its recognized performance, the rDPS:3-21G (reduced diffuse polarization function and shell augmented) basis set introduced by Zuber and Hug[46] was employed in the TDHF calculations. The calculations were performed using both the DALTON[47] and Gaussian 03[48] quantum chemistry packages. A typical incident light wavelength of 532 nm was adopted in all optical tensor calculations. A Maxwell-Boltzmann *T*-dependence factor has been added to eqs 5.1 and 5.2 with T = 298.15 K to account for the *T*- $([1 - \exp(-\hbar\Delta\omega_p/(k_bT))]^{-1})$ dependence of the vibrational level population. In the spectra, each transition is represented by a Lorentzian function with fwhm of 10 cm^{-1}, which is more or less what is observed in the experimental spectra.[49] In order to compare the simulated VROA spectra, we evaluate the overlaps between them[5]. The "*S*" quantity is then defined as the ratio between the intensity (I_a) overlap of the two spectra and the square root of their self-overlap:

$$S_{ab} = \frac{\langle I_a | I_b \rangle}{\sqrt{\langle I_a | I_a \rangle \langle I_b | I_b \rangle}} \qquad (5.3)$$

This quantity amounts to 1 or -1 when the spectra are identical or opposite, respectively.

5.1.3 Spectra and their Interpretation

The Raman spectra for the mixture of the four compounds - the isotactic compound, the syndiotactic compound, and the racemic mixture of the atactic compounds - are reported in Figure 5.3. They correspond to the recorded spectra (not shown here) from which the background of fluorescence was removed using the Fityk program.[50] At first glance, the spectra for the atactic, isotactic, and syndiotactic species look very similar to each other. Nevertheless, one can point out variations in the shape of the bands (the band at 820 or 1460 cm^{-1}, for instance) due to small shifts in the normal-mode frequencies between the different stereoisomers.

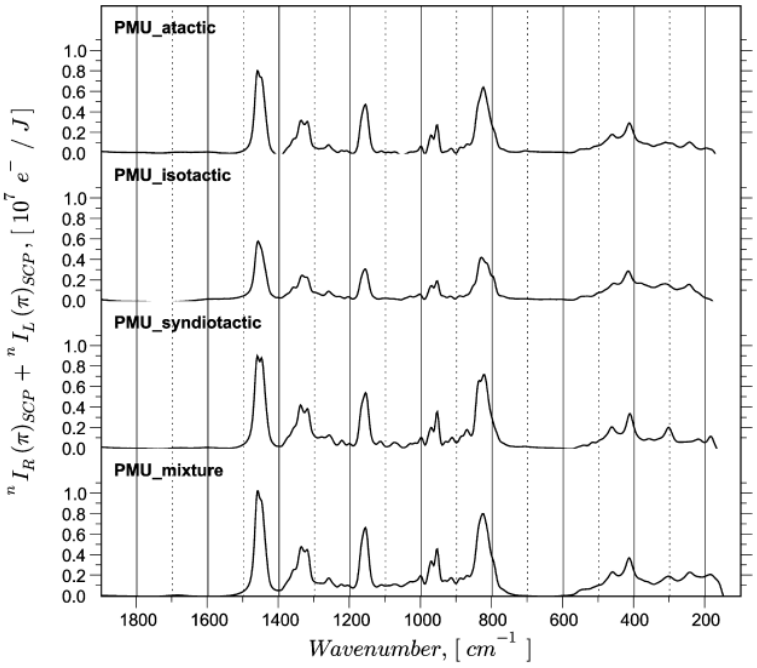

Figure 5.3 : Experimental Raman backward-scattering spectra of PMU compounds after background removal. Laser power 300 mW, wavelength 532 nm, recording time 10 min.

Structural aspects: the most stable Conformers.

In order to simulate the Raman/VROA spectra of each stereoisomer, one needs to determine the most favorable conformations and evaluate the Raman/VROA spectra for each of them. For the isotactic and syndiotactic compounds, only one conformer, TGTGTGTG and TTTTTTTT, respectively, have been considered, since they represent by far the most stable conformations in both cases. For the atactic species, one needs to consider more than one conformation. By molecular mechanics (using the OPLS force field[51]) and subsequent B3LYP/6-31G* calculations, five conformations were found in a range of 1 kJ/mol while the next conformer is 7 kJ/mol higher than the minimum. The torsion angles obtained at the B3LYP/6-31G* level are listed in Table 5.1. Their values are very close to the ideal 180°, 60°, and -60° values, corresponding to trans, gauche-(+), and gauche-(-) conformations, respectively.

Table 5.1 : Torsion angles, relative energies, Maxwell-Boltzmann distribution weights, and conformation labels of the most stable conformers of (4*R*,8*R*)-PMU as determined at the B3LYP/6-31G* level of approximation[a]

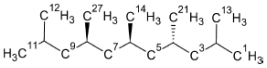

Δ*E*, kJ/mol (B3LYP/6-31G*)	0.000	0.473	0.543	0.986	1.033
	25.2%	20.9%	20.3%	17.0%	16.6%
Δ*E*, kJ/mol (MP2/6-31G*)	1.559	1.296	2.142	0.295	0.000
	15.5%	17.3%	12.3%	25.8%	29.1%
torsion angle[b]	conformer 1	conformer 2	conformer 3	conformer 4	conformer 5
$C_1-C_2-C_3-C_4$	−176.2	−176.1	−176.5	−59.2	59.9
$C_4-C_3-C_2-C_{13}$	60.2	60.3	59.9	177.2	−176.5
$C_2-C_3-C_4-C_5$	−174.5	−174.4	−179.1	−61.3	−179.2
$C_3-C_4-C_5-C_6$	176.3	176.4	61.0	−179.9	60.8
$C_4-C_5-C_6-C_7$	−60.8	−60.8	−175.9	−60.9	179.7
$C_5-C_6-C_7-C_8$	**179.8**	179.5	175.6	179.4	60.2
$C_6-C_7-C_8-C_9$	**175.8**	**179.3**	**179.6**	**179.3**	**60.1**
$C_7-C_8-C_9-C_{10}$	**−174.7**	**−61.4**	**−61.4**	**−61.4**	**−179.4**
$C_8-C_9-C_{10}-C_{11}$	60.2	**177.0**	**177.0**	**177.0**	−176.6
$C_8-C_9-C_{10}-C_{12}$:	**−176.2**	−59.4	−59.4	−59.4	**59.9**
$C_2-C_3-C_4-C_{21}$	61.2	61.3	58.1	174.4	58.0
$C_6-C_5-C_4-C_{21}$	−59.4	−59.3	−174.7	−57.1	−174.9
$C_4-C_5-C_6-C_{14}$	174.9	175.0	60.0	174.9	57.1
$C_8-C_7-C_6-C_{14}$	−57.5	**−57.8**	**−60.3**	**−57.9**	**−175.6**
$C_6-C_7-C_8-C_{27}$	−59.9	−57.9	−57.6	−57.9	−175.6
$C_{10}-C_9-C_8-C_{27}$	61.1	174.4	174.3	174.3	57.9
conformation of the "right" segment of PMU	TG′TG′ (P)	TG′TG′ (P)	GTGT (M)	TG′TG′TG′ (P)	GTGTGT (M)
	3−4−5−6−7−8−27	3−4−5−6−7−8−27	13−2−3−4−5−6−7	13−2−3−4−5−6−7−8−27	13−2−3−4−5−6−7−8−27
conformation of the "left" segment of PMU	**TTTT**	**TG′TG′ (P)**	**TG′TG′ (P)**	**TG′TG′ (P)**	**GTGT (M)**
	12−10−9−8−7−6−5	11−10−9−8−7−6−14	11−10−9−8−7−6−14	11−10−9−8−7−6−14	12−10−9−8−7−6−14

[a] The labels corresponding to the torsion angles of the backbone are written in bold. [b] Regular patterns in the values of the successive torsion angles along the chain are highlighted in bold or underlined.

One observes regular patterns in the values of the successive torsion angles along the chain (highlighted in bold or underlined in Table (5.1). So, each conformer has been theoretically divided into two halves, to which a conformational label can be attributed. For instance, conformer 1 is built from the combination of an all-trans and a right-handed helical segments. The Raman and VROA spectra obtained by summing the spectra of each conformer of the atactic compound weighted by the B3LYP/6-31G* Boltzmann factors are given in Figure 5.4, respectively, together with the spectra for the TGTGTGTG conformer of the (4*R*,6*s*,8*S*)-PMU (isotactic compound) and the TTTTTTTT conformer of the (4*R*,6*r*,8*S*)-PMU (syndiotactic compound). Figures 5.5 and 5.6 display the individual Raman and VROA spectra for each conformer of the atactic compound.

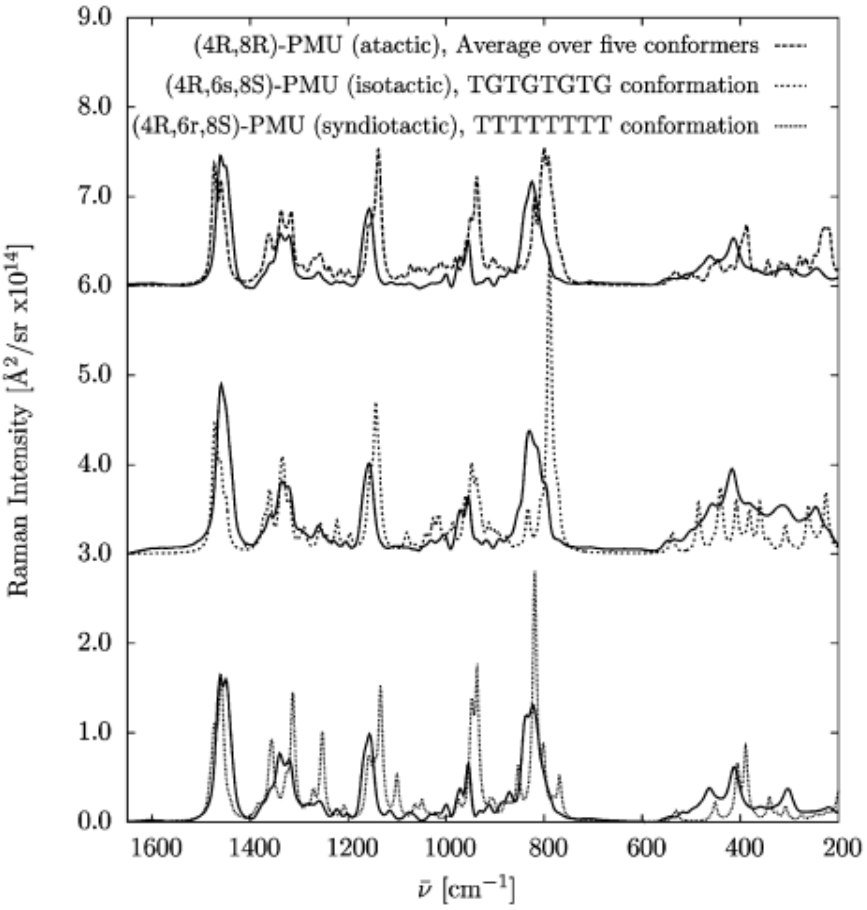

Figure 5.4 : Simulated Raman polarized spectra of (4*R*,6*s*,8*S*)-PMU and (4*R*,6*r*,8*S*)-PMU molecules in their most favorable conformation as well as the (4*R*,8*R*)-PMU spectrum for which the average over the five most stable conformers is performed using the Boltzmann distribution based on the B3LYP/6-31G* energies. The experimental spectra are superimposed over the corresponding calculated ones using solid lines. Each transition is represented by a Lorentzian function with fwhm of 10 cm^{-1}. The optical wavelength is 532 nm and a multiplicative factor of 0.96 was used to scale the vibrational frequencies.

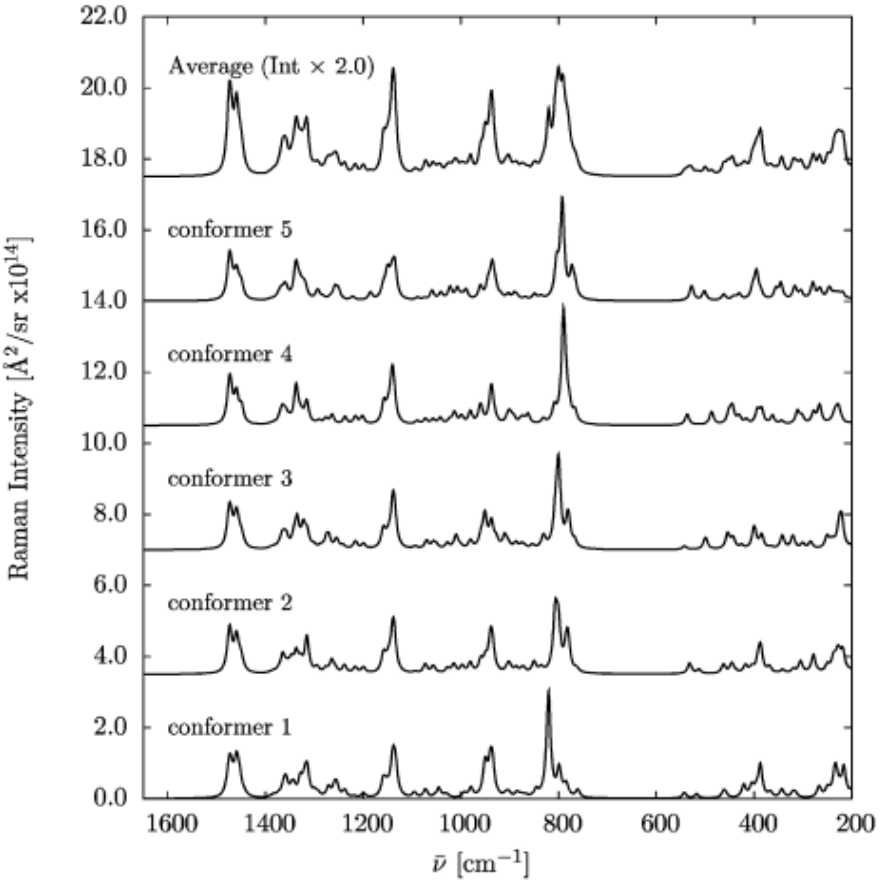

Figure 5.5 : Simulated Raman polarized spectra of the five most stable conformers of the (4*R*,8*R*)-PMU molecule as well as the average spectrum obtained using the Boltzmann distribution based on the B3LYP/6-31G* energies of the five conformers. Each transition is represented by a Lorentzian function with fwhm of 10 cm^{-1}. The optical wavelength is 532 nm and a multiplicative factor of 0.96 was used to scale the vibrational frequencies.

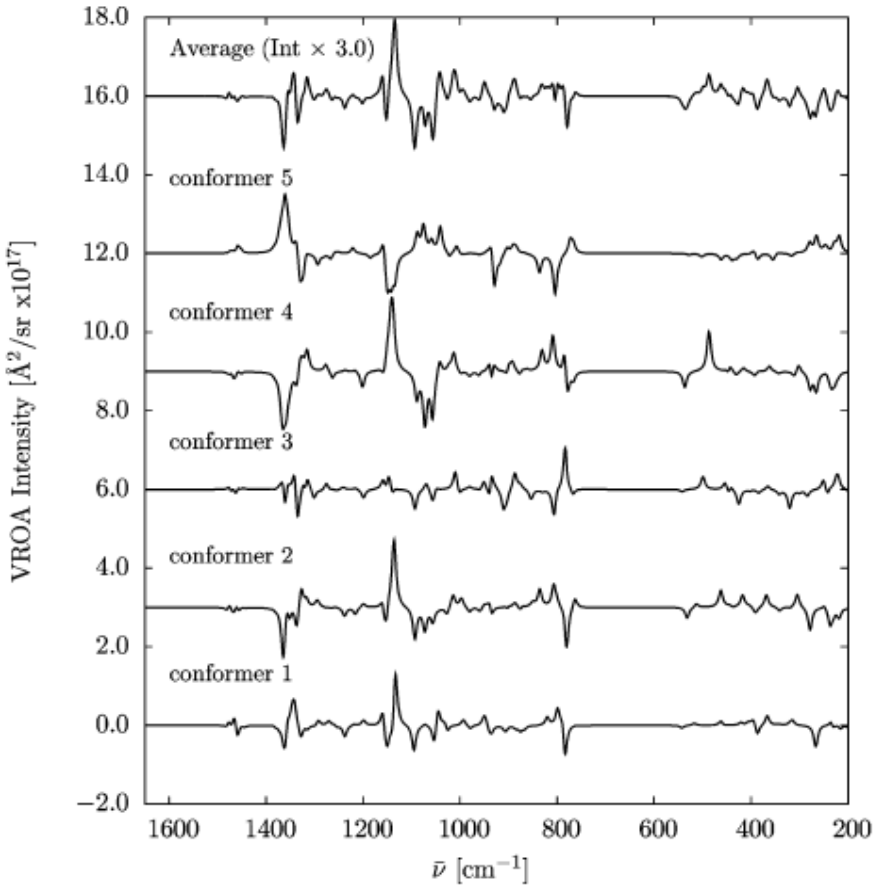

Figure 5.6 : Simulated VROA backward-scattering spectra of the five most stable conformers of the (4*R*,8*R*)-PMU molecule as well as the average spectrum obtained using the Boltzmann distribution based on the B3LYP/6-31G* energies of the five conformers. Each transition is represented by a Lorentzian function with fwhm of 10 cm^{-1}. The optical wavelength is 532 nm and a multiplicative factor of 0.96 was used to scale the vibrational frequencies.

Analysis of the Raman Spectra.

For the three stereoisomers, simulated and measured Raman spectra are in close agreement (Figure 5.4). Some specific features associated with each stereoisomer are indeed well-reproduced by the calculations. For instance, the band at 1460 cm^{-1} consists of two slightly separated peaks for

the atactic and syndiotactic compounds, while in the spectrum of the isotactic, it mostly reduces to one merged peak. The band at 960 cm^{-1} on the experimental spectrum of the syndiotactic compound is clearly made of two peaks with a ratio 1:2, the lower wavenumber one being the most intense. This is also reproduced by the calculated spectrum. A similar observation is made for the band close to 960 cm^{-1} in the experimental and theoretical spectra of the atactic compound, while the isotactic ones consist more of two peaks with similar intensities. A third remarkable signature is the band at 820 cm^{-1}. In the simulated spectra, the differences between the peaks (positions and relative intensities) of the three stereoisomers are obvious. So, for the isotactic compound, the most intense peak is located at 789 cm^{-1}, while for the syndiotactic, the most intense peak is at much larger wavenumber (819 cm^{-1}). These shifts are not fully reproduced in the experimental spectra, though; the shapes of the bands are modified between the spectra of the different stereoisomers. For the atactic species, one could have argued about the choice of the weight given to the spectrum of each conformer to account for such differences between theory and experiment. Nevertheless, by taking the MP2/6-31G* energies rather than the B3LYP/6-31G* values, one does not find significant differences. In addition, the peaks around 1160 cm^{-1} are also well reproduced by the simulations, but they do not appear to be sensitive to the configuration. The same applies to the triplet of transitions in the 1320-1360 cm^{-1} region for which the distinction between the peaks is less marked in the experimental spectra. Out of the five bands in the 700-1600 cm^{-1} frequency zone, representative modes of the isotactic and syndiotactic isomers are sketched in Figure 5.7. They correspond to the bands located around 810, 1140, and 1460 cm^{-1}. These modes involve hydrogen wagging motions and C-C stretching, as well as the umbrella motion of the hydrogen atoms of the lateral methyl groups.

Additional insight into the relation between the spectra and the molecular structures can be retrieved from the overlaps between the simulated spectra. Indeed, the overlap between the Raman spectra for the TGTGTGTG conformer of the (4*R*,6*s*,8*S*)-PMU (isotactic) compound and the TTTTTTTT conformer of the (4*R*,6*r*,8*S*)-PMU (syndiotactic) compound amounts to 0.645. This value, which represents the similitude in the Raman spectra between the two regular $(TT)_N$ and the $(TG)_N$ structures, is the smallest overlap observed here between any pair of theoretical Raman spectra. The Raman spectra for the different conformers of the (4*R*,8*R*)-PMU compound are very similar to each other (Figure 5.5). To distinguish them, the overlaps between the spectrum of the TGTGTGTG conformer of the (4*R*,6*s*,8*S*)-PMU compound and the spectra of conformers 1-5 were calculated. They amount to 0.698, 0.823, 0.822, 0.965, 0.911, respectively. Similarly, the corresponding overlaps for the TTTTTTTT conformer of the (4*R*,6*r*,8*S*)-PMU compound are 0.932, 0.781, 0.753, 0.648, 0.694, respectively.

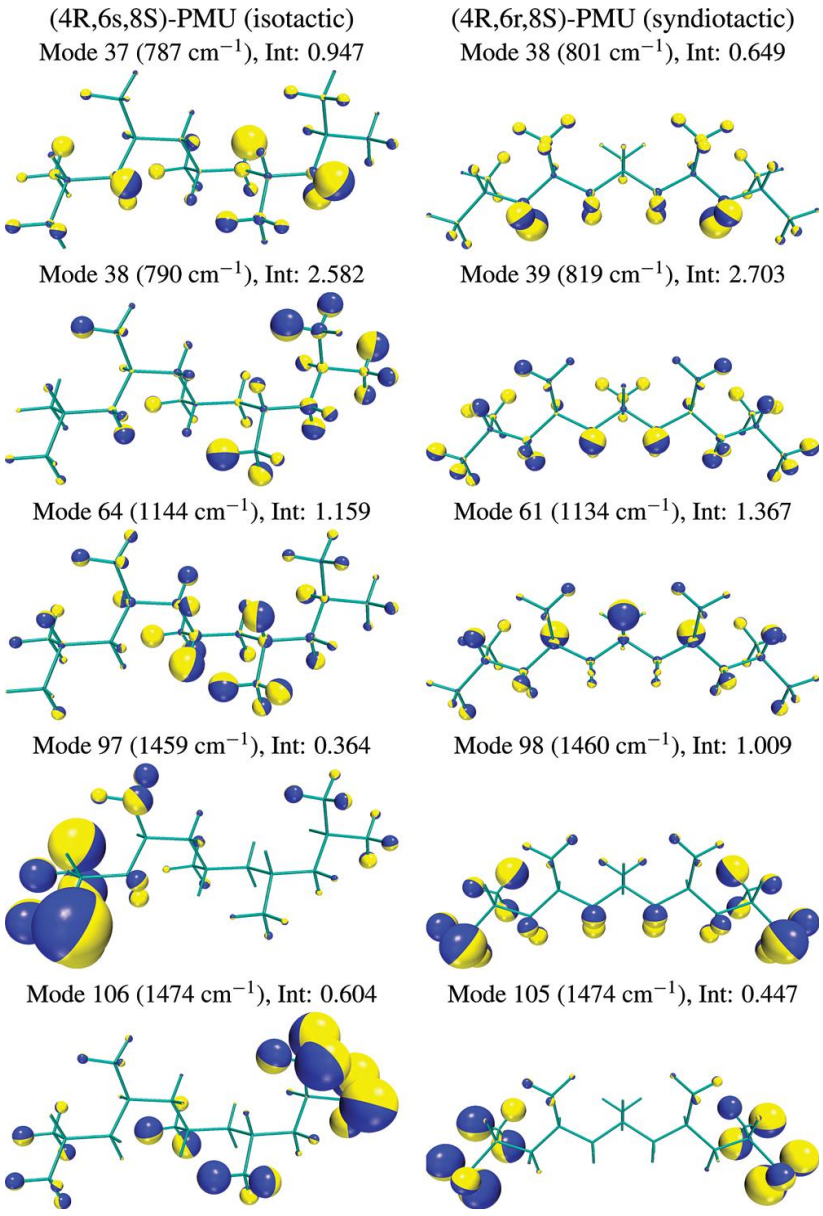

Figure 5.7 : Sketch of the five normal modes of the TGTGTGTG conformer of (4*R*,6*s*,8*S*)-PMU and of the TTTTTTTT conformer of (4*R*,6*r*,8*S*)-PMU that dominate the Raman spectra. The direction of atomic displacements is perpendicular to the junction plane between the two hemispheres of distinct color, while their amplitudes are proportional to the radius of the sphere. The Raman intensities are also given and are expressed in $Å^2$/sr.

These values are consistent with the conformations of the atactic chains (Table 5.1). Indeed, the signatures of conformer 1 are more closely related to those of the $(TT)_N$ structure while the Raman patterns of conformers 4 and 5 are closer to those of the $(TG)_N$ structure. Note that these overlap values depend on the choice of fwhm to represent each transition but that their relative values remain similar. Indeed, as a matter of illustration, the overlaps have been calculated on the basis of spectra plotted with a fwhm of 15 cm^{-1}. In that case, the overlaps between the spectra of the isotactic chain and the five atactic conformers amount to 0.788, 0.900, 0.906, 0.981, 0.951, as given in the same order as previously.

Analysis of the VROA Spectra.

Even if our samples are nonchiral (or racemic mixture) and therefore that no VROA spectrum could be recorded, simulated VROA spectra are reported and analyzed. The overlap between the VROA spectrum of the TGTGTGTG conformer of the (4*R*,6*s*,8*S*)-PMU compound (Figure 5.8) and the spectra of conformers 1-5 (Figure 5.6) amount to -0.077, -0.518, 0.012, -0.800, 0.765, respectively. These values are very interesting when put in relation to the torsion angle sequences of the conformers (Table 5.1).

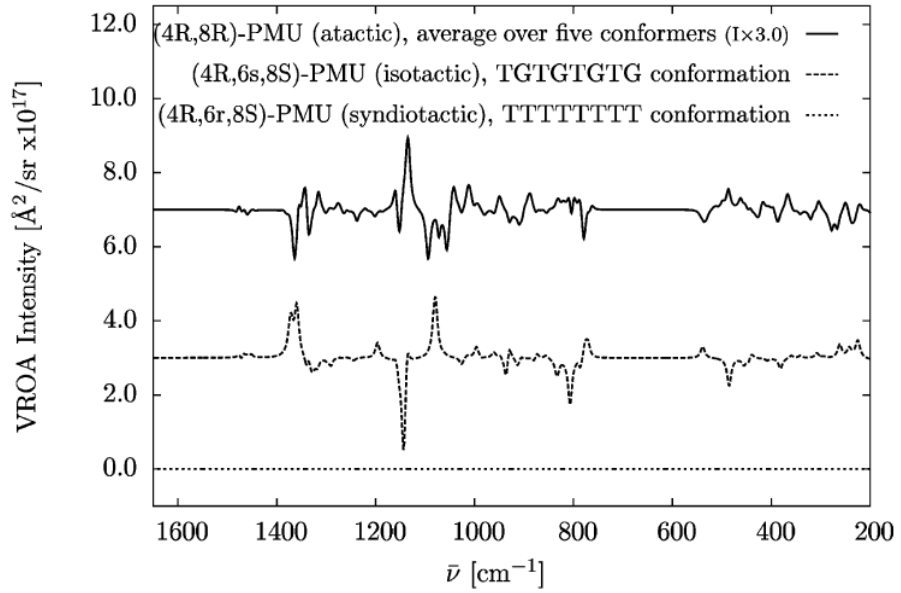

Figure 5.8 : Simulated VROA backward-scattering spectra of (4*R*,6*s*,8*S*)-PMU and (4*R*,6*r*,8*S*)-PMU molecules in their most favorable conformation as well as the (4*R*,8*R*)-PMU spectrum for which the average over the five most stable conformers is performed using the Boltzmann distribution based on the B3LYP/6-31G* energies. Each transition is represented by a Lorentzian function with fwhm of 10 cm^{-1}. The optical wavelength is 532 nm and a multiplicative factor of 0.96 was used to scale the vibrational frequencies.

As already said, the structures of the conformers of (4*R*,8*R*)-PMU are not as regular as the $(TG)_N$ structure of the isotactic compound or as the $(TT)_N$ structure of the syndiotactic species. On the other hand, these structures can be considered to be build of two segments and each of these brings its own fingerprints to the VROA spectrum of the conformer. So, one observes that the overlaps for conformers 2, 4, and 5, which exhibit some 3-fold helical structures typical of TG conformations, are important and increase from conformer 2 to conformers 4 and 5, since the helical segments are longer for the latter two. Moreover, the sign of the overlaps is directly related to the difference of helical pitches, right- or left-handed, of the

structures in comparison. Conformer 3 has a completely different pattern and therefore a very small overlap with the spectrum of the $(TG)_N$ structure, which can be explained by the fact that this chain combines the two opposite helical pitches, leading to a quasi-cancellation of the two fingerprints and a resulting weak intensity. The overlap for conformer 1 is quite small (in absolute value), which is again explained by the short helical content of the chain. Then, the overlap between the VROA spectrum for the (4*R*,8*R*)-PMU, obtained from a Boltzmann averaging of the spectra of the five conformers and the VROA spectrum of the TGTGTGTG conformer of the (4*R*,6*s*,8*S*)-PMU (isotactic compound) amounts to -0.392 (Figure 5.8). This value indicates that even after averaging over the five conformations, the global VROA spectrum still displays VROA signatures, here dominated by the $(TG')_N$ structure. Thus, on the spectrum, one observes the typical couplet (positive-negative) at around 1100 cm^{-1} attributed to the presence of the 3-fold helical TG′TG′ conformation of the polypropylene chain.[5] As a matter of comparison, for the Raman spectra, the overlap value between the atactic (averaged over the five conformations) and the isotactic spectra is 0.891, while it is 0.835 between the atactic and the syndiotactic spectra. This shows that the Raman spectrum of the (4*R*,8*R*)-PMU (Figure 5.4) combines the signatures of the $(TG)_N$ structure of the isotactic configuration as well as the signatures of the $(TT)_N$ structure of the syndiotactic configuration but that their distinction is more subtle than using VROA spectra.

5.1.4 Conclusions

We have revisited the pentamethylundecane (PMU) synthesis and designed a novel key intermediate, namely, 2,4,8,10-tetramethyl-6-methyleneundecane, allowing the one-step preparation of PMU as a mixture of the four stereoisomers and the three-step preparation of the separated isomers. This process involves the hydroboration of **1**, giving the primary

alcohol **2**; the tosylation of **2**; and its substitution with hydride (Figure 5.1). The chromatographic separation of the stereoisomers could be performed either on the alcohol **2** or on the tosylate **3**. At the preparative scale, the two meso isomers of PMU (isotactic and syndiotactic PMUs) and the racemic mixture of atactic PMU were successfully provided. Unfortunately, the analytical resolution of the atactic mixture (chiral HPLC) could not be scaled up to furnish substantial amounts of the pure enantiomers. Among the different techniques to characterize the compounds, this study has particularly focused on the Raman spectroscopy by conducting a joined experimental and theoretical characterization on the isotactic compound, the syndiotactic compound, and the racemic mixture of the two atactic species, as well as on the mixture of all the four stereoisomers. A good agreement is found between the experimental and theoretical Raman spectra. Though, the Raman spectra are weakly affected by the change of configuration, by studying the overlap between the simulated spectra, we have shown that the two regular structures, the TGTGTGTG conformer of (4*R*,6*s*,8*S*)-PMU and the TTTTTTTT conformer of (4*R*,6*r*,8*S*)-PMU, present the smallest overlap between any pair of Raman spectra. Then, the Raman spectra of the five conformers of the atactic (4*R*,8*R*)-PMU display signatures matching to different degrees those of both regular structures, which are directly correlated to the pattern of torsion angles along the chain backbone. The vibrational Raman optical activity spectra have also been simulated and the fingerprints between the spectra of the five conformers have been shown to be related to the fingerprints of the regular $(TG)_N$ 3-fold helical structure modulated by the pattern of the successive torsion angles along the backbone. Indeed, each structure can be considered to be build of two segments and each of these brings it own fingerprints to the VROA spectrum of the conformer. Since the $(TT)_N$ syndiotactic compound has no VROA signatures, only the segments with a 3-fold helical structure contribute to the

VROA signatures, which make the VROA spectroscopy very sensitive to the helicity, as demonstrated here.

5.1.5 Acknowledgement

The authors thank Prof. Werner Hug and Mrs Elena Hasanova for their contributions in recording the spectra and for fruitful discussions. V.L. thanks the Fund for Scientific Research (F.R.S.-FNRS) for his Postdoctoral Researcher position. This work was supported by the Belgian Government (IUAP No. P06-27 "Functional Supramolecular Systems"). The calculations have been performed on the Interuniversity Scientific Computing Facility (ISCF), installed at the FUNDP, for which the authors gratefully acknowledge the financial support of the F.R.S.-FRFC and of the "Loterie Nationale" under Contract No. 2.4.617.07.F, and of the FUNDP.

5.1.6 References and Notes

[1] Yellin, N.; Levin, I. W. *Biochim. Biophys. Acta* **1977**, *489*, 177–190.

[2] Zerbi, G.; Abbate, S. *Chem. Phys. Lett.* **1981**, *80*, 455–457.

[3] Snyder, R. G.; Strauss, H. L.; Elliger, C. A. *J. Phys. Chem.* **1982,** *86*, 5145–5150.

[4] Orendorff, C.; Ducey, M.; Pemberton, J. *J. Phys. Chem. A* **2002**,*106*, 6991–6998.

[5] Lamparska, E.; Liégeois, V.; Quinet, O.; Champagne, B. *Chem-PhysChem* **2006**, *7*, 2366–2376.

[6] Orendorff, C.; Pemberton, J. *Anal. Chem.* **2005**, *77*, 6069–6077.

[7] Clavell-Grunbaum, D.; Strauss, H. L.; Snyder, R. G. *J. Phys. Chem. B* **1997**, *101*, 335–343.

[8] Furakawa, Y.; Tasumi, M. In *Modern Polymer Spectroscopy*; Zerbi, G., Ed.; Wiley-VCH: New York, 1999; Chapter 4, pp 207-237.

[9] Lucotti, A.; Tommasini, M.; Fazzi, D.; Zoppo, M. D.; Chalifoux, W. A.; Ferguson, M. J.; Zerbi, G.; Tykwinski, R. R. *J. Am. Chem. Soc.* **2009**, *131*, 4239–4244.

[10] Mukherjee, V.; Singh, N. P.; Yadav, R. A. *Spectrochim. Acta A* **2009**, *73*, 249–256.

[11] Nagabalasubramanian, P. B.; Periandy, S.; Mohan, S.; Govindarajan, M. *Spectrochim. Acta A* **2009**, *73*, 277–280.

[12] Costante, J.; Hecht, L.; Polavarapu, P. L.; Collet, A.; Barron, L. D. *Angew. Chem., Int. Ed.* **1997**, *36*, 885–887.

[13] Hug, W. *In Handbook of Vibrational Spectroscopy*; Chalmers, J. M., Griffiths, P. R., Eds.; John Wiley and Sons: Chichester, 2002; Vol. 1, p 175.

[14] Pecul, M.; Rizzo, A.; Leszczynski, J. *J. Phys. Chem. A* **2002**, *106*, 11008–11016.

[15] Reiher, M.; Liégeois, V.; Ruud, K. *J. Phys. Chem. A* **2005**, *109*, 7567–7574.

[16] Haesler, J.; Schindelholz, I.; Riguet, E.; Bochet, C. G.; Hug, W. *Nature* **2007**, *446*, 526–529.

[17] Haesler, J.; Hug, W. *Chimia* **2008**, *62*, 482–488.

[18] Uchiyama, T.; Sonoyama, M.; Hamada, Y.; Dukor, R. K.; Nafie, L. A.; Hayashi, F.; Oosawa, K. *Vib. Spectrosc.* **2008**, *48*, 65–68.

[19] Kapitan, J.; Zhu, F.; Hecht, L.; Gardiner, J.; Seebach, D.; Barron, L. D. *Angew. Chem., Int. Ed.* **2008**, *47*, 6392–6394.

[20] Mukhopadhyay, P.; Zuber, G.; Beratan, D. N. *Biophys. J.* **2008**, *95*, 5574–5586.

[21] Jacob, Ch. R.; Luber, S.; Reiher, M. *Chem.sEur. J.* **2009**, *15*, 13491–13508.

[22] Luber, S.; Reiher, M. *J. Phys. Chem. B* **2010**, *114*, 1057–1063.

[23] Liégeois, V.; Champagne, B. *J. Comput. Chem.* **2009**, *30*, 1261– 1278.

[24] Liégeois, V.; Jacob, Ch. R.; Champagne, B.; Reiher, M. *J. Phys. Chem. A* **2010**, *114*, 7198–7212.

[25] Drillieres, S.; Mestanza, R.; Graebling, D. *Int. Polym. Proc.* **1998**, *13*, 149–153.

[26] Van Drumpt, J. D.; Oosterwijk, H. H. J. *J. Polym. Sci., Polym. Chem.* **1976**, *14*, 1495–1511.

[27] Hulse, G. E.; Kersting, R. J.; Warfel, D. R. *J. Polym. Sci., Polym. Chem.* **1981**, *19*, 655–667.

[28] Tabata, M.; Sohma, J.; Yokota, K.; Yamaoka, H.; Matsuyama, T. *Radiat. Phys. Chem.* **1990**, *36*, 551–558.

[29] Jois, Y.; Bronk, J. *Polymer* **1996**, *37*, 4345–4356.

[30] Ranganathan, S.; Baker, W.; Russell, K.; Whitney, R. *J. Polym. Sci., Polym. Chem.* **1999**, *37*, 3817–3825.

[31] Clark, D.; Baker, W.; Russell, K.; Whitney, R. *J. Polym. Sci., Poly Chem.* **2000**, *38*, 2456–2468.

[32] Sulek, P.; Knaus, S.; Liska, R. *Macromol. Symp.* **2001**, *176*, 155– 165.

[33] Knaus, S.; Spoljaric-Lukacic, L.; Liska, R.; Saf, R. *Eur. Polym. J.* **2005**, *41*, 2240–2254. Raman and VROA Signatures of PMU Diastereoisomers *J. Phys. Chem. B, Vol. 114, No. 36, 2010*,**11759**

[34] Benedetti, E.; Pucci, S.; Pino, P.; Schettino, V. *Spectrochim. Acta A* **1973**, *A 29*, 1313–1320.

[35] Zambelli, A.; Locatelli, P.; Bajo, G.; Bovey, F. A. *Macromolecules* **1975**, *8*, 687–689.

[36] Suter, U. W.; Pucci, S.; Pino, P. *J. Am. Chem. Soc.* **1975**, *97*, 1018–1023.

[37] Ferro, D. R.; Zambelli, A.; Provasoli, A.; Locatelli, P.; Rigamonti, E. *Macromolecules* **1980**, *13*, 179–186.

[38] Horst, B. T.; Feringa, B. L.; Minnaard, A. J. *Org. Lett.* **2007**, *9*, 3013–3015.

[39] Liang, B.; Novak, T.; Tan, Z.; Negishi, E. *J. Am. Chem. Soc.* **2006**, *128*, 2770–2771.

[40] Pino, P.; Pucci, S.; Benedetti, E.; Bucci, P. In *Sintesi Organiche*; Con. Naz. Ric: Rome, 1968; pp 91-95.

[41] For further information regarding corona detection, please refer to the manufacturer's website: http://www.coronacad.com.

[42] Barron, L. D.; Buckingham, A. D. *Mol. Phys.* **1971**, *20*, 1111.

[43] Barron, L. D. *Molecular Light Scattering and Optical Activity*; Cambridge University Press: Cambridge, 2004.

[44] Buckingham, A. D. *Ad*v. *Chem. Phys.* **1967**, *12*, 107.

[45] Liégeois, V.; Ruud, K.; Champagne, B. *J. Chem. Phys.* **2007**, *127*, 204105.

[46] Zuber, G.; Hug, W. *J. Phys. Chem. A* **2004**, *108*, 2108–2118.

[47] DALTON, a molecular electronic structure program, Release 2.0, **2005**; see http://www.kjemi.uio.no/software/dalton/dalton.html.

[48] Frisch, M. J. et al. *Gaussian 03, Re*V*ision B. 04*, Gaussian, Inc., Wallingford, CT, **2004**.

[49] Zuber, G.; Hug, W. *Hel*V. *Chim. Acta* **2004**, *87*, 2208–2234.

[50] Wojdyr, M. Open source GPL'd peak profiling program Fityk; http://www.unipress.waw.pl/fityk.

[51] Jørgensen, W. L.; Tirado-Rives, J. *J. Am. Chem. Soc.* **1988**, *110*, 1657–1666.

5.2 Polypropylene Ionic Thermoplastic Elastomers: Synthesis and Properties

Dimitri D.J. Rousseaux,[1] Xavier Drooghaag,[1] Michel Sclavons,[2] Pierre Godard,[2] Véronique Carlier,[2] Jacqueline Marchand Brynaert[1]

Published as Polym. Degrad. Stab. ***2010****, 95, 363-368*

[1]Unité de Chimie Organique et Médicinale, Place Louis Pasteur 1, B-1348 Louvain-la-Neuve, Belgium
[2]Unité de Physique et de Chimie des Hauts Polymères, Place Croix du Sud 1, B-1348 Louvain-la-Neuve, Belgium.

Abstract

Polypropylene ionic thermoplastic elastomers have been prepared by melt radical grafting of maleic anhydride onto polypropylene in the presence of N-bromosuccinimide followed by neutralization of the resulting elastomeric grafted polypropylene using sodium salts. Sodium hydroxide and sodium acetate were compared in aqueous solution, as anhydrous or hydrated powders. The neutralization reaction was followed by Fourier transform infrared spectroscopy, allowing the development of a method to determine the effective neutralization degree. Important physical changes were recorded upon neutralization. Especially thermal stability, shear storage modulus and complex viscosity in the flow region were largely increased as a function of the neutralization degree.

5.2.1 Introduction

Ionomers are macromolecules composed of a small but significant proportion of constitutional units (less than 10 %) containing an ionic and/or ionizable group.[1] The ionic moieties are usually obtained by full or partial neutralization of the acid groups by metal salts. The acid groups are mainly carboxylic acids but also sulfonic and phosphonic acids are being used. The ionic groups cause a micro-phase separation of the ionic moieties (ionic aggregation) within the non-ionic matrix and act as physical crosslinks.[2-7] The ionic aggregation induces strong modifications in the physical, mechanical and rheological properties of the material. Nevertheless, ionomers can be melt-processed due to the reversibility of the crosslinking based on the increased mobility of the ionic moieties at high temperature. Ionomers of low glass-transition non-crystalline polymers can be used as ionic thermoplastic elastomers (TPEs) if the ionic aggregates are sufficiently weakened at the processing temperatures.[8,9] TPEs are meltprocessable polymers composed of a continuous elastomeric phase reinforced by a dispersed hard phase acting as thermo-reversible junction points.[10] Different types of carboxylated ionic TPEs have been studied in the past, for example: Kutsumizu et al. investigated non-crystalline poly(ethylene-co-methacrylic acid) ionomers;[11,12] more recently, the group of Goossens-van Duin studied extensively ionomers based on maleated ethylene/propylene copolymers.[9,13-16] In this paper, carboxylated ionic TPEs of polypropylene (PP) will be introduced. PP elastomeric ionomers are based on the elastomeric polypropylene-graft-maleic anhydride (elPP-g-MA) as described in section 2.2 of chapter 2. Both the precursor elPP-g-MA and the ionomers are synthesized by melt-processing. The neutralization reaction is monitored by infrared spectroscopy and a method is proposed to determine the effective neutralization degree (ND). Various forms of sodium hydroxide and sodium acetate are used to compare their efficiency for elPP-g-MA neutralization.

The influence of the base nature and amount on the ND is studied. Thermal and rheological properties of the ionomers are examined and discussed as a function of the ND.

5.2.2 Experimental Section

Materials

Isotactic homopolymer PP powder (Moplen HF500N) was purchased from Basell. The free radical initiator was Luperox 101XLS50 from Arkema (2,5-bis(tert-butyl-peroxy)-2,5-dimethylhexane (DHBP), 50 wt.% blend with silica). Maleic anhydride (MA, Acros, 99 % purity), N-bromosuccinimide (NBS, Acros, 99 % purity), sodium acetate (NaAc) trihydrate (Aldrich, 99 % purity) and anhydrous (Aldrich, 99 % purity), sodium hyroxide (NaOH) in pellets (Aldrich, 99+ % purity) and in powder (Aldrich, 97 % purity) and toluene (Fisher, analytical grade) were used as received.

Synthesis of elPP-g-MA and the corresponding ionomers

elPP-g-MA was synthesized by reactive extrusion as described in section 2.2.2 of chapter 2. Briefly, isotactic polypropylene was treated with 3.26 wt.% of supported peroxide, 5 wt.% of maleic anhydride and 0.8 wt.% of N-bromosuccinimide. elPP-g-MA was produced in a Brabender single screw extruder equipped with a screw of L/D = 20. The barrel was heated on three zones at 220, 240 and 260 °C, respectively, and the screw speed was set to 30 rpm.

All the ionomers were synthesized by reactive blending in a Brabender Plasticorder equipped with an electrically heated W50EH mixing device of 40 g capacity. The mixing speed was set to 100 rpm and the temperature at 220 °C. The alkaline base was added to the molten elPP-g-MA either in fine

powder, or in 2.5 molar aqueous solution, and the reaction was stopped after 5 min by quenching the molten ionomer at room temperature.

Characterizations

elPP-g-MA samples were first washed as described in section 2.2.2 of chapter 2. The anhydride content was determined by acid-base titration according to a standard procedure:[17] 1 g of washed polymer was dissolved in 150 ml of refluxing toluene. After complete dissolution, five drops of 1% w/v bromothymol blue in methanol were added and the solution was titrated by a 0.05N solution of tetrabutyl ammonium hydroxide (TBAOH). The titration was stopped when the color change was stable. The AM content was calculated from the volume and concentration of TBAOH.

Crystallinity and glass transition temperature (T_g) measurements of elPP-g-MA and ionomers were performed on a second heating ramp from -50 to 220 °C at 10 °C/min using a Mettler Toledo DSC 821e module. The device was calibrated with indium and zinc.

Number- and weight-average molar mass (Mn and Mw, respectively) of the elPP-g-MA were measured on a Waters Alliance GPCV 2000 equipped with two Styragel HT 6E and one Styragel HT 2 columns. A differential refractometer and a viscometer were used as detectors. The mobile phase was 1,2,4-trichlorobenzene (TCB). The concentration of the sample was 2 mg/mL in TCB and dissolution was achieved by shaking at 160 °C for 1 h. The injection volume was 215 µL. Temperature was held constant at 145 °C throughout the analysis. The system was calibrated prior to the analysis with PS standards according to ISO 16014-2 specification.

FTIR spectra of compression-molded films were recorded on a Nicolet Nexus 670 FTIR apparatus, over a spectral range from 4000 to 400 cm^{-1} at a

resolution of 4 cm^{-1}. All the FTIR spectra were normalized by setting the peak height of the 973 cm^{-1} absorption band to an absorbance of 1 A.U. This band, which is assigned to isotactic helices, is usually considered as an internal reference for the comparison of films of different thicknesses.[18] The FTIR spectra were mathematically analyzed by an iterative curve-fitting method developed in the Igor software provided by Wavemetrics, Inc. The absorption bands area in the carbonyl frequency range of the anhydride (1750-1830 cm^{-1}) and the carboxylic acid (1650-1750 cm^{-1}) were approximated by a Voigt function.

Thermal analyses were performed on Mettler Toledo TGA/SDTA 851e using a heating rate of 10 °C/min under air atmosphere (100 ml/min) from 25 to 600 °C.

Rheological properties were measured using a Rubber Process Analyser RPA 2000 from Alpha Technologies. Frequency sweep tests were performed at 120 °C and at a strain rate of 10 % over an angular frequency ranging from 300 to 1 rad/s.

5.2.3 Results and discussion

elPP-g-MA characterization

The main characteristics of the starting isotactic PP and the elPP-g-MA are summarized in Table 5.2. elPP-g-MA reaches a grafting level of 3.5 wt.% and its molar mass is clearely reduced in comparison with the starting PP. The degradation of the molar mass is caused by the well-established β-scission side reaction occurring during reactive processing. The crystallinity of elPP-g-MA is strongly reduced with respect to the starting iPP, due to the epimerization reaction occuring in the presence of

peroxide and NBS (see section 2.2 of chapter 2 for the detailed study of this reaction).

Table 5.2 : Characteristics of PP and elPP-g-MA.

	PP	elPP-g-MA
Grafting level (wt%MA)	/	3.5
Crystallinity (%)	46.2	1.6
Mn	65k	22k
Mw	245k	60k

Ionomer ND determination

The neutralization reaction can be assessed by FITR by monitoring the decrease of the carbonyl symmetric stretching vibration of the succinic anhydride band at 1790 cm^{-1}. The asymmetric stretching of the succinic anhydride band is visible at 1864 cm^{-1} but is weaker than the symmetric one. The grafted succinic anhydride moieties can be neutralized twice (Figure 5.9), the first neutralization step being easier because the first acid dissociation constant (pKa_1 = 4.2) is weaker than the second one (pKa_2 = 5.6).

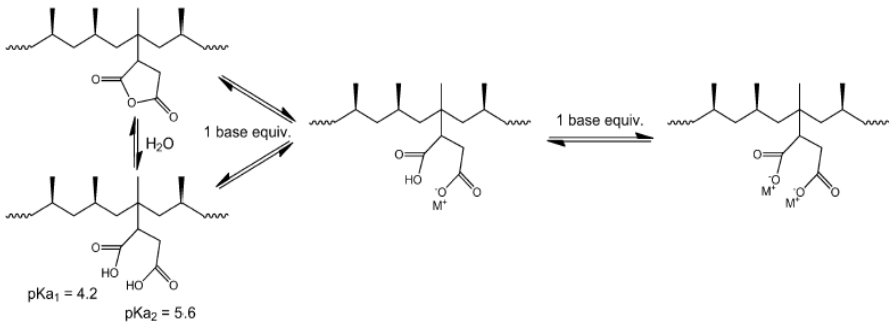

Figure 5.9 : two-steps neutralization of elPP-g-MA

After the first neutralization step, the anhydride ring is opened into a carboxylate group and a carboxylic acid. Figure 5.10 shows an enlargement

of the carbonyl region of the FTIR spectra of the starting elPP-g-MA and the ionomer neutralized with 0.5 equivalents (equiv.) of 2.5M NaOH solution. The elPP-g-MA spectrum shows only two absorption bands, characteristic for cyclic anhydrides at 1863 cm^{-1} (weak, asymmetrical stretching) and 1790 cm^{-1} (strong, symmetrical stretching). As shown in Figure 5.10, the intensity of the anhydride bands decreases upon neutralization while two new bands appear at 1715 cm^{-1} and 1570 cm^{-1}. These new bands correspond to the carbonyl stretching of carboxylic acid and metal-carboxylate, respectively.[9,16]

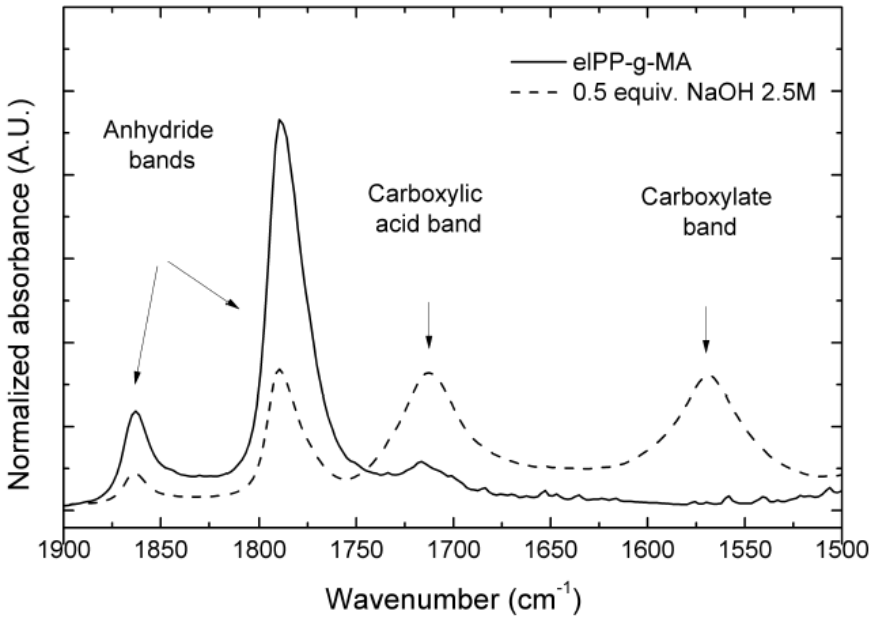

Figure 5.10 : Enlargement of the carbonyl region of the FTIR spectra for elPP-g-MA and 0.5 equiv. NaOH 2.5 M ionomer.

If the ND was calculated on the basis of the decrease of the anhydride band at 1790 cm^{-1} from elPP-g-MA ($Aanh_{elPP\text{-}g\text{-}MA}$) to ionomer ($Aanh_{ionomer}$), using Equation 5.4, it would be overestimated due to the carboxylic acid functions contribution. To solve this problem, elPP-g-MA was hydrolyzed in a water atmosphere in order to open properly the anhydride functions into

diacids. Figure 5.11 shows an enlargement of the carbonyl region of the FTIR spectra for dry elPP-g-MA (starting material) and wet elPP-g-MA. Wet elPP-g-MA was then melt-pressed into films at 200 °C. By melt-pressing the wet sample during increasing times, the diacid functions progressively closed to form anhydrides (Figure 5.12). The evolution of the acid band area as a function of the anhydride band area for several meltpressed samples is presented in Figure 5.13. A linear regression, using Equation 5.8, can be used to convert the anhydride band area (Aanh) into acid (Aacid) in order to calculate a corrected acid band area (Aacid corr). The corrected acid band area is the area of the acid band that would have been measured if all anhydride functions were hydrolyzed into acid and this value corresponds to the Y intercept (Y_0) of Equation 5.5. The corrected acid band area can be calculated by measuring the anhydride and acid bands areas of a sample using Equation 5.7. A corrected neutralization degree (cND) based on the decrease of the corrected acid band area from elPP-g-MA ($A_{\text{acidcorr elPP-g-MA}}$) to ionomer ($A_{\text{acidcorr ionomer}}$) can be calculated using Equation 5.8.

$$ND = \frac{A_{anh_{\text{ionomer}}}}{A_{anh_{\text{elPP-g-MA}}}} \cdot 100 \tag{5.4}$$

$$A_{acid} = (A_{anh} \cdot S) + Y_0 \tag{5.5}$$

$$A_{acid\_corr} = Y_0 \tag{5.6}$$

$$A_{acid\_corr} = A_{acid} - (A_{anh} \cdot S) \tag{5.7}$$

$$cND = \frac{A_{acid\_corr_{\text{ionomer}}}}{A_{acid\_corr_{elPP-g-MA}}} \cdot 100 \tag{5.8}$$

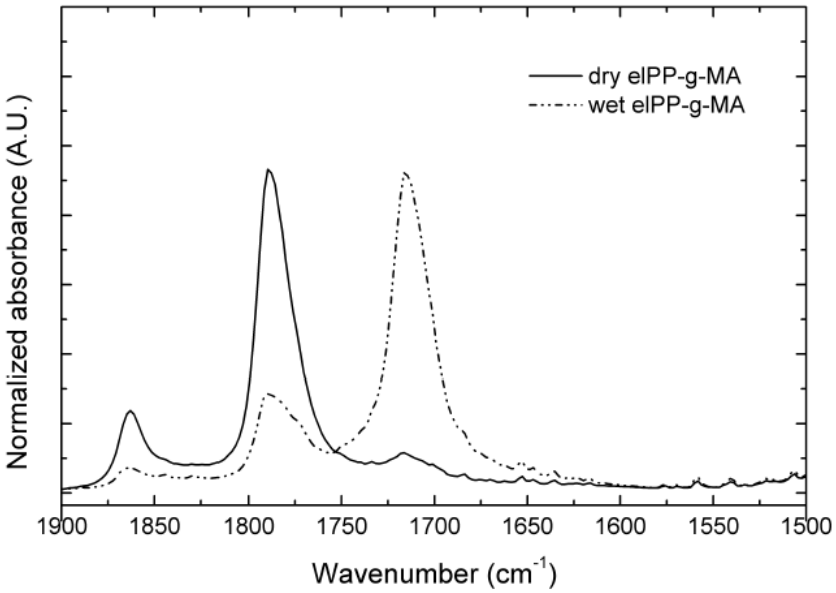

Figure 5.11 : Enlargement of the carbonyl region of the FTIR spectra for dry and wet elPPg-MA.

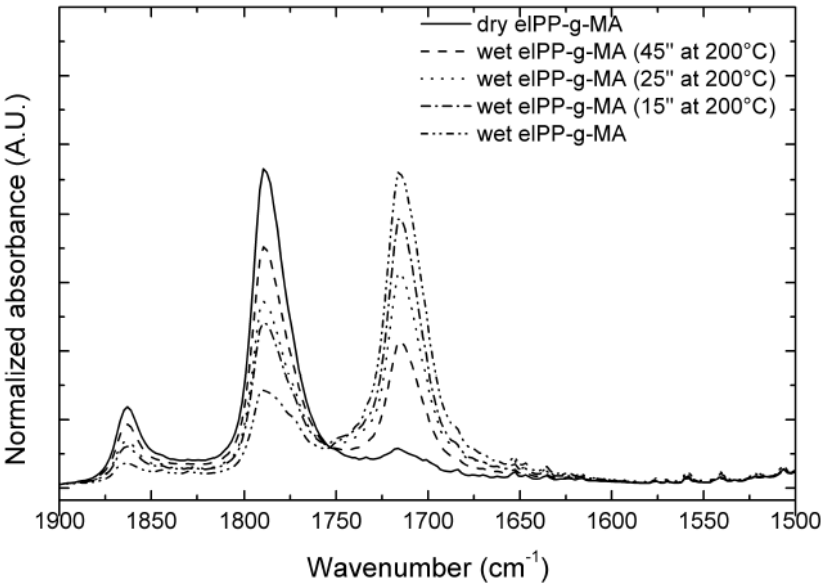

Figure 5.12 : Enlargement of the carbonyl region of the FTIR spectra for melt-pressed wet elPP-g-MAs for increasing times.

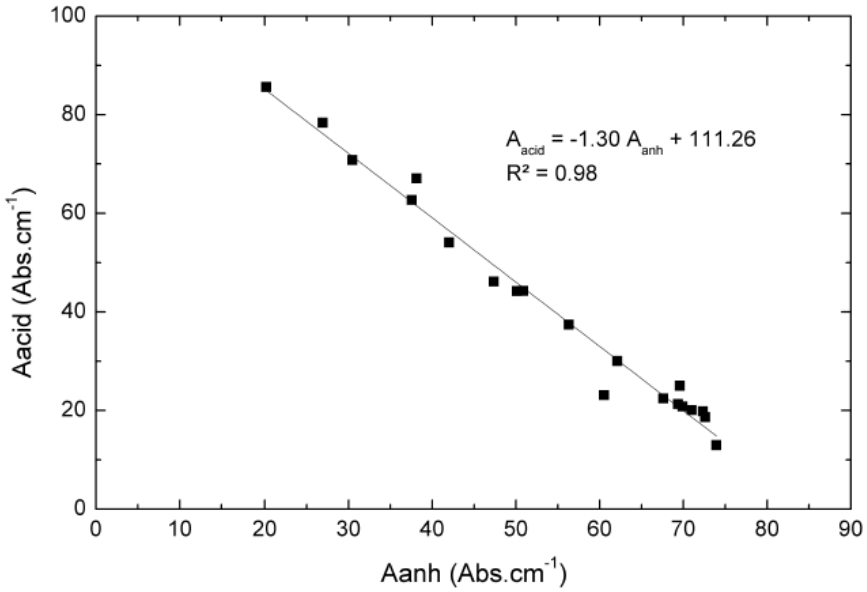

Figure 5.13 : Acid band area (Aacid) evolution as a function of the anhydride band area (Aanh) for the melt-pressed elPP-g-MAs.

Influence of the nature of the base on the ND

The influence of the nature of the base on the neutralization degree has been studied. Two different bases were used: sodium hydroxide and sodium acetate. These bases were added under various forms to the molten elPP-g-MA. One base equiv. refers to the amount of base required to neutralize all the anhydride functions twice. NaOH was added in 2.5M aqueous solution (NaOH 2.5M) at 0.1, 0.2, 0.3, 0.5 and 0.75 equiv. or as powdered solid (NaOH sol.) at 0.75 equiv. NaAc was added as hydrated solid ($NaAc.3H_2O$ sol.) and as 2.5 molar aqueous solution (NaAc 2.5M) at 0.1, 0.2, 0.5, 0.75 and 1 equiv. or as anhydrous solid (NaAc anh. sol.) at 1 equiv. Figure 5.14 shows the evolution of the cND of ionomers, as a function of the added amount of base.

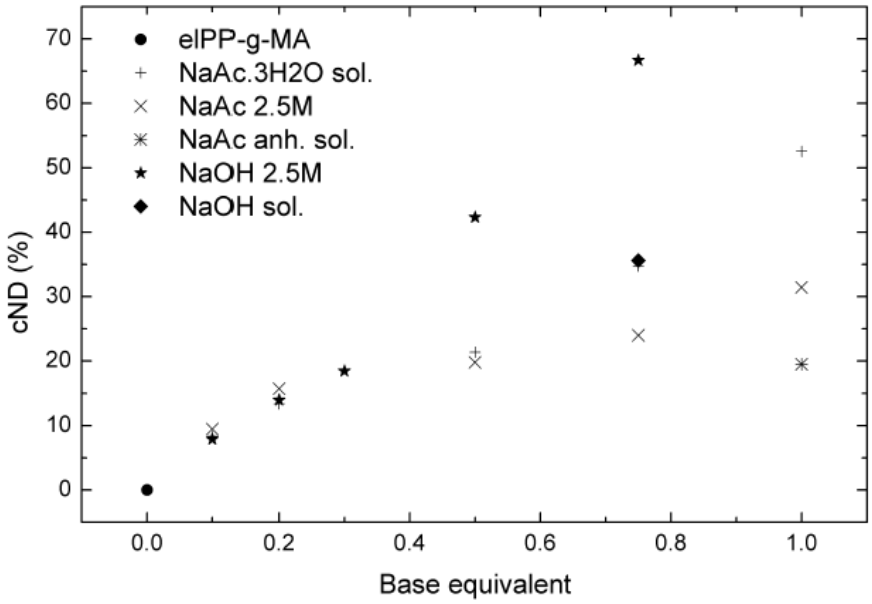

Figure 5.14 : Ionomers cND evolution versus base equivalent.

Up to 0.2 equiv., the cND is the same for all ionomers, and proportional to the base amount. Differences are observed above 0.2 equiv. The cND of the ionomers synthesized with NaOH 2.5M continues to rise proportionally to the base amount, indicating that the reaction yield is maintained. The cND of the ionomer synthesized with 0.75 equiv. of NaOH sol. is about the half of the one synthesized with 0.75 equiv. of NaOH 2.5M. Over 0.2 equiv., the cND of the ionomers synthesized with NaAc.$3H_2O$ sol. continues to rise but less importantly than with NaOH 2.5M while the cND of the ionomers synthesized with NaAc 2.5M reaches a plateau. The cND of the ionomer prepared with 1 equiv. of NaAc anh. sol. is 2.7 times lower than the one with 1 equiv. of NaAc.$3H_2O$ sol. and 1.6 times lower than the one with 1 equiv. of NaAc 2.5M. The neutralization reaction requires water to ionize the base. Although hygroscopic, NaOH sol. powder contains much less water than NaOH in solution. This explains the observed difference in cND between NaOH 2.5M and NaOH sol. The difference in cND observed between the

ionomers neutralized by NaOH and NaAc results from their pKa which are 15.7 for NaOH (H_2O/OH^-) and 4.76 for NaAc ($CH_3CO_2H/CH_3CO_2^-$). NaOH is a stronger base than NaAc and is therefore more efficient to neutralize elPP-g-MA under the same conditions. Considering the pKa difference between the grafted succinic moieties and the bases, a complete reaction is theoretically expected with NaOH and an equilibrated reaction with NaAc. However, the neutralization reaction is displaced towards the products formation since the reaction residue (H_2O for NaOH, CH_3CO_2H for NaAc) is evaporated during the ionomer synthesis. The difference in cND observed between the ionomers neutralized by NaAc.$3H_2O$ sol. and NaAc 2.5M cannot be rationalized. As for NaOH, the presence of water, either from salt hydration for NaAc.$3H_2O$ sol., or from solution for NaAc 2.5M, explains the higher cND obtained when neutralizing elPP-g-MA with a water-containing NaAc salt rather than with NaAc anh. sol. The neutralization efficiency order for all bases is the following: NaOH 2.5M > NaOH sol. ≈ NaAc.$3H_2O$ sol. > NaAc 2.5M > NaAc. anh. sol. The ionomer prepared with 0.75 equiv. of NaOH 2.5M reaches a critical neutralization degree value. When synthesizing this ionomer, the torque increased until the blender-knives broke the ionic network and expelled it. The crosslinking density reaches a plateau and a higher neutralization degree cannot be obtained. For that reason, the characterization of this sample is omitted.

Ionomer characterizations

While the DSC trace of elPP-g-MA (not shown here, but similar to the one presented in section 2.2.3 of chapter 2) exhibits a glass-transition around -4.2 °C and a weak broad melting peak, the DSC traces of the ionomers show only a glass-transition, in any case similar to the one of elPP-g-MA.

Thermogravimetric analysis was performed on the ionomers. In order to compare all the samples, the temperature at 10 % weight loss, which corresponds to the onset of the degradation, is plotted as a function of the cND in Figure 5.15. There is a signifficant increase in the onset temperature (T_o) with respect to the cND. At high ND, the T_o is measured about 60 °C higher than for elPP-g-MA. This phenomenon can be explained by the ionic crosslinking which holds together the polymer segments resulting from thermal degradation (of the ionomer). As the neutralization degree increases, the crosslinking density increases proportionally. Hence the polymer segments are tied together and the onset temperature is raised.

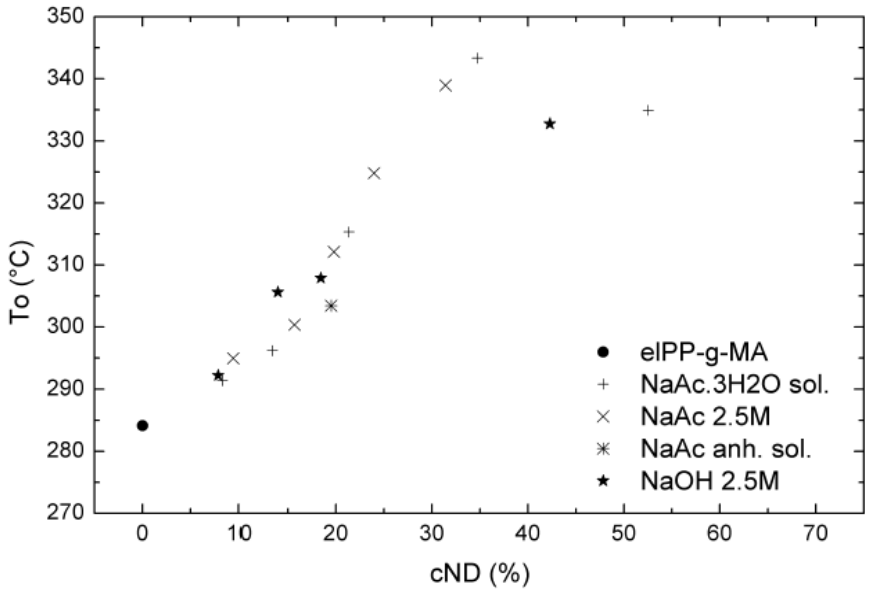

Figure 5.15 : Ionomers onset temperature (To) versus cND.

Rheology.

Frequency sweep experiments were performed on all the samples. To facilitate the comparison between the different samples, only the values of shear elastic modulus and complex viscosity, taken at 12 rad/s, are

presented. Figures 5.16 and 5.17 show the evolution of the shear elastic modulus (G') and the complex viscosity (η*) respectively, as a function of the cND. Both the shear elastic modulus and the complex viscosity increase about 2 decades with the cND. The phenomenon is explained by the matrix reinforcement as a result of the ionic crosslinking. By increasing the neutralization degree, the extent of ionic aggregation rises and enhances the reinforcement effect.

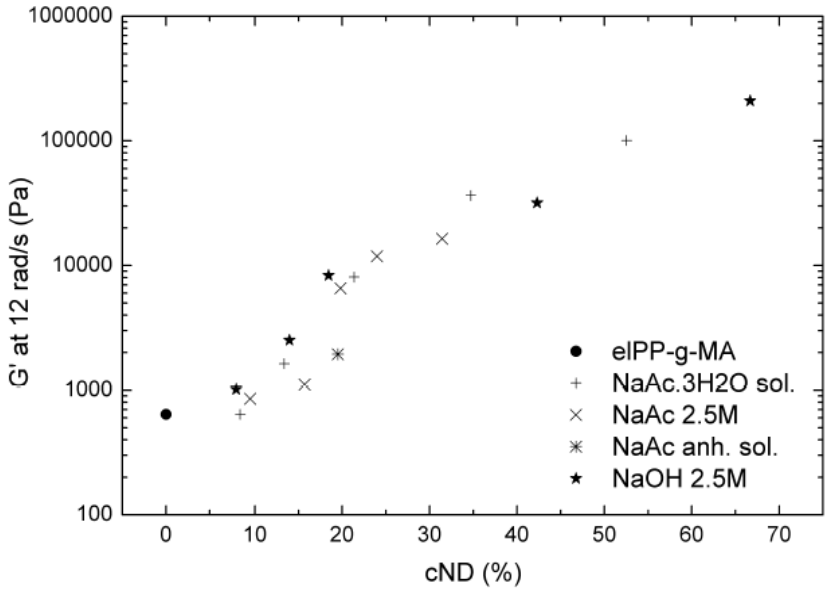

Figure 5.16 : Ionomers shear elastic modulus (G') at 12 rad/s versus cND.

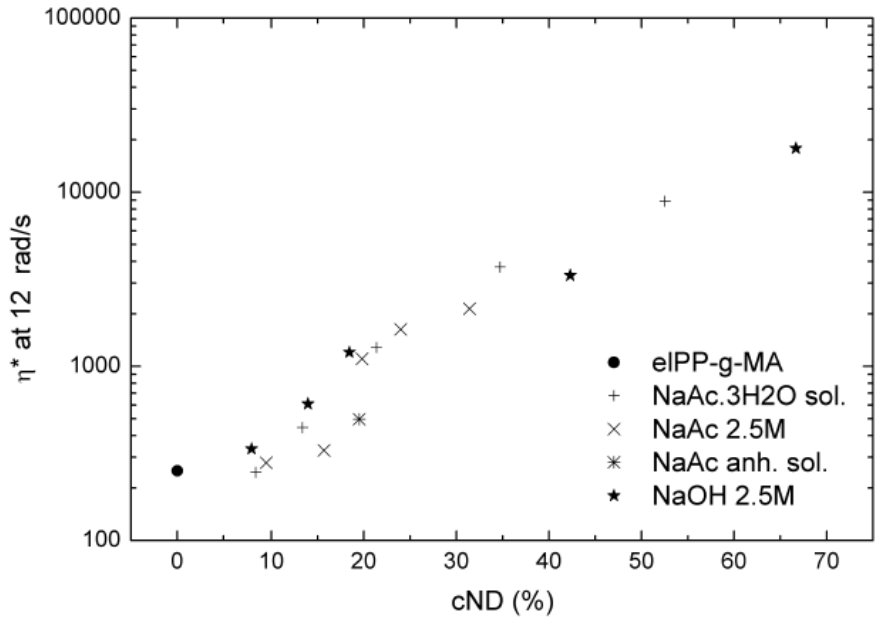

Figure 5.17 : Ionomers complex viscosity (η*) at 12 rad/s versus cND.

5.2.4. Conclusions

Elastomeric highly-functionalized polypropylene-graft-maleic anhydride was produced and characterized. From this material, new carboxylated ionic thermoplastic elastomers of polypropylene were successfully synthesized. Two sodium bases were used under different physical forms to compare their effciency to neutralize the elastomeric polypropylene-graft-maleic anhydride. It was shown that water, either from salt hydration or from salt aqueous solution, is required to ionize the base in order to allow the acid-base reaction to occur. A method was developed to determine the effective neutralization degree by infrared spectroscopy. The choice of the base has a strong influence on the neutralization degree. Sodium hydroxide allowed the neutralization yield to be kept almost constant even at high neutralization degree. However, as the neutralization yield never reaches 100 %, the excess of the added sodium hydroxide may

lead to corrosion. Sodium acetate is a weak base but the neutralization reaction is displaced towards product formation since the reaction residue (acetic acid) is evaporated during the ionomer synthesis. Furthermore, no corrosion is expected with sodium acetate. For these reasons, sodium acetate is preferred over sodium hydroxide. The ionomer physical properties were improved strongly. The thermal stability in air atmosphere, shear storage modulus and complex viscosity in the flow region were largely increased as a function of the neutralization degree.

5.2.5. Acknowledgement

The authors thank La Région Wallonne and FRIA (Fonds pour la formation à la Recherche dans l'Industrie et dans l'Agriculture) for financial support. J. Marchand-Brynaert is Senior Research Associate of the FRS-FNRS (Fonds National de la Recherche Scientifique, Belgium). Prof. A. Jonas is acknowledged for help and useful discussions about the FTIR fitting routine and Prof. J. Devaux for his kind support.

5.2.6. References

[1] M. Hess, R.G. Jones, J. Kahovec, Kitayama T., P. Kratochvil, P. Kubisa, W. Mormann, R. F. T. Stepto, D. Tabak, J. Vohldal, and E. S. Wilks. Terminology of polymers containing ionizable or ionic groups and of polymers containing ions (IUPAC recommendations 2006). Pure Appl. Chem., 78(11), 2067-2074, 2006.

[2] L. Holliday. Ionic Polymers. Applied Science Publishers, London, 1975.

[3] A. Eisenberg. Ions in Polymers. American Chemical Society, Washington, DC, 1980.

[4] L. A. Utracki and R. A. Weiss. Multiphase polymers: blends and ionomers, volume 1. American Chemical Society, Washington, DC, 1989.

[5] S. Schlick. Ionomers: Characterisation, Theory and Applications. CRC Press, Boca Raton, Florida, 1996.

[6] M. R. Tant, K. A. Mauritz, and G. L. Wilkes. Ionomers: synthesis, structure, properties and applications. Springer, London, 1997.

[7] A. Eisenberg and J-S. Kim. Introduction to ionomers. Wileyinterscience, New-York, 1998.

[8] S. Bagrodia, G. L. Wilkes, and J. P. Kennedy. New polyisobutylene based model elastomeric ionomers: Rheological behavior. Polym. Eng. Sci., 26(10), 662-672, 1986.

[9] M. A. J. van der Mee, R. M. A. Abee, G. Portale, J. G. P. Goossens, and M. van Duin. Synthesis, structure, and properties of ionic thermoplastic elastomers based on maleated ethylene/propylene copolymers.Macromolecules, 41(14), 5493-5501, 2008.

[10] W. J. Work, K. Horie, M. Hess, and R. F. T. Stepto. Definition of terms related to polymer blends, composites, and multiphase polymeric materials (IUPAC recommendations 2004). Pure Appl. Chem., 76(11), 1985-2007, 2004.

[11] S. Kutsumizu, H. Tagawa, Y. Muroga, and S. Yano. Small-angle X-ray scattering investigation of noncrystalline poly(ethylene-comethacrylic acid) ionomers. Macromolecules, 33(10), 3818-3827, 2000.

[12] S. Kutsumizu, K. Tadano, Y. Matsuda, M. Goto, H. Tachino, H. Hara, E. Hirasawa, H. Tagawa, Y. Muroga, and S. Yano. Investigation of microphase separation and thermal properties of noncrystalline ethylene ionomers. 2. IR, DSC, and dielectric characterization. Macromolecules, 33(24), 9044-9053, 2000.

[13] M. E. L. Wouters, J. G. P. Goossens, and F. L. Binsbergen. Morphology of neutralized low molecular weight maleated ethylenepropylene

copolymers (MAn-g-EPM) as investigated by smallangle X-ray scattering. Macromolecules, 35(1), 208-216, 2002.

[14] M. E. L. Wouters, V. M. Litvinov, F. L. Binsbergen, J. G. P. Goossens, M. van Duin, and H. G. Dikland. Morphology of ethylene-propylene copolymer based ionomers as studied by solid state NMR and small angle x-ray scattering in relation to some mechanical properties. Macromolecules, 36(4), 1147-1156, 2003.

[15] B. P. Grady, J. G. P. Goossens, and M. E. L. Wouters. Morphology of zinc-neutralized maleated ethylene-propylene copolymer ionomers : Structure of ionic aggregates as studied by x-ray absorption spectroscopy. Macromolecules, 37(23), 8585-8591, 2004.

[16] C.X. Sun, M.A.J. van der Mee, J.G.P. Goossens, and M. van Duin. Thermoreversible cross-linking of maleated ethylene/propylene copolymers using hydrogen-bonding and ionic interactions. Macromolecules, 39, 3441-3449, 2006.

[17] M. Sclavons, P. Franquinet, V. Carlier, G. Verfaillie, I. Fallais, R. Legras, M. Laurent, and F. C. Thyrion. Quantification of the maleic anhydride grafted onto polypropylene by chemical and viscosimetric titrations, and FTIR spectroscopy. Polymer, 41(6), 1989-1999, 2000.

[18] D. R. Burfield and P. S. T. Loi. The use of infrared spectroscopy for determination of polypropylene stereoregularity. J. Appl. Polym. Sci., 36(2), 279-293, 1988.

5.3 Thermorheological Behavior of Various Short- and Long-Chain Branched Polyethylenes and Their Correlations with the Molecular Structure

Ute Kessner,[1] Joachim Kaschta,[1] Florian J. Stadler,[2] Cécile S. Le Duff,[3] Xavier Drooghaag,[3]and Helmut Münstedt,[1]

*Published as Macromolecules **2010**, 43, 7341-7350*

[1]Institute of Polymer Materials, Friedrich-Alexander-University Erlangen-Nürnberg, Martensstr. 7, D-91058 Erlangen, Germany.
[2]School of Semiconductor and Chemical Engineering, Chonbuk National University,
664-14, 1-ga Deokjin-dong, Deokjin-gu, Jeonju, Jeonbuk, 561-756, Republic of Korea.
[3]Institute of Condensed Matter and Nanosciences, Université catholique de Louvain, Bâtiment Lavoisier, Place Louis Pasteur, 1, 1348 Louvain-la-Neuve, Belgium.

Abstract

This paper deals with the characterization of a broad range of linear polyethylenes (PE) by means of thermorheology. It is demonstrated in which way the thermorheological behavior can be related to the comonomer type and content of copolymers. In the first part of this paper, well-established analytical and rheological methods are applied to distinguish linear and branched samples. The resolution limit of these methods is demonstrated by the investigation of a blend from a linear-low density PE (LLDPE) and a branched low density PE (LDPE). Special attention is paid to nuclear-magnetic resonance (NMR) spectroscopy in order to reliably determine the

comonomer type and content of the samples chosen. The main focus of this paper lies on thermorheological investigations and correlations with the molecular structure. The comparatively high sensitivity of such investigations is highlighted: even small amounts of long-chain branches (LCB) are revealed. The activation energy (E_a) of linear samples increases with growing comonomer length and content, respectively. As such, thermorheology is demonstrated to be an interesting rheological "tool" to get an insight into branching structures. Moreover, the experimental effort is relatively small as solely usual dynamic-mechanical experiments at different temperatures are required.

5.3.1 Introduction

Commercial linear low-density polyethylenes (LLDPE) are polymerized by Ziegler-Natta (ZN) or metallocene (m) catalysts using ethylene and an α-olefin, which is typically butene, hexene, or octene, respectively. Single-site catalysts (SSC) even allow the insertion of very few long-chain branches (LCB) into linear polyethylenes (PE) improving the processing properties. As such, the molecular structure and consequently the physical properties of these copolymers vary distinctly. Several studies in the literature aim to characterize the molecular structure of commercial as well as experimental LLDPE grades with analytical and rheological means in order to develop new grades and to improve the efficiency of catalysts.[1-4] The aim of this paper is to present a rheological "tool" to probe the molecular structure of PE, which is simple to handle compared to the common analytical characterization methods. For this purpose, the thermorheological behavior and the determination of activation energies (E_a) are suitable methods, as they reliably discriminate between thermorheologically simple LLDPE and thermorheologically complex long-chain branched low-density polyethylenes (LDPE) or long-chain branched

metallocene linear low-density polyethylenes (LCB-mLLDPE), respectively.[5] Some studies in the literature already deal with the relationship between the thermorheological behavior and the molecular structure of linear polyethylenes. These are summarized in the next section in order to derive the motivation and goals of this paper.

5.3.2 Literature Survey

Influence of the Length of Side Groups - Homopolymers

High-density polyethylenes (HDPE) possess activation energies E_a around 26-28 kJ/mol independent of the molar mass (M) and the polydispersity (PDI).[3,6-8] The homopolymerization of higher α-olefins leads to an increase of E_a with increasing monomer mass as the rotational potential of the backbone units rises.[7] For example, for isotactic polypropylene (iPP), which differs from HDPE by replacing hydrogen atoms by methyl groups, activation energies between 6 and 44 kJ/mol are reported.[7-13] Higher values up to 58.5 kJ/mol were determined by Eckstein et al.,[10] while Rojo et al. found an E_a around 50 kJ/mol,[14] in case of syndiotactic polypropylenes. However, the influence of tacticity is not completely understood. Homopolymers of higher α-olefins like polyisobutylene even reach activation energies around 45 kJ/mol,[15] while 49-66 kJ/mol is found for poly-1-butene.[7,16,17]

Influence of the Length of Side Groups - Copolymers

Kolodka et al.[18] copolymerized iPP with a poly(ethylene-co-propylene) macromer with a number-average molar mass (Mn) of 2500 g/mol, which is below the critical entanglement length. E_a of around 40 kJ/mol was obtained independently of the branching frequency. Furthermore, activation energies of around 30-33 kJ/mol are found in the literature for PE differing in the comonomer type and content.[9,19-21] The E_a values reported could not be

correlated with the molecular structure. However, Hussein et al.[22] concluded from their results that E_a of poly-(ethylene-octene) is higher than poly(ethylene-butene) at the same branching content.

Influence of the Comonomer Content

Some authors[4,23,24] identified a relationship between E_a and the number of side chains or comonomer content, respectively. An increase from around 23 kJ/mol at 0 wt% up to 40 kJ/mol at 30 wt% hexene was determined in the range studied. Stadler et al.[3] found such a dependence to be valid regardless of the comonomer type inserted. Wood-Adams and Costeux[25] published E_a values of poly(ethylene-butene) copolymers. E_a increased from 26 kJ/mol at 0 wt %, characteristic of HDPE, to around 33 kJ/mol at 7 wt% comonomer content. At still higher butene contents, E_a was found to be constant. These results are consistent with other studies.[26-28] An increase of E_a with comonomer content was also found by Hussein et al.[22] for poly(ethylene-butene) and poly(ethylene-octene). However, it cannot be concluded from this study whether E_a becomes constant or still increases at higher comonomer content. Some papers report even higher E_a for LLDPE but state that LCB may be an issue.[2]

Influence of the Comonomer Distribution

The catalyst chosen affects the homogeneity of the comonomer incorporation. From the literature, it is known that ZN catalysts, in general, lead to heterogeneous comonomer distributions. By comparison, the structure of polymers catalyzed with single-site catalysts is more homogeneous. Additionally, heterogeneities of the comonomer distribution may appear with both catalyst types.[29-31] Nevertheless, no differences in the thermorheological behavior between m- and ZN-catalyzed LLDPE are reported in the literature.

Influence of Very Few Long-Chain Branches

Investigations of the correlations between the thermorheological behavior and the molecular structure of linear PE are often complicated by the presence of a small amount of LCB, which may be not detectable with analytical methods. Vega et al.[24] and Wood-Adams and Costeux[25] described a synergistic effect of short-chain and long-chain branching on E_a. Furthermore, E_a of long-chain branched HDPE and LLDPE increased with the number of LCB. By contrast, Wasserman and Graessley[8] did not observe an elevated E_a for samples suspected to contain few LCB. Thus, the question remains whether few LCB noticeably affect the thermorheological behavior. Nevertheless, it is known from the literature that a significant amount of LCB, for example in LDPE and LCB-mLLDPE, results in thermorheological complexity and leads to a higher E_a compared to LLDPE.

5.3.3 Motivation

It is well-established in the literature that linear PE is thermorheologically simple. Furthermore, it is known that the molar mass and the polydispersity have no influence on the thermorheological behavior. LCB, however, affect the temperature dependence drastically, such that reliable correlations with the linear structure of PE (i.e., the comonomer length and content) are not possible, if a few LCB are present. A complete and comprehensive molecular characterization of the samples investigated is missing in many studies cited above. Moreover, the analytical and rheological characterization methods used were not sensitive enough to reveal small amounts of LCB and/or are time and cost consuming.[32,33] Therefore, contradictory results on "apparently" linear PE are found in the literature. Furthermore, inconsistencies are obvious, as different methods for the evaluation of E_a were applied in these studies. Summarizing the various findings, the prerequisites to establish relationships between the

thermorheological behavior, especially E_a, and the comonomer length and content of LLDPE should exclude the presence of any LCB and apply a method for the determination of E_a which is independent of the experimental quantity used. An approach to a defined method was previously published,[34] and it is applied in this paper. A broad range of linear polyethylenes is investigated with common analytical and rheological methods as well as with thermorheology. A detailed molecular characterization of the samples is carried out to detect small amounts of LCB and to get a comprehensive insight into the molecular structure. The temperature-dependent viscoelastic behavior is related to the molecular structure taking into account the detection limits and restrictions of the methods used.

5.3.4 Characterization Methods

Size ExclusionChromatography coupled with Multiangle Laser-Light Scattering

The determination of the molar masses (M_n, number-average; M_w, weight-average), their distribution as well as the radii of gyration was carried out using a high-temperature size exclusion chromatograph ((SEC), PL 220, Varian Inc.) equipped with Shodex columns [UT 807 (1x) and UT 806M (3x)] and coupled with a multiangle laser-light scattering (MALLS) apparatus (Wyatt Dawn EOS, Wyatt Corp.). The temperature was 140 °C and the solvent 1,2,4-trichlorobenzene (TCB).

^{13}C Nuclear Magnetic Resonance (^{13}C NMR) Spectroscopy.

^{13}C nuclear-magnetic resonance spectroscopy was applied in order to determine the comonomer type and content. These NMR measurements were performed in different laboratories and by different operators. A good agreement between the results of different setups was obtained. The reproducibility of such measurements was checked on a poly(ethylene-

hexene) sample (L6-4). The measurement uncertainty is estimated to be 10 % at the maximum. The main part of the NMR results originates from the Université catholique de Louvain (Département de Chimie). Details of these measurements are briefly given below. Further information on the measurement and evaluation of NMR data as well as on the quantitative determination of the comonomer content can be found in the literature.[35-39]

Preparation of Samples for the NMR Analysis.

About 100 mg of each polymer were dissolved under argon in 2.5 mL of deuterated tetrachloroethane (TCE-d_2), preheated at 135 °C. To obtain a complete dissolution, the samples were rotated at 40 rpm in the NMR spectrometer at 135 °C for up to 1 h.

Acquisition of 1D ^{13}C NMR spectra.

NMR spectra were acquired on a Bruker Avance DRX500 spectrometer operating at 500.13 MHz for ^{1}H (125.77 MHz for ^{13}C) and equipped with a 10 mm Bruker Selective Observe ^{13}C probe for temperatures up to 400 °C. The probe temperature was set at 135 °C for the duration of the experiments. Spectra were referenced to the TCE-d_2 peaks at 6.00 ppm for ^{1}H and 73.70 ppm for ^{13}C. One dimensional ^{1}H spectra were recorded prior to ^{13}C experiments to ensure that the best field homogeneity was attained for each sample. One-dimensional ^{13}C were recorded using 32768 points and an acquisition time of 0.59 s. Between 3000 and 4000 scans were acquired per sample with a sweep width of 27.6 kHz and a delay of 15 s between scans, using inverse-gated Waltz16 ^{1}H decoupling. The signal was Fourier transformed using an exponential multiplication function with a line broadening of 2 Hz and zero-filled to a final spectral resolution of 0.42 Hz per point. Sample spinning was not found to significantly improve the resonances line shape, so all spectra were measured without it. A

J-modulated spin-echo experiment was also measured to determine the number of ^{1}H coupled to ^{13}C in order to support the assignments of peaks.

Rheological Experiments.

The resins were stabilized with 0.5 wt.% Irganox 1010 and 0.5.wt % Irgafos 168 from the Ciba company. Disks of 25 mm diameter and 2 mm height were pressed. The rheological experiments were conducted under nitrogen atmosphere with a Bohlin Gemini C-VOR rheometer. Dynamic-mechanical data were recorded for at least four different temperatures in the range from 130 to 210 °C at angular frequencies ω between 0.01 and 300 s^{-1}. Whenever the terminal regime at 150 °C was not reached, creep experiments were carried out to determine the zeroshear viscosity. Details about creep experiments can be found in the literature.[40] A new sample was inserted in the rheometer whenever the temperature was changed in order to minimize gap errors. Thermal stability as well as reproducibility were ensured.

5.3.5 Materials

A broad range of different commercial and experimental PE grades was chosen which allow the systematical characterization of the relationship between comonomer content, type and distribution. As these samples result, on the one hand, from commercial manufacturers and, on the other hand, from a project subjected to a nondisclosure agreement (samples mLLDPE L4-5 and L6-3), no information about the polymerization conditions can be given. Nevertheless, at least the catalyst is known. Particular attention was paid toward the possible presence of a small amount of long-chain branches. Thus, a blend of 95 vol % mLLDPE L6-1 and 5 vol % LDPE 2 (LL/L 95/5) was investigated to get an insight into the effect of a small amount of long-chain branched material (cf. Table 5.3) (Preparation: Kneader, 60 rpm, 160 °C, 10 min). Tables 4.3-4.6 summarize the results of the molecular

characterization. The comonomer content nc is an average of the different NMR measurements carried out. Table 5.3 contains the samples the properties of which are known. Therefore, they are used as "reference materials". For example, mHDPE 1 and mHDPE 2 were intensively investigated in terms of an IUPAC round robin test and are known as linear homopolymers. (mHDPE 1 was not investigated rheologically in this work; its zero-shear viscosity at 150 °C shown in the following was taken from Stadler et al.[41]). mLLDPE L6-1 and LDPE 2 were extensively studied before and results on the blend L/LL 95/5 were already partly discussed.[5,34] In Table 4.4, the samples with butene as the comonomer are listed. Its content ranges from 0.7 mol % to 7.6 mol %. Hexene and octene comonomers cover a smaller range but the factor of about three in their concentrations will be large enough for differentiation (cf. Table 5.5 and Table 5.6). The nomenclature of the samples is chosen in the way that "L" stands for the linear structure anticipated, the first number for the carbon atoms of the comonomer and the second one denominates the sample within one category.

Table 5.3 : Molecular Characteristics of the "Reference Materials" and the Blend LL/L 95/5

sample	M_w [kg/mol]	M_w/M_n
mHDPE 1	205	2.6
mHDPE 2	45	2.7
LDPE 2	230	13.7
mLLDPE L6−1	113	3.2
blend from mLLDPE L6−1 and LDPE 2: LL/L 95/5	112	3.0

Table 5.4 : Molecular Characteristics of the Poly(ethylene-butene) Copolymers

sample	catalyst	comonomer	n_c [mol %]	M_w [kg/mol]	M_w/M_n
L4−1	ZN	butene	0.7	85	3.7
L4−2	ZN	butene	2.7	148	4.2
L4−3	ZN	butene	2.8	88	3.6
L4−4	ZN	butene	3.7	128	4.2
L4−5	m	butene	5.4	108	2.0
L4−6	m	butene	5.7	112	2.5
L4−7	ZN	butene	7.6	85	3.7

Table 5.5 : Molecular Characteristics of the Poly(ethylene-hexene) Copolymers

sample	catalyst	comonomer	n_c [mol %]	M_w [kg/mol]	M_w/M_n
L6−1	m	hexene	1.2	113	3.2
L6−2	m	hexene	2.6	124	2.9
L6−3	m	hexene	2.6	83	2.5
L6−4	m	hexene	3.0	116	2.5

Table 5.6 : Molecular characteristics of the poly(ethylene-octene) Copolymers

sample	catalyst	comonomer	n_c [mol %]	M_w [kg/mol]	M_w/M_n
L8−1	ZN	octene	1.1	129	4.5
L8−2	ZN	octene	1.6	135	4.6
L8−3	ZN	octene	3.8	96	4.9

5.3.6 Results

Analytical Characterization.

The branching architecture of the samples was analytically investigated by means of the well-established relationships between the radius of gyration $\langle r_g^2 \rangle^{0.5}$ and the molar mass M_{LS}.[41,42] It should be mentioned that the lower resolution limit of the experimental setup used lies at a radius of gyration of around 20 nm. First, the question whether the samples contain small amounts of LCB is addressed by means of SEC coupled with MALLS. Parts a and b

of Figure 5.18 compare $\langle r_g^2 \rangle^{0.5}$ and the differential molar-mass distribution dW/d(log M), respectively, as a function of M_{LS} for mHDPE 1, mHDPE 2, mLLDPE L6-1, LDPE 2 and the blend LL/L 95/5.

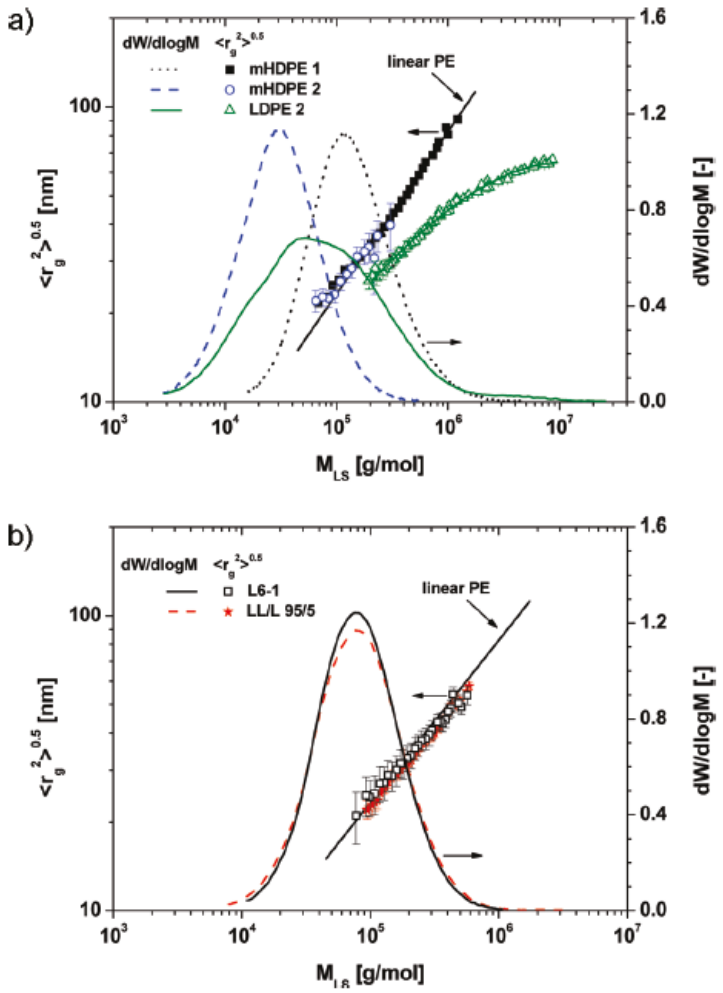

Figure 5.18 : $\langle r_g^2 \rangle^{0.5}(M_{LS})$ and dW/d(log$M$) as a function of M_{LS} of (a) the comopolymers and (b) mLLDPE L6-1 and the blend LL/L 95/5.

The power-law relationship between $\langle r_g^2 \rangle^{0.5}$ and M_{LS} of linear PE is valid for mHDPE 1 and mHDPE 2. The linear fit of the double-logarithmically plotted $\langle r_g^2 \rangle^{0.5}$ (M_{LS}) values of mHDPE 1 serves as a

reference for linear molecules in the following. While mLLDPE L6-1 fulfils this relationship, LDPE 2 deviates from the straight line. This is due to the LCB causing a coil contraction of the molecules.[34] The long chain branched fraction of the blend LL/L 95/5 is not reflected by this plot as $\langle r_g^2 \rangle^{0.5}$ follows the $\langle r_g^2 \rangle^{0.5}$ (M_{LS}) relationship of the linear PE within the measurement uncertainty. The dW/d(log M) curves of the linear samples are typical of the narrow molar mass distribution characteristics for metallocene-catalyzed PE. In comparison, a broad distribution is observed in case of the LDPE polymerized by a free radical process. The molar mass distributions dW/d(log M) of the neat LLDPE and the blend LL/L 95/5 are quite similar. Therefore, the molecular analysis with SEC and MALLS has to be regarded as not being capable to reveal low amounts of long-chain branched molecules within a linear matrix, if they are of the order given by the blend. $\langle r_g^2 \rangle^{0.5}$ as well as dW/d(log M) as a function of M_{LS} of the copolymers following the relationship for the linear PE are only partly presented. No hints to the presence of LCB are obtained for most of the samples of Table 5.4 to Table 5.6. There are some few exceptions, however, which will be discussed in the following. Figure 5.19a shows somewhat surprising results of the ZNLLDPE L4-2 and L4-4 in comparison to the linear reference (i.e., mHDPE 1). The two ZN-LLDPE samples deviate at high M_{LS} from the $\langle r_g^2 \rangle^{0.5}$ (M_{LS})-relationship of linear PE. dW/d(log M) as a function of M_{LS} of these samples exhibits a broad molar mass distribution with high molar mass components. (The results were affirmed by comparative measurements at two other laboratories.) From these results, it could be assumed that the ZNLLDPE L4-2 and L4-4 are linear PE with a small portion of LCB molecules at high M_{LS}, but for ZN-catalysts an incorporation of LCB is not known. On the other hand, a contraction of molecules resulting in lower $\langle r_g^2 \rangle^{0.5}$ than that of linear counterparts is known from the literature for linear samples with a high comonomer content.[43]

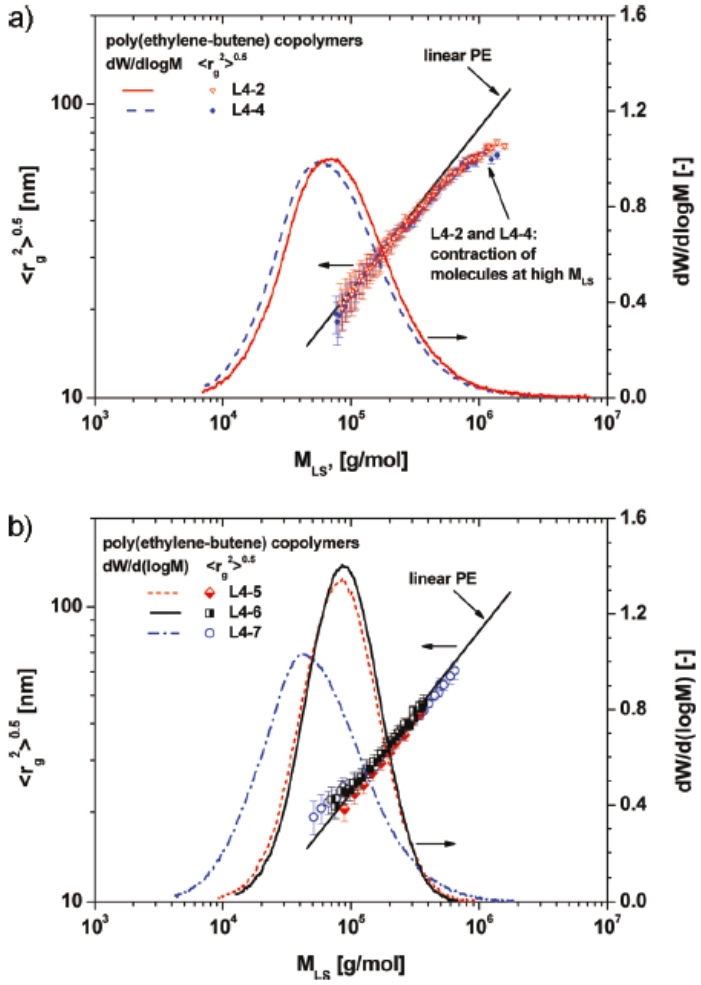

Figure 5.19 : (a) $\langle r_g^2 \rangle^{0.5}(M_{LS})$ and dW/d(log M) as a function of M_{LS} of poly(ethylene-butene) copolymers showing deviations from the linear structure (b) $\langle r_g^2 \rangle^{0.5}$ and dW/d(log M) as a function of M_{LS} of several poly(ethylene-butene) copolymers.

Sun et al.[43] investigated the influence of short-chain branches on $\langle r_g^2 \rangle^{0.5}(M_{LS})$ of structurally uniform α-olefin copolymers of ethylene with propene, butene, hexene and octene. Their results of $\langle r_g^2 \rangle^{0.5}(M_{LS})$ could be described by a power-law analogous to that of the linear PE homopolymers. However, the proportionality constant decreased systematically with

increasing comonomer length and content which can be interpreted as a contraction of $\langle r_g^2 \rangle^{0.5}$ over the whole range of M_{LS}. Such a trend was found beginning with 5 wt % comonomer in the copolymers, however, a significant deviation from the homopolymer serving as a reference was observed above a comonomer content of around 20-30 wt %. According to these findings, a very inhomogeneous comonomer distribution of the ZN-catalyzed products L4-2 and L4-4 with a low comonomer content at low M and a high comonomer content at high M could be the reason for the contraction of $\langle r_g^2 \rangle^{0.5}$ at high M_{LS}. However, ZN catalysts are known to preferentially insert comonomers in the regime of lower M, while molecules in the regime of higher molar masses are less side-chain branched. Furthermore, the average comonomer content of the samples investigated in the terms of this thesis is comparatively low and, thus, a pronounced deviation from the linear reference due to short chain branches is implausible. In addition, Figure 5.19b and Figure 5.20 show exemplarily several butene and hexene copolymers, which were found to be linear according to the results of SEC-MALLS. The linear samples shown here coincide with the linear reference, i.e. mHDPE 1, indicating the absence of LCB. The molar mass distributions of the ZN-catalyzed samples are in general broader than those of the m-catalyzed samples. $\langle r_g^2 \rangle^{0.5}(M_{LS})$ of the ZN-catalyzed poly(ethylene-octene) samples is shown in Figure 5.21. These samples coincide with the reference line of linear PE in good approximation. However, $\langle r_g^2 \rangle^{0.5}(M_{LS})$ of ZN-LLDPE L8-3 with the highest but still relatively low comonomer content of the octane samples shows a faint contraction of the molecules resulting in lower $\langle r_g^2 \rangle^{0.5}$ values over the whole M_{LS} range in comparison to the $\langle r_g^2 \rangle^{0.5}$ of mHDPE 1 or the copolymers with lower comonomer contents, respectively. The slope of a linear fit through its values is similar to that of the reference line of linear PE. Though, this small contraction is still in the order of the measurement uncertainty, this trend is in agreement with the results of Sun et

al.[43] on the influence of SCB on $\langle r_g^2 \rangle^{0.5}(M_{LS})$. These authors demonstrated a similar contraction of the molecules of several PE copolymers which increases with increasing side-chain frequency. The fact that the samples L4-6 and L4-7, which possess a comonomer content even higher than that of L8-3, coincide with the reference line of linear PE can also be understood by the results of Sun et al.[43] as the coil dimensions correlate with the comonomer type. The influence of an incorporated butane comonomer on the coil size is weaker than that of an octane comonomer.

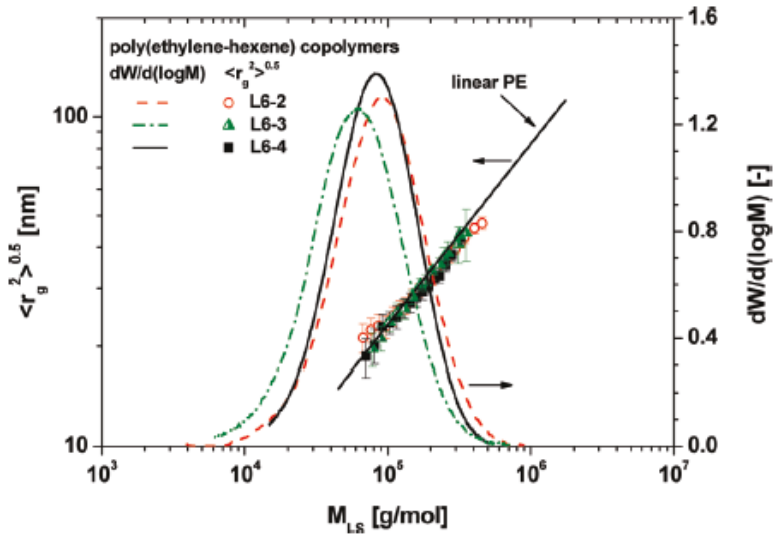

Figure 5.20 : $\langle r_g^2 \rangle^{0.5}(M_{LS})$ and dW/d(log M) as a function of M_{LS} of the poly(ethylene-hexene) copolymers.

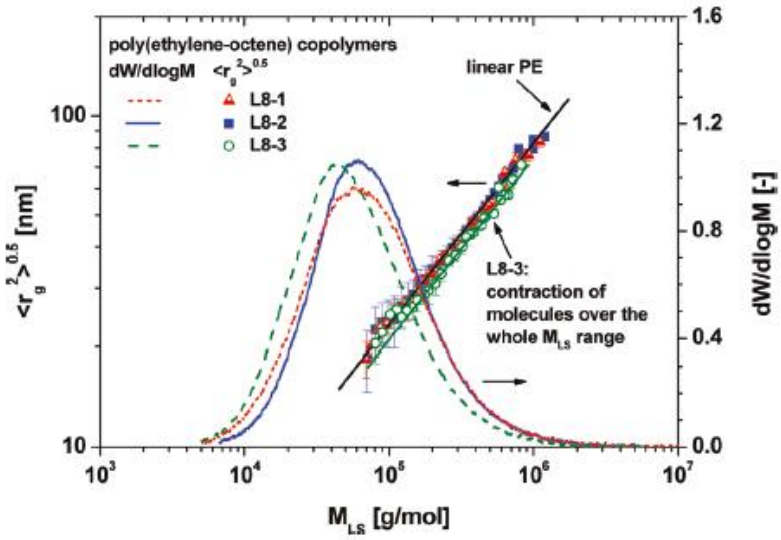

Figure 5.21 : $\langle r_g^2 \rangle^{0.5}(M_{LS})$ and dW/d(log M) as a function of M_{LS} of the poly(ethylene-octene) copolymers.

Rheological Characterization.

The double-logarithmic plot of the zero-shear viscosity η_0 as a function of the absolute weight-average molar mass M_w allows a qualitative discrimination of the branching architecture. $\eta_0(M_w)$ of the samples investigated is depicted in Figure 5.22. The zero-shear viscosities are averages from several reproducible measurements. η_0 was determined from dynamic-mechanical experiments, whenever the terminal regime was reached. Otherwise, the values given result from creep experiments which are appropriate to cover longer times.

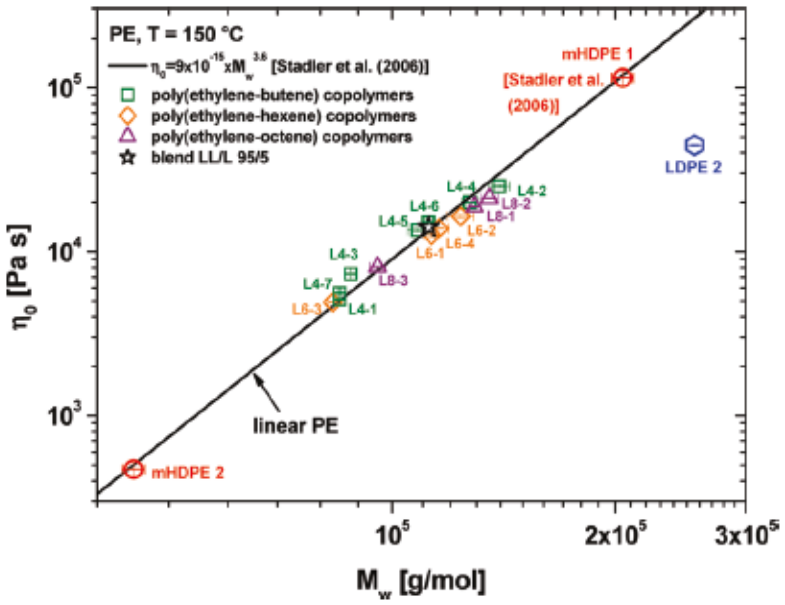

Figure 5.22 : $\eta_0(M_w)$ of the polyethylenes investigated.

The zero-shear viscosities of HDPE were found to be proportional to $M_w^{3.6}$.[41] This relationship is valid for mHDPE 1 and mHDPE 2, too. LDPE 2 significantly deviates from the reference line of linear materials indicating statistically (or treelike) branched molecules.[34,44] (Values higher than those of the reference line are attributed toward star-like branched molecules in the literature[44]). The $\eta_0(M_w)$ relationship holds for PE copolymers in good approximation too, as frequently shown in the literature.[28,44] All the linear samples investigated in this paper fulfill the well-established power-law dependence within the accuracy of the analytical and rheological measurements. In order to probe the influence of few LCB on the $\eta_0(M_w)$-relationship the results of the blend LL/L 95/5 are depicted too. The viscosities of the blend LL/L 95/5 and the matrix mLLDPE L6-1 differ only by about 10%. Within the experimental accuracy, the $\eta_0(M_w)$-relationship cannot reveal a small amount of LCB in LLDPE. As a consequence, $\eta_0(M_w)$

is not accurate enough to answer the question whether ZN-LLDPE L4-2 and L4-4 contain any LCB as indicated by $\langle r_g^2 \rangle^{0.5}(M_{LS})$ (cf. Figure 5.19a).

Thermorheological Behavior.

The detection of LCB by means of the analytical and rheological characterization is limited due to the low sensitivity toward LCB of the methods applied. However, it is known from the literature that thermorheology is very sensitive with respect to LCB. Therefore, it can be expected that further information on the samples may be gained from the thermorheological behavior. In case of thermorheologically simple polymers, all relaxation times τ involved exhibit the same temperature dependence :

$$\tau(T) = a_T(T, T_0) \cdot \tau(T_0) \tag{5.9}$$

with T being the actual and T_0 the reference temperature. The shift factor a_T is a function of the temperature allowing the construction of master curves from rheological properties. For temperatures significantly higher than T_g an Arrhenius equation of the type :

$$a_T = \exp\left[\frac{E_a}{R}\left(\frac{1}{T} - \frac{1}{T_0}\right)\right] \tag{5.10}$$

is valid (R is the universal gas constant, T the absolute temperature of the measurement, T_0 the reference temperature, and E_a the activation energy). In general, the shift factors of PE are known to follow such an Arrhenius dependence. Equation 5.9 does not hold for thermorheologically complex materials as in such a case not all the relaxation times do shift with the same temperature-dependent factor. For many materials such a behavior can be described by a stress-dependent activation energy, for example. This

quantity can be used for a qualitative discussion of the thermorheological complexity.

Qualitative Classification: δ(|G*|) Plots.

For a coarse classification of the materials with respect to their thermorheological behavior, the phase angle δ as a function of the magnitude of the complex modulus |G*| at different temperatures is used.[45] Such a plot is exemplarily shown in Figure 5.23 for the "reference materials" mHDPE 2, LDPE 2, and mLLDPE L6-1 and the blend LL/L 95/5. In some cases, the curves were shifted along the |G*|-axis by the factors indicated, for the matter of a better distinction. The curves of mHDPE 2 and mLLDPE L6-1, measured at different temperatures, superimpose indicating thermorheological simplicity.

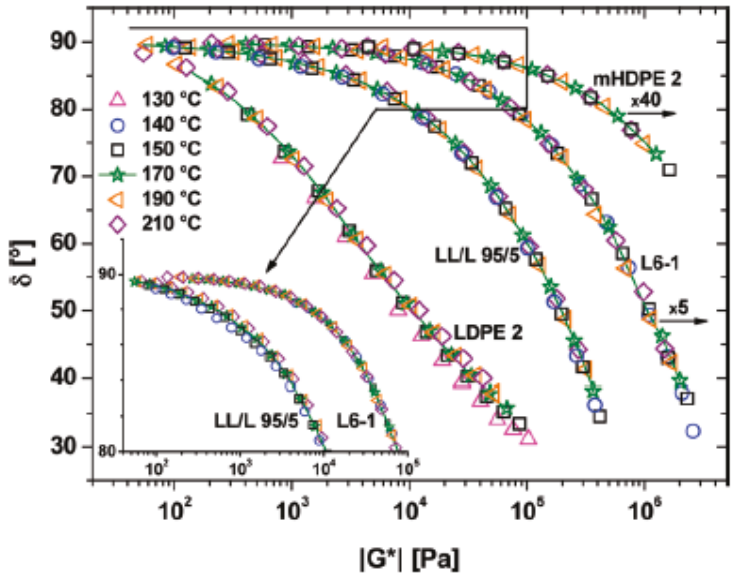

Figure 5.23 : δ(|G*|,T) of the homopolymermHDPE2, the blendLL/L 95/5 and its components.

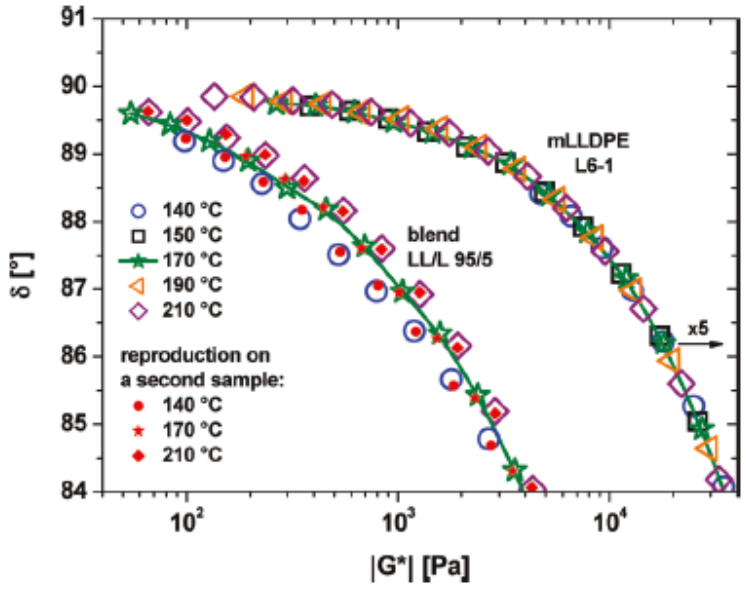

Figure 5.24 : Demonstration of the reproducibility of dynamic-mechanical data to judge the significance of a slight thermorheological complexity by means of δ(|G*|,T).

In contrast to them, LDPE 2 splits systematically with temperature typical of a pronounced thermorheological complexity. This kind of thermorheological complexity was extensively discussed in a previous paper.[34] The influence of very few long-chain branched molecules on the thermorheological behavior of a linear PE can be seen from the blend LL/L 95/5. The curves of the blend coincide with each other at lower δ or shorter relaxation times, respectively, while a slight but systematic split with temperature can be observed at high δ (cf. inset of Figure 5.23). This feature can be attributed to longer relaxation times at which the molecules carrying LCB come into play. Such a kind of thermorheological complexity—though more pronounced— was observed in the case of an LCB-mLLDPE before.[5] From this result one can conclude that δ(|G*|,T) reflects the low amount of LCB, which could neither be detected by SEC coupled with MALLS nor by $\eta_0(M_w)$. In order to judge the significance of δ(|G*|,T) toward the evaluation of a slight thermorheological

complexity like that of the blend LL/L 95/5, however, the uncertainty of the dynamic-mechanical measurements performed has to be known. Figure 5.23 shows a section of δ(|G*|,T) for mLLDPE L6-1 and the blend LL/L 95/5 at high phase angles. For the blend LL/L 95/5, the curves at three different temperatures are exemplarily plotted with the reproduction measurements performed on a second sample as indicated by the full symbols which come to lie within the open ones (cf. Figure 5.24). The measurement uncertainty was found to be typically around ±1%. Consequently, the thermorheological complexity of the blend LL/L 95/5 at high δ is reproducible and significant, though the split-up is quite small. Furthermore, the curves of the mLLDPE L6-1 at high δ superimpose in good agreement such that the comparison between the two materials plotted clearly indicates thermorheological simplicity for the mLLDPE L6-1 and thermorheological complexity for the blend LL/L 95/5. δ(|G*|,T) of almost all the samples superimpose as well as the curves of the mLLDPE L6-1. Therefore, they are not plotted here. Thermorheological simplicity can be stated with exception of mLLDPE L4-6 and mLLDPE L6-4. Even the ZN-LLDPE samples L4-2 and L4-4 appear thermorheologically simple, although, the SEC-MALLS results indicated the presence of LCB at high molar masses (cf. Figure 5.19a). Two explanations could be given for this finding. As the branching is mainly restricted to comparatively high molar mass components (cf. Figure 5.20a), the lowest applied angular frequency of about 0.01 s^{-1} may still be too high to probe the internal long relaxation times connected with the long-chain branched molecules. The dynamic-mechanical experiments, especially, for these two samples demonstrate that the terminal regime is not completely reached. The second explanation is related to the assumption that the decrease of the radius of gyration may originate from an extremely inhomogeneous distribution of short-chain branches. As E_a of linear PE molecules with different amounts of SCB are not much different, however, the resulting thermorheological complexity will be so small (see Literature Survey) that

the time-temperature superposition principle will be found valid in good approximation. The poly(ethylene-butene) mLLDPE L4-6 as well as the poly(ethylene-hexene) copolymer mLLDPE L6-4 turned out to show a small but reproducible thermorheological complexity : a systematic split at high δ occurred (cf. Figure 5.25 and Figure 5.26). For comparison the results of L4-5 containing almost the same butene content as L4-6 and L6-3 are shown in detail, too. These materials exhibit thermorheological simplicity, however.

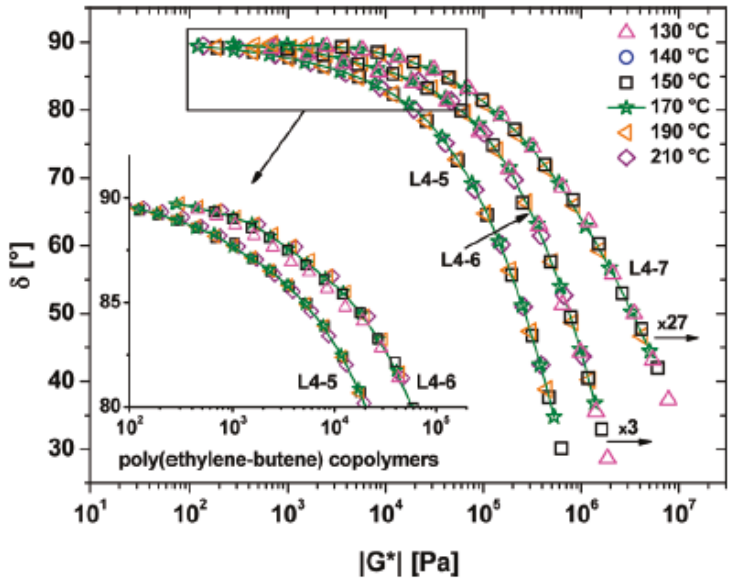

Figure 5.25 : δ(|G*|,T) of several poly(ethylene-butene) copolymers.

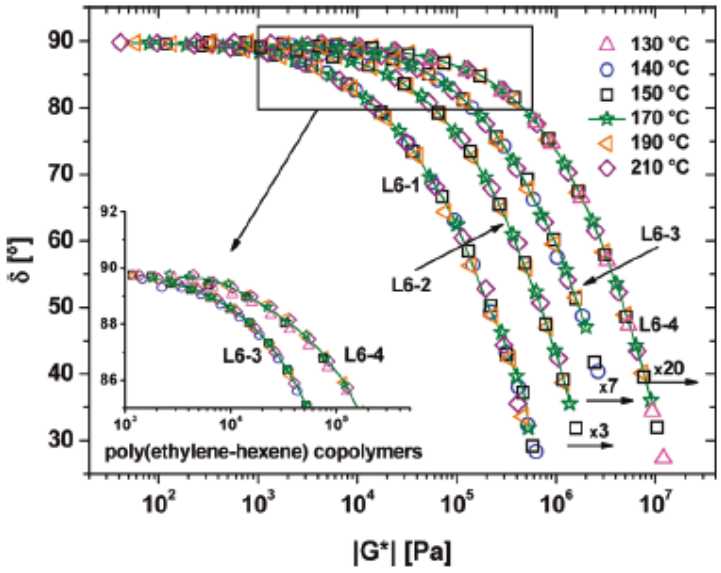

Figure 5.26 : δ(|G*|,T) of the poly(ethylene-hexene) copolymers.

From these results, it can be assumed that L4-6 and L6-4 contain a small amount of LCB analogous to the blend investigated (cf. Figure 5.23). As shown for the blend, this small fraction cannot be detected with the common molecular analyses (cf. Figure 5.18b). Thermorheology seems to be sensitive enough to reveal such fine details of the molecular structure. It should be mentioned that L4-6 and L6-4 are commercial grades originating even from the same polymerization process. These conclusions are supported by the results of Resch,[46] who found a decrease of the linear steady-state compliance with increasing temperature in case of these two samples pointing toward a thermorheological complexity, too. In summary, it could be shown that linear PE is thermorheologically simple even if an inhomogeneous comonomer distribution due to the insertion by ZN-catalysts is probable. Moreover, a comonomer content up to 7.6 mol % does not result in thermorheological complexity.

Quantitative Evaluation : E_a in Dependence on the Molecular Structure.

In order to determine reliable and comparable activation energies the evaluation method chosen is crucial. Besides a shift along the time or frequency axis, a weak modulus shift $b_{T,\text{Rouse}} = \rho_0 T_0/\rho T$ considering the change of the density ρ and temperature according to the Rouse theory comes into play.[47,48]

In general, the modulus shift b_T is given as:

$$G(\omega, T_0) = b_T G(a_T \omega, T) \tag{5.11}$$

From δ(|G*|,T), it is evident that the curves of purely linear PE measured at different temperatures superimpose within the accuracy of the experiments. This finding does not exclude the existence of the well-known density correction, however, as it is too small to be seen in this type of plot and, therefore, can be neglected. Furthermore, the moduli of LDPE vertically shift distinctly more strongly than LLDPE as demonstrated in a previous paper.[34] As a consequence, E_a of LDPE becomes a function of the quantity chosen for its determination, if the vertical shift factor is neglected. To overcome these difficulties, b_T can generally be excluded by evaluating the temperature dependence using tan δ(ω,T) or δ(ω,T), respectively:

$$\begin{aligned} \tan\delta(\omega, T_0) &= \frac{G''(\omega, T_0)}{G'(\omega, T_0)} = \frac{b_T \cdot G''(a_T\omega, T)}{b_T \cdot G'(a_T\omega, T)} \\ &= \tan\delta(a_T\omega, T) \end{aligned} \tag{5.12}$$

G’ is the storage modulus and G’’ the loss modulus. E_a can be determined from the phase angle measured as a function of ω at different temperatures (cf. Figure 5.27a). If ω at distinct δ are plotted semi logarithmically versus the reciprocal absolute temperature 1/T, straight lines are obtained as indicated in Figure 5.27b.

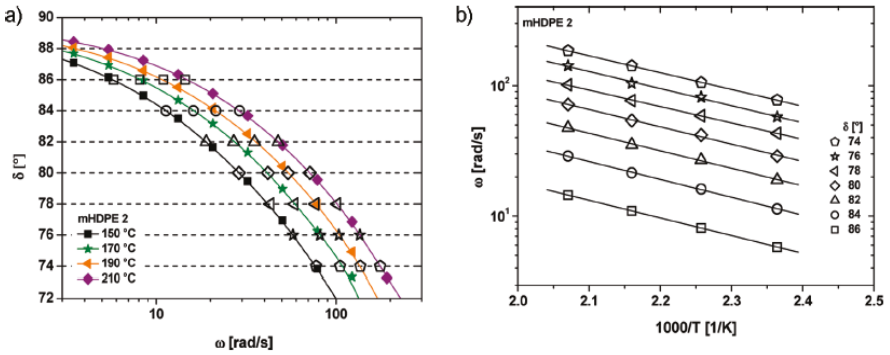

Figure 5.27 : (a) δ(ω,T) of mHDPE 2. (b) Arrhenius diagrams of mHPDE 2 at different constant δ.

Then, E_a can be calculated from the slopes of linear fits according to:

$$\omega(T) = \omega(T_0)\exp\left(-\frac{E_a}{RT}\right) \qquad (5.13)$$

Figure 5.28 shows $E_a(\delta)$ of several samples.

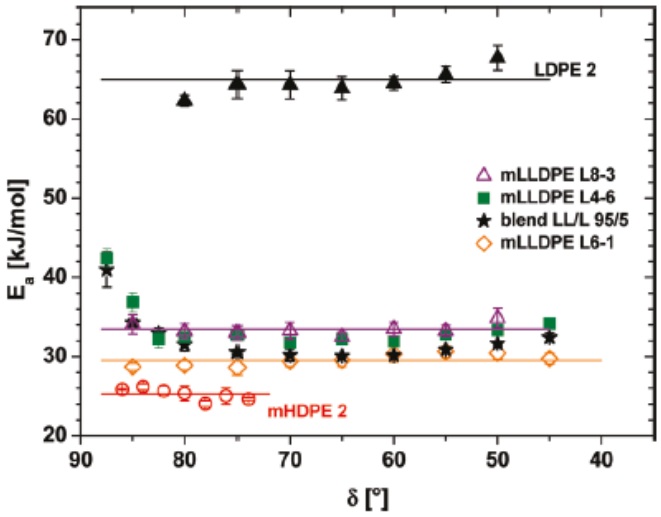

Figure 5.28 : Activation energy as a function of the phase angle.

Within the accuracy of the measurements constant E_a values are found for mHDPE 2, mLLDPE L6-1 and LDPE 2, respectively. On the other side, E_a of the thermorheologically complex blend LL/L 95/5 deviates from that of the neat mLLDPE L6-1. Especially at high δ values, which correspond to long relaxation times, an increase of E_a appears, which can be attributed to the presence of LCB. This increase is found in a δ range which agrees with that of the split of the δ(|G*|,T)-curves shown in Figure 5.23. Similar results were found for mLLDPE L4-6. The thermorheological complexity of this sample found from δ(|G*|,T) (cf. Figure 5.25) is reflected by the increase of E_a at high δ. Taking the results on mLLDPE L4-6 into account, it can be concluded that this material contains a small amount of LCB in addition to the linear molecules. The rheological functions of such a "blend" exhibit a temperature-dependent change of their shape as previously discussed and seen from LL/L 95/5.[5] Therewith, this kind of thermorheological complexity differs from that found for statistically branched LDPE, as the latter possesses an average E_a, which is valid for all of its molecules and such for all of its relaxation times if evaluated from δ(ω,T). δ(|G*|,T) of mLLDPE

L6-4, shown in Figure 5.26, shows a small split-up at δ close to 90°. But for this material, an E_a dependent on δ could not be found. This very slight thermorheological complexity at angles close to 90° is not reflected in $E_a(\delta)$. It is quite likely, however, that mLLDPE L6-4 also contains a few LCB, as it originates from the same manufacturer and production route as mLLDPE L4-6. Therefore, the following discussion on the influence of the type and content of comonomers on the activation energies does not comprise results from these two grades as any LCB would disturb the analysis. In order to find correlations between E_a and the molecular structure of the copolymers, the $E_a(\delta)$ values of the thermorheologically simple PE are plotted as a function of the comonomer content in Figure 5.29.

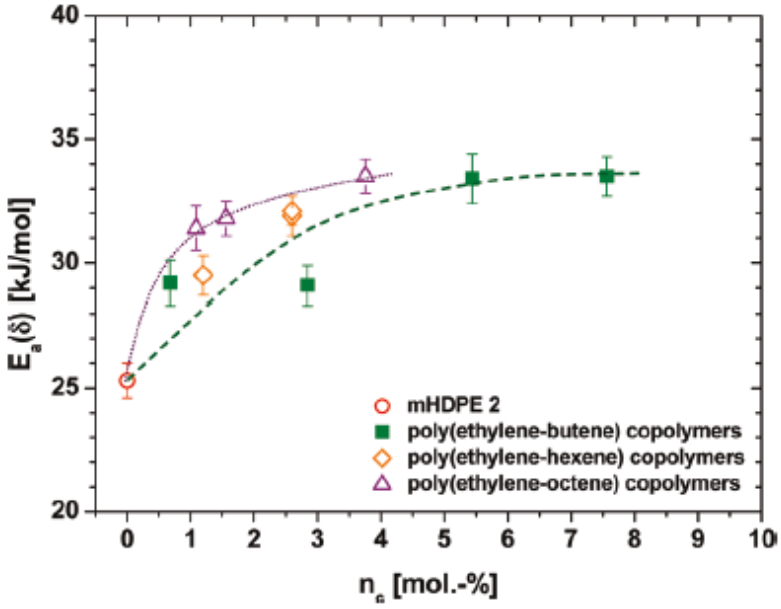

Figure 5.29 : Activation energy of different linear PE as a function of the comonomer content (lines are drawn to guide the eye).

The homopolymer mHDPE 2 exhibits the lowest E_a of around 25 kJ/mol. (For comparison, Stadler et al.[3] found 27 kJ/mol for mHDPE 1 and mHDPE 2 evaluated from G'(ω,T)). The insertion of butene comonomers up to

4 mol% results in an increase of E_a up to 29 kJ/mol. Increasing the butene content even more leads to E_a values up to 33.5 kJ/mol (for L4-5 and L4-7). From the results it seems to be probable that E_a reaches a plateau at high comonomer contents as reported by Wood-Adams and Costeux.[25] Additionally, E_a of the poly(ethylene-hexene) and poly(ethylene-octene) copolymers are presented. Again, an increase of E_a with increasing comonomer content is observable. However, E_a of the samples with hexene as comonomer is higher than E_a of the poly(ethylene-butene) copolymers at the same comonomer content. A similar tendency is found with the poly(ethylene-octene) copolymers. E_a of these products exceeds that of the poly(ethylene-butene) and poly(ethylene-hexene) copolymers at the same comonomer content, hence, E_a increases with the length of the side branches.

5.3.7 Discussion

Comparison of the Characterization Methods Applied.

The common analytical characterization by means of the relationships between $\langle r_g^2 \rangle$ and M_{LS} and the rheological one using η_0 and M_w, respectively, are not sensitive enough to detect some few long-chain branched molecules in linear PE as demonstrated by the blend LL/L 95/5. The significance of $\langle r_g^2 \rangle(M_{LS})$ for the blend LL/L 95/5 is limited according to several points of view. First of all, the lower detection limit of the SEC-MALLS setup used is 20 nm. Furthermore, the radii of gyration of the LDPE 2 have been truncated at molar masses below 200 kg/mol as indications of a disturbance of the separation of the SEC became visible (cf. Figure 5.18, parts a and b).[34] The highest molar masses of the neat mLLDPEL6-1, however, range up to around 600 kg/mol, those of the LDPE 2 reach values up to 10000 kg/mol. Therefore, in the blend above 600 kg/mol the molecules of the LDPE 2 should appear. However, $\langle r_g^2 \rangle(M_{LS})$ of the blend agrees with that of the neat mLLDPE L6-1 over the whole M_{LS} range and, moreover, $dW/d(\log M)$ as a

function of M_{LS} of the mLLDPE L6-1 remains unchanged by the addition of 5 vol% LDPE 2. That means, the amount of the LCB molecules is too low to be reflected by the SEC-MALLS setup. However, a contraction of $\langle r_g^2 \rangle$ at high M_{LS} pointing toward LCB was detected for the ZN-LLDPE samples L4-2 and L4-4. From this result it has to be concluded that these samples surprisingly possess long-chain branched molecules of a high molar mass. The relationship between η_0 and M_w, however, does not reflect any LCB in the LLDPE samples investigated. Even the blend LL/L 95/5 and the ZN-LLDPE, which contain LCB according to $\langle r_g^2 \rangle(M_{LS})$, appear as purely linear. This result demonstrates that $\eta_0(M_w)$ is not sensitive enough to reveal the small amounts of LCB in the samples. The high sensitivity of the thermorheological behavior toward a few LCB in linear PE, however, could be demonstrated. $\delta(|G^*|,T)$ of the blend LL/L 95/5 indicates a thermorheological complexity, as the curves at angles close to 90 ° systematically split. Furthermore, thermorheological complexity was also observed for the mLLDPE samples L4-6 and L6-4 which were classified as purely linear according to $\langle r_g^2 \rangle(M_{LS})$ and $\eta_0(M_w)$. $E_a(\delta)$ of thermorheologically complex samples is not constant, but increases at angles close to 90 °, which correspond to long relaxation times related to long-chain branches. Moreover, a thermorheological complexity of these two samples is also observed by means of the temperature dependence of the linear steady-state compliance determined by creep-recovery experiments.[46] In conclusion, the relaxation times of the long-chain branched molecules in the samples mLLDPE L4-6 and L6-4 are covered by dynamic-mechanical as well as creep-recovery experiments, respectively. However, in contrast to the results of the analytical investigations, no hints toward the LCB in the ZN-LLDPE samples L4-2 and L4-4 detected by SEC-MALLS could be gained from $\delta(|G^*|,T)$. An explanation for this finding is the limited frequency or time range covered by dynamic-mechanical experiments typically performed down to $\omega = 10^{-2}$ s^{-1}. At this frequency, the terminal regime is reached for

purely linear samples of moderate M, while it may be far away for ZN-LLDPE L4-2 and L4-4, as it is well-known that long chain branched molecules of high molar masses possess long relaxation times. Therefore, the relaxation times corresponding to the long-chain branched high molar mass tails of these two ZN-LLDPE are not fully covered by the dynamic-mechanical experiments performed. In order to check this assumption, creep and creep-recovery experiments were carried out with the ZN-LLDPE sample L4-2 at 150 and 190 °C. The linear steady-state compliance J_e^0 was determined at long recovery times around 4000 s for 150 °C and 1500 s at 190 °C. These recovery times correspond to angular frequencies of 2.5×10^{-4} s^{-1} and 6.7×10^{-4} s^{-1}, respectively. Details about such experiments can be found in prior publications.[5,34] A distinct temperature dependence of J_e^0 was found, which is comparable to that of the thermorheologically complex mLLDPE samples L4-6 and L6-4.[43] J_e^0 of the ZN-LLDPE L4-2 decreases from $(12.2 \pm 0.4) \times 10^{-4}$ Pa^{-1} at 150 °C to $(8.6 \pm 0.3) \times 10^{-4}$ Pa^{-1} at 190 °C. This finding demonstrates that the ZN-LLDPE L4-2 is thermorheologically complex, too, and confirms the finding of long-chain branched molecules of high molar mass by SEC-MALLS (cf. Figure 5.19a).

Relationship between E_a and the Comonomer Length and Content.

The main finding of this paper, namely the relationship between the activation energy and the type and content of the comonomers investigated, will be discussed in the following. It can be assumed that the probability P of a local displacement of a molecular segment is given as the product of the probabilities P_v and P_a:

$$P = P_v \, . \, P_a \qquad (5.14)$$

Thereby, P_v describes the probability that a sufficient free volume is available for the molecular segment and P_a the probability to overcome the

potential barrier for the segmental motion. At temperatures near the glass transition temperature T_g, the influence of P_v dominates, i.e., the free volume available determines the probability of the displacement of molecular segments. In that case, the so-called WLF equation holds. The free volume increases with increasing temperature and, thus, the relevance of P_v decreases. At higher temperatures, enough free volume for molecular displacements is available and the limiting factor is P_a which is determined by the thermal activation of segmental motion. Thus, the Arrhenius equation 5.10 holds. The latter situation is valid for the PE samples investigated as all measurements were carried out far above T_g and the shift factors follow eq 5.10. Consequently, the thermal activation dominates the segmental motions. E_a is a measure of the potential barrier, which has to be overcome. It is obvious now that E_a increases, if the segments become bulkier. The comonomer type inserted and following from that the length of the side chain is decisive for the resistance of the segment with respect to its displacement. This model easily explains the enhancement of the activation energy from butene to octene as comonomer. Furthermore, it is not difficult to imagine that the hindrance of the segmental motion becomes the more pronounced the higher the concentration of the side groups is.

5.3.8 Conclusions

The results obtained demonstrate that thermorheological measurements are very sensitive and powerful to probe details of the molecular structure of PE. Comparing the established characterization methods $\langle r_g^2 \rangle(M_{LS})$ and $\eta_0(M_w)$, the following can be stated :

• The $\langle r_g^2 \rangle(M_{LS})$-relationship valid for linear PE is not sensitive enough to reveal small amounts of LCB in linear PE as demonstrated by means of the blend of 5 vol% LDPE added to a hexene copolymer (LL/L 95/5).

• The $\eta_0(M_w)$-relationship which has been shown to differentiate between linear and long-chain branched molecules does not detect small amounts of LCB as demonstrated by means of the blend LL/L 95/5. All the samples investigated appear linear, if solely classified according to $\eta_0(M_w)$, though a contraction of $\langle r_g^2 \rangle$ and thermorheological complexity were observed for several of them.

The qualitative classifications of the thermorheological behavior by $\delta(|G^*|,T)$ leads to the following conclusions :

• Thermorheologically simple and complex polymers can sensitively be discriminated by $\delta(|G^*|,T)$.

• The small amount of LCB in the blend LL/L 95/5 could successfully be revealed. Furthermore, the high sensitivity of $\delta(|G^*|,T)$ allowed to find a thermorheological complexity pointing toward the presence of LCB for two samples (L4-6 and L6-4) which seemed to be linear according to $\langle r_g^2 \rangle(M_{LS})$ and $\eta_0(M_w)$.

• The sensitivity of $\delta(|G^*|,T)$ with respect to thermorheological complexity can only be exploited, if the frequency range applied matches the internal time scale of the molecules responsible for a thermorheological complex behavior. This fact explains the result that a thermorheologically simple behavior was found for two samples (L4-2 and L4-4), which contain long-chain branched molecules of high molar mass according to SEC-MALLS.

The following conclusions can be drawn from the quantitative evaluation of the thermorheological behavior using the activation energy E_a in dependence on the phase angle δ :

• Differences in the thermorheological behavior between m-catalyzed (more homogeneous comonomer distribution) and ZN-catalyzed (less homogeneous comonomer distribution) copolymers were not observed.

• $E_a(\delta)$ determined from $\delta(\omega,T)$ was found to be constant for most of the linear PE investigated and the LDPE. $E_a(\delta)$ of linear samples containing a few long chain branched molecules increases at high phase angle, if the longest relaxation times are covered within the frequency range measured.
• $E_a(\delta)$ of linear PE increases with growing comonomer length and content. A maximal E_a of 33.5 kJ/mol is reached at the highest comonomer content investigated, i.e., 7.6 mol % butene.
• $E_a(\delta)$ representing the potential barrier for the flow of a polymer melt can be correlated with the mobility of the molecular segment, which has to be displaced. It is obvious that the mobility depends on the bulkiness of the molecular segment, and thus E_a increases with growing comonomer length and content. The results demonstrate that E_a can be used as a direct probe of the molecular structure of short-chain branched polymers.

5.3.9 Summary

The molecular structure of a broad range of likely linear PE samples, a blend of LLDPE and LDPE as well as a LDPE are investigated by means of well-established analytical and rheological relationships. The results from these methods are compared with the conclusions drawn from investigations of the thermorheological behavior. Thermorheology is found to be a very sensitive probe of the molecular structure. It is shown that the evaluation of $\delta(|G^*|,T)$ as well as $E_a(\delta)$ detects even few LCB in a linear PE if the frequency range of the dynamic-mechanical experiment matches the molecular time scale. Furthermore, $E_a(\delta)$ correlates with the comonomer type and content of linear PE. It becomes the larger the longer the comonomer and the higher its concentration. As such, thermorheology offers an interesting method to get an insight into molecular structures, particularly, those connected with the branching architecture. Investigations of this kind are comparatively simple and fast as only well established dynamic

mechanical experiments at different temperatures are needed. The results of this paper convincingly demonstrate, however, that the application of different methods and the careful assessment of their findings are necessary to obtain a reliable characterization of the molecular structure of branched polyethylenes.

5.3.10 Acknowledgment

The authors express their gratitude to Prof. J. Marchand-Brynaert and Prof. C. Bailly (Université catholique de Louvain, Département de Chimie) for their support of the NMR analysis. M. Sc. H. Müller (University Erlangen-Nürnberg) is thanked for the preparation and the measurements of the blend, Mrs. I. Herzer for performing the molecular characterization with great care, and Dr. D. Ferri (Polymeri Europa) for providing several samples as well as for the support with comparative NMR measurements.

5.3.11 References and Notes

[1] Aguilar, M.; Vega, J. F.; Sanz, E.; Martinez-Salazar, J. Polymer 2001, 42, 9713–9721.

[2] Starck, P.; Malmberg, A.; Löfgren, B. J. Appl. Polym. Sci. 2002, 83, 1140–1156.

[3] Stadler, F. J.; Gabriel, C.; Münstedt, H. Macromol. Chem. Phys. 2007, 208, 2449–2454.

[4] Vega, J. F.; Martin, S.; Exposito, M. T.; Martinez-Salazar, J. J. Appl. Polym. Sci. 2008, 109, 1564–1569.

[5] Kessner, U.; Münstedt, H. Polymer 2010, 51, 507–513.

[6] Raju, V. R.; Smith, G. G.; Marin, G.; Knox, J. R.; Graessley, W. W. J. Appl. Polym. Sci. 1979, 17, 1183–1195.

[7] Laun, H. M. Prog. Colloid Polym. Sci. 1987, 75, 111–136.

[8] Wasserman, S. H.; Graessley, W. W. Polym. Eng. Sci. 1996, 36, 852–861.

[9] Mavridis, H.; Shroff, R. N. Polym. Eng. Sci. 1992, 32, 1778–1791.

[10] Eckstein, A.; Friedrich, C.; Lobbrecht, A.; Spitz, R. Acta Polym. 1997, 48, 41–46.

[11] Eckstein,A.; Suhm, J.; Friedrich, C.; Maier, R.-D.; Sassmannshausen, J.; Bochmann, M.; Mülhaupt, R. Macromolecules 1998, 31, 1335–1340.

[12] Ye, Z.; AlObaidi, F.; Zhu, S. Ind. Eng. Chem. Res. 2004, 43, 2860–2870.

[13] Auhl, D., Molekulare Struktur und rheologische Eigenschaften strahlenmodifizierter Polypropylene. Ph.D. Thesis, Friedrich-Alexander Universität Erlangen-Nürnberg: Nürnberg, Germany, 2006

[14] Rojo, E.; Fernandez, M.; Munoz, M. E.; Santamaria, A. Polymer 2006, 47, 7853–7858.

[15] Wang, J.-S.; Porter, R. S.; Knox, J. R. J. Polym. Sci., Part B: Polym. Lett. 1970, 8, 671–675.

[16] Hadinata, C.; Gabriel, C.; Ruellman, M.; Laun, H. M. J. Rheol. 2005, 49, 327–349.

[17] Mendelson, R. A. Polym. Eng. Sci. 1968, 8, 235–240.

[18] Kolodka, E.; Wang, W.-J.; Zhu, S.; Hamielec, A. E. Macromolecules 2002, 35, 10062–10070.

[19] Schlund, B.; Utracki, L. A. Polym. Eng. Sci. 1987, 27, 359–366.

[20] Kim, Y. S.; Chung, C. I.; Lai, S. Y.; Hyun, K. S. J. Appl. Polym. Sci. 1996, 59, 125–137.

[21] Malmberg, A.; Kokko, E.; Lehmus, P.; Löfgren, B.; Seppälä, J. V. Macromolecules 1998, 31, 8448–8454.

[22] Hussein, A. I.; Hameed, T.; Williams, M. C. J. Appl. Polym. Sci. 2006, 102, 1717–1728.

[23] Arnett, R. L.; Thomas, C. P. J. Phys. Chem. 1980, 84, 649–652.

[24] Vega, J. F.; Santamaria, A. Macromolecules 1998, 31, 3639–3647.

[25] Wood-Adams, P.; Costeux, S. Macromolecules 2001, 34, 6281–6290.

[26] Carella, J. M.; Graessley, W. W. Macromolecules 1984, 17, 2775–2786.

[27] Cassano, G. A.; Valles, E. M.; Quinzani, L. M. J. Rheol. 2000, 44, 47–63.

[28] Lohse, D. J.; Milner, S. T.; Fetters, L. J.; Xenidou, M. Macromolecules 2002, 35, 3066–3075.

[29] Zhang, M.; Lynch, D. T.; Wanke, S. E. Polymer 2001, 42, 3067–3075.

[30] Kong, J.; Fan, X.; Xie, Y.; Qiao, W. J. Appl. Polym. Sci. 2004, 94, 1710–1718.

[31] Biazek, M.; Czaja, K.; Sacher-Majewska, B. Thermochim. Acta 2005, 429, 149–154.

[32] Shroff, R. N.; Mavridis, H. Macromolecules 1999, 32, 8454–8464.

[33] Garcia-Franco, C. A.; Lohse, D. J.; Robertson, C. G.; Georjon, O. Eur. Polym. J. 2008, 44, 376–391.

[34] Kessner, U.; Kaschta, J.; Münstedt, H. J. Rheol. 2009, 53, 1001–1016.

[35] Randall, J. C. Polym. Rev. 1989, 29, 201–317.

[36] Liu, W.; Ray, D. G., III; Rinaldi, P. L. Macromolecules 1999, 32, 3817–3819.

[37] Liu, W.; Rinaldi, P. L.; McIntosh, L. H.; Quirk, R. P. Macromolecules 2001, 34, 4757–4767.

[38] Sahoo, S. K.; Zhang, T.; Reddy, D. V.; Rinaldi, P. L.; McIntosh, L. H.; Quirk, R. P. Macromolecules 2003, 36, 4017–4028.

[39] Klimke, K., Optimised polyolefin branch quantification by 13C NMR spectroscopy. Ph.D. Thesis, Johannes Gutenberg-Universität Mainz: Mainz, Germany, 2006.

[40] Gabriel, C.; Kaschta, J.;Münstedt, H. Rheol. Acta 1998, 37, 7–20.

[41] Stadler, F. J.; Piel, C.; Kaschta, J.; Rulhoff, S.; Kaminsky, W.; Münstedt, H. Rheol. Acta 2006, 45, 755–764.

[42] Beer, F.; Capaccio, G.; Rose, L. J. Appl. Polym. Sci. 1999, 73, 2807–2812.

[43] Sun, T.; Brant, P.; Chance, R. R.; Graessley, W. W. Macromolecules 2001, 34, 6812–6820.

[44] Gabriel, C.; Münstedt, H. Rheol. Acta 2002, 41, 232–244.

[45] van Gurp, M.; Palmen, J. Rheol. Bull. 1998, 67, 5–8.

[46] Resch, J. A., Elastic and viscous properties of polyolefin melts with different molecular structure investigated in shear and elongation. Ph.D. Thesis, Friedrich-Alexander Universität Erlangen-Nürnberg: Nürnberg, Germany, 2010.

[47] Rouse, P. E., Jr. J. Chem. Phys. 1953, 21, 1272–1280.

[48] Ferry, J. D. Viscoelastic properties of polymers, 3rd ed.; John Wiley & Sons: New York, 1980.

Chapter Six

Main Conclusions and Future Work

6.1 Main Conclusions

The experience and skills acquired previously by our team from the AMPP project in the field of controlled-crystallinity polypropylene obtained by reactive extrusion of isotactic polypropylene could be successfully applied to the grafting of maleic anhydride. Typical radical grafting of maleic anhydride onto polypropylene leads to low molecular weight grafted products. Grafting levels are usually very low (~1 wt.% or less) and located exclusively at chain extremities. Several graft structures co-exist and consist mainly in succinic rings, poly(maleic anhydride) and unsaturated rings (itaconic structures were suggested by other authors). Conversely, when processed in the presence of N-bromossuccinimide, highly-grafted polypropylene elastomers with preserved molecular weights were produced. The high grafting levels, up to 2.8 wt.%, enabled high-temperature NMR identification of the grafts without prior ^{13}C enrichment. The grafts structure consisted in a great majority of succinic anhydride rings distributed along the PP backbone. As expected the starting isotacticity and hence the resulting crystallinity of the products were greatly reduced, providing their elastomeric behavior.

Those original new materials were successfully used as an alternative source of ionic thermoplastic elastomers upon hydrolysis and neutralization of the anhydride functions. Several bases were investigated and the obtained ionomers were fully characterized.

The NBS mediated grafting of maleic anhydride was attempted onto high-density polyethylene to evaluate if crosslinking could be prevented. Although a lower amount of gel was observed upon Soxhlet extraction, the graft content could not be drastically improved. Also, FTIR analyses revealed that the graft structure was unaffected by bromine radicals,

indicating that the grafting mechanism in the presence of NBS is different on HDPE than on PP.

Several bromine-free mediators borrowed from controlled radical polymerization techniques were involved in melt-grafting of maleic anhydride onto iPP. None of them was efficient in both improving the graft content and preserving the molecular weights, sometimes contradicting the patent literature. Particular attention was paid to the grafting reaction mediated with nitroxides. Although nitroxides did not succeed in improving the grafting process, they gave additional clues regarding the assignment of the 1775 cm^{-1} absorption band in the FTIR spectra of PP-g-MA that still remained unclear at the time. The band at 1775 cm^{-1} is associated with the band at 1840 cm^{-1} and are due to grafted maleic entities. This also explains why a residual absorption band remains at 720 cm^{-1} (C-H out of plane deformation of maleic anhydride) even on washed PP-g-MA (i.e. rid of ungrafted maleic anhydride).

The synthesis of the model compound of polypropylene, namely 2,4,6,8,10-pentamethylundecane, that was established during the AM-PP project could be rather easily adapted to a larger scale. However, the preparative-scale separation of the diastereoisomers of PMU turned out to be really tricky. Although the analytical scale separation of the intermediate 6-p-toluenesulfonyloxymethyl-2,4,8,10-tetramehtylundecane was successfully achieved, a very poor resolution was observed at preparative scale. Our efforts were therefore devoted to the separation of the intermediate 6-hydroxymethyl-2-4-8-10-tetramethylundecane with a detection method based on the Corona CAD® technology, specially adapted for molecules devoid of chromophore. Once again the analytical-scale separation of the diastereoisomers was successful but scaling up the separation appeared delicate. Pure fractions of each diastereoisomers could be recovered and

converted into PMU. Although several hundred milligrams of the syndiotactic and atactic models could be recovered, only a few milligrams of the isotactic model could be obtained.

A sample of each pure diastereoisomer was given to the *Unité de Chimie Physique Théorique et Structurale* from the *Facultés Universitaires Notre-Dame de la Paix* to try and correlate the experimental and theoretically-simulated Raman spectra of those polypropylene models. Interestingly, a good agreement between experimental and simulated spectra was observed.

Even though the amount of isotactic PMU was too small to be engaged in model epimerization reactions, it was decided to substitute the isotactic model by atactic or syndiotactic models to study the epimerization process. The modification of the stereochemistry of the models could be very easily observed and quantified by GC. Using the same relative concentrations in peroxide and NBS than those engaged in reactive extrusion, the destruction of the initial stereo-regularity of the syndiotactic model compound remained below 10 %. Interestingly, the GC traces of the crude products were remarkably clean despite their dark brown color. No by-products or reaction intermediates could be isolated or identified through GC or NMR spectroscopy. No evidence of grafted-bromine was observed. It was also demonstrated that epimerization actually occurred even in the absence of peroxide but to a lower extent. DSC measurements indicated that degradation of both the peroxide and NBS occurred at much lower temperature when they are mixed together in a hydrocarbon substrate. Unfortunately, the grafting reaction could not be reproduced at the time on the model compounds.

Aside from the main topic of this thesis, the skills developed in the field of high temperature ^{13}C NMR contributed to an international project based on polyethylene rheology. The goal was to use the thermorheological behavior of molten polyethylenes of various chain architectures as a probe for their molecular structure, e.g. the presence of short- and long-chain branches. High temperature NMR was required to accurately characterize the molecular structure (type and quantity of co-monomers) of the samples

6.2 Future Work

The grafting of reactive polar entities such as maleic anhydride onto a hydrophobic non-reactive polymer creates amphiphilic molecules that can be used as compatibilizers between polar and non-polar materials. The NBS-mediated melt-grafting of maleic anhydride onto PP is a flexible process for the manufacture of a range of innovative compatibilizers with enhanced reactivity and tailored physico-chemical properties. Those interesting features were exploited in a couple of side-projects where NBS-mediated PP-g-MA plays a major role.

A project in the continuity of this Thesis was started as another Ph.D. Thesis led by Dimitri Rousseaux, entitled *"Polypropylene/Clay Nanocomposites Revisited"*, that aims to engage NBS-mediated PP-g-MA derivatives (i.e ionomers) as compatibilizers of PP/clay nanocomposites.

Also, because of their higher reactivity and higher molecular weights, NBS-mediated PP-g-MA was considered in the manufacture of sizing for glass fiber for polypropylene reinforcement. A very interesting project called "*EMULFIVE*", and funded by the Walloon Region, consists in grafting PEG chains onto a part of the grafted maleic anhydride to give the PP-g-MA a more pronounced amphiphilic character for the future

preparation of stable PP-g-MA emulsions. The addition of innovative photo-activable bridging molecular clips will further improve the reinforcement.

Concerning the mechanistic investigations on the model compounds, further work is required to comprehend the epimerization and grafting reactions in the presence of NBS, and more particularly the fate of bromine radicals. Lower temperatures are required to prevent maleic anhydride distillation off the reactive mixture. As gas chromatography does not provide information concerning side-products and reaction intermediates, the experimental setup and analytical tools must be revised and adapted to the analyses of highly volatile compounds. Blank experiments (NBS-peroxide couple only) should be conducted as well and grating in the presence of much lower concentrations of maleic anhydride should be attempted to remain within the solubility limits for homogeneous reaction.